Oxidative Medicine and Cellular Longevity

# Genetic and Chemical Effects on Somatic and Germline Aging

Lead Guest Editor: Myon-Hee Lee
Guest Editors: Huai-Rong Luo, Soo Han Bae, and Adriana San-Miguel

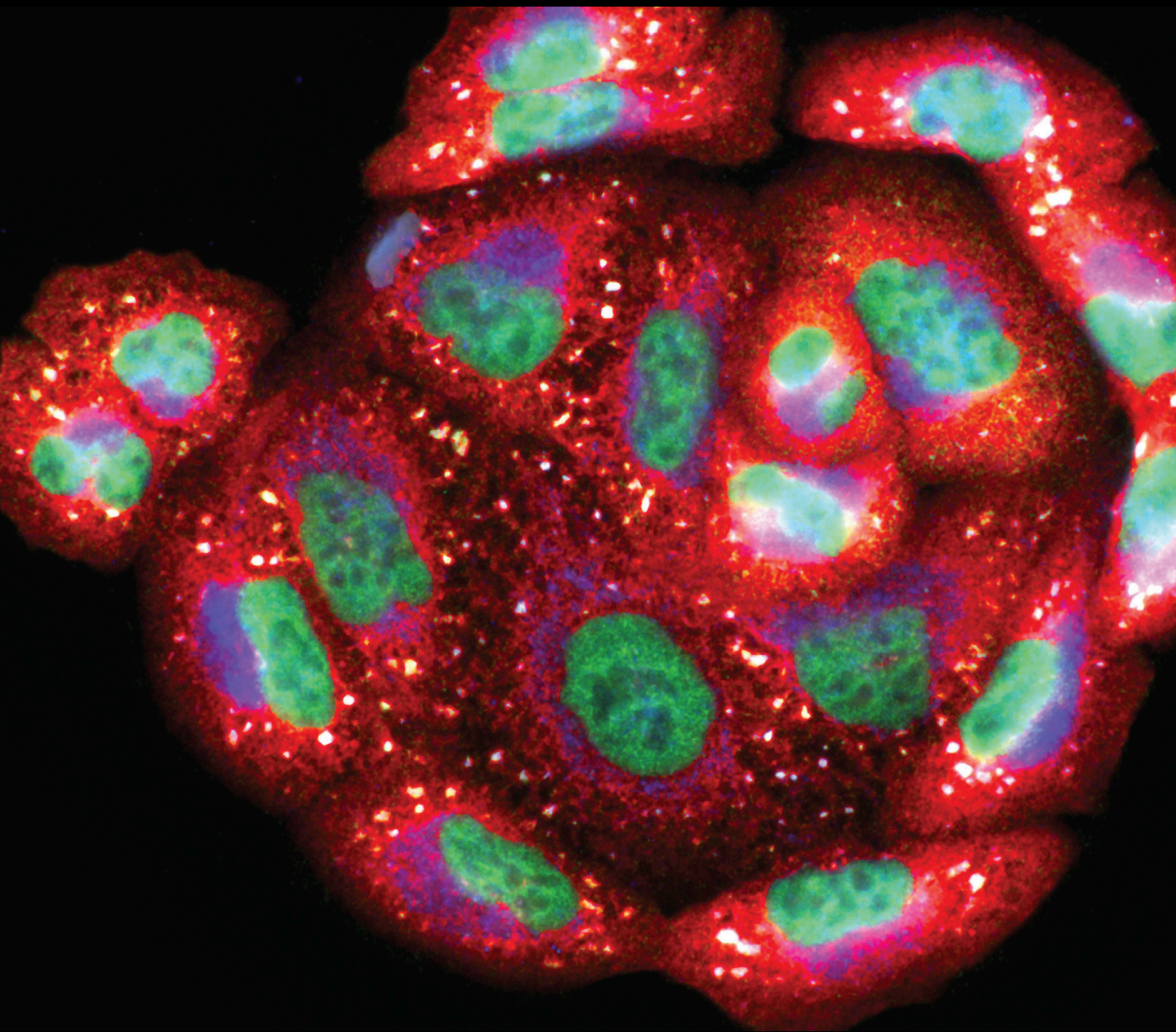

# Genetic and Chemical Effects on Somatic and Germline Aging

Oxidative Medicine and Cellular Longevity

# Genetic and Chemical Effects on Somatic and Germline Aging

Lead Guest Editor: Myon-Hee Lee
Guest Editors: Huai-Rong Luo, Soo Han Bae, and Adriana San-Miguel

# Contents

**The Effects of Age and Reproduction on the Lipidome of Caenorhabditis elegans**
Qin-Li Wan, Zhong-Lin Yang, Xiao-Gang Zhou, Ai-Jun Ding, Yuan-Zhu Pu, Huai-Rong Luo, and Gui-Sheng Wu
Research Article (14 pages), Article ID 5768953, Volume 2019 (2019)

**Triclosan: An Update on Biochemical and Molecular Mechanisms**
Mohammad A. Alfhili and Myon-Hee Lee
Review Article (28 pages), Article ID 1607304, Volume 2019 (2019)

Hindawi
Oxidative Medicine and Cellular Longevity
Volume 2020, Article ID 4684890, 2 pages
https://doi.org/10.1155/2020/4684890

*Editorial*

# Genetic and Chemical Effects on Somatic and Germline Aging

**Myon-Hee Lee**[1], **Huai-Rong Luo**[2], **Soo Han Bae**[3] **and Adriana San-Miguel**[4]

[1]*Department of Internal Medicine (Division of Hematology/Oncology), Brody School of Medicine at East Carolina University, Greenville, NC 27834, USA*
[2]*Key Laboratory for Aging and Regenerative Medicine, Department of Pharmacology, School of Pharmacy, Southwest Medical University, Luzhou, Sichuan 646000, China*
[3]*Severance Biomedical Science Institute, Yonsei Biomedical Research Institute, Yonsei University College of Medicine, 50 Yonsei-ro, Seodaemun-gu, Seoul 03722, Republic of Korea*
[4]*Department of Chemical and Biomolecular Engineering, NC State University, Raleigh, NC 27695, USA*

Correspondence should be addressed to Myon-Hee Lee; leemy@ecu.edu

Received 22 October 2019; Accepted 23 October 2019; Published 4 January 2020



Somatic aging is a complex process characterized by gradual deterioration of physiological function that is observed at the genetic, molecular, and cellular levels. The role of genetic and chemical factors in the aging phenomenon extends to various research fields, including stem cell biology, diabetes, and cancer. Although the fundamental mechanisms behind the aging process are still poorly understood, increasing evidence shows that a progressive and irreversible accumulation of oxidative injury, caused by reactive oxygen species (ROS), impacts negatively on the aging process and contributes to impaired physiological function, increased incidence of age-related disease, and shortened lifespan.

In addition to somatic aging, several studies have shown that reproductive capabilities similarly decline with age (also termed germline aging). Germline tissue is the only tissue designed to support the development of an entire organism, and therefore, it may be the ultimate source of stem cells for tissue replacement in diseased or injured individuals. Specifically, germline aging manifests as diminished germline stem cell (GSC) capacity and reduced germ cell numbers. Several reports have demonstrated that signals from the reproductive system influence somatic aging and *vice versa*. However, mechanisms governing this intricate process remain ill defined.

Therefore, this special issue will focus on the impact of genetic (e.g., miR-22, SIRT-1, AT1R, TGF-$\beta$1, Smad2/3, daf-12/16, NRF2) and chemical factors (e.g., triclosan, salidroside, folic acid, Lycium barbarum polysaccharide, porphyran, lipidome) on antioxidant defense mechanisms and age-induced somatic and germline aging, using both invertebrate and vertebrate model organisms, which may address fundamental biological questions regarding aging and development.

X. Zhang et al. demonstrated that sleep deprivation induces serious telomere dysfunction and a subsequent senescence-associated secretory phenotype (SASP). In addition, authors showed for the first time that folic acid (also known as vitamin $B_9$) supplementation could reverse telomere damage and the secretion of senescence-associated cytokines in both mice and humans.

R. He et al. reported that upregulation of TRPC3 is involved in atrial fibrosis in aging and spontaneously hypertensive rats. Furthermore, pharmacological TRPC3 selected blocker or knockdown of TRPC3 both attenuates Ang II-induced atrial fibroblasts migration, proliferation, and the expression of fibrotic biomarkers. $Ca^{2+}$-permeable TRPC3 mediates atrial fibrosis through the $Ca^{2+}$/AT1R/TGF-$\beta$1/p-Smad2/3 signaling pathway, suggesting which may be a potential therapeutic target of the pathogenesis of atrial fibrillation during aging and hypertension.

G.-X. Mao et al. studied the effects of salidroside, a compound isolated from Rhodiola rosea L., on cellular senescence. The authors found that salidroside delays cellular

senescence in human fibroblasts partly by increasing mitochondrial biogenesis. The authors also show that salidroside induces expression of SIRT1, a necessary step in of mitochondrial biogenesis. Finally, the authors studied the role of the miR-22 miRNA in SIRT1 expression and revealed that increased SIRT1 expression is an in part result of miR-22 inhibition.

Z. Zhang et al. reported that the Lycium barbarum polysaccharides (LBP) extracted from Lycium barbarum show a positive effect on longevity, the abilities to withstand environmental stress, reproduction, and maintenance of muscle integrity mainly through *sir-2.1*, *daf-12*, and *daf-16* using the nematode *C. elegans* as a model system.

M. Chen et al. reported that the proper differentiation of gonad somatic cells is essential for germ cell meiosis. Aberrant development of gonad somatic cells leads to ectopic expression of meiosis-associated genes in germ cells, subsequently causes meiosis arrest before prophase I. In $Wt1^{-/flox}$; *Cre-ER™* mice, inactivation of *Wt1* by the injection of tamoxifen at E9.5 blocks the differentiation of Sertoli and granulosa cells and causes most germ cells migrate outside of genital ridge. STRA8, SYCP3, and $\gamma$H2AX proteins are detected in germ cells of both male and female $Wt1^{-/flox}$; *Cre-ER™* gonads, whereas no thread-like SYCP3 signal is observed.

S.-H. Kim et al. reported the antioxidant and antiaging effect of phosphatidylcholine and the underlying mechanism involved in phosphatidylcholine-induced longevity using the nematode *Caenorhabditis elegans* as a model system. Specifically, the authors demonstrated that phosphatidylcholine delays age-related decline of motility by the upregulation of longevity-assurance genes, *hsp-16.2* and *sod-3*.

A. R. Ghanam et al. investigated the age-associated expression of three molecular hallmarks of aging: SA-$\beta$-gal, $P16^{INK4a}$, and retrotransposable elements (RTEs), in different mouse tissues during chronological aging, and revealed variable expression patterns of these markers in different tissues with aging. $P16^{INK4a}$ shows consistent increases with age in most tissues, while expression of RTEs is variable among different tissues examined. These data suggest that biological changes occurring with physiological aging may be useful in choosing the appropriate timing of therapeutic interventions to slow the aging process or keep more susceptible organs healthier in the aging process.

Q.-L. Wan et al. used a comprehensive high-resolution lipidome to show the relationship between longevity and lipid metabolism using *C. elegans* as a model system. The authors demonstrated that signals from the reproductive tissues may affect animal lifespan at least in part by regulating FOXO/DAF-16-mediated metabolic changes.

M. A. Alfhili and M. H. Lee provide an update on current knowledge regarding the therapeutic and toxic potential of triclosan, a chlorinated phenolic antimicrobial agent and a potential inhibitor of NRF2-mediated oxidative stress response. Specifically, this review emphasizes on the biochemical and molecular alterations, either brought about by or in response to TCS exposure at both the cellular and organismal levels.

## Conflicts of Interest

The authors declare no conflict of interest.

## Acknowledgments

Finally, the editors are very grateful to all the authors who submitted their research articles and reviews to this special issue. They also thank all the reviewers for their valuable contribution to this special issue.

*Myon-Hee Lee*
*Huai-Rong Luo*
*Soo Han Bae*
*Adriana San-Miguel*

Hindawi
Oxidative Medicine and Cellular Longevity
Volume 2019, Article ID 4569614, 14 pages
https://doi.org/10.1155/2019/4569614

*Research Article*

# Folic Acid Supplementation Suppresses Sleep Deprivation-Induced Telomere Dysfunction and Senescence-Associated Secretory Phenotype (SASP)

**Xiaoning Zhang**,[1,2] **Yuwen Wang**,[1] **Rui Zhao**,[1] **Xianyun Hu**,[3] **Baoren Zhang**,[4] **Xin Lv**,[5] **Zhenglong Guo**,[6] **Zhiqiang Zhang**,[7] **Jinghua Yuan**,[8] **Xu Chu**,[1] **Fei Wang**,[9] **Guang Li**,[1] **Xin Geng**,[10] **Yang Liu**,[11] **Lei Sui**,[12] **and Feng Wang**[1,13]

[1]*Department of Genetics, School of Basic Medical Sciences, Tianjin Medical University, Tianjin 300070, China*
[2]*Institute of Basic Medicine, Shandong First Medical University & Shandong Academy of Medical Sciences, Shandong 250012, China*
[3]*Department of Medical Examination, Tianjin Worker's Hospital, Tianjin 300050, China*
[4]*Department of General Surgery, Tianjin General Surgery Institute, Tianjin Medical University General Hospital, Tianjin 300052, China*
[5]*Department of Nutrition and Food Science, School of Public Health, Tianjin Medical University, Tianjin 300070, China*
[6]*Department of Cell Biology, School of Basic Medical University, Tianjin Medical University, Tianjin 300070, China*
[7]*Department of Pathology, Tianjin Hospital of ITCWM, Nankai Hospital, Tianjin 300100, China*
[8]*School of Medicine, Hangzhou Normal University, Zhejiang 310036, China*
[9]*Department of Neurology, General Hospital, Tianjin Medical University, Tianjin 300052, China*
[10]*Department of Biochemistry and Molecular Biology, School of Basic Medical Sciences, Tianjin Medical University, Tianjin 300070, China*
[11]*Department of Radiobiology, Institute of Radiation Medicine, Chinese Academy of Medical Sciences and Peking Union Medical College, Tianjin 300192, China*
[12]*Department of Prosthodontics, Tianjin Medical University School and Hospital of Stomatology, Tianjin 300070, China*
[13]*Tianjin Key Laboratory of Exercise Physiology and Sports Medicine, Tianjin University of Sport, Tianjin 300381, China*

Correspondence should be addressed to Yang Liu; liuyang@irm-cams.ac.cn, Lei Sui; suilei@tmu.edu.cn, and Feng Wang; wangf@tmu.edu.cn

Received 4 May 2019; Revised 4 September 2019; Accepted 13 September 2019; Published 17 December 2019

Guest Editor: Myon-Hee Lee



Sleep deprivation is reported to cause oxidative stress and is hypothesized to induce subsequent aging-related diseases including chronic inflammation, Alzheimer's disease, and cardiovascular disease. However, how sleep deprivation contributes to the pathogenesis of sleep deficiency disorder remains incompletely defined. Accordingly, more effective treatment methods for sleep deficiency disorder are needed. Thus, to better understand the detailed mechanism of sleep deficiency disorder, a sleep deprivation mouse model was established by the multiple platform method in our study. The accumulation of free radicals and senescence-associated secretory phenotype (SASP) was observed in the sleep-deprived mice. Moreover, our mouse and human population-based study both demonstrated that telomere shortening and the formation of telomere-specific DNA damage are dramatically increased in individuals suffering from sleeplessness. To our surprise, the secretion of senescence-associated cytokines and telomere damage are greatly improved by folic acid supplementation in mice. Individuals with high serum baseline folic acid levels have increased resistance to telomere shortening, which is induced by insomnia. Thus, we conclude that folic acid supplementation could be used to effectively counteract sleep deprivation-induced telomere dysfunction and the associated aging phenotype, which may potentially improve the prognosis of sleeplessness disorder patients.

## 1. Introduction

Sleep is a physiological state that is vital for the quality of life of an individual and occupies 1/4-1/3 of the time in one day in most humans. During sleep, most of the body's systems are in a state of synthesis, helping to restore the immune, nervous, skeletal, and muscular systems, which are important to maintain emotion, memory, and cognitive functions [1]. However, sleep deprivation (SD) or chronic sleep restriction has become a relevant health problem caused by social factors, such as wide usage of electronic products and networks, night-shift work or overtime work schedules, and chronic diseases [2–4]. Previous studies have shown that sleep deprivation leads to a number of aging-related diseases, including chronic inflammation, Alzheimer's disease, and cardiovascular disease [5–10] and even causes mortality when individuals are severely deprived of sleep [11, 12].

A main cause of sleep deprivation-induced disease is increased oxidative damage [13]. Oxidative stress is a phenomenon caused by an imbalance between the production and accumulation of reactive oxygen species (ROS) in cells and tissues and the ability of a biological system to detoxify these reactive products [14]. A large number of studies have shown that oxidative stress and increased ROS production could lead to cell trauma and cause several diseases [14–18].

Telomeres are a type of repetitive nucleotide sequence ($5'$-$(TTAGGG)_n$-$3'$) at the ends of all chromosomes that protect the chromosome from deterioration or fusion with neighboring chromosomes. Due to their high guanine content, telomeres are considered common fragile sites of the genome and are highly sensitive to damage and are shortened by chronic oxidative stress, toxin damage, and radiation exposure [19, 20]. When telomeres become critically short or sufficiently damaged, DNA damage signaling is triggered, leading to various senescence-related disorders [10].

Folate, also known as the natural form of vitamin B9 in food, which is the generic term for a family of compounds including folic acid (a synthetic, parent compound of this family which does not exist in nature) and its derivatives is a critical cofactor in one-carbon metabolism, including nucleotide metabolism, maintaining the cellular redox status and methylation metabolism [21, 22]. Folate is also required for nucleotide synthesis and is implicated in cell proliferation, DNA repair, and genomic stability [23]. Current studies have shown that folic acid functions in the treatment of neural tube defect (NTD), cardiovascular disease (CVD), and stroke [24–26].

In this study, we used a multiple classical platform technique to investigate the hypothesis that folic acid supplementation prevents sleep deprivation-induced oxidative stress and telomere dysfunction in an animal model. Furthermore, we recruited human volunteers to investigate the correlation between sleep quality, folic acid, and telomere length.

## 2. Materials and Methods

### 2.1. Animal Experiments

*2.1.1. Animals and Sleep Deprivation.* Wild-type male C57BL/6J mice (4~5 weeks) were purchased from Huafukang Bioscience Co., Inc. (BJ, CN). Mice were randomly divided into two groups with similar mean body weights (14 mice per group): the FAD group (mice were fed a folic acid-deficient diet) and the FAS group (mice were fed a folic acid-supplemented diet).

All mice were fed one purified diet based on the AIN93M standard formula [27] without the addition of folic acid (FAD) or with the addition of 8 mg/kg folic acid (FAS) (for the composition of the experimental diets, see Supplementary Table 1). All diets were manufactured by Trophic Animal Feed High-Tech Co., Ltd. (JS, CN). Before sleep deprivation, mice were fed a folic acid-deficient or folic acid-supplemented diet for 78 days. FAD and FAS mice were both randomly subdivided into two groups: wide platform control groups (WC+FAD and WC+FAS) and sleep deprivation groups (SD+FAD and SD+FAS) (seven mice per group). Mice were sleep deprived using the multiple classical platform technique, as described previously (the experimental design is shown in Figure 1(a)) [28, 29]. Briefly, mice in a group were placed on narrow platforms ($\Phi$ 3 cm, 12 platforms per container) in a water tank (41 cm × 34 cm × 17 cm) surrounded by water up to 1 cm beneath the surface (schematic photo in Supplementary Figures 1A and 1B). In this method, mouse sleep was disrupted when the mice fell into the water after muscle atonia. The duration of sleep deprivation was 20 h, which ran from 1:00 pm to 9:00 am the following day, and was conducted over 7 days; the mice slept for 4 h every day. Control group mice were placed on a large platform ($\Phi$ 6 cm, 8 platforms per container) in the water tank where the mice were able to sleep and move at will. Mice were maintained under specific pathogen-free conditions (temperature controlled 22.5 ± 0.5°C) with a 12-12 h light-dark cycle (lights were turned on at 7:30 am and turned off at 7:30 pm) according to institutional guidelines. Experimental protocols and animal care methods were approved by the Animal Care and Use Committee of Tianjin Medical University (TMUaMEC 2017012).

*2.1.2. Folate Concentration Assays.* Serum folate concentration was determined by a competitive protein-binding assay with a Siemens automated chemiluminescence system (BER, DE), according to the manufacturer's instructions. The detectable concentration ranged from 1 to 24 ng/mL, since the serum folate levels were high, and the samples were diluted by a factor of 5 to 20 with normal saline.

*2.1.3. ROS Levels and SOD Activity Assays.* The liver and testis were homogenized (1 : 20, *w*/*v*) in ice-cold phosphate-buffered saline (PBS). The homogenate was centrifuged at 9000 ×g at 4°C for 15 min to remove cell debris. The supernatant was harvested and incubated with dichlorodihydrofluorescein diacetate (DCFH-DA) (Wanlei Life Sciences Co., Ltd., LN, CN) at 37°C for 30 min to assess intracellular ROS generation. Fluorescence was examined using a Multifunctional Enzyme Marker (Tecan, Männedorf, CH) at excitation/emission wavelengths of 485/525 nm. Total SOD activity was detected by a Total SOD Assay Kit with WST-8 (Wanlei Life Sciences Co., Ltd.) according to the manufacturer's

instructions. The absorbance was assessed at 550 nm using a Microplate Reader (Bio-Rad, CA, USA).

*2.1.4. Enzyme-Linked Immunosorbent Assay.* The levels of IL-4, IL-6, TNF-$\alpha$, p53, and $p16^{INK4a}$ in plasma were detected by an enzyme-linked immunosorbent assay (ELISA) according to the manufacturer's instructions.

*2.1.5. Fluorescence In Situ Hybridization (FISH) and $\gamma$-H2AX Immunofluorescence-Telomere FISH (IF-FISH).* Fluorescence in situ hybridization (FISH) of telomeres was performed on methanol/acetic acid-fixed bone marrow cells and paraffin-embedded sectioned testis tissue as previously described [30] using a Cy3-conjugated PNA telomere oligonucleotide probe (Panagene, Daejeon, KR). $\gamma$-H2AX immunofluorescence-telomere FISH was carried out as described by Kasbek and colleagues [31]. FISH was performed as previously described, and immunofluorescence was performed using anti-phospho-histone H2AX primary antibody (Ser 139); endogenous peroxides of testis-specimens were blocked with goat serum followed by deparaffinization and rehydration, and antigen retrieval was performed by heating in a microwave. The primary antibody and the Alexa Fluor® 488-conjugated secondary antibody were both diluted 1 : 500. Stained cells were photographed using an Olympus inverted microscope or confocal microscope (Olympus FV1000, JP).

*2.1.6. cDNA Library Preparation and Sequencing.* cDNA libraries of testis cells were constructed and sequenced at the Novogene Bioinformatics Institute (BJ, CN). Clean data were obtained after filtering out reads with adaptors and poly-N sequences > 10% and low-quality reads from raw data through in-house Perl scripts. The Q20, Q30, and GC content of the clean reads were calculated. All downstream analyses were based on the good-quality clean reads. Differentially expressed genes (DEGs) with $|\log_2(\text{fold change})| > 0$ and $P$ values < 0.05 were considered significant. In order to unveil the pathways that may be associated with the identified DEGs, KEGG pathway enrichment analysis was performed using the NovoMagic v3.0 website (https://magic.novogene.com/) (Supplementary Tables 2 and 3).

*2.1.7. Quantitative Real-Time Polymerase Chain Reaction (qPCR).* The RNA-sequencing results were validated by quantitative real-time polymerase chain reaction (qPCR). Total RNA of the testis tissues was extracted using a TRIzol reagent (Invitrogen, NY, USA), and 1 $\mu$g of RNA was reverse-transcribed using HiScript II Q Select RT SuperMix for qPCR (Vazyme Biotech, JS, CN) according to the manufacturer's instructions. To evaluate the expression of the involved genes, quantitative real-time PCR detection was performed with AceQ qPCR SYBR Green Master Mix (Vazyme Biotech) on the Rotor-Gene Q 2000 real-time PCR system (Qiagen, Düsseldorf, DE). All of the specific primers were synthesized by GENEWIZ, Inc. (JS, CN), and the sequences of each primer are listed in Supplementary Table 4. Each sample was tested and analyzed in triplicate. GAPDH was used as the endogenous control.

*2.1.8. Assessment of Sperm Motility.* The sperm motility assessment of all mice was performed as previously described [32]. One testis from each animal was placed into a 35 mm dish containing 1.5 mL of normal saline and ruptured using syringes with 26 G needles. Then, the sperms were gently squeezed out of the testes. Dishes containing released sperm were incubated at 37°C for 30 min in a 5% $CO_2$ air incubator, followed by removal of the testes, mixing of the sperm suspension by gentle swirling, and subsequent assessment of sperm motility. Sperm suspensions were diluted 1 : 10 in normal saline (37°C), loaded onto a prewarmed glass slide (37°C), covered with a prewarmed glass coverslip, and rested for 20 s before analysis. Sperm motility was blind-assessed at 37°C using a microscope at ×200 magnification. At least 200 sperms from five fields were counted in each sperm sample within 2 min of removal from the incubator.

### 2.2. Human Research

*2.2.1. Participants and Samples.* This study was carried out in accordance with the approved guidelines of the Committees for Ethical Review of Research Involving Human Subjects at Tianjin Medical University and Tianjin Worker's Hospital. Informed consent was obtained from all participants.

Participants were recruited from Tianjin Worker's Hospital. In total, 96 participants (41 males and 55 females) underwent the initial screening. All participants filled out the Pittsburgh Sleep Quality Inventory (PSQI) [33] to assess their sleep quality in the month preceding the start of the experiment, in which nineteen individual items generate seven "component" scores: subjective sleep quality, sleep latency, sleep duration, habitual sleep efficiency, sleep disturbances, use of sleeping medication, and daytime dysfunction. The sum of the scores for the seven yields the PSQI score. Good sleepers were the individuals whose PSQI scores were between 0 and 9, and the "poor" sleepers were those whose PSQI scores were between 10 and 21 (depressed patients were excluded). One portion of the participants ($N = 63$) showed good sleep quality (scores less than 9), while the rest of the participants ($N = 33$) were in the poor sleep quality range (scores between 10 and 21). As described previously, the normal and low reference values for folate was at >7.2 ng/mL and <7.2 ng/mL [22], so each group was divided into two subgroups according to the folate concentration: 7.2 ng/mL (<16.4 nmol/L) and >7.2 ng/mL (>16.4 nmol/L); thus, all participants were divided into 4 subgroups: good sleep with lower folate (GS+LF) ($N = 26$), poor sleep with lower folate (PS+LF) ($N = 21$), good sleep with higher folate (GS+HF) ($N = 37$), and poor sleep with higher folate (PS+HF) ($N = 12$). Demographic characteristics of the study population are shown in Supplementary Tables 5–7.

All samples were used anonymously. Peripheral blood was collected from each participant into ethylenediaminetetraacetic acid anticoagulant tubes and heparin-anticoagulant tubes.

*2.2.2. Routine Blood Examination and Telomere FISH of Leukocytes.* Routine blood examination and serum folate levels were detected. The telomere length of the leukocytes was determined by FISH.

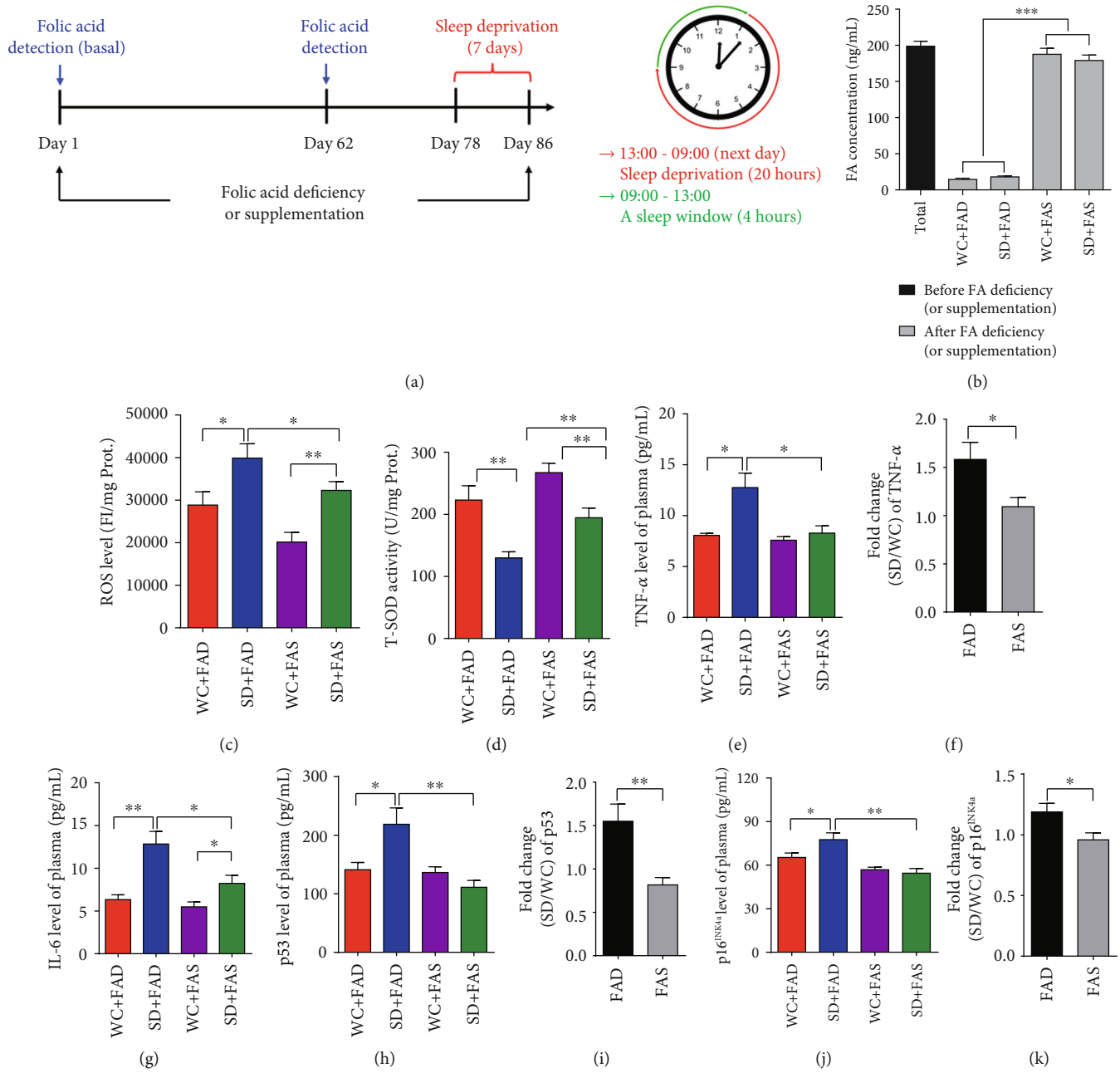


FIGURE 1: Folic acid attenuates sleep deprivation-induced oxidative stress and SASP disorder. (a) Experimental design. A schematic diagram showing that mice were fed a long-term folic acid-supplemented diet for more than two months, and sleep deprivation was performed for 20 h/day (01:00 pm to 09:00 am the following day) for 7 days. (b) The folic acid concentration in serum before and after folic acid deficiency (or supplementation). (c) Reactive oxygen species (ROS) in the liver was assayed using DCFH-DA as a probe. (d) Antioxidative capacity in the liver was detected by the total SOD assay kit with WST-8. (e, f) Secretion of tumor necrosis factor-$\alpha$ (TNF-$\alpha$) in the plasma, detected by ELISA, and the fold change (SD/WC) in the FAD or FAS groups. (g) Secretion of interleukin-6 (IL-6) in the plasma, detected by ELISA. (h–k) The abundance of p53 and $p16^{INK4a}$ in the plasma was detected by ELISA and the fold change (SD/WC) in the FAD or FAS groups. Data are presented as the mean ± SEM ($N = 7$ per group). $^{*}P < 0.05$; $^{**}P < 0.01$; and $^{***}P < 0.001$.

*2.3. Statistical Analysis.* Data are presented as the mean ± standard error of the mean (mean ± SEM). Statistical analysis was performed using SPSS 20.0 software (SPSS Inc., Chicago, USA). Two-way ANOVA was used for comparisons among groups, and a post hoc contrast by least significant difference (LSD) $t$-test was applied to confirm the significance. Two-tailed $P$ values < 0.05 were considered statistically significant.

## 3. Results

*3.1. Folic Acid Attenuates Sleep Deprivation-Induced Oxidative Stress and SASP.* Somnipathy is a common disease and a concomitant symptom with certain diseases. It has been reported that high-grade somnipathy induces severe disorders, including circadian rhythm disorders, endocrine dyscrasia, and systemic inflammation [12, 34]. Additionally, folic acid is reported to play an important role in preventing neural tube defects and cardiovascular disease and reducing inflammation through its role as a one-carbon donor, which suggests that folic acid supplementation might benefit individuals with sleep deprivation-related disorders. To further investigate the effect of sleep deprivation on aging-related disease and the reversal effect of folic acid, a mouse model was established using the multiple classical platform technique [28, 29] for 7 days (wide platform control group (WC) *vs.* sleep deprivation group (SD)), and mice were sleep deprived for 20 h per day from 1:00 pm to 9:00 am the following day (for the experiment design, see Figure 1(a)). Before sleep deprivation, the mice were fed a folic acid-deficient diet (FAD) ($N = 14$) or an 8 mg/kg folic acid-supplemented diet (FAS) ($N = 14$) for 78 days. The serum folic acid concentration was tracked during the process. We observed that the folic acid concentration level was high (~200 ng/mL for total mice) before the customized food, since the ordinary mouse diet has relatively high folic content (4~8 mg/kg) (Figure 1(b)). As predicted, the folate concentration of the mice fed different folic acid diets showed dramatic differences (<20 ng/mL for the FAD group and >180 ng/mL for the FAS group, Figure 1(b)). Interestingly, sleep deprivation was found to lead to increased physiological dysfunctions, including ruffled fur, anemia, and mobility retardation; folic acid supplementation greatly reversed these disorders (data not shown). Additionally, the body weight was tracked every day during the folic acid feeding and sleep deprivation process. The results showed that folic acid supplementation had no effect on body weight in non-sleep-deprived mice (WC+FAD and WC+FAS) ($N = 7$ per group). However, sleep deprivation induced visible weight loss, which was abated in folic acid-fed mice (Supplementary Figure 1C) (SD+FAD *vs.* SD+FAS) ($N = 7$ per group), suggesting that folic acid supplementation may help to resolve the sleep deprivation-induced physical effects.

Oxidative stress is caused by an imbalance between prooxidants and antioxidants in cells and tissues [14]. Proteins and lipids are oxidatively modified under oxidative stress and then lose/change their cellular functions [35]. It has been reported that wakefulness requires a great amount of oxygen, resulting in a significant leakage and accumulation of reactive oxygen species (ROS), such as the superoxide anion radical ($O_2^{\cdot-}$), hydroxyl radicals ($^{\cdot}OH$), and the nonradical hydrogen peroxide ($H_2O_2$), from mitochondria during oxidative phosphorylation [35, 36]. Superoxide dismutase (SOD), catalase (CAT), and glutathione peroxidase (GPx) are the three major enzymes in charge of transforming free radicals into more stable chemical forms [35]. To determine the effect of folic acid on oxidative stress induced by sleep deprivation, we assessed the ROS level and antioxidant SOD activity in liver tissues that contain large amounts of mitochondria and are actively engaged in energy metabolism. As expected, the level of ROS was increased in the sleep deprivation group (SD+FAD *vs.* WC+FAD, SD+FAS *vs.* WC+FAS) ($N = 7$ per group), which could then be reduced by folic acid supplementation (Figure 1(c)) (SD +FAS *vs.* SD+FAD). In contrast, SOD, which specifically converts superoxide radicals to hydrogen peroxide, had the opposite change (Figure 1(d)). For instance, SOD activity was inhibited by sleep deprivation and induced by folic acid supplementation. Interestingly, we observed that folic acid supplementation could also decrease the production of ROS and promote the activity of SOD even in the non-sleep-deprived control mice (WC+FAD and WC+FAS), indicating that folic acid plays an important role in systemically mediating the redox status *in vivo*. Similarly, the antioxidative effect was also observed in testis cells (another tissue abundant with mitochondria) (Supplementary Figure 2). However, the fold change of both ROS and SOD by folic acid between the FAD group ((SD +FAD)/(WC+FAD)) and the FAS group ((SD+FAS)/(WC +FAS)) did not show visible differences, suggesting that the antioxidative function of folic acid is not specific to the sleep-deprived mice (data not shown).

Elevated ROS simulate cellular senescence and induce the alternative SASP [37]. SASP is a characteristic feature of senescent cells that secrete a predictable profile of cytokines, chemokines, and proteases. In this study, to evaluate SASP alterations, the concentration of SASP biomarkers, including IL-4, IL-6, and TNF-$\alpha$ in blood samples was measured by ELISA ($N = 7$ per group). Compared to that of the control (WC+FAD) group, the secretion of IL-4, IL-6, and TNF-$\alpha$ cytokines in the blood was increased in the sleep deprivation (SD+FAD) group of mice fed the no folic acid diet. However, the increased cytokine secretion was eliminated by folic acid supplementation (WC+FAS and SD+FAS). In contrast to the effect of folic acid on redox status, folic acid supplementation had little effect on the secretion of cytokines in control mice without sleep disturbance (WC+FAD *vs.* WC+FAS) (Figures 1(e) and 1(g); IL-4 data not shown). However, we compared the effect of folic acid between the sleep deprivation group and the control group and calculated the fold change in cytokine secretion. We observed that the secretion of TNF-$\alpha$ was dramatically reduced by the addition of folic acid ($1.583 \pm 0.176$-fold for (SD+FAD)/(WC+FAD) *vs.* $1.092 \pm 0.094$-fold for (SD+FAS)/(WC+FAS), $P < 0.05$) (Figure 1(f)), suggesting that folic acid plays an important role in SASP induction specifically in sleep-deprived mice.

The p53 and Rb signaling pathways are the two main signaling pathways for cellular senescence, which mediate the presentation of SASP. To further confirm the activation of the aging response signal pathways, the levels of the related regulators, including p53 and $p16^{INK4a}$, were also detected by ELISA. We observed that sleep deprivation could activate both the p53 and Rb ($p16^{INK4a}$) pathways (Figures 1(h)–1(k)), which may result from the increased level of ROS. Additionally, consistently, the increase of both p53 and Rb ($p16^{INK4a}$) induced by sleep deprivation was suppressed by folic acid supplementation ($1.583 \pm 0.176$-fold

for (SD+FAD)/(WC+FAD) *vs.*$1.092 \pm 0.094$-fold for (SD +FAS)/(WC+FAS), $P < 0.05$) (Figures 1(i) and 1(k)). Nuclear factor NF-$\kappa$B plays an important role in SASP signaling pathway due to its induction expression of pro-inflammatory factors including cytokines, chemokines, and adhesion molecules. Thus, we detected the expression of NF-$\kappa$B in testis sections by immunohistochemistry staining using NF-$\kappa$B antibody; however, we did not observe any significant change between different groups (Supplementary Figure 3). The results aforementioned showed that the secretion of the SASP biomarkers may vary between solid tissues and the circulatory system. Taken together, our data show that folic acid attenuates the sleep deprivation-induced aging response through inflammatory cytokines and aging-related protein secretion but not through the direct regulation of redox status regulation.

*3.2. Telomere Dysfunction Could Be Ameliorated by Folic Acid Supplementation.* Due to their high guanine content, telomeres are considered fragile sites of the genome and can be attacked by ROS, chemistry, ionizing radiation (IR), etc. [38, 39], and the dysfunction of telomeres leads to genomic instability and cellular senescence [40]. To investigate whether telomere function is affected by sleep deprivation and folic acid supplementation, the telomere length was determined by quantitative fluorescence in situ hybridization (Q-FISH), and telomere-specific DNA damage was determined by colocalization of $\gamma$-H2AX and telomeres.

For telomere length detection, telomeric DNA was labeled by the Cy3 conjugated PNA probe, and the average telomere length was reflected by the fluorescent signal intensity in bone marrow cells. The data revealed that abnormal sleep rhythm led to a shortening of the average telomere length, which could be partially rescued by folic acid supplementation (Figures 2(a) and 2(b)). The telomere length (fluorescent signal intensity) distribution analysis revealed that the distribution peak moved to the left in the sleep deprivation sample. Moreover, a large number of cells (~15%) with super short telomeres (AFUs 0-10) were detected in the sleep-deprived folic acid-deficient group, suggesting that abnormal sleep rhythm may lead to telomere damage or losses other than telomere shortening (Figure 2(c)). To our surprise, compared to the SD+FAD mice, folic acid-supplemented mice (SD+FAS) had a marked recovery of the telomere loss phenotype, and the percentage of short telomeres decreased from 15% to 2% (Figure 2(c)). Additionally, this rescue effect on the non-sleep-deprived mice was clear (5.38% to 1.36%), suggesting that folic acid supplementation resolves sleep deprivation-induced telomere shortening/damage by promoting telomere DNA repair, which might be related to the suppression of p53 or other unknown causes.

To further understand the toxic effect of sleep deprivation and folic acid on reproduction, the telomere length and telomere DNA damage-induced foci were analyzed in testis tissues; the mobility/activity of sperm was also determined. Similar to the bone marrow cell results, the loss of telomeric DNA was found to be greatly resolved by folic acid supplementation (Supplementary Figures 4A–4C). Furthermore, the immunofluorescence colocalization data demonstrated that sleep deprivation-induced DNA damage occurred on both telomeres and other sequences of the genome. However, folic acid supplementation reduced the number of telomere dysfunction-induced foci (TIFs), and the fold change in TIFs after sleep deprivation was significantly decreased in the FAS group ($1.076 \pm 0.090$) compared to that of the FAD group ($1.426 \pm 0.100$) ($P < 0.05$) (Figure 3(c)), suggesting that folic acid supplementation improves telomere damage to a great extent. The number of cells with TIFs did not change when the mice with normal sleep rhythms were fed folic acid-supplemented diets. Telomere shortening or telomere damage has been suggested to play a triggering role in asthenospermia; thus, the sperm performance of mice was analyzed. Our results revealed that the percentage of active sperm, especially the forward motile sperm, was significantly decreased after sleep deprivation (24% to 16%) but increased after folic acid supplementation (16% to 26%) (Figures 3(d) and 3(e)). In addition, we also found that mice suffering from sleep deprivation had more inactive sperms (59% to 69%), which could also be rescued by folic acid supplementation (69% to 58%) (Figure 3(f)). To our surprise, folic acid supplementation also improved the sperm motility performance in mice with normal sleep rhythms, suggesting that folic acid rescues sleep deprivation-induced asthenospermia through its telomere protection function and at least one another pathway.

*3.3. Folic Acid Recovered the Transcriptome Altered by Sleep Deprivation.* To understand the mechanism by which folic acid effectively ameliorates the negative physical response caused by sleep deprivation, we performed RNA-sequencing (RNA-seq) to identify differentially expressed genes (DEGs) that play key roles in this process. Heat map and volcano plot analysis showed the DEGs in WC +FAD, SD+FAD, and SD+FAS mice (2 of each) (Figures 4(a)–4(c)). A total of 1667 DEGs, including 810 upregulated and 857 downregulated, were found in SD +FAD mice compared with WC+FAD mice. In contrast, 496 upregulated and 692 downregulated genes were found in SD+FAS mice compared with SD+FAD mice. The DEGs upregulated in SD+FAD mice but downregulated in SD +FAS or SD+FAD mice overlapped. The Kyoto Encyclopedia of Genes and Genomes (KEGG) analysis demonstrated that these DEGs are significantly associated with cellular metabolism and oxidative phosphorylation-related pathways (i.e., oxidative phosphorylation pathway, metabolism of xenobiotics by cytochrome P450 pathway, thyroid hormone signaling pathway, protein processing in endoplasmic reticulum, and telomere length regulation) (Figures 4(d) and 4(e); Supplementary Tables 2 and 3). Four DEGs (*Cox6a1*, *Cox8a*, *Ndufa12*, and *Ndufb8*) related to the oxidative phosphorylation pathway were selected for further analysis, and the level of transcription was determined (Figures 4(f) and 4(g); Supplementary Figure 5). As expected, the expression of the genes was elevated by sleep deprivation but inhibited after folic acid supplementation, which illustrates that sleep deprivation plays an important role in promoting the related cellular metabolism and

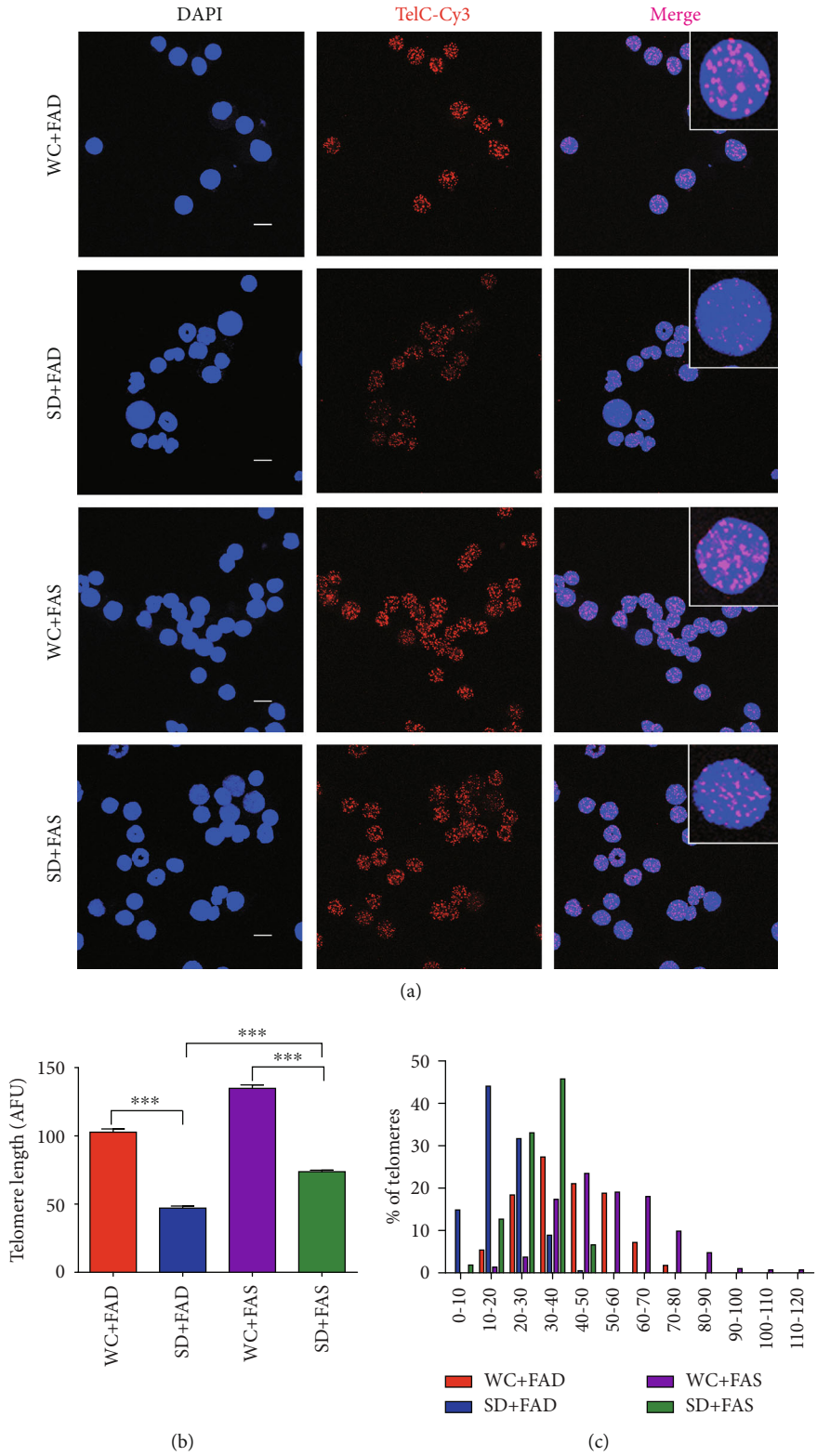


FIGURE 2: Folic acid restrains telomere shortening induced by sleep deprivation. (a) The telomere length of bone marrow cells was detected by quantitative fluorescence in situ hybridization (Q-FISH) and is shown as average fluorescence units (AFUs). Scale bars are 10 $\mu$m. (b) Scatter plot of telomere AFUs for more than 200 cells of all mice. (c) The histogram displays the distribution of relative telomere length as AFUs. Data are presented as the mean ± SEM ($N = 7$ per group). $^{***}P < 0.001$.

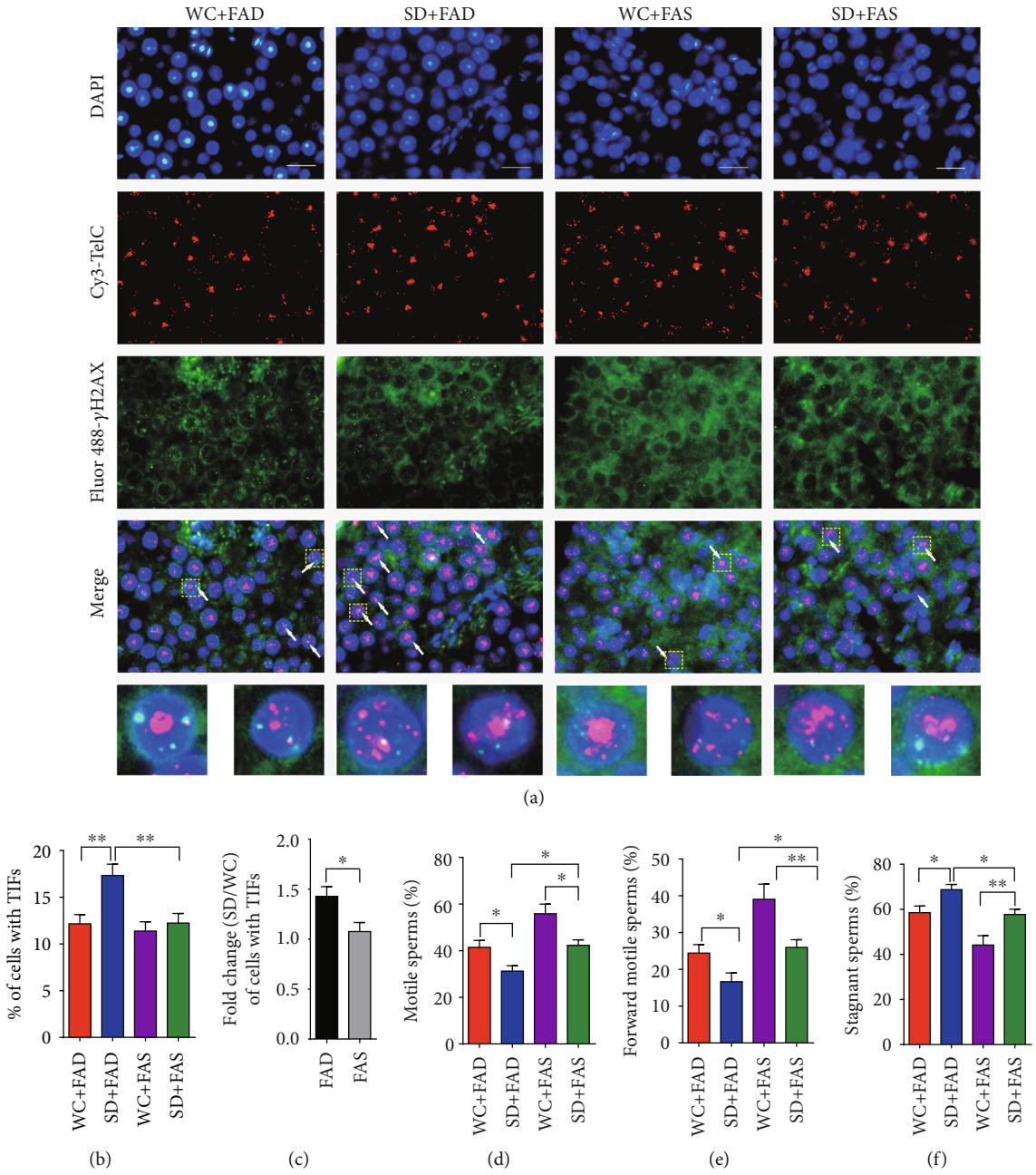


Figure 3: Folic acid ameliorates telomere dysfunction and rescues spermatozoa motility defects induced by sleep deprivation. (a) Telomere damage shown by the colocalization of the telomere signals and DNA damage marker $\gamma$-H2AX (TIFs). Scale bars are 10 $\mu$m. (b, c) Representative TIFs of telomere damage images of all groups and the fold change (SD/WC) in the FAD or FAS groups. (d) Percentage of motile sperm. (e) Percentage of the forward motile sperm. (f) Percentage of stagnant sperm. Data are presented as the mean ± SEM ($N = 7$ per group). $^{*}P < 0.05$ and $^{**}P < 0.01$.

oxidative phosphorylation, which could be subsequently suppressed by folic acid. Taken together, our RNA-seq data show that in addition to protecting telomeres, folic acid resolves sleep deprivation-induced disorder by suppressing the oxidative phosphorylation process. Additionally, a differentially expressed gene named *Tep1*, which encodes a component of the telomerase-associated protein responsible for telomerase activity, was identified by RNA-seq. The transcription of *Tep1* was suppressed by sleep deprivation but elevated in folic acid supplementation samples. Tep1 has been reported to play an essential role in telomere length regulation, which might be the reason for the telomere elongation observed in folic acid-supplemented mice.

*3.4. Elongated Leukocyte Telomere Length Is Associated with a High Serum Concentration Level of Folic Acid in Humans.* Telomeres are shortened with cell division, and telomere length is considered a marker of biological age [41–43]. In our mouse experiments, we observed that folic acid supplementation could greatly ameliorate sleep deprivation-

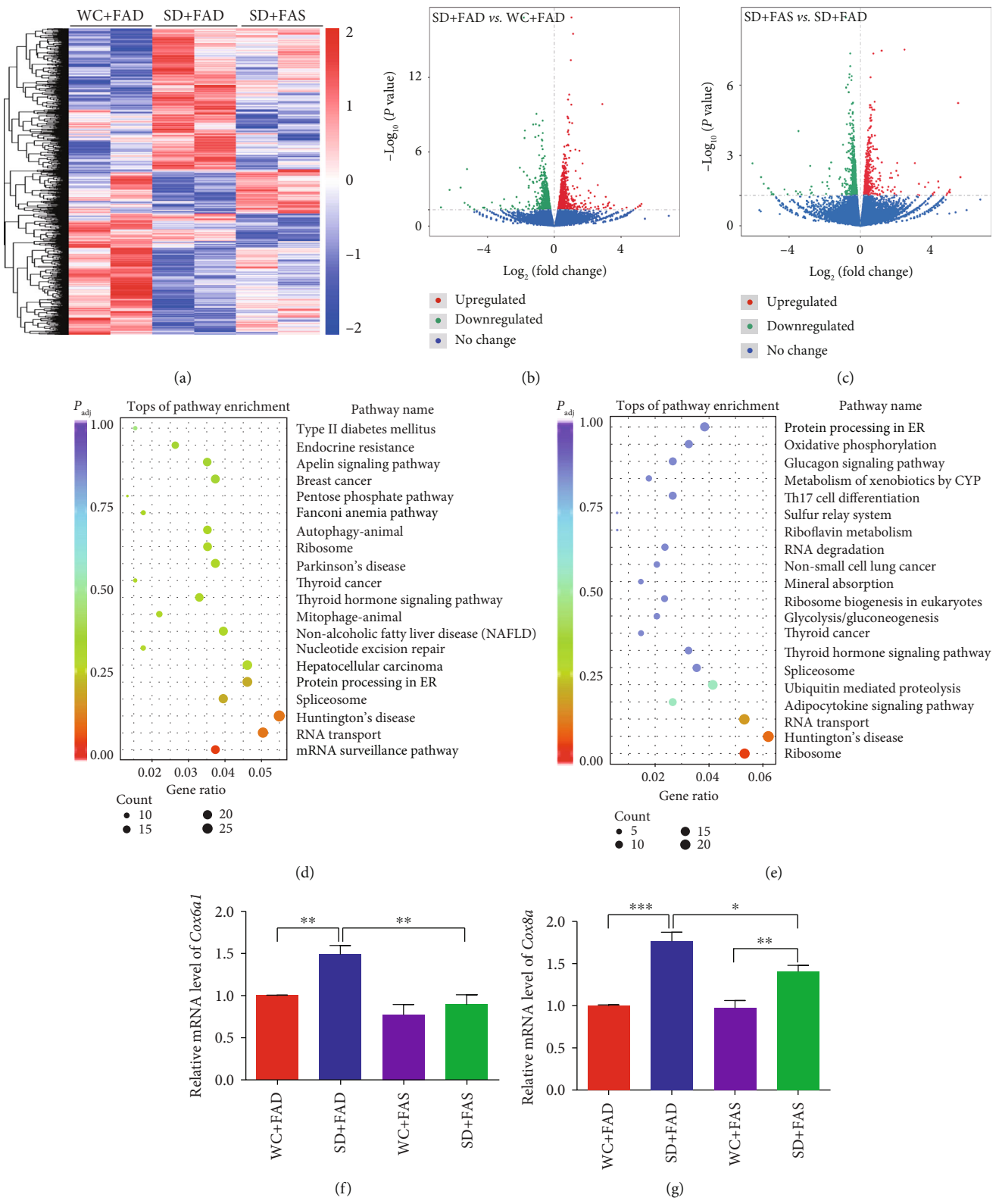


FIGURE 4: Transcriptome profile analysis. (a) Heat map of gene expression in WC+FAD, SD+FAD, and SD+FAS mice ($N = 2$ per group). (b) Volcano plot showing the transcript levels differentially expressed between SD+FAD and WC+FAD mice. (c) Volcano plot showing the transcript levels differentially expressed between SD+FAS and SD+FAD mice. (d) Top representative pathways of enriched DEGs in the SD+FAD *vs.* WC+FAD group. (e) Top representative pathways of enriched DEGs in the SD+FAS *vs.* SD+FAD group. (f) Relative expression of *Cox6a1* detected by real-time PCR. (g) Relative expression of *Cox8a* detected by real-time PCR. Data are presented as the mean ± SEM ($N = 7$ per group). $^{*}P < 0.05$; $^{**}P < 0.01$; and $^{***}P < 0.001$.

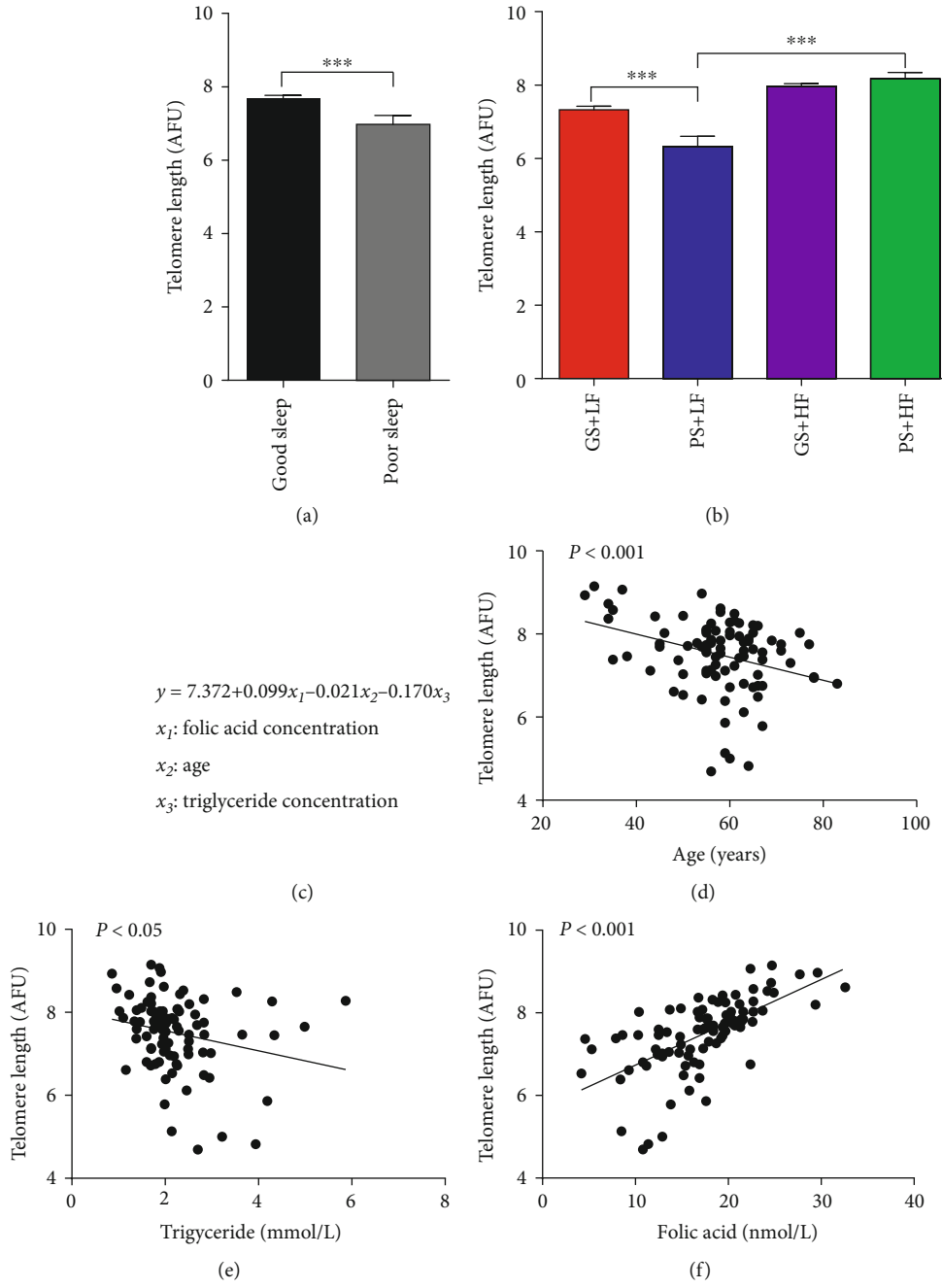


Figure 5: Elongated leukocyte telomere length is associated with a high concentration level of plasma folic acid in humans. (a) The leukocyte telomere length of the participants divided into two groups according to the sleep score. (b) The leukocyte telomere length of the participants divided into four groups according to both sleep score and blood folate concentration. (c) A multiple regression analysis was performed for all the individuals. (d) The correlation between leukocyte telomere length and age. (e) The correlation between leukocyte telomere length and triglycerides. (f) The correlation between leukocyte telomere length and blood folate concentration. Data are presented as the mean ± SEM . $^{***}P < 0.001$.

induced telomere damage/shortening. To investigate the telomere effect of sleep quality and folic acid supplementation in the human population, leukocyte telomere length was assessed by Q-FISH. A total of 98 individuals were included, and 2 were excluded due to incomplete information (detailed information is shown in Supplementary Tables 5–7). The sleep quality of the participants was determined by the PSQI score. Two-thirds of the participants ($N = 63$) showed good sleep quality (scores less than 9), while the rest of the participants ($N = 33$) were in the poor sleep quality range (scores between 10 and 21). The individuals were divided into four groups according to the sleep score and blood folate concentration. Overall, the poor sleep group showed a shorter telomere length compared to that of the good sleep group (Figure 5(a)). The clinical parameters, including age, body mass index (BMI),

folate concentration, and the routine blood indices, were put in a multiple regression equation (Figure 5(c)), and the $\beta$ value was generated to analyze the association of these variables with telomere length. Our data demonstrated that the leukocyte telomere length of the population was significantly inversely associated with age and triglyceride concentration and positively correlated with blood folate (Figures 5(d)–5(f); Supplementary Table 8). The population with lower levels of serum folate (PS+LF) showed weaker telomere fluorescence compared to the population with good sleep and lower serum folate levels (GS+LF). However, in contrast, the telomere length of the GS+HF group and the PS+HF group showed no significant change. Moreover, both groups with higher folate levels (GS+HF group and PS+HF group) had longer telomeres than the groups with lower folate levels (GS+LF group and PS+LF group) (Figure 5(b)). Consistent with our mouse results, our human population-based study indicates that poor sleep quantity could significantly shorten telomere length or damage telomeres, which may ultimately contribute to aging- and aging-related diseases; a high baseline concentration of folate in blood could greatly reverse the effects of sleep deficiency.

## 4. Discussion

Sleep deprivation has been reported to be associated with various human pathologies, including inflammation, cardiovascular disease, Alzheimer's disease, reproductive system dysfunction, other aging-related issues, and even death [5, 44]. The most acceptable hypothesis for these observations is that the imbalance between prooxidants and antioxidants trigged by wakefulness may play an essential role in contributing to the associated disorders [45]. However, an effective treatment method for sleep deficiency-induced disorder has not yet been developed. In our study, we observed that sleep deprivation could lead to free radical accumulation and corresponding systemic damage, as previously reported [45]. Interestingly, our data revealed that sleep deprivation induces serious telomere dysfunction and a subsequent SASP. Further investigation in the human population demonstrated that poor sleep quality led to severe telomere shortening. More importantly, we showed for the first time that folic acid supplementation could reverse telomere disorder and the secretion of senescence-associated cytokines in both mice and humans.

Folate, also known as vitamin B9, is an essential compound involved in many important biochemical processes [46]. Folate is essential for the body to make DNA, RNA, and amino acids during periods of rapid growth, such as infancy and pregnancy [47]. Recent studies have provided evidence showing that folate plays an important role in preventing NTD, cardiovascular disease, and stroke, which are diseases related to oxidative stress [24]. Since folate acts on the methionine metabolic cycle, being related to the endogenous antioxidants glutathione (GSH) and glutathione peroxidase, the most likely explanation for our findings is that folic acid could resolve the sleep deprivation-associated disturbances through its antioxidant activity. Consistently, we observed that the accumulation of ROS could be abrogated and that the activity of SOD could be induced by the addition of folic acid. However, the fold change of ROS and SOD was the same between sleep-deprived mice and non-sleep-deprived control mice after folic acid supplementation, suggesting that the antioxidation activity of folic acid is not specific to the wakefulness of mice. The subsequent results showed that folic acid treatment inhibited the secretion of senescence-associated cytokines (especially TNF-$\alpha$) and telomere shortening/damage only for the sleep-deprived mice. To our knowledge, this is the first study showing that folic acid could help resolve the sleep deprivation-induced aging-related phenotype change and could thus provide a major advance in the understanding of the function of folic acid.

In addition, folic acid and its intermediate metabolite tetrahydrofolic acid play an essential role in the synthesis of S-adenosylmethionine (SAM), which functions as a cofactor and methyl group donor for DNA methylation [48]. We speculate that folic acid may protect cells via an epigenetic modification. Folic acid could inhibit the stress response process and aging-related inflammatory response by mediating the expression of genes involved in regulating SASP or oxidative stress, such as p53 and Rb, through methylation or demethylation of the promoter. Our RNA-seq data showed that the expression levels of the genes involved in oxidative phosphorylation were greatly altered by folic acid supplementation.

Telomeres which are a type of repetitive nucleotide sequence ($5'$-$(TTAGGG)_n$-$3'$) at the ends of all chromosomes are considered common fragile sites of the genome. Telomeres are shortened with cell division, and telomere length is considered a marker of biological age [41, 42]. Due to their high guanine content, telomeres are highly sensitive to damage and shortening by several endogenous or exogenous factors, such as chronic oxidative stress, toxin damage, and radiation exposure [19, 20]. When telomeres become critically short or sufficiently damaged, the dysfunction triggers DNA damage signaling, leading to genomic instability and cell senescence [10, 40]. Thus, sleep deprivation, which is reported to trigger oxidative stress, leads to telomere-specific DNA damage and subsequent aging [49]. The tissues and cells with a high level of metabolic activity are easily to get free radical accumulation and subsequent DNA damage. Thus, the reproductive system is very sensitive to the external and internal stresses. Moreover, testis is one type of the tissues with telomerase activity. It has been reported that the telomerase played an import role in DNA damage response and damaged DNA repair. Our current data showed that sleep deprivation could lead to telomere damage not only in telomerase-negative cells but also in telomerase-positive cells. Interestingly, we observed that folic acid upregulated the expression of the telomerase-associated protein TEP1, which is essential for telomere elongation and telomere damage repair. Thus, we suspect that in addition to regulating oxidative status, folic acid plays a direct role in telomere length maintenance.

In summary, our study implicates folic acid as an effective vitamin to counteract telomere dysfunction and the associated senescence phenotype induced by sleep deprivation.

Although the detailed mechanism needs to be further addressed, our findings indicate that to obtain a better treatment outcome of sleep deficiency-related disorders, the recovery of subsequent oxidative stress and related damage is greatly needed.

## Data Availability

The data used to support the findings of this study are available from the corresponding authors upon request.

## Conflicts of Interest

The authors declare there are no competing interests.

## Acknowledgments

This work was supported by grants from the National Natural Science Foundation of China (Nos. 91649102, 31471293, 31771520, 81772243, 81671054, and 81771135), the National Key R&D Program of China (No. 2017YFC1001904), the Natural Science Foundation of Tianjin City (Nos. 17JCYBJC42700 and 16JCZDJC32800), the Key Project of Tianjin Natural Science Fund (No. 19JCZDJC35600), the Non-profit Central Research Institute Fund of Chinese Academy of Medical Sciences (2018RC310020), the Fundamental Research Funds for the Central Universities (3332019003), the Tianjin Medical University 13th 5-year postgraduate Innovation Fund (No. YJSCX201705), and the Innovation Project of Shandong Academy of Medical Sciences.

## Supplementary Materials

Supplementary Figure 1: folic acid ameliorates weight loss induced by sleep deprivation. (A) Schematic photo of the sleep deprivation group. Mice were sleep deprived in a water tank containing multiple classical platforms (diameter in 3 cm). (B) Schematic photo of the control platform group. The control group mice were placed on large platforms (diameter in 6 cm). (C) Long-term weight change ($n = 7$ per group). Supplementary Figure 2: oxidative stress in testis cells. (A) Reactive oxygen species (ROS) in the testis cells was assayed using DCFH-DA as a probe ($n = 7$ per group). (B) Antioxidative capacity in the testis cells was detected by the total superoxide dismutase (SOD) assay kit with WST-8 ($n = 7$ per group). Data was represented as the mean ± SEM. $^{*}P < 0.05$; $^{**}P < 0.01$; $^{***}P < 0.001$. Supplementary Figure 3: the expression of NF-$\kappa$B in testis cells. The testis sections immunohistochemically stained against NF-$\kappa$B of each group. Scale bars are 100 $\mu$m. Supplementary Figure 4: folic acid restrains telomere shortening of testis cells induced by sleep deprivation. (A) Telomere length of testis cells was detected by quantitative fluorescence in situ hybridization (Q-FISH) and shown with average fluorescence unit (AFU). Scale bars are 10 $\mu$m. (B) Scatter plot of AFU for more than 300 cells of all mice. (C) Histogram displays distribution of relative telomere length. Data was represented as the mean ± SEM ($n = 7$ per group). $^{***}P < 0.001$. Supplementary Figure 5: relative expression of Ndufa12 and Ndufb8 detected by real-time PCR. (A) Relative mRNA level of Ndufa12 ($n = 7$ per group). (B) Relative mRNA level of Ndufb8. Data was represented as the mean ± SEM ($n = 7$ per group). $^{*}P < 0.05$. Supplementary Table 1: composition of the experimental diets. Supplementary Table 2: the differentially expressed genes found in SD+FAD vs. WC+FAD group and related pathways identified with KEGG analysis. Supplementary Table 3: the differentially expressed genes found in SD+FAS vs. SD+FAD group and related pathways identified with KEGG analysis. Supplementary Table 4: primer sequences for real-time PCR detection. Supplementary Table 5: demographic characteristics of the study population. Clinical parameters are shown as the mean ± SD. Supplementary Table 6: demographic characteristics of the study population divided into two groups according to the sleep score. Clinical parameters are shown as the mean ± SD. Supplementary Table 7: demographic characteristics of the study population divided into four groups according to both sleep score and blood folic acid concentration. Clinical parameters are shown as the mean ± SD. Supplementary Table 8: linear regression analysis of the correlation between the leukocyte telomere length (AFU) and general characteristics. *(Supplementary Materials)*

## References

[1] D. J. Gottlieb and D. L. Bhatt, "More evidence that we could all use a good night's sleep*," *Journal of the American College of Cardiology*, vol. 73, no. 2, pp. 145–147, 2019.

[2] E. Ghanem, S. Al Bitar, R. Dib, and C. S. Kabrita, "Sleep restriction alters the temporal expression of major histocompatibility complex class ii molecules in murine lymphoid tissues," *Behavioural Brain Research*, vol. 362, pp. 152–159, 2019.

[3] L. Exelmans and J. Van den Bulck, "Bedtime mobile phone use and sleep in adults," *Social Science & Medicine*, vol. 148, pp. 93–101, 2016.

[4] C. C. Caruso, "Negative impacts of shiftwork and long work hours," *Rehabilitation Nursing*, vol. 39, no. 1, pp. 16–25, 2014.

[5] J. M. Mullington, M. Haack, M. Toth, J. M. Serrador, and H. K. Meier-Ewert, "Cardiovascular, inflammatory, and metabolic consequences of sleep deprivation," *Progress in Cardiovascular Diseases*, vol. 51, no. 4, pp. 294–302, 2009.

[6] J. K. Holth, S. K. Fritschi, C. Wang et al., "The sleep-wake cycle regulates brain interstitial fluid tau in mice and CSF tau in humans," *Science*, vol. 363, no. 6429, pp. 880–884, 2019.

[7] C. A. Everson, C. J. Henchen, A. Szabo, and N. Hogg, "Cell injury and repair resulting from sleep loss and sleep recovery in laboratory rats," *Sleep*, vol. 37, no. 12, pp. 1929–1940, 2014.

[8] M. L. Andersen, D. A. Ribeiro, C. T. Bergamaschi et al., "Distinct effects of acute and chronic sleep loss on DNA damage in rats," *Progress in Neuro-Psychopharmacology & Biological Psychiatry*, vol. 33, no. 3, pp. 562–567, 2009.

[9] E. S. Arnardottir, E. V. Nikonova, K. R. Shockley et al., "Blood-gene expression reveals reduced circadian rhythmicity in individuals resistant to sleep deprivation," *Sleep*, vol. 37, no. 10, pp. 1589–1600, 2014.

[10] E. H. Blackburn, E. S. Epel, and J. Lin, "Human telomere biology: a contributory and interactive factor in aging, disease

risks, and protection," *Science*, vol. 350, no. 6265, pp. 1193–1198, 2015.

[11] A. N. Vgontzas, J. Fernandez-Mendoza, D. Liao, and E. O. Bixler, "Insomnia with objective short sleep duration: the most biologically severe phenotype of the disorder," *Sleep Medicine Reviews*, vol. 17, no. 4, pp. 241–254, 2013.

[12] M. R. Irwin, R. Olmstead, and J. E. Carroll, "Sleep disturbance, sleep duration, and inflammation: a systematic review and meta-analysis of cohort studies and experimental sleep deprivation," *Biological Psychiatry*, vol. 80, no. 1, pp. 40–52, 2016.

[13] K. H. Alzoubi, O. F. Khabour, B. A. Rashid, I. M. Damaj, and H. A. Salah, "The neuroprotective effect of vitamin E on chronic sleep deprivation-induced memory impairment: the role of oxidative stress," *Behavioural Brain Research*, vol. 226, no. 1, pp. 205–210, 2012.

[14] G. Pizzino, N. Irrera, M. Cucinotta et al., "Oxidative stress: harms and benefits for human health," *Oxidative Medicine and Cellular Longevity*, vol. 2017, Article ID 8416763, 13 pages, 2017.

[15] L. Doridot, M. Jeljeli, C. Chene, and F. Batteux, "Implication of oxidative stress in the pathogenesis of systemic sclerosis via inflammation, autoimmunity and fibrosis," *Redox Biology*, no. article 101122, 2019.

[16] M. Muriach, M. Flores-Bellver, F. J. Romero, and J. M. Barcia, "Diabetes and the brain: oxidative stress, inflammation, and autophagy," *Oxidative Medicine and Cellular Longevity*, vol. 2014, Article ID 102158, 9 pages, 2014.

[17] N. García, C. Zazueta, and L. Aguilera-Aguirre, "Oxidative stress and inflammation in cardiovascular disease," *Oxidative Medicine and Cellular Longevity*, vol. 2017, Article ID 5853238, 2017.

[18] S. K. Saha, S. B. Lee, J. Won et al., "Correlation between oxidative stress, nutrition, and cancer initiation," *International Journal of Molecular Sciences*, vol. 18, no. 7, article e1544, 2017.

[19] J. M. J. Houben, H. J. J. Moonen, F. J. van Schooten, and G. J. Hageman, "Telomere length assessment: biomarker of chronic oxidative stress?," *Free Radical Biology & Medicine*, vol. 44, no. 3, pp. 235–246, 2008.

[20] N. Pawlas, A. Płachetka, A. Kozłowska et al., "Telomere length, telomerase expression, and oxidative stress in lead smelters," *Toxicology and Industrial Health*, vol. 32, no. 12, pp. 1961–1970, 2016.

[21] S. Cui, X. Lv, W. Li et al., "Folic acid modulates _VPO1_ DNA methylation levels and alleviates oxidative stress-induced apoptosis in vivo and in vitro," *Redox Biology*, vol. 19, pp. 81–91, 2018.

[22] F. Ma, T. Wu, J. Zhao et al., "Plasma homocysteine and serum folate and vitamin B12 levels in mild cognitive impairment and Alzheimer's disease: a case-control study," *Nutrients*, vol. 9, no. 7, p. 725, 2017.

[23] W. Li, R. Tang, F. Ma, S. Ouyang, Z. Liu, and J. Wu, "Folic acid supplementation alters the DNA methylation profile and improves insulin resistance in high-fat-diet-fed mice," *The Journal of Nutritional Biochemistry*, vol. 59, pp. 76–83, 2018.

[24] R. D. Wilson, R. D. Wilson, F. Audibert et al., "Pre-conception folic acid and multivitamin supplementation for the primary and secondary prevention of neural tube defects and other folic acid-sensitive congenital anomalies," *Journal of Obstetrics and Gynaecology Canada*, vol. 37, no. 6, pp. 534–549, 2015.

[25] Y. Li, T. Huang, Y. Zheng, T. Muka, J. Troup, and F. B. Hu, "Folic acid supplementation and the risk of cardiovascular diseases: a meta-analysis of randomized controlled trials," *Journal of the American Heart Association*, vol. 5, no. 8, article e003768, 2016.

[26] X. Wang, X. Qin, H. Demirtas et al., "Efficacy of folic acid supplementation in stroke prevention: a meta-analysis," *Lancet*, vol. 369, no. 9576, pp. 1876–1882, 2007.

[27] P. G. Reeves, F. H. Nielsen, and G. C. Fahey Jr., "AIN-93 purified diets for laboratory rodents: final report of the American Institute of Nutrition ad hoc writing committee on the reformulation of the AIN-76a rodent diet," *The Journal of Nutrition*, vol. 123, no. 11, pp. 1939–1951, 1993.

[28] R. H. Silva, V. C. Abílio, A. L. Takatsu et al., "Role of hippocampal oxidative stress in memory deficits induced by sleep deprivation in mice," *Neuropharmacology*, vol. 46, no. 6, pp. 895–903, 2004.

[29] B. Qin and Y. Deng, "Overexpression of circadian clock protein cryptochrome (CRY) 1 alleviates sleep deprivation-induced vascular inflammation in a mouse model," *Immunology Letters*, vol. 163, no. 1, pp. 76–83, 2015.

[30] X. Feng, S. J. Hsu, C. Kasbek, M. Chaiken, and C. M. Price, "CTC1-mediated C-strand fill-in is an essential step in telomere length maintenance," *Nucleic Acids Research*, vol. 45, no. 8, pp. 4281–4293, 2017.

[31] C. Kasbek, F. Wang, and C. M. Price, "Human TEN1 maintains telomere integrity and functions in genome-wide replication restart," *The Journal of Biological Chemistry*, vol. 288, no. 42, pp. 30139–30150, 2013.

[32] B. C. Borges, D. Garcia-Galiano, S. da Silveira Cruz-Machado et al., "Obesity-induced infertility in male mice is associated with disruption of Crisp4 expression and sperm fertilization capacity," *Endocrinology*, vol. 158, no. 9, pp. 2930–2943, 2017.

[33] D. J. Buysse, C. F. Reynolds III, T. H. Monk, S. R. Berman, and D. J. Kupfer, "The Pittsburgh sleep quality index: a new instrument for psychiatric practice and research," *Psychiatry Research*, vol. 28, no. 2, pp. 193–213, 1989.

[34] G. Dispersyn, F. Sauvet, D. Gomez-Merino et al., "The homeostatic and circadian sleep recovery responses after total sleep deprivation in mice," *Journal of Sleep Research*, vol. 26, no. 5, pp. 531–538, 2017.

[35] H. Sies, "Oxidative stress: a concept in redox biology and medicine," *Redox Biology*, vol. 4, pp. 180–183, 2015.

[36] K. H. Al-Gubory, C. Garrel, P. Faure, and N. Sugino, "Roles of antioxidant enzymes in corpus luteum rescue from reactive oxygen species-induced oxidative stress," *Reproductive Biomedicine Online*, vol. 25, no. 6, pp. 551–560, 2012.

[37] G. Salazar, "NADPH oxidases and mitochondria in vascular senescence," *International Journal of Molecular Sciences*, vol. 19, no. 5, p. 1327, 2018.

[38] P. Wang, J. Geng, J. Gao et al., "Macrophage achieves self-protection against oxidative stress-induced ageing through the Mst-Nrf2 axis," *Nature Communications*, vol. 10, no. 1, p. 755, 2019.

[39] T. von Zglinicki, "Oxidative stress shortens telomeres," *Trends in Biochemical Sciences*, vol. 27, no. 7, pp. 339–344, 2002.

[40] J. Yuan, Y. Liu, J. Wang et al., "Long-term persistent organic pollutants exposure induced telomere dysfunction and senescence-associated secretary phenotype," *The Journals of*

*Gerontology. Series A, Biological Sciences and Medical Sciences*, vol. 73, no. 8, pp. 1027–1035, 2018.

[41] Y. Zhu, X. Liu, X. Ding, F. Wang, and X. Geng, "Telomere and its role in the aging pathways: telomere shortening, cell senescence and mitochondria dysfunction," *Biogerontology*, vol. 20, no. 1, pp. 1–16, 2019.

[42] J. Liu, L. Wang, Z. Wang, and J. P. Liu, "Roles of telomere biology in cell senescence, replicative and chronological ageing," *Cells*, vol. 8, no. 1, p. 54, 2019.

[43] M. Herrmann, I. Pusceddu, W. Marz, and W. Herrmann, "Telomere biology and age-related diseases," *Clinical Chemistry and Laboratory Medicine*, vol. 56, no. 8, pp. 1210–1222, 2018.

[44] J. H. Choi, S. H. Lee, J. H. Bae et al., "Effect of sleep deprivation on the male reproductive system in rats," *Journal of Korean Medical Science*, vol. 31, no. 10, pp. 1624–1630, 2016.

[45] G. Villafuerte, A. Miguel-Puga, E. M. Rodríguez, S. Machado, E. Manjarrez, and O. Arias-Carrión, "Sleep deprivation and oxidative stress in animal models: a systematic review," *Oxidative Medicine and Cellular Longevity*, vol. 2015, Article ID 234952, 15 pages, 2015.

[46] A. M. Gazzali, M. Lobry, L. Colombeau et al., "Stability of folic acid under several parameters," *European Journal of Pharmaceutical Sciences*, vol. 93, pp. 419–430, 2016.

[47] C. R. Sudfeld and E. R. Smith, "New evidence should inform who guidelines on multiple micronutrient supplementation in pregnancy," *The Journal of Nutrition*, vol. 149, no. 3, pp. 359–361, 2019.

[48] P. R. Mandaviya, L. Stolk, and S. G. Heil, "Homocysteine and DNA methylation: a review of animal and human literature," *Molecular Genetics and Metabolism*, vol. 113, no. 4, pp. 243–252, 2014.

[49] M. A. Kang, E. Y. So, A. L. Simons, D. R. Spitz, and T. Ouchi, "DNA damage induces reactive oxygen species generation through the H2AX- Nox1/Rac1 pathway," *Cell Death & Disease*, vol. 3, no. 1, article e249, 2012.

Hindawi
Oxidative Medicine and Cellular Longevity
Volume 2019, Article ID 4025496, 15 pages
https://doi.org/10.1155/2019/4025496

*Research Article*

# Upregulation of Transient Receptor Potential Canonical Type 3 Channel via AT1R/TGF-$\beta$1/Smad2/3 Induces Atrial Fibrosis in Aging and Spontaneously Hypertensive Rats

**Rongfang He,[1,2] Juan Zhang,[1] Dan Luo,[1] Yiyan Yu,[1] Tangting Chen,[1] Yan Yang,[1] Fengxu Yu,[3] and Miaoling Li[1,3]**

[1]*Key Laboratory of Medical Electrophysiology of Ministry of Education, Medical Electrophysiology Key Lab of Sichuan Province, Collaborative Innovation Center for Prevention and Treatment of Cardiovascular Disease, Institute of Cardiovascular Research, Southwest Medical University, Luzhou 646000, China*
[2]*Infectious Disease Department, The Affiliated Hospital of Southwest Medical University, Luzhou 646000, China*
[3]*Affiliated Hospital of Southwest Medical College, Cardiothoracic Surgery, Luzhou 646000, China*

Correspondence should be addressed to Fengxu Yu; yuluchuan@swmu.edu.cn and Miaoling Li; limiaolingcc@swmu.edu.cn

Received 6 May 2019; Revised 11 August 2019; Accepted 13 September 2019; Published 23 November 2019

Guest Editor: Huai-Rong Luo



Fibroblast proliferation and migration are central in atrial fibrillation (AF) promoting structure remodeling, which is strongly associated with aging and hypertension. Transient receptor potential canonical-3 channel (TRPC3) is a key mediator of cardiac fibrosis and the pathogenesis of AF. Here, we have observed the increased TRPC3 expression that induced atrial fibrosis which possibly is either mediated by the aging process or related to hypertensive progression. In this study, we measured the pathological structure remodeling by H&E staining, Masson staining, and transmission electron microscope (TEM). The protein expression levels of fibrotic biomarkers and TRPC3 were measured by Western blotting with atrial tissues from normotensive Wistar Kyoto rats (WKY 4m-o (4 months old)), old WKY (WKY 24m-o (24 months old)), spontaneously hypertensive rat (SHR 4m-o (4 months old)), and old SHR (SHR 24m-o (24 months old)). To illuminate the molecular mechanism of TRPC3 in atrial fibrosis of aging rats and SHR, we detected the inhibited role of TRPC3 selective blocker ethyl-1-(4-(2,3,3-trichloroacrylamide) phenyl)-5-(trifluoromethyl)-1H-pyrazole-4-carboxylate,pyrazole-3 (Pyr3) on angiotensin II (Ang II) induced fibrosis in neonatal rat atrial fibroblasts. The pathological examination showed that the extracellular matrix (ECM) and collagen fibrils were markedly increased in atrial tissues from aged and hypertensive rats. The protein expressions of fibrotic biomarkers (collagen I, collagen III, and transforming growth factor-$\beta$1 (TGF-$\beta$1)) were significantly upregulated in atrial tissues from the WKY 24m-o group, SHR 4m-o group, and SHR 24m-o group compared with the WKY 4m-o group. Meanwhile, the expression level of TRPC3 was significantly upregulated in WKY 24m-o and SHR 4m-o atrial tissues compared to WKY 4m-o rats. In isolated and cultured neonatal rat atrial fibroblasts, Ang II induced the atrial fibroblast migration and proliferation and upregulated the expression levels of TRPC3 and fibrotic biomarkers. TRPC3 selected blocker Pyr3 attenuated the migration and proliferation in neonatal rat atrial fibroblasts. Furthermore, Pyr3 significantly alleviated Ang II-induced upregulation of TRPC3, collagen I, collagen III, and TGF-$\beta$1 through the molecular mechanism of the TGF-$\beta$/Smad2/3 signaling pathway. Similarly, knocking down TRPC3 using short hairpin RNA (shTRPC3) also attenuated Ang II-induced upregulation of TGF-$\beta$1. Pyr3 preconditioning decreased Ang II-induced intracellular $Ca^{2+}$ transient amplitude elevation. Furthermore, AT1 receptor was involved in Ang II-induced TRPC3 upregulation. Hence, upregulation of TRPC3 in aging and hypertension is involved in an atrial fibrosis process. Inhibition of TRPC3 contributes to reverse Ang II-induced fibrosis. TRPC3 may be a potential therapeutic target for preventing fibrosis in aging and hypertension.

## 1. Introduction

Atrial fibrillation (AF) is the most common arrhythmia in clinical practice, and pharmacological approaches have weak effects on AF treatment. One of the crucial reasons is hard to reverse the process of myocardial fibrosis. The structural remodeling is an important contributor to the AF substrates. The structural remodeling caused by atrial fibrosis promotes the occurrence and progression of AF [1, 2]. The incidence of AF increases with age [3, 4]. Hyperactivation of the renin-angiotensin-aldosterone system (RAAS) in hypertension is also closely related to the occurrence of AF [5]. Aging and hypertension both induce atrial fibrosis [6]. Preventing atrial fibrosis may be one of the key targets for the treatment of AF [7].

The hallmark of atrial fibrosis is fibroblast migration, proliferation, and extracellular matrix (ECM) protein deposition. Aging and hypertension are pivotal risk factors for atrial fibrosis. The classic mechanisms of fibroblast proliferation and matrix deposition are involved in the upregulation of collagen I, collagen III, activation of TGF-$\beta$1, and downstream Smad signaling pathways. Periostin also plays an important role in cardia remodeling [8]. However, the factors that cause the activation of these signaling pathways are varied, such as myocardial ischemia, apoptosis, and activation of the RAAS system. Its mechanism is not fully clarified. Finding targets to inhibit atrial fibrosis is helpful to the treatment and prevention of AF.

Excessive $Ca^{2+}$ influx mediates the process of atrial fibrosis during atrial fibrillation. Canonical transient receptor potential 3 (TRPC3) channel is a non-voltage gated and nonselective cation channel that regulates $Ca^{2+}$ homeostasis. Recently, TRPC3 channel was identified as a mediator of myocardial fibrosis. The electrophysiological data showed [9] that the expression of TRPC3 was increased in fibroblasts from AF patients and a rapid pacing dog model of AF. In a rapid pacing dog model, TRPC3 blockade prevents AF substrate development. However, up to date, it is not clear whether TRPC3 upregulation promotes atrial fibrosis related to aging process or hypertension [10]. Calcium influx through TRPC3 was increased in vascular smooth muscle cells and aortic tissue from SHR compared with WKY. Increased TRPC3 in the vasculature is important for blood pressure regulation. Upregulation of TRPC3 induces in cerebrovascular remodeling during hypertension via transactivation of epidermal growth factor receptor- (EGFR-) dependent signaling pathways [11–13]. Enhancement of TRPC3 activity at the cytoplasmic and mitochondrial levels contributes to redox signaling and calcium dysregulation in the vasculature from SHR [14]. An increase in the molecular coupling between inositol 1,4,5-trisphosphate receptor (IP3R) and TRPC3 augments endothelin-1- (ET-1-) induced vasoconstriction during hypertension [15]. Sierra-Valdez et al. analyzed the structure-function relation of TRPC3 and found that cytoplasmic domain was the target of channel allosteric modulated site [16]. From the above studies, however, it is not illuminated that fibroblasts were activated by TRPC3 during hypertension. Aging also is susceptible to fibrogenesis; the molecular mechanism has not fully illuminated [12]. Here, we undertook this study to test the following hypotheses: (1) the expression level of TRPC3 from atrial fibroblast is upregulated in aging and hypertension, which is involved in atrial fibrosis; (2) TRPC3 was upregulated through TGF-$\beta$1/Smad signaling pathways to promote atrial remodeling.

## 2. Materials and Methods

*2.1. Chemicals and Reagents.* Ang II (#HY-13948) was purchased from MedChemExpress company (MCE, USA), and Pyr3 (# P0032) and PD123 319 (#P186) were purchased from Sigma-Aldrich (Saint Louis, MO, USA). Collagenase (tape 2) was obtained from Worthington Biochemical. Fetal bovine serum (FBS) was purchased from GIBCO-BRL Life Technologies (Grand Island, NY). Antibodies against TGF-$\beta$1, GAPDH, and periostin were obtained from Cell Signaling Technology (Beverly, MA, USA). Antibodies against TRPC3 were obtained from Alomone Laboratories (Jerusalem, Israel), and antibodies against collagen I, collagen III, angiotensin II type 1 receptor (AT1R), angiotensin II type 2 receptor (AT2R), Smad2/3, and phosphorylated Smad2/3 were obtained from Abcam (Cambridge, MA, USA). A 24-well transwell system (8.0 $\mu$m porous membrane, Corning, NY, USA) was used to measure cell migration.

*2.2. Experimental Animals.* Healthy male normotensive Wistar Kyoto rats (WKY 4m-o, 4 months old), old WKY (WKY 24m-o, 24 months old), spontaneous hypertensive rat (SHR 4m-o, 4 months old), and old SHR (SHR 24m-o, 24 months old) were obtained from the animal care center of Southwest Medical University (Luzhou, China). During the whole experiments, the rats had free access to a standard chow diet and tap water ad libitum and the rats were housed at a constant room temperature (~25°C) and humidity in a 12 h day/12 h night cycles. All animal experiments were performed with the Guide for the Care and Use of Laboratory Animals from the US National Institutes of Health and were approved by the Ethical Committee on Animal Care and Use of Southwest Medical University (Luzhou, China).

*2.3. Histopathological Examination (H&E Staining and Masson's Staining).* The atrial specimens from WKY and SHR were fixed in 10% PBS neutral formalin, dehydrated, washed, and paraffin-embedded. The paraffin-embedded specimens were sectioned and stained with hematoxylin-eosin staining (H&E staining) and Masson's stain. In H&E-stained atrial tissues, the nucleic acids stain dark blue and the proteins stain red to pink. In Masson-stained atrial tissues, the extracellular matrix collagen was stained blue and cardiomyocytes were stained red.

*2.4. Transmission Electron Microscopy Examination.* WKY and SHR were anesthetized with 1% pentobarbital sodium (40 mg/kg), and the atrial tissues were isolated into 0.5mm$^3$ sized small chunks, immediately placed in 4% glutaraldehyde fixed for 2 h (4°C), cleaning the small chunks with PBS (0.1 M) for 3 times, and then fixed with 1% osmium tetroxide for 2 h. The small chunks of atrial tissues were gradient dehydration by ethanol and acetone and epoxy resin immersion, embedding, and polymerization. Preparation of 0.5 $\mu$m

thickness of semithin slices was used to locate the required atrial myocytes by a light microscope and then made 60 nm thickness of ultrathin slices, stained by uranium acetate and lead citrate. The last step was observed by an electron microscope (type H-7500) and photographed with a Gatan-780 CCD.

*2.5. Cell Culture.* Atrial tissues from neonatal (1~3 days old) Sprague-Dawley rats were excised (15 neonates/preparation) and then washed with phosphate-buffered saline solution (PBS) for 3 times. The atrial tissues were cut into 2~3 chunks and transferred to a 25 ml glass jar with 10 mL Trypsin (EDTA, 0.25%) at 4°C for overnight (12~16 h). After that, added 10 mL Dulbecco's modified Eagle's medium (DMEM) with 10% fetal bovine serum (FBS) into the glass jar, incubated in a 37°C humidified atmosphere containing 5% $CO_2$ for 5 min. The supernatant was discarded and subjected to enzymatic digestion for 1 min at 37°C with collagenase II (1 mg/ml) and bovine serum albumin (5 mg/mL, BSA) in PBS. The supernatant was discarded and added with the same enzymatic digested solution (10 mL) for 10 min at 37°C; the supernatant was collected, and the enzyme digestion process was repeated 2 times. All the collected supernatants were transferred to a 50 ml tube for centrifugation for 5 min (1000 rpm). To separate the cardiomyocytes from fibroblasts, the cells were seeded in a six-well culture plate with DMEM and kept in a $CO_2$ (5%) incubator for 120 min. The upper layer cardiomyocytes were discarded, and the plate was washed with PBS for 3 times and then kept in an incubator with DMEM (10%FBS) for 24 h. After the fibroblasts were grown to confluence and starved of serum for 12 h, then treatment with two protocols was performed. One of the protocol was separately administered with drug into each well with control (no treatment), Ang II (1 $\mu$mol/L), and Ang II with Pyr3 (10 $\mu$mol/L) for 48 h, and then the expression levels of protein TRPC3, TGF-$\beta$1, periostin, collagen I, collagen III, Smad2/3, and p-Smad2/3 were measured. The second protocol was separately administered with control (no treatment), Ang II, Ang II with valsartan (10 $\mu$mol/L, Ang II subtype-1 receptor (AT1R) antagonist), and Ang II with PD123 319 (10 $\mu$mol/L, Ang II subtype-2 receptor (AT2R) antagonist) for 48 h, and then the expression levels of protein TRPC3 were measured.

*2.6. Design of TRPC3 RNA Interference (RNAi) Sequence and Construction of Short Hairpin (sh) RNA-Expressing Lentiviral Vectors.* Three designed TRPC3-specific sequences were selected to use the online short interfering RNA tools with the reference sequence of TRPC3; the target sequences of TRPC3-1 (5′-GGACAGAAATGCTAATTAT-3′), TRPC3-2 (5′-GAACGAAGGTGAACTGAAA-3′), and TRPC3-3 (5′-GGGTCAAACTTGCCATTAA-3′) were homologous with those of TRPC3-specific mRNA. The sequences of TRPC3-1 are the best ones for TRPC3 RNA interference. Lentiviral vector carrying shRNA TRPC3 gene used the vector aGV248. shRNA TRPC3 was transfected into the cultured fibroblasts according to the manufacturer's instructions. Briefly, when the fibroblasts were confluence to 80% in 6-well plates, respectively added Blank (no Lentiviral vector ) or 15 $\mu$l Lentiviral vector (LV-shCtrl), 15 $\mu$L carrying shRNA TRPC3 gene Lentiviral vector (LV-shTRPC3, 1E+9TU/mL), and virus transfection strengthening agent (HitransG A & P, 100 $\mu$L) to mix together. After 24 hours post transduction, the media mixtures were removed and replaced with DMEM. A fluorescence microscope was used to monitor the transfection efficiency. The fibroblasts were cultured for another 48 hours, and then the protein expression of TRPC3 and TGF-$\beta$1 was measured.

*2.7. Cell Proliferation Assays (Wound Healing and Transwell Migration Assays).* In wound healing assay, when the fibroblasts were grown to confluence, a linear wound was made by 1 ml pipette tip cross in the confluent cell layer. The fibroblasts in each well were washed three times to remove detached cells and debris and then treated with Ang II, Ang II with Pyr3, and Pyr3 alone in each well. After that, the wells were imaged at 0 h, 24 h, and 48 h after treatment. The size of wounds was measured by ImageJ software. In transwell assay, after fibroblasts are prepared, the suspension should be diluted to an optimal density for seeding. Transwells are placed on a 24-well plate. The suspension of fibroblasts was added into the transwell with no air bubbles. At the same time, fibroblasts were treated with Ang II, Ang II with Pyr3, and Pyr3 alone in each transwell. Following incubation for 48 h, the membranes of transwells are fixed by dipping in 70% ethanol solution. After drying the membranes, fibroblast staining solution is added for approximately 30 minutes at room temperature. And then, the transwell was washed with PBS. Finally, the membrane can be excised and placed on a microscope slide. Cells on the underside of the membrane represent the number of cells that have migrated.

*2.8. $Ca^{2+}$ Transient Measurements.* Cultured fibroblasts were seeded in 96-well plates. After confluence to 90%, the fibroblasts were used to measure the calcium transients. The fibroblasts were washed twice in PBS and then incubated with intracellular calcium indicator Fura-2-acetoxymethyl (Fura-2/AM, 1 $\mu$mol/L, Invitrogen, USA; #F1221) for 30 min at 37°C; at the end of the loading period, the fibroblasts were washed twice with PBS, and intracellular free $Ca^{2+}$ imaging was measured by a cell imaging Multi-Mode reader (Cytation 5, BioTek). Fluorescence of the Fura-2/AM-loaded fibroblasts was measured using two excitation wavelengths: 340 nm and 380 nm, and an emission wavelength: 510 nm. The ratio of 340/380 was calculated, which represents the relative intracellular free $Ca^{2+}$ fluorescence intensity. The experiment protocols were performed with ($n = 6$) or without of Pyr3 ($n = 6$) in $Ca^{2+}$-free Tyrode's solution for 1 min, followed with or without Pyr3 in $Ca^{2+}$-free Tyrode's solution with Ang II (1 $\mu$mol/L) for 4 min, and then with or without Pyr3 in Ang II (1 $\mu$mol/L) with 1.8 mmol/L $Ca^{2+}$ Tyrode's solution for 4 min.

*2.9. Quantitative Real-Time PCR (qRT-PCR).* Total RNA was extracted from WKY 4m-o ($n = 8$), WKY 24m-o ($n = 8$), SHR 4m-o ($n = 8$), and SHR 24m-o ($n = 8$) using NucleoZOL reagents (MACHEREY-NAGEL, Germany). The cDNA was generated from 1 $\mu$g of total RNA using the ReverTra-Plus

kit (TOYOBO), and real-time PCR was carried out using the QuantiNova SYBR Green PCR Kit (QIAGEN, Germany) following the manufacturer's instructions. The relative gene expression levels of the TRPC3, Col1, Col3, and TGF-$\beta$1 were normalized to the housekeeping gene GAPDH. The mRNA expression levels were calculated by the $2^{-\Delta\Delta Ct}$ method. The primer sequences used were as follows: Trpc3 forward 5′-GTGTCTGGTCGTGTTGGTCGT-3′, reverse 5′-GATGAAGGAGGCAGCGTGAG-3′; Col1a1 forward 5′-CATGCCGTGACCTCAAGATG-3′, reverse 5′-TGTACCAGTTCTTCTGAGGCACA-3′; Col3a1 forward 5′-AGTGGCCATAATGGGGAACG-3′, reverse 5′-GCTGACCATCTGATCCAGGG-3′; Tgfb1 forward 5′CTGCTGACCCCCACTGATAC-3′, reverse 5′-AGCCCTGTATTCCGTCTCCT-3′; GAPDH forward 5′-CGGCAAGTTCAACGGCACAG-3′, reverse 5′-CGCCAGTAGACTCCACGACAT-3′.

*2.10. Western Blotting.* Proteins were extracted using RIPA buffer (Beyotime) containing protease and phosphatase inhibitors (Roche, Germany). The supernatants were collected after centrifugation at 4°C (12000 rpm, 15 min), and the protein concentration was detected with bicinchoninic acid (BCA assay, Beyotime, China). The protein samples (25 $\mu$g) were separated with 10% sodium dodecyl sulfate-polyacrylamide (SDS-PAGE) gel electrophoresis and transferred to polyvinylidene difluoride membranes (PVDF, Bio-Rad Laboratories, Hercules, CA, USA). 5% of nonfat dry milk in TBST was used to block the membrane for 1 h at room temperature. Primary antibodies including TRPC3 (1 : 1000), collagen I (1 : 1000), collagen III (1 : 1000), TGF-$\beta$1 (1 : 1000), periostin (1 : 1000), AT1R (1 : 1000), AT2R (1 : 1000), GAPDH (1 : 1000), Smad2/3 (1 : 1000), and phosphorylated Smad2/3 (1 : 1000), which were incubated at 4°C overnight. After incubation with primary antibody, the PVDF membranes were washed for 10 min 3 times in TBST. And then the membranes were incubated with horseradish peroxidase-conjugated secondary antibody (1 : 10000, Santa Cruz Biotechnology, Santa Cruz, USA) for 1 hour at room temperature. The immunoblotting bands were shown via an enhanced chemiluminescent detection kit (Gel Imaging System, Bio-Rad). The image was acquired and analyzed by Quantity One Software.

*2.11. Statistical Analysis.* All the data were presented as the mean ± standard deviation (SD). The differences were analyzed by GraphPad prism software 7.0. Quantitative data were analyzed by one-way ANONA tests followed by post hoc analysis. All values with $P < 0.05$ represented a significant difference.

## 3. Results

*3.1. Animal Characteristics.* Detailed animal characteristics are shown in Table 1; there was a significant difference of body weight in WKY 24m-o ($n = 8$, $P < 0.01$) and SHR 24m-o ($n = 8$, $P < 0.05$) compared to WKY 4m-o, and a significant difference of body weight was also shown between WKY 24m-o and SHR 24m-o ($n = 8$, $P < 0.01$). Systolic and diastolic blood pressures were significantly higher in SHR 4m-o and SHR 24m-o compared to WKY 4m-o and WKY 24m-o ($n = 8$, $P < 0.01$). There was no significant difference in heart rate and blood glucose.

*3.2. Pathological and Ultrastructural Changes in the Atrium from Aging and Hypertensive Rat.* Aging and hypertension are the independent risk factors of atrial structure remodeling. Collagen is the main component of extracellular matrix. In this study, the atrial slices of H&E staining showed significantly increased extracellular matrix (ECM) in atrial tissues from WKY 24m-o, SHR 4m-o, and SHR 24m-o, while rarely ECM could be seen in WKY 4m-o (Figure 1). The cardiac muscles were divided into many branches by ECM. The space between each branch was wider, and the cell nucleus is misaligned. Furthermore, the atrial slice of SHR 24m-o was observed to be significantly misaligned and the muscle was divided into reticular structures (Figure 1(c)). The slices of Masson's staining showed apparent blue color in WKY 24m-o, SHR 4m-o, and SHR 4m-o (shown with arrows, Figure 2(a)). Muscle filament of atrial myocytes was regular organization, but the collagenous fibrils were distinctly observed by TCM in WKY 24m-o, SHR 4m-0, and SHR 4m-0 (Figure 2(b)).

*3.3. Upregulation of TRPC3 and Fibrotic Biomarkers in the Atrium from WKY and SHR with Aging.* Morphologically, myocardial fibrosis was found in old WKY, young SHR, and SHR with aging. Fibrotic biomarkers included collagen I, collagen III, and TGF-$\beta$1; TRPC3 also is associated with fibrosis. The mRNA level of TRPC3 was significantly increased in WKY 24m-o ($P < 0.05$, $n = 8$) and SHR 4m-o ($P < 0.05$, $n = 8$) compared to WKY 4m-o (Figure 3(d)), in accordance with the protein expression level. The mRNA level of COL-1 was significantly increased in WKY 24m-o ($P < 0.05$, $n = 8$), SHR 4m-o ($P < 0.01$, $n = 8$), and SHR 24m-o ($P < 0.05$, $n = 8$) compared to WKY4m-o (Figure 3(a)), and the mRNA level of COL-III was also markedly increased in WKY 24m-o ($P < 0.01$, $n = 8$), SHR 4m-0 ($P < 0.05$, $n = 8$), and SHR 24m-0 ($P < 0.01$, $n = 8$) (Figure 3(b)). The COL-I protein level was significantly increased in all the SHR groups compared to WKY 4m-o (Figure 3(a)). The COL-III protein level was significantly increased in WKY 24m-o and SHR 4m-o (Figure 3(b)). TGF-$\beta$1 is a fibrosis marker; the mRNA and protein expression levels of TGF-$\beta$1 were all increased in SHR, WKY, and SHR in aging compared to the WKY 4m-o group (Figure 3(c)). The data indicated that the upregulation of TRPC3 was accompanied with the upregulation of a fibrotic biomarker in aging and hypertension.

*3.4. TRPC3 Is Involved in Ang II-Induced Cell Migration and Proliferation.* TRPC3 is upregulation in aging and hypertension. To understand the mechanisms of TRPC3 associated with atrial fibrosis, we treated the neonatal atrial fibroblasts with fibrotic agent Ang II (1 $\mu$mol/L) with or without TRPC3 inhibitor Pyr3 (10 $\mu$mol/L) for 48 hours to measure the cell migration and proliferation. Figure 4(a) shows images of the wound at 0 hour and 48 hours. Wound healing assay indicated that Ang II significantly increased the

Table 1: Body weight, blood pressure, heart rate and blood glucose from WKY and SHR with or without aging.

| | WKY 4m-o ($n = 8$) | WKY 24m-o ($n = 8$) | SHR 4m-o ($n = 8$) | SHR 24m-o ($n = 8$) |
|---|---|---|---|---|
| Weight | 325.00 ± 34.33 | 407.50±41.74$^{**}$ | 328.75 ± 38.79 | 358.12±16.46$^{*,\#\#}$ |
| Systolic blood pressure (mmHg) | 113.87 ± 13.59 | 134.00 ± 7.34 | 189.62±23.79$^{**,\#\#}$ | 184.87±19.72$^{**,\#\#}$ |
| Diastolic blood pressure (mmHg) | 91.75 ± 26.47 | 94.25 ± 10.87 | 141.12±16.64$^{**,\#\#}$ | 130.37±18.39$^{**,\#\#}$ |
| Heart rate (bmp/min) | 356.12 ± 56.12 | 345.17 ± 36.17 | 389.28 ± 32.16 | 357.54 ± 43.17 |
| Blood glucose (mmol/L) | 6.05 ± 0.86 | 6.75 ± 1.29 | 6.21 ± 1.53 | 6.85 ± 1.30 |

Each value represents the mean ± SD; $n = 8$ rats per group. $^{*}P < 0.05$ and $^{**}P < 0.01$ compared to WKY 4m-o; $^{\#}P < 0.05$ and $^{\#\#}P < 0.01$ compared to WKY 24m-o.

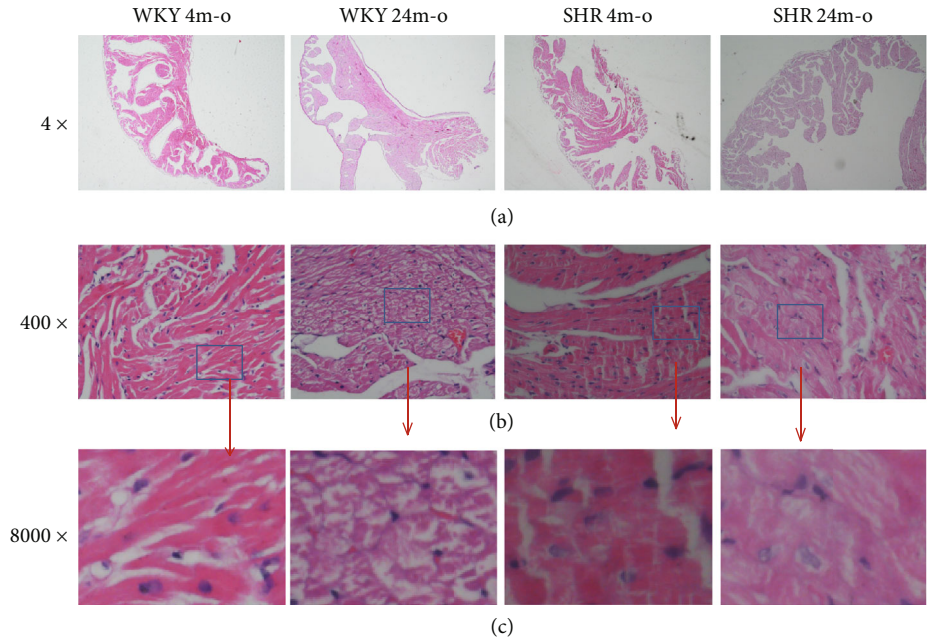


Figure 1: Atrial structural remodeling measured by H&E staining from WKY 4m-o, WKY 24m-o, SHR 4m-o, and SHR 24m-o rats. Representative H&E staining: (a) magnification ×4, (b) magnification ×400, and (c) magnified the blue grid from (b).

proliferation of fibroblasts compared to the control group and TRPC3 blocker Pyr3 attenuated Ang II-induced proliferation (Figure 4(a), $n = 5$). To accurately calculate the number of migrated fibroblasts, transwell migration assay was used to detect the response. Data calculated the number of fibroblasts migrating outside of the bottom membrane. The result showed that Ang II markedly increased fibroblast migration and Pyr3 decreased the migration under the condition of Ang II stimulation ($n = 4$, $P < 0.01$). The two methods demonstrated that Pyr3 prevents Ang II-induced fibrotic response in fibroblasts.

*3.5. Role of TRPC3 Selected Blocker Pyr3 in the Intracellular $Ca^{2+}$ Response Induced by Ang II.* When cultured cardiac fibroblasts were treated in a calcium-free medium (Figures 5(a) and 5(b)), the resting calcium ratio values (ratio, Fura340/-Fura380) in control (0.746 ± 0.001, $n = 6$) were higher than those in Pyr3 preconditioning (0.732 ± 0.006), but data showed no significantly statistical differences. Application of Ang II (1 $\mu$mol/L) in the calcium-free solution evoked a calcium transient in both control and Pyr3 preconditioning. The data showed that Pyr3 significantly decreased calcium transient under the condition of calcium-free solution ($P < 0.05$, $n = 6$), and then solution was changed to 1.8 mmol/L $CaCl_2$ with 1 $\mu$mol/L Ang II; the calcium transient was significantly more enhanced in both control and Pyr3 preconditioning, while the calcium transient in Pyr3 preconditioning is significantly lower than that in control ($P < 0.05$, $n = 6$).

*3.6. Suppression of TRPC3 Prevents Ang II-Induced Deposition of Extracellular Matrix Proteins.* The above data showed that the expression of TRPC3 was elevated in the atrium from aging and hypertensive rats. Furthermore, the inhibition of TRPC3 significantly attenuated fibroblast migration and proliferation, but the exact mechanism is unclear. So, the contribution of TRPC3 on atrial fibrosis was further explored in cultured fibroblasts from neonatal rat atrial tissues, after the fibroblasts were grown to confluency to 70-80% of 6-well plate. In the treatment of Ang II (1 $\mu$mol/L)

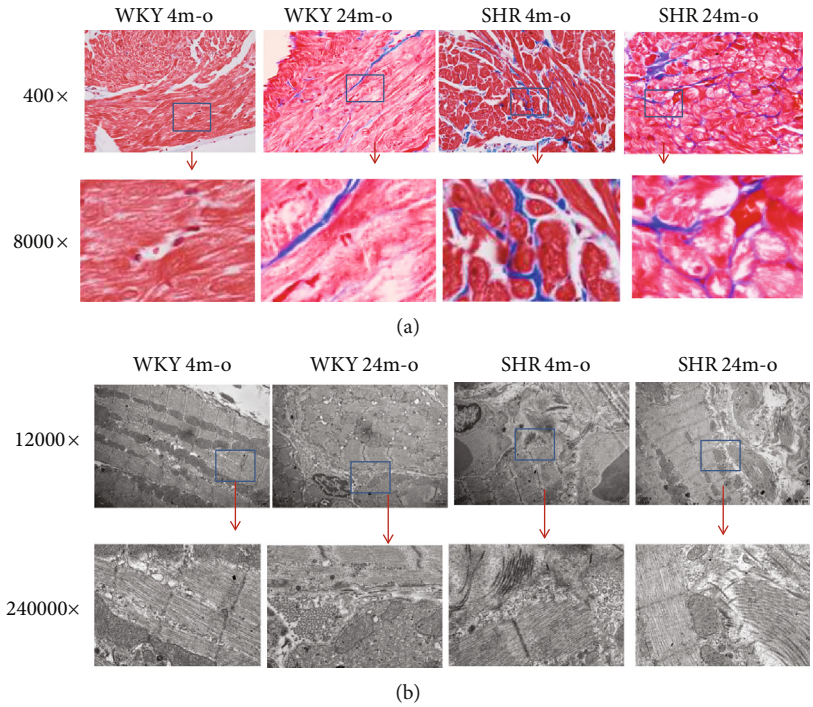


Figure 2: Atrial structural remodeling measured by Masson's staining and TEM in WKY 4m-o, WKY 24m-o, SHR 4m-o, and SHR 24m-o rats. (a) In Masson's staining, the collagen was stained blue, and cardiomyocytes were stained red. In the top panel, magnification is ×400; in the bottom panel, magnification is ×8000, magnifying the blue grid from the top panel. (b) TEM photos: in the top panel, magnification is ×12000; in the bottom panel, magnification is ×240000, magnifying the blue grid from the top panel.

with or without Pyr3, or Pyr3 alone for 48hours, the experiment was repeated five times. 48 h later, the cells were obtained to detect the protein level by Western blotting. In Figure 6, compared with the control group, the protein level of TRPC3 was significantly increased under the condition of Ang II stimulation, while Pyr3 inhibited Ang II-induced upregulation of TRPC3. In the treatment of the fibroblasts with Pyr3 alone, the expression of TRPC3 was unchanged. The data suggested that Ang II stimulation could upregulate the expression of TRPC3. On the normal condition, TRPC3 shows low expression level in fibroblasts (Figure 6(a), $n = 6$). Furthermore, Ang II significantly upregulated the expression levels of fibrotic biomarkers COL-1 and COL-III (Figure 6(b), $n = 6$, $P < 0.01$; Figure 6(c), $n = 6$, $P < 0.05$). Moreover, Pyr3 reversed Ang II-induced upregulation of COL-I (Figure 6(b), $n = 6$, $P < 0.05$) and COL-III (Figure 6(c), $n = 6$, $P < 0.01$). Periostin is produced by myocardial fibroblasts and also a mediator in cell-matrix crosstalk association with fibroproliferative diseases in the myocardium. In cultured fibroblasts, the expression of periostin was elevated by Ang II. Pyr3 prevents Ang II-induced upregulation of periostin. Taken together, the data showed that the inhibition of TRPC3 attenuated the deposition of extracellular matrix protein.

*3.7. Downregulation of TRPC3 by LV-shTRPC3 Suppresses the Protein Expression of TGF-β1.* TGF-β1 is a pivotal biomarker of fibrosis. To further define the role of TRPC3 involved in myocardial fibrosis, lentiviral vector carrying shRNA TRPC3 gene was used to simulate the similar effect of TRPC3 selected blocker. In Figure 7, Blank indicated that no lentiviral vector was added in fibroblasts, shCtrl indicated that lentiviral vector treated the fibroblasts with no shTRPC3, and LV-shTRPC3 indicated that the fibroblasts transfected with lentiviral vector carrying shRNA TRPC3. Data showed that Blank and shCtrl had no effect on the expression of TRPC3 and TGF-β1; however, shTRPC3 induced significantly the downregulation of the expressions of both TRPC3 (Figure 7(b)) and TGF-β1 (Figure 7(c)). It means that the downregulation of TRPC3 is involved in decreasing TGF-β1 expression.

*3.8. Ang II-Induced TRPC3 Upregulation through AT1 Receptor.* Ang II plays a key role in the modulation of many functions through strong affinity to the angiotensin II type 1 receptor (AT1R) and angiotensin II type 2 receptor (AT2R). Whether the role of Ang II acts on TRPC3 through its receptor remains unclear. First, we detected the expression levels of AT1R and AT2R in WKY and SHR with or without aging. Compared to the WKY 4m-o group, the expression level of AT1R was apparently increased in WKY 24m-o (Figure 8(a), $n = 8$, $P < 0.05$) and SHR 4m-o (Figure 8(a), $n = 8$, $P < 0.01$). But there was no significant difference between the WKY 4m-o and SHR 24m-o groups (Figure 8(a), $n = 8$, $P > 0.05$). No significant difference was found in AT2R expression from the four groups. We speculate that AT1R may be the key protein to regulate the function of TRPC3. In order to determine the effects, we measured the role of AT1R blocker valsartan (10 μmol/L) and AT2R blocker PD123 319 (10 μmol/L) on TRPC3 expression. In

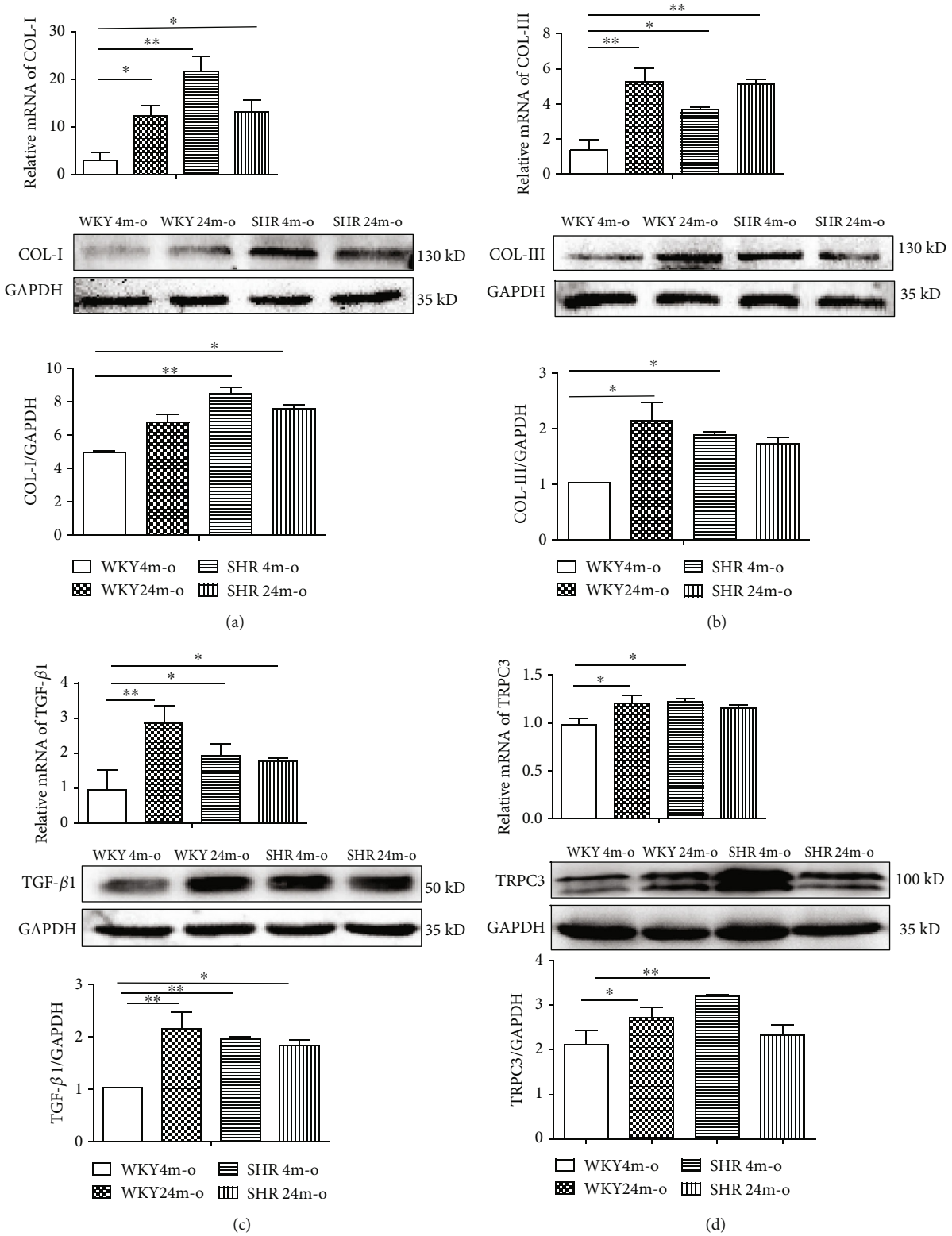


Figure 3: Upregulation of fibrotic biomarkers and TRPC3 in the atrium from SHR and WKY with aging. The relative mRNA and protein expressions of collagen I (left, upper panel, COL-I) (a), collagen III (right, upper panel, COL-III) (b), TGF-$\beta$1 (left, bottom panel) (c), and TRPC3 (right, bottom panel) (d). All values are presented as the mean ± SD of 8 rats. $^{*}P < 0.05$ and $^{**}P < 0.01$ significantly different compared with WKY 4m-o.

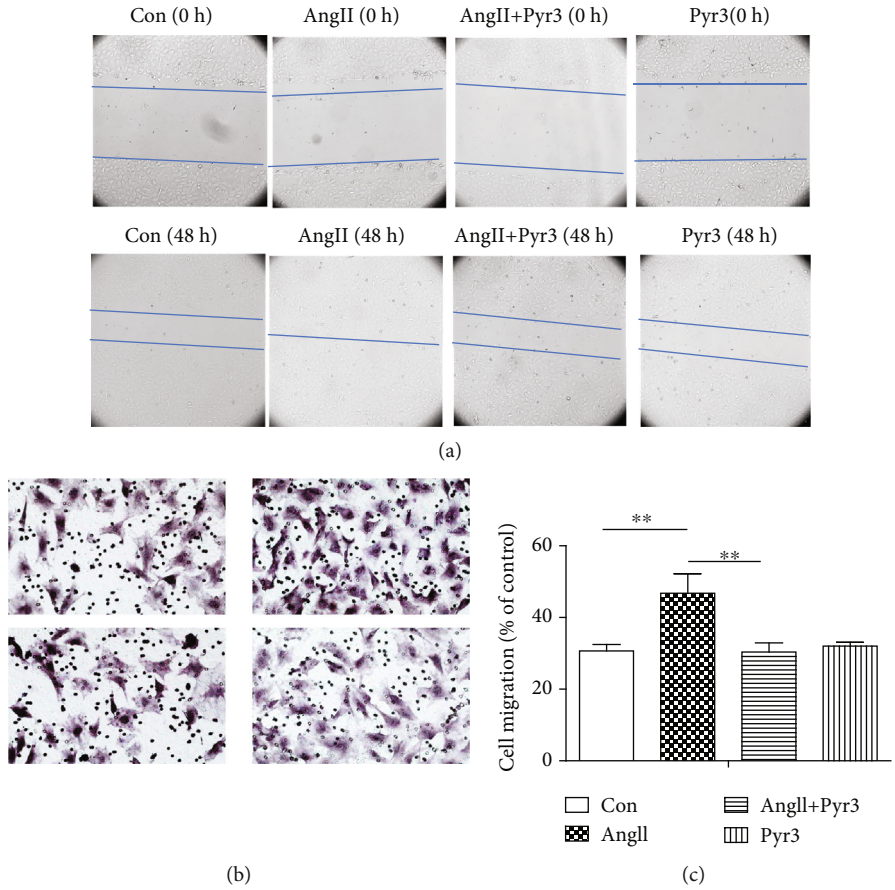


Figure 4: TRPC3 inhibition prevents Ang II-induced cell migration and proliferation. (a). After wound healing assay, the wound of the 24-well cultured confluent neonatal rat atrial fibroblasts was imaged before and after administration of Pyr3 (10 $\mu$mol/L) and Ang II with or without Pyr3 (10 $\mu$mol/L) for 48 h; the wound edges were imaged under a 10x objective. (b) Accurately measure cell migration by transwell assay. Transwells are placed in wells, and cell suspension is pipetted into the upper chambers, incubating the cells with administration of Pyr3 (10 $\mu$mol/L) and Ang II with or without Pyr3 (10 $\mu$mol/L) for 48 h; image the migrated fibroblasts from underside membrane, count the migrated cells on a grid under magnification ×200, and count 5 high power fields to calculate the average cell number per field. All data shown are the mean values ± SD and are expressed as % of the control value (first bar). $^*P < 0.05$ versus control (the first $^*$) and versus Ang II (the second $^*$).

cultured neonatal rat atrial fibroblasts, Western blotting data showed that valsartan inhibited the upregulation of TRPC3 induced by Ang II, while PD123 319 has no action on the upregulation induced by Ang II. The results in Figure 8 demonstrated that Ang II may regulate the function of TRPC3 by AT1R, while not by AT2R.

*3.9. TRPC3 Blockade Suppresses the TGF-β1/Smad2/3 Signaling Pathway.* TGF-$\beta$1 plays a key role in atrial fibrosis. Therefore, TGF-$\beta$1 may be involved in Ang II-induced upregulation of TRPC3. In cultured neonatal rat atrial fibroblasts, with treatment of Ang II with or without Pyr3, the expression of TGF-$\beta$1 was significantly increased with Ang II stimulation. As we speculated, Pyr3 attenuated the upregulation induced by Ang II treatment. Pyr3 alone had no effect on the expression of TGF-$\beta$1 (Figure 9(a)). TGF-$\beta$1/Smad3 is the critical signaling pathway in fibrosis. Therefore, the expression of Smad2/3 and phosphorylation of Smad2/3 (p-Smad2/3) were determined. The results showed that the total protein of Smad2/3 was no apparent different treatment by Ang II with or without Pyr3. However, the P-Smad2/3 and the ratio of P-Smad2/3/Smad2/3 were significantly attenuated induced by Pyr3. As a whole, these results demonstrated that Pyr3 inhibited the atrial fibrosis through TGF-$\beta$1/Smad2/3 signaling pathway.

## 4. Discussion

Atrial fibrosis induces structural remodeling which is a substrate of AF occurrence and persistence. Aging and hypertension are known risk factors for cardiovascular disease, especially during AF [17]. TRPC3 is a nonselective $Ca^{2+}$ permeant cation channel, which mediates a calcium influx involved in cardiac fibrosis [18]. Some studies showed that TRPC3 was increased in vasculature [10] and peripheral blood monocytes in hypertension [19]. To date, no study has investigated the fibrotic response of atrial fibroblast TRPC3 underlying aging and hypertension. The aim of this study is to elucidate the mechanism of TRPC3 upregulation-induced fibrosis in aging and hypertension. The present study

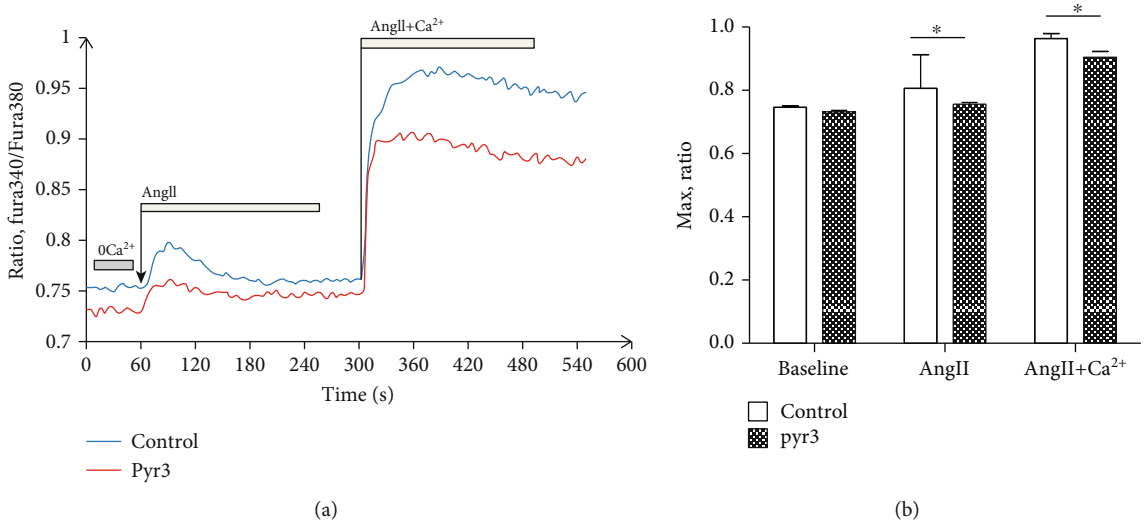


Figure 5: Intracellular $Ca^{2+}$ rises induced by Ang II with or without extracellular $Ca^{2+}$. Intracellular free $Ca^{2+}$ detected by ratio values of Fura340/380. During the fluorescence calcium acquisition process, in the control group, fibroblasts were perfused with $Ca^{2+}$-free Tyrode's solution for 1 minute, following perfusion with $Ca^{2+}$-free Tyrode's solution with Ang II (1 $\mu$mol/L) for 4 minutes, and then perfused with 1.8 mmol/L $Ca^{2+}$ Tyrode's solution with Ang II (1 $\mu$mol/L) for 4 minutes. In the Pyr3 group, fibroblasts were perfused with $Ca^{2+}$-free Tyrode's solution with Pyr3 (10 $\mu$mol/L) for 1 minute, following perfusion with $Ca^{2+}$-free Tyrode's solution with Ang II (1 $\mu$mol/L) for 4 minutes containing Pyr3 (10 $\mu$mol/L), and then perfused with 1.8 mmol/L $Ca^{2+}$ Tyrode's solution with Ang II (1 $\mu$mol/L) for 4 minutes containing Pyr3 (10 $\mu$mol/L). (a) The changes of fluorescence calcium microphotographs, traces, and quantitative ratio values. (b) The statistical graph of fluorescence calcium ratio values. Baseline bar shows the mean values of $Ca^{2+}$-free Tyrode's solution, Ang II bar shows the peak values of calcium transient of $Ca^{2+}$-free Tyrode's solution with Ang II (1 $\mu$mol/L), and Ang II+$Ca^{2+}$ bar shows the peak values of calcium transient with 1.8 mmol/L $Ca^{2+}$ Tyrode's solution with Ang II (1 $\mu$mol/L).

showed that fibrosis was evidenced in the atrium during aging and hypertension. Pathological changes measured by a light microscope and a transmission electron microscope showed an excessive deposition of extracellular matrix. In addition, atrial TRPC3 expression was upregulated in the atrium from SHR, aged WKY and SHR. To mimic this pathological state in cultured atrial fibroblasts, Ang II stimulation plays this effect. Ang II treated the fibroblasts with or without TRPC3 channel selected blocker Pyr3. The results showed that Pyr3 could attenuate the migration, proliferation, and deposition of profibrotic biomarker proteins induced by Ang II. Furthermore, Pyr3 prevented Ang II-induced atrial fibrosis via AT1R involved in the downregulation of the TGF-$\beta$1/Smad2/3 signaling pathway.

TRPC3 has been implicated in many cardiovascular diseases, such as myocardial hypertrophy [20], heart failure [18, 20], myocardial infarction [21], and AF [22]. The known main mechanism is involved in the calcineurin/NFAT signaling pathway to promote $Ca^{2+}$ influx via TRPC3 and induces mechanical stress, hypertrophy, and heart failure. These studies focused on the profibrotic effects on cardiomyocytes or the cells from other organs or systems; there are seldom papers that reported the effects on fibroblasts. Actually, even more importantly, the pathophysiology action of TRPC3 is involved in cardiac fibroblasts directly inducing migration and proliferation. AF increases with age and induces age-dependent atrial fibrosis. Harada et al. reported that TRPC3 regulated cardiac fibroblast proliferation by controlling $Ca^{2+}$ influx via the extracellular signal regulated kinase (ERK) signaling pathway to upregulate the expression of TRPC3 in vivo AF dog model [9]. We also demonstrated that Pyr3 significantly decreased the calcium transient amplitude in Ang II with extracellular $Ca^{2+}$-free or 1.8 mmol/L $Ca^{2+}$. Aging and hypertension are the key factors to promote atrial fibrosis and eventually lead to AF. Protein aggregation is a hallmark for aging. Ayyadevara et al. [23] first reported that protein aggregation existed during natural aging, chronic hypertension, and myofibroblast aging in vitro [24]. Ang II-induced hypertension shows many of the same aggregated characteristics seen in natural aging, such as fibroblast proliferation and migration, and leads to fibrosis. Hypertensive and aged hearts show similar dysfunction of the heart and related most likely to the development of fibrosis. Based on these proteomic studies, hypertension appears to accelerate or mimic some aspects of natural physiologic aging. Furthermore, young individuals with hypertension exhibit arterial changes similar to those in older persons with normal blood pressure [25, 26]. The same from the abovementioned, in this study, we observed the similar fibrosis features by a light microscope (H&E staining, Masson's staining) and a transmission electron microscope. The atrial tissues from WKY 24m-o, SHR 4m-o, and SHR 24m-o rats all showed significant deposition of ECM and proliferation. In observing the ultrastructure of atrial myocytes under transmission electron microscopy, there were obvious collagenous fibrils between cells. And then, we also measured significant upregulation of protein expression, such as TRPCR3, profibrotic COL-I, COL-III, periostin, and TGF-$\beta$1 in young SHR, aged WKY, and aged SHR compared to young WKY [27]. It means that aging, the same as hypertension, induced upregulation of

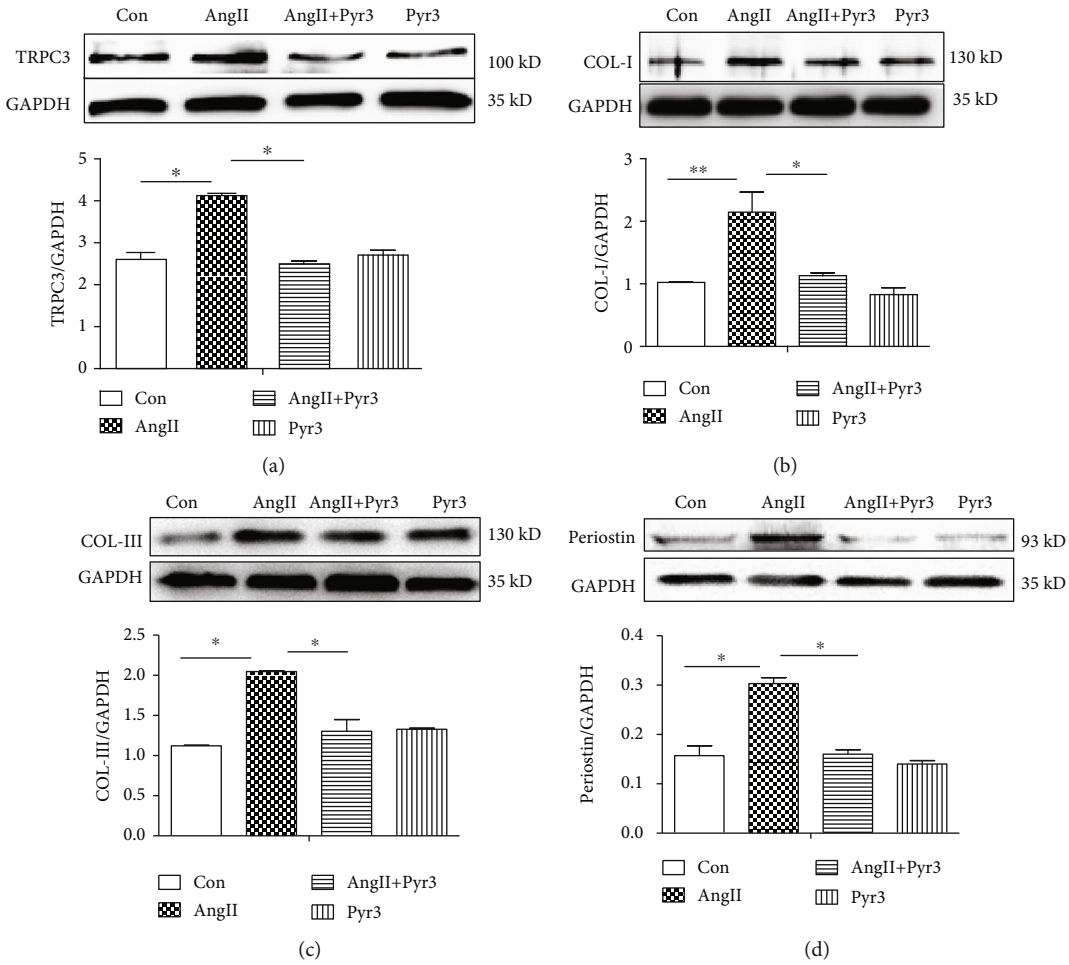


Figure 6: TRPC3 inhibition prevents Ang II-induced deposition of extracellular matrix protein. In cultured fibroblast, administrated Ang II (1 $\mu$mol/L) with or without Pyr3 (10 $\mu$mol/L) to measure the protein expression of TRPC3 (a), COL-1 (b), COL-III (c), and periostin (d) by Western blotting. The ratio of TRPC3, COL-I, COL-III, and periostin normalized to GAPDH was calculated. The analyzed data was shown from 5 independent experiments. All data presents the mean values ± SD. $^*P < 0.05$ shows a significant difference from control or from treatment with Ang II.

TRPC3 accompanied with excessive deposition of extracellular matrix. Our studies demonstrated that atrial TRPC3 expression was upregulated during aging and hypertension, which was accompanied with the enhancement of fibrotic markers.

However, in Figures 4(b) and 4(d), data showed that compared with the WKY 4m-o group, the protein expressions of COL-I and TRPC3 in the SHR 24m-o group were not significantly increased compared with those in the SHR 4m-o group and WKY 24m-o group. The possible reason is that it is not sensitive to response to higher blood pressure, especially response to Ang II in aged hypertensive rats. Myocardial fibrosis already exists in elderly hypertensive rats, so they are less sensitive to changes in blood pressure.

Researchers also found that upregulation of TPRC3 enhances EGFR transactivation, which is involved in hypertension-induced cerebrovascular remodeling by the signaling pathway TRPC3/ADAM17 [11, 13, 28]. Increased proportion and assembly of TRPC3 and TRPC6 contribute to cell depolarization in hypertensive mesenteric vascular smooth muscle cells [29]. In SHR, elevation coupling between type 1 inositol 1,4,5-trisphosphate receptor (IP3R) and TRPC3 enhances cell contraction of mesenteric arteries [15]. TRPC3 also is involved in regulating mitochondrial function and reactive oxygen species (ROS) generation [30, 31]. In SHR, enhancement of TRPC3 activity at the cytoplasmic and mitochondrial levels contributes to $Ca^{2+}$ dysregulation and redox signaling activity in the vasculature [14]. Additionally, excessive migration of monocytes in essential hypertension is related to upregulation of TRPC3 [19, 32]. These research data demonstrated that TPRC3 is increased in mesenteric arteries, cerebrovasculature, mitochondria, and monocytes, which is consistent with our results in atrial tissues from young SHR, WKY, and SHR in aging.

Excessive activation of fibroblasts is the most direct cause of myocardial fibrosis. Fibrosis also is a feature of AF. Hypertension is susceptible to AF occurrence. TRPC3 blockade prevents AF substrate development in an AF model. TRPC3 of fibroblasts plays a pivotal role in AF process via the ERK/microRNA-26/NFAT (nuclear factor of activated T-lymphocytes) signaling pathway. The data

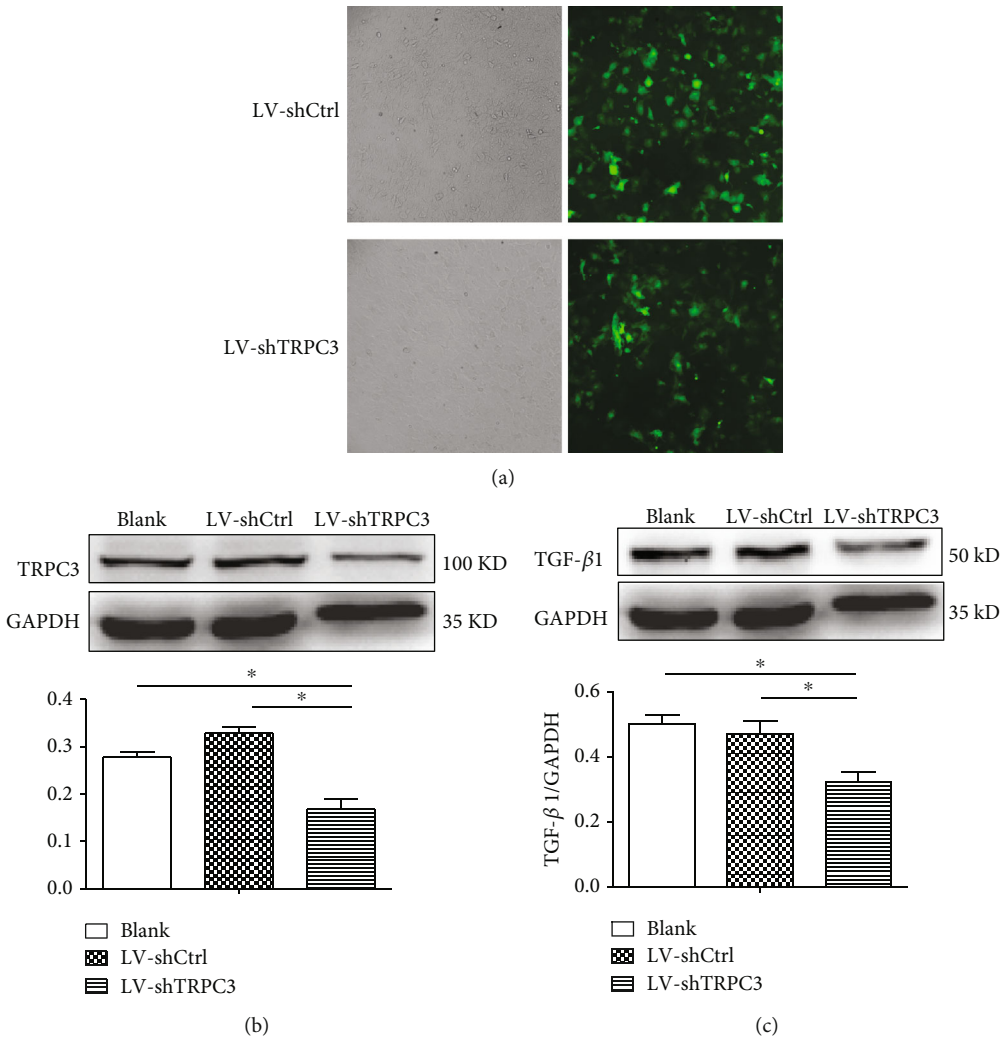


Figure 7: Downregulation of TRPC3 by LV-shTRPC3 suppressed the protein expression of TGF-$\beta$1. (a) GFP expression in fibroblasts under a fluorescence microscope after 72 h of infection. (b) The protein expression by Western blot analysis of TRPC3 in Blank, LV-shCtrl, and LV-shTRPC3. (c) The protein expression by Western blot analysis of TGF-$\beta$1 in Blank, LV-shCtrl, and LV-shTRPC3 ($n = 5$). $^*P < 0.05$ shows a significant difference from Blank or LV-shCtrl with LV-shTRPC3.

indicated that TRPC3 may be a novel potential therapeutic target for AF-induced fibrosis [9]. Additionally, Saliba et al. reported that TRPC3 presented in renal fibroblasts and control fibroblast proliferation and activation through the $Ca^{2+}$-mediated ERK signaling pathway [33]. Our data also implied that the TRPC3 was increased in the atrium from aging and hypertensive rats and accompanied with profibrotic protein upregulation.

RAAS activity plays an important role in functional and structural changes of vasculature that occurs with aging and hypertension [34, 35]. RAAS is involved in the aging and hypertension process. Angiotensin-converting enzyme inhibitor (ACEI) and AT1 receptor blocker could decrease age-associated vascular damage. To understand the mechanism of the relation between upregulated TRPC3 and atrial fibroblasts under aging and hypertension, the cultured neonatal atrial fibroblasts were treated with Ang II with or without TRPC3 inhibitor Pyr3. The data showed that Ang II increased the proliferation, migration, and expression of TRPC3, COL-I, COL-III. Pyr3 prevents Ang II-induced TRPC3 upregulation and profibrotic collagen deposition. It confirmed that Ang II mimics the response of aging and hypertension. TRPC3 also is involved in the proliferation and migration in atrial fibroblasts.

In fact, it is not clear how Ang II regulates the activity of TRPC3. In general, Ang II possesses a physiological function through angiotensin-converting enzymes or by acting through receptors. TRPC3 is a receptor-operated channel modulated by Gq PCRs; the activation of AT1R may induce cation influx via TRPC3 or TRPC6 in mouse cardiomyocytes [32]. The results demonstrate that Ang II promotes the slow increase in the $Ca^{2+}$ transient; TRPC3 and PLC inhibition significantly suppressed the increase of intracellular $Ca^{2+}$ induced by both the sustained stretch and Ang II. The data indicate that the activation of TRPC3/6 by sustained stretch is mediated via the signaling pathway AT1R-Gq-PLC-DAG [36–38]. In cultured fibroblasts, in this study, Ang II treatment with AT1R inhibitor valsartan or AT2R inhibitor

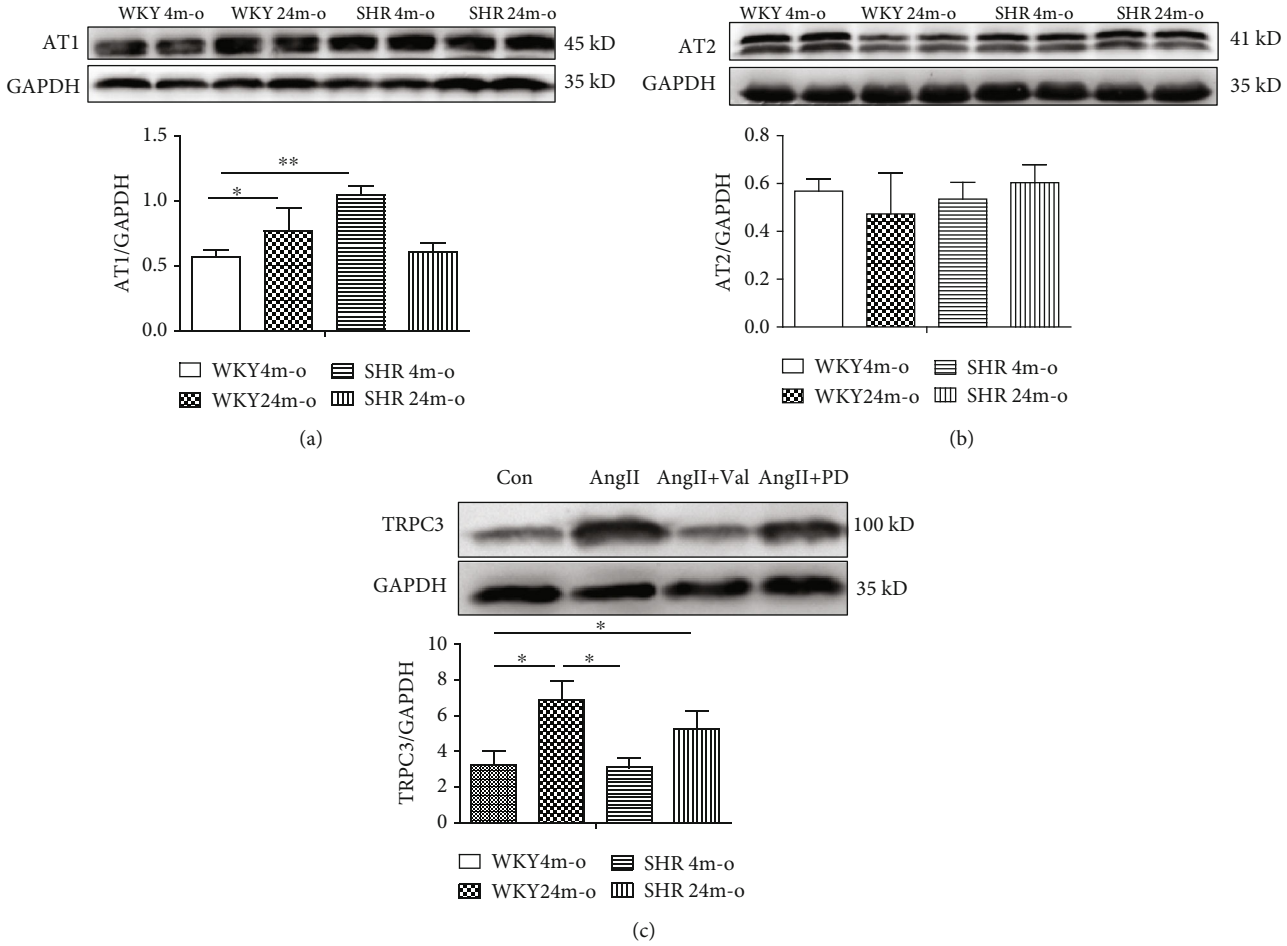


Figure 8: AT1R blocker inhibited Ang II-induced TRPC3 upregulation. The protein expressions of ATR1 (a) and AT2R (b) are measured by Western blotting from WKY and SHR with or without aging. (c) The protein expression of TRPC3 was measured by after treatment with Ang II (1 $\mu$mol/L), Ang II with AT1R blocker valsartan (Val, 10 $\mu$mol/L), or Ang II with AT2R blocker PD123 319 (PD, 10 $\mu$mol/L) for 48hours. The analyzed data was shown from 5 independent experiments. All data presents the mean values ± SD. $^*P < 0.05$ shows a significant difference from control or from treatment with Ang II.

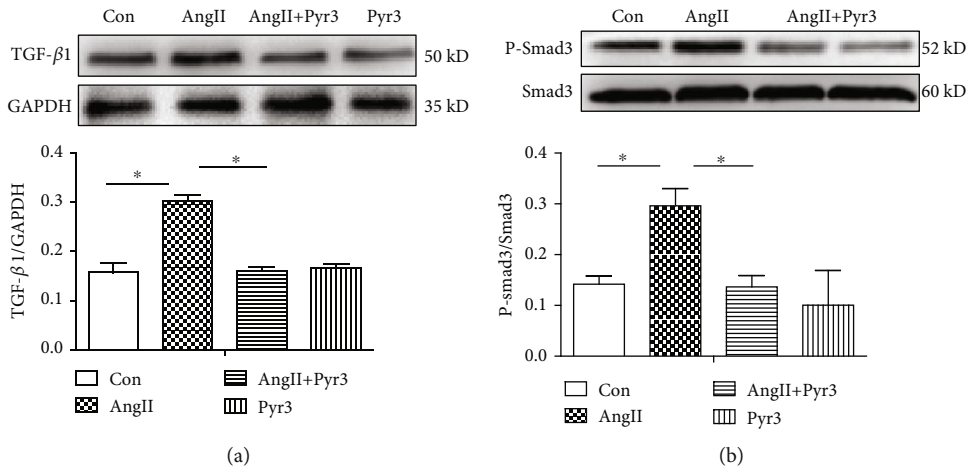


Figure 9: Suppression of the TGF-$\beta$1/Smad2/3 signaling pathway with TRPC3 blockade. The atrial fibroblasts were exposed to Ang II with or without Pyr3. The protein expressions of TGF-$\beta$1 (a), P-Smad2/3, and Smad2/3 (b) are measured by Western blotting. The ratio of TGF-$\beta$1, Smad2/3, and P-Smad2/3 normalized to GAPDH was calculated. The ratio of P-Smad2/3/Smad2/3 shows the phosphorylation state. The analyzed data was shown from 5 independent experiments. All data presents the mean values ± SD. $^*P < 0.05$ shows a significant difference from control or from treatment with Ang II.

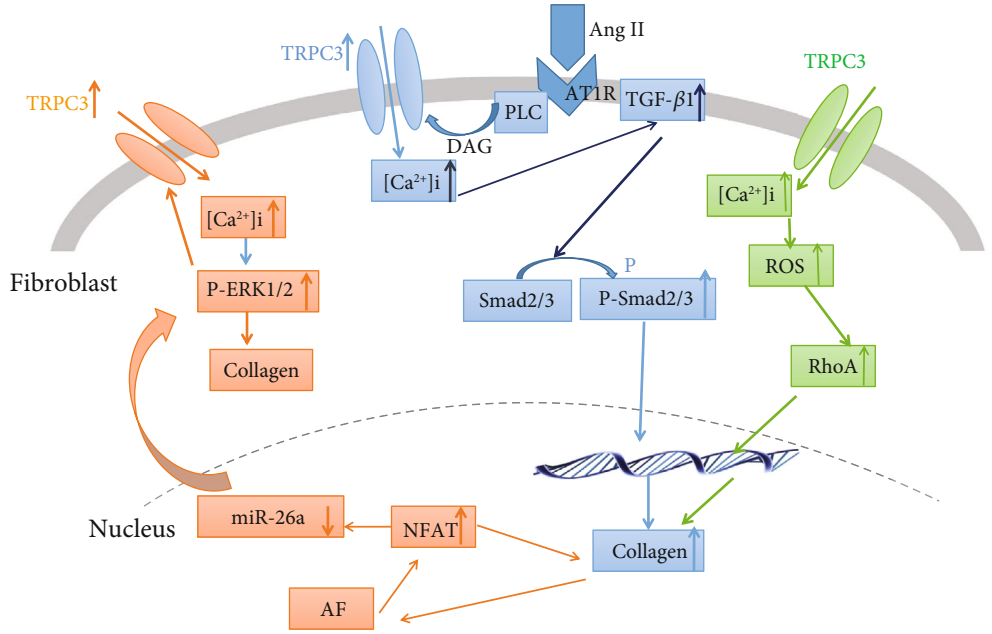


Figure 10: The summary of the signaling pathway of TRPC3 upregulation in fibroblasts involved in fibrosis. The blue signaling pathway is evidenced by this study, and the red and green ones were reported by published papers.

PD123 319 was used. Valsartan significantly inhibits Ang II-induced TRPC3 enhancement, while PD123 319 has no remarkable action on TRPC3 expression. Our experiment demonstrated that Ang II upregulated TRPC3 via AT1R, which is consistent with the above study by Yamaguchi et al. in isolated mouse ventricular myocytes.

TGF-$\beta$1 is a central mediator of fibrosis. Ang II is involved in fibrosis via the TGF-$\beta$1/Smad3 signaling pathway. Cytoskeleton, such as microtubule, is associated with Rho guanine nucleotide exchange factor (GEF-H1), which is involved in TRPC3-mediated RhoA activation induced by mechanical stress in cardiomyocytes and transforming growth factor (TGF-$\beta$) stimulation in cardiac fibroblasts [39]. TRPC6 interaction with TRPC3-NOX2 protein complex attenuates the hyperglycemia-induced heart failure in mice [18]. TRPC3 inhibition or $Ca^{2+}$ removal inhibits renal fibroblast proliferation and myofibroblast differentiation by suppressing the phosphorylation of extracellular signal regulated kinase (ERK1/2) in cultured fibroblasts. In our study, Pyr3 inhibited Ang II-induced TGF-$\beta$1 upregulation. Furthermore, lentiviral vector carrying shRNA TRPC3 gene also inhibited TGF-$\beta$1 expression. In addition, Pyr3 also inhibited the expression of phosphorylated Smad2/3. Our results demonstrated that Pyr3 prevented Ang II-induced atrial fibrosis by the TGF-$\beta$1/smad2/3 signaling pathway. Figure 10 summarizes the signaling pathway of the TRPC3 in fibroblasts, which are involved in myocardial fibrosis. The blue one is the signaling pathway evidenced in this study, and the red and green ones were reported by published papers.

## 5. Conclusions

TRPC3 is increased in the atrium from aging and hypertensive rats accompanied with atrial fibrosis. The upregulation of TRPC3 from atrial fibroblasts is involved in fibrosis via the AT1R/TGF-$\beta$1/p-Smad2/3 signaling pathway. TRPC3 may be a potential therapeutic target under the pathophysiology states such as aging and hypertension.

## Data Availability

The data used to support the findings of this study are available from the corresponding authors upon request.

## Conflicts of Interest

The authors declare that there is no conflict of interests.

## Authors' Contributions

Rongfang He, Juan Zhang, Dan Luo, Yiyan Yu, and Tangting Chen carried out the experiments. Yan Yang provided the experimental animals. Miaoling Li and Fengxu Yu designed the experiments and wrote the manuscript. Rongfang He, Juan Zhang, and Dan Luo contributed equally to this work.

## Acknowledgments

This work was supported by the Foundation of National Natural Science Foundation of China (No. 81470022), Collaborative Innovation Center for Prevention and Treatment of Cardiovascular Disease of Sichuan Province, and Science & Technology Department of Sichuan Province (19YYJC1958). The authors gratefully acknowledge Dr. Yan Yang (Institute of Cardiovascular Research, Southwest Medical University) for providing the animals.

## References

[1] Q. Wang, Y. Yu, P. Zhang et al., "The crucial role of activin a/ALK4 pathway in the pathogenesis of Ang-II-induced atrial

fibrosis and vulnerability to atrial fibrillation," *Basic Research in Cardiology*, vol. 112, no. 4, p. 47, 2017.

[2] M. S. Dzeshka, G. Y. Lip, V. Snezhitskiy, and E. Shantsila, "Cardiac fibrosis in patients with atrial fibrillation: mechanisms and clinical implications," *Journal of the American College of Cardiology*, vol. 66, no. 8, pp. 943–959, 2015.

[3] F. Rahman, G. F. Kwan, and E. J. Benjamin, "Erratum: global epidemiology of atrial fibrillation," *Cardiology*, vol. 13, no. 8, p. 501, 2016.

[4] F. Rahman, G. F. Kwan, and E. J. Benjamin, "Global epidemiology of atrial fibrillation," *Nature Reviews Cardiology*, vol. 11, no. 11, pp. 639–654, 2014.

[5] M. S. Dzeshka, A. Shantsila, E. Shantsila, and G. Y. H. Lip, "Atrial fibrillation and hypertension," *Hypertension*, vol. 70, no. 5, pp. 854–861, 2017.

[6] M. S. Kallistratos, L. E. Poulimenos, and A. J. Manolis, "Atrial fibrillation and arterial hypertension," *Pharmacological Research*, vol. 128, pp. 322–326, 2018.

[7] T. Chen, M. Li, X. Fan, J. Cheng, and L. Wang, "Sodium tanshinone IIA sulfonate prevents angiotensin II-induced differentiation of human atrial fibroblasts into myofibroblasts," *Oxidative Medicine and Cellular Longevity*, vol. 2018, Article ID 6712585, 10 pages, 2018.

[8] I. Kii, "Practical application of periostin as a biomarker for pathological conditions," *Advances in Experimental Medicine and Biology*, vol. 1132, pp. 195–204, 2019.

[9] M. Harada, X. Luo, X. Y. Qi et al., "Transient receptor potential canonical-3 channel-dependent fibroblast regulation in atrial fibrillation," *Circulation*, vol. 126, no. 17, pp. 2051–2064, 2012.

[10] D. Liu, D. Yang, H. He et al., "Increased transient receptor potential canonical type 3 channels in vasculature from hypertensive rats," *Hypertension*, vol. 53, no. 1, pp. 70–76, 2009.

[11] M. Wang, Y. B. Tang, M. M. Ma et al., "TRPC3 channel confers cerebrovascular remodelling during hypertension via transactivation of EGF receptor signalling," *Cardiovascular Research*, vol. 109, no. 1, pp. 34–43, 2016.

[12] M. Chen, J. Liu, Y. Lu et al., "Age-dependent alpha-synuclein accumulation is correlated with elevation of mitochondrial TRPC3 in the brains of monkeys and mice," *Journal of Neural Transmission*, vol. 124, no. 4, pp. 441–453, 2017.

[13] P. W. Piresand and S. Earley, "A TRPC3 signalling complex promotes cerebral artery remodelling during hypertension," *Cardiovascular Research*, vol. 109, no. 1, pp. 4-5, 2016.

[14] B. Wang, S. Xiong, S. Lin et al., "Enhanced mitochondrial transient receptor potential channel, canonical type 3-mediated calcium handling in the vasculature from hypertensive rats," *Journal of the American Heart Association*, vol. 6, no. 7, 2017.

[15] A. Adebiyi, C. M. Thomas-Gatewood, M. D. Leo, M. W. Kidd, Z. P. Neeb, and J. H. Jaggar, "An elevation in physical coupling of type 1 inositol 1,4,5-trisphosphate ($IP_3$) receptors to transient receptor potential 3 (TRPC3) channels constricts mesenteric arteries in genetic hypertension," *Hypertension*, vol. 60, no. 5, pp. 1213–1219, 2012.

[16] F. Sierra-Valdez, C. M. Azumaya, L. O. Romero, T. Nakagawa, and J. F. Cordero-Morales, "Structure-function analyses of the ion channel TRPC3 reveal that its cytoplasmic domain allosterically modulates channel gating," *Journal of Biological Chemistry*, vol. 293, no. 41, pp. 16102–16114, 2018.

[17] A. Harvey, A. C. Montezano, R. A. Lopes, F. Rios, and R. M. Touyz, "Vascular fibrosis in aging and hypertension: molecular mechanisms and clinical implications," *Canadian Journal of Cardiology*, vol. 32, no. 5, pp. 659–668, 2016.

[18] T. Numaga-Tomita, S. Oda, T. Shimauchi, A. Nishimura, S. Mangmool, and M. Nishida, "TRPC3 channels in cardiac fibrosis," *Frontiers in Cardiovascular Medicine*, vol. 4, p. 56, 2017.

[19] Z. Zhao, Y. Ni, J. Chen et al., "Increased migration of monocytes in essential hypertension is associated with increased transient receptor potential channel canonical type 3 channels," *PLoS One*, vol. 7, no. 3, article e32628, 2012.

[20] N. Onohara, M. Nishida, R. Inoue et al., "TRPC3 and TRPC6 are essential for angiotensin II-induced cardiac hypertrophy," *The EMBO Journal*, vol. 25, no. 22, pp. 5305–5316, 2006.

[21] P. Hang, J. Zhao, B. Cai et al., "Brain-derived neurotrophic factor regulates TRPC3/6 channels and protects against myocardial infarction in rodents," *International Journal of Biological Sciences*, vol. 11, no. 5, pp. 536–545, 2015.

[22] L. Hanand and J. Li, "Canonical transient receptor potential 3 channels in atrial fibrillation," *European Journal of Pharmacology*, vol. 837, pp. 1–7, 2018.

[23] S. Ayyadevara, F. Mercanti, X. Wang et al., "Age- and hypertension-associated protein aggregates in mouse heart have similar proteomic profiles," *Hypertension*, vol. 67, no. 5, pp. 1006–1013, 2016.

[24] M. De Luca, "The role of the cell-matrix interface in aging and its interaction with the renin-angiotensin system in the aged vasculature," *Mechanisms of Ageing and Development*, vol. 177, pp. 66–73, 2019.

[25] A. Harvey, A. C. Montezano, and R. M. Touyz, "Vascular biology of ageing–implications in hypertension," *Journal of Molecular and Cellular Cardiology*, vol. 83, pp. 112–121, 2015.

[26] M. Litwin, J. Feber, and M. Ruzicka, "Vascular aging: lessons from pediatric hypertension," *Canadian Journal of Cardiology*, vol. 32, no. 5, pp. 642–649, 2016.

[27] Y. Mitamura, M. Murai, C. Mitoma, and M. Furue, "NRF2 activation inhibits both TGF-$\beta$1- and IL-13-mediated periostin expression in fibroblasts: benefit of cinnamaldehyde for antifibrotic treatment," *Oxidative Medicine and Cellular Longevity*, vol. 2018, Article ID 2475047, 10 pages, 2018.

[28] X. Xiao, H. X. Liu, K. Shen, W. Cao, and X. Q. Li, "Canonical transient receptor potential channels and their link with cardio/cerebro-vascular diseases," *Biomolecules & Therapeutics*, vol. 25, no. 5, pp. 471–481, 2017.

[29] I. Alvarez-Miguel, P. Cidad, M. T. Pérez-García, and J. R. López-López, "Differences in TRPC3 and TRPC6 channels assembly in mesenteric vascular smooth muscle cells in essential hypertension," *The Journal of Physiology*, vol. 595, no. 5, pp. 1497–1513, 2017.

[30] S. G. Tang, X. Y. Liu, S. P. Wang, H. H. Wang, A. Jovanović, and W. Tan, "Trimetazidine prevents diabetic cardiomyopathy by inhibiting Nox2/TRPC3-induced oxidative stress," *Journal of Pharmacological Sciences*, vol. 139, no. 4, pp. 311–318, 2019.

[31] Y. Saliba, V. Jebara, J. Hajal et al., "Transient receptor potential canonical 3 and nuclear factor of activated T cells C3 signaling pathway critically regulates myocardial fibrosis," *Antioxidants & Redox Signaling*, vol. 30, no. 16, pp. 1851–1879, 2019.

[32] D. Y. Liu, A. Scholze, R. Kreutz et al., "Monocytes from spontaneously hypertensive rats show increased store-operated and second messenger-operated calcium influx mediated by

transient receptor potential canonical type 3 channels," *American Journal of Hypertension*, vol. 20, no. 10, pp. 1111–1118, 2007.

[33] Y. Saliba, R. Karam, V. Smayra et al., "Evidence of a role for fibroblast transient receptor potential canonical 3 $Ca^{2+}$ channel in renal fibrosis," *Journal of the American Society of Nephrology*, vol. 26, no. 8, pp. 1855–1876, 2015.

[34] A. C. Montezano, A. N. D. Cat, F. J. Rios, and R. M. Touyz, "Angiotensin II and vascular injury," *Current Hypertension Reports*, vol. 16, no. 6, p. 431, 2014.

[35] R. M. Touyz, "Intracellular mechanisms involved in vascular remodelling of resistance arteries in hypertension: role of angiotensin II," *Experimental Physiology*, vol. 90, no. 4, pp. 449–455, 2005.

[36] Y. Yamaguchi, G. Iribe, T. Kaneko et al., "TRPC3 participates in angiotensin II type 1 receptor-dependent stress-induced slow increase in intracellular $Ca^{2+}$ concentration in mouse cardiomyocytes," *The Journal of Physiological Sciences*, vol. 68, no. 2, article 519, pp. 153–164, 2018.

[37] G. Y. Zhang, X. Li, C. G. Yi et al., "Angiotensin II activates connective tissue growth factor and induces extracellular matrix changes involving Smad/activation and p38 mitogen-activated protein kinase signalling pathways in human dermal fibroblasts," *Experimental Dermatology*, vol. 18, no. 11, pp. 947–953, 2009.

[38] B. Liu, X. He, S. Li, B. Xu, L. Birnbaumer, and Y. Liao, "Deletion of diacylglycerol-responsive TRPC genes attenuates diabetic nephropathy by inhibiting activation of the TGF$\beta$1 signaling pathway," *American Journal of Translational Research*, vol. 9, no. 12, pp. 5619–5630, 2017.

[39] T. Numaga-Tomita, N. Kitajima, T. Kuroda et al., "TRPC3-GEF-H1 axis mediates pressure overload-induced cardiac fibrosis," *Scientific Reports*, vol. 6, no. 1, article 39383, 2016.

Hindawi
Oxidative Medicine and Cellular Longevity
Volume 2019, Article ID 5276096, 13 pages
https://doi.org/10.1155/2019/5276096

*Research Article*

# Salidroside Delays Cellular Senescence by Stimulating Mitochondrial Biogenesis Partly through a miR-22/SIRT-1 Pathway

**Gen-Xiang Mao**,[1] **Xiao-Gang Xu**,[1] **San-Ying Wang**,[1] **Hui-Fen Li**,[2] **Jing Zhang**,[1] **Zhong-Shan Zhang**,[3] **Hui-Li Su**,[1] **Sha-Sha Chen**,[1] **Wen-Min Xing**,[1] **Ya-Zhen Wang**,[1] **Ji-Huan Dai**,[1] **Guo-Fu Wang**,[1] **Sean X. Leng**,[2] **and Jing Yan**[1]

[1]*Zhejiang Provincial Key Lab of Geriatrics & Geriatrics Institute of Zhejiang Province, Department of Geriatrics, Zhejiang Hospital, Hangzhou 310013, China*
[2]*Division of Geriatric Medicine and Gerontology, Department of Medicine, Johns Hopkins University School of Medicine, Baltimore, MD 21224, USA*
[3]*Department of Pharmacology, Huzhou University, Huzhou 313000, China*

Correspondence should be addressed to Gen-Xiang Mao; maogenxiang@163.com, Sean X. Leng; sleng1@jhmi.edu, and Jing Yan; zjicu@vip.163.com

Received 7 May 2019; Revised 6 August 2019; Accepted 24 August 2019; Published 12 September 2019

Guest Editor: Adriana San-Miguel



Calorie restriction (CR) is a nongenetic intervention with a robust effect on delaying aging in mammals and other organisms. A mild stimulation on mitochondrial biogenesis induced by CR seems to be an important action mode for its benefits. Here, we reported that a component isolated from *Rhodiola rosea L.*, salidroside, delays replicative senescence in human fibroblasts, which is related to its stimulation on mitochondrial biogenesis by activating SIRT1 partly resulted from inhibition on miR-22. Salidroside increased the mitochondrial mass that accompanied an increment of the key regulators of mitochondrial biogenesis including PGC-1$\alpha$, NRF-1, and TFAM and reversed the mitochondrial dysfunction in presenescent 50PD cells, showing a comparable effect to that of resveratrol. SIRT1 is involved in the inducement of mitochondrial biogenesis by salidroside. The declined expression of SIRT1 in 50PD cells compared with the young 30PD cells was prevented upon salidroside treatment. In addition, pretreatment of EX-527, a selective SIRT1 inhibitor, could block the increased mitochondrial mass and decreased ROS production induced by salidroside in 50PD cells, resulting in an accelerated cellular senescence. We further found that salidroside reversed the elevated miR-22 expression in presenescent cells according to a miRNA array analysis and a subsequent qPCR validation. Enforced miR-22 expression by using a Pre-miR-22 lentiviral construct induced the young fibroblasts (30PD) into a senescence state, accompanied with increased senescence-related molecules including p53, p21, p16, and decreased SIRT1 expression, a known target of miR-22. However, salidroside could partly impede the senescence progression induced by lenti-Pre-miR-22. Taken together, our data suggest that salidroside delays replicative senescence by stimulating mitochondrial biogenesis partly through a miR22/SIRT1 pathway, which enriches our current knowledge of a salidroside-mediated postpone senility effect and provides a new perspective on the antidecrepitude function of this naturally occurring compound in animals and humans.

## 1. Introduction

Aging is the most significant risk factor for a range of degenerative disorders. One of the earlier molecular theories of aging is that reactive oxygen species (ROS) damage macromolecules progressively over time, leading to a gradual decline in cellular function [1]. ROS are mainly produced as by-products of electron transport for ATP generation by mitochondria, the cells' power plant for energy generation. Calorie restriction (CR) is arguably the most robust,

nongenetic intervention that increases lifespan and reduces the rate of aging in mammals and other organisms. CR has been demonstrated to delay aging as well as the progression of age-associated disorders such as Alzheimer's disease (AD) and diabetes [2–4]. The underlying mechanisms for the beneficial effects of CR remain unknown and likely involve many processes. For instance, substantial evidence supports that CR reduces oxidative stress via stimulating the mitochondrial biogenesis. Mitochondria under CR conditions have less oxygen consumption and generate less ROS than controls. Many investigators have observed that resveratrol (RES), a SIRT1 activator, closely mimics the effects of CR. In addition, resveratrol has been shown to stimulate mitochondrial biogenesis and induce amelioration of oxidative stress [5–8]. Interestingly, resveratrol was reported to delay cellular senescence in cultured human fibroblasts [9, 10]. Therefore, developing therapeutics to improve mitochondrial biogenesis and/or its function is an attractive strategy to delay aging and prevent age-associated diseases [11]. However, difficulties and controversies are abundant in applying CR and resveratrol treatment in humans. Novel strategies to potentially induce mitochondrial biogenesis and delay cellular senescence should be explored.

Though the precise reason for the decrease in the rate of mitochondrial biogenesis during aging is currently unknown, it seems that both extra- and intracellular regulatory factors of mitochondrial biogenesis are implicated [11]. Despite the complexity of the various signaling pathways that converge to regulate mitochondrial biogenesis, they all seem to share the common key component of the peroxisome proliferator-activated receptor $\gamma$ coactivator 1 (PGC-1) family of cotranscription factors. Specifically, PGC-1$\alpha$ has been shown to act as a common intracellular mediator during mitochondrial biogenesis [12]. PGC-1$\alpha$ enhances the expression of nuclear respiration factors (NRF-1 and NRF-2) and mitochondrial transcription factor A (TFAM), which are transcription factors that trigger the expression of genes coding for both nuclear subunits of the respiratory chain and proteins involved in mitochondrial DNA transcription and replication [13, 14]. Aging-associated reduction in mitochondrial biogenesis in aged animals shown by lower gene expression in the PGC-1$\alpha$ signaling pathways including decreased mRNA and protein contents for PGC-1$\alpha$, NRF1/2, and TFAM accompanied with an increased oxidative stress level was observed when compared to the young controls [15]. In mammalian studies of CR or resveratrol treatment, an activation of SIRT1 was observed that resulted in deacetylation of PGC-1$\alpha$ in a nicotinamide adenine dinucleotide- (NAD-) dependent manner, leading to PGC-1$\alpha$ activation and CR- or resveratrol-induced mitochondrial biogenesis [6].

MicroRNAs (miRNAs) represent a class of naturally occurring small, 18- to 28-nucleotide-long, noncoding RNAs that negatively regulate the stability and translation of target protein-coding mRNAs at the 3′ untranslated region (UTR). Recently, accumulating evidences suggest some miRNAs, such as let-7, miR-34a, and miR-22, can modulate senescence progression by regulating the expression of senescence-related molecules such as p53 and SIRT1 [16–19].

Salidroside (SAL), a phenylpropanoid glycoside isolated from *Rhodiola rosea L.*, is a popular medicinal plant used in traditional Chinese medicine. It is reputed to improve depression, enhance work performance, eliminate fatigue, and treat symptoms of asthenia subsequent to intense physical and psychological stress. Our previous studies have indicated that SAL showed a potent antiaging effect in an accelerated mouse aging model induced by D-galactose [20]. It also protects human fibroblast 2BS cells from premature senescence induced by $H_2O_2$ or UVB exposure in human diploid fibroblasts [21, 22], identified as stress-induced premature senescence (SIPS), which is mainly caused by oxidative stress and subsequent DNA damage. Besides, we found that SAL delays the replicative senescence of human diploid fibroblasts 2BS cells, which may be related to its stimulatory role on mitochondrial biogenesis. In the current study, the stimulatory effect of SAL on mitochondrial biogenesis will be investigated in 2BS cells as well as its related molecular mechanisms. We will attempt to ascertain the precise mechanisms of SAL regarding its antiaging effect *in vitro* beyond oxidative stress or DNA damage and thus inspire a new idea for prevention or delay of aging and age-associated diseases.

## 2. Materials and Methods

*2.1. Reagents.* Salidroside (SAL) was purchased from the National Institute for the Control of Pharmaceutical and Biological Products (Beijing, China). Resveratrol (3,5,4′-trihydroxystilbene), $H_2$DCFDA (2′,7′-dichlorodihydrofluorecein diacetate), NAO (nonyl acridine orange), and JC-1 (5,5′,6,6′-tetrachloro-1,1′,3,3′-tetraethyl benzimidazole carbocyanine iodide) were purchased from Sigma-Aldrich. Selisistat (EX-527) was from MedChemExpress (MCE). Dulbecco's modified Eagle's medium (DMEM), fetal bovine serum (FBS), and trypsin were obtained from Invitrogen, USA. Primary anti-PGC-1$\alpha$ antibody was obtained from Novus Biologicals, LLC, USA. Antibodies for SIRT1, Rb, $p21^{Waf1}$, and $p16^{INK4a}$ were from Cell Signaling Technology, Inc. Anti-NFR-1 and anti-TFAM antibodies were Abcam products. Anti-p53 and anti-$\beta$-actin primary antibodies were purchased from Santa Cruz Biotechnology, Inc., USA.

*2.2. Cell Culture.* The 2BS cell line isolated from human fetal lung fibroblasts was originally established by the National Institute of Biological Products (Beijing, China) and has been well characterized and widely used as a cellular senescence model [23–25]. Cells are considered to be young at earlier than 30 population doubling (PD) and replicative senescent around 55PD or later. The cells were grown in DMEM supplemented with 10% FBS, 100 U/mL penicillin, and 100 mg/mL streptomycin in an incubator at 37°C with 5% $CO_2$. The cultured cells were split in ratios of 1 : 2 or 1 : 4 when the confluence of the culture was over 85%. The cumulative population doublings (CPDs) were calculated as $\log_2 (D/D_0)$, where $D$ and $D_0$ are defined as the density of cells at the time of harvesting and seeding, respectively. As replicative senescent fibroblasts are hard to harvest for various detections, all experiments were performed using cells that

were at 50PD as near-senescence (presenescence) cells unless indicated otherwise.

*2.3. Senescence-Associated β-Galactosidase (SA-β-gal) Staining.* The activity of senescence-associated β-galactosidase (at pH 6) is a biomarker of replicative senescence first reported by Dimri et al. [26]. The percentage of SA-β-gal-positive cells out of the total number of cells was counted. Average percentages were obtained from three independent experiments.

*2.4. Intracellular Reactive Oxygen Species (ROS) Measurement.* The intracellular ROS level was determined by flow cytometry analysis. Before submitting for flow cytometry analysis, cells were trypsinized and collected for an incubation with the ROS probe 2′,7′-dichlorodihydrofluorecein diacetate ($H_2$DCFDA, 10 μM) in the dark. The intracellular fluorescence (FL1, green) intensity was measured, and a relative level (set control as 100%) was calculated. Images of cells stained by $H_2$DCFDA were acquired by Leica fluorescence microscopy.

*2.5. Measurement of a Mitochondrial Mass.* A mitochondrial mass was determined by using the nonyl acridine orange (NAO) probe, which specifically binds to cardiolipin, a specific phospholipid that is found almost exclusively in the inner mitochondrial membrane and is widely considered as a mitochondrial mass marker [3]. For flow cytometry assay, cells were treated as indicated above, detached and fixed with 70% ethanol, and stored until use at -20°C. Then, ethanol was removed by centrifugation, and cells were washed in PBS and stained with 10 μM NAO in 1 mL of PBS. After incubating for 10-20 min at room temperature in the dark, cells were washed in PBS for three times and submitted for flow analysis. Relative change in mean fluorescence for green fluorescence at 530 nm was calculated which reflects the mitochondrial mass.

*2.6. Measurement of Adenosine Triphosphate (ATP).* Intracellular ATP was measured by using the ATP colorimetric/-fluorometric assay kit supplied by Abcam (ab83355). Briefly, cells rinsed by cold PBS were lysed in 100 μL of ATP assay buffer and centrifuged at 15,000g for 2 min. The supernatant was collected and transferred to a new tube, and then, 20-40 μL of 4 M perchloric acid were added to remove proteins by centrifugation at 12,000g for 2 min. The supernatant was collected, and a buffer containing 2 M KOH was added to neutralize the sample and remove the excess perchloric acid. After centrifugation for 15 min at 12,000g to pellet insoluble materials, the supernatant was added to a 96-well plate and developed according to the manufacturer's instructions. The absorbance was read at 570 nm using an automatic ELISA plate reader. The ATP content was calculated based on a standard curve generated at the same time.

*2.7. Flow Cytometric Analysis of Mitochondrial Membrane Potential (ΔΨm).* Changes in the ΔΨm were analyzed by using JC-1. JC-1 is a positively charged fluorescent compound which is taken up by mitochondria proportionally to the inner mitochondrial membrane potential [27]. ΔΨm was determined by the ratiometric analysis of orange fluorescence emitted by JC-1 aggregates (FL2, red) and that emitted by the free probe (FL1, green). Briefly, 2BS cells seeded in six-well plates were treated with SAL (10 μM) for indicated time. Then, cells were dissociated and were incubated in 1 mL of PBS supplemented with 10% FBS containing 0.5 μg/mL JC-1 for 1 h in the dark. Cells were then washed twice with PBS and submitted for flow cytometric analysis. The ratio of FL2 versus FL1 reflects the level of ΔΨm. Images of JC-1 staining were acquired using Leica fluorescence microscopy.

*2.8. Western Blot Analysis.* Cells were rinsed with iced PBS and then lysed with cell lysis buffer containing protease inhibitor cocktail (Cell Signaling Technology, USA). Protein concentrations were determined by the BCA protein assay kit (Pierce Chemical Co.). A total of 50 μg of protein extracts were loaded and electrophoresed on a 4-15% SDS polyacrylamide gel and transferred to the polyvinylidene fluoride (PVDF) membrane (Bio-Rad, USA). The membranes were subsequently probed with specific primary antibodies. The secondary antibody used for detection was linked with horseradish peroxidase. The enhanced chemiluminescence (ECL) method was used to detect the conjugated horseradish peroxidase. The optical density (OD) of each band was measured using ImageJ for semiquantitative analysis.

*2.9. miRNA Microarray.* Total RNAs were harvested from 2BS fibroblasts at different PD with or without SAL treatment by using the traditional acid guanidinium-phenol-chloroform extraction method and quantified with a spectrophotometer (NanoDrop; Thermo Fisher Scientific). Microarray analysis of the miRNA expression (miRbase 19.0) was performed by using a service provider (LC Science).

*2.10. Real-Time qPCR.* Total RNA was extracted from the cells and tissues using the miRNeasy Mini kit (QIAGEN). The expression of mature miR-22 was quantified according to a kit (Hs_miR-22_1 miScript Primer Assay targets miRNA: hsa-miR-22-3p, QIAGEN, MS00003220) by using a real-time PCR system LightCycler 480 (Roche). The expression of miRNA was defined from the threshold cycle, and relative expression levels were calculated using the $2^{-\Delta\Delta Ct}$ method after normalization with reference to the expression of U6 small nuclear RNA (QIAGEN, MS00033740).

*2.11. Lentivirus Infection.* Lentivirus expressing Pre-miR-22 was generated with LV3-GFP lentiviral vectors (Lenti-Pre22) provided by GenePharma Inc. (Shanghai, China). For pilot studies, cells were infected with control vector (Lenti-C) or Lenti-Pre22 at various multiplicities of infection (MOI) accompanied with 1-5 μg/mL polybrene, and a MOI of 5 with 2 μg/mL polybrene was optimal to transfect the 2BS cells.

*2.12. Data Analysis.* All experiments were repeated in triplicate. The results were expressed as mean ± SD. One-way ANOVA analysis (SPSS 19.0) was used for data comparisons

within multiple groups, with $P$ value less than 0.05 considered to be statistically significant.

## 3. Results

*3.1. SAL Delays Replicative Senescence of Human 2BS Fibroblasts.* Our previous studies indicated that the optimal dose range of SAL for its protection against stress-induced premature senescence (SIPS) in human diploid 2BS fibroblasts is 5-20 $\mu$M [21, 22]. In this study, we first observed the effects of SAL on replicative lifespan and biomarkers related to cellular senescence in human 2BS fibroblasts. Cells were cultured in a SAL-supplemented medium from 30PD until they became replicative senescent. SAL significantly delayed replicative senescence of 2BS cells by at least 8 PDs (see Table 1). The two concentrations of SAL (5 $\mu$M and 10 $\mu$M) showed a similar gain in PDs. The growth rate of SAL-treated cells was dramatically increased compared to that of the control cells (Table 1). For the SA-$\beta$-gal activity, a biomarker of cellular senescence, only sporadic SA-$\beta$-gal-positive cells were observed in young control cells (Figure 1(a)). As anticipated, SA-$\beta$-gal activity was markedly elevated in 55PD control cells ($91.7 \pm 7.1\%$), while cells at 55PD cultured in a 10 $\mu$M SAL-supplemented medium from 30PD showed a much lower positive rate ($28.3 \pm 4.9\%$). Moreover, SAL treatment for 48 h significantly suppressed the elevated production of intracellular ROS in near-senescent 2BS cells (50PD), which was comparable to that of resveratrol (RES) (Figure 1(b)), an antioxidant reported to be a SIRT1 activator and delays replicative senescence in human fibroblasts [9]. The above results show that SAL could delay the replicative senescence process of 2BS cells.

*3.2. SAL Induces an Increment of Mitochondrial Biogenesis in 2BS Fibroblasts.* Compared with the young control cells (30PD), late PD 2BS (50PD) showed a decreased fluorescent intensity of NAO, suggesting a lower mitochondrial mass in 50PD cells. Upon treated with SAL at 10 $\mu$M for 48 h, the mitochondrial mass level reflected by the NAO fluorescent intensity in 50PD 2BS was pulled up closed to the young level, which is comparable to that of resveratrol (RES) (Figure 2). Then, the alteration of typical signaling pathways involved in the mitochondrial biogenesis was subsequently considered. As shown in Figure 3, the key regulators of mitochondrial biogenesis including PGC-1$\alpha$, NRF-1, and TFAM were significantly increased in 50PD 2BS incubated with SAL, and a similar effect was observed in resveratrol-treated cells.

*3.3. Effect of SAL on the Mitochondrial Function in 2BS Fibroblasts.* Since SAL induced an increment of mitochondrial biogenesis in human fibroblasts, we next asked whether it affects the mitochondrial function. Mitochondrial membrane potential ($\Delta\Psi$m) and ATP production were used for assessment of a mitochondrial function. In flow cytometric assays of JC-1-stained cells, FL2 (orange) fluorescence reports the J aggregate form of JC-1 which reflects the level of $\Delta\Psi$m. The FL1 green signal reports the nonaggregate form of the dye and provides a measure to assess variations of dye loading. In untreated young control cells (30PD), flow cytometric analysis revealed a larger population of cells with high $\Psi$m based on FL2/FL1 fluorescence than that of 50PD cells which was partly reversed by SAL and RES treatment (Figure 4(a)). The declined ATP production in late PD cells was also partly reversed by SAL or RES treatment (Figure 4(b)). These results suggest that SAL can rescue the mitochondrial dysfunction via $\Delta\Psi$m and ATP production in fibroblasts.

Table 1: The effect of salidroside on the life spans of 2BS cells in CPDs.

| Group | Treatment | Time of transfer to a special medium | $n$ | CPDs | Average PDs per week |
|---|---|---|---|---|---|
| I | Control | — | 3 | $55.3 \pm 3.7$ | $1.6 \pm 0.1$ |
| II | SAL (5 $\mu$M) | 30PD | 3 | $62.8 \pm 4.1$ | $2.1 \pm 0.2^*$ |
| III | SAL (10 $\mu$M) | 30PD | 3 | $63.5 \pm 5.3$ | $2.2 \pm 0.2^*$ |

*Note.* Human fibroblast 2BS cells at 30PD were cultured in DMEM supplemented with salidroside (SAL) at 5 $\mu$M and 10 $\mu$M, respectively. When the confluence of the culture was reached 70-80%, the cells were split in ratios of 1 : 2 or 1 : 4 and were continually cultured in the indicated medium. Control cells were cultured in a 0.01% supplemented medium. CPDs (cumulative population doublings) were calculated as log2 ($D/D_0$), where $D$ and $D_0$ were defined as the density of cells at the time of harvesting and seeding, respectively. The last culture was defined as the subculture that could not be confluent in 15 days. Data were obtained from three independent experiments ($^*P < 0.05$ vs. $I$).

*3.4. SAL Stimulates Mitochondrial Biogenesis Related to the SIRT1 Activation.* Since SIRT1 is highly related to mitochondrial biogenesis through activation on PGC1$\alpha$ [3], it is interesting to detect the SIRT1 expression. Consistent with previous reports, lower SIRT1 protein expression was observed in late PD fibroblasts in comparison to that of young human fibroblasts [28]. SAL dose dependently increased the SIRT1 protein expression in 50PD 2BS, with 10 $\mu$M offering an optimal effect, which was similar to that of resveratrol (Figure 5(a)). For the time course study, SAL started to improve the SIRT1 protein expression at 6 h and maintained this stimulatory effect at least till 48 h (Figure 5(b)). Then, we used a selective SIRT1 inhibitor, Selisistat (EX-27) [29, 30], to test whether SAL-induced mitochondrial biogenesis is dependent on SIRT1 activation. According to the previous studies [30, 31] and our pilot studies, EX-527 at 10 $\mu$M was used to inhibit SIRT1 activity and did not cause cell death in 2BS fibroblasts. It was added to the medium 2 h earlier before the SAL or RES treatment and was present until cell harvest. As shown in Figure 6(a), both SAL- and RES-induced increments of mitochondrial mass were suppressed by EX-527 intervention in 50PD cells. Meanwhile, EX-527 pretreatment abolished their inhibition on intracellular ROS production in 50PD 2BS cells (Figure 6(b)). Moreover, an enhanced SA-$\beta$-gal activity was induced by EX-527 in presenescent cells coincubated with SAL (Figure 6(c)). The above results suggested that inhibition on mitochondrial biogenesis accompanied with an increment of ROS induces cellular senescence rapidly.

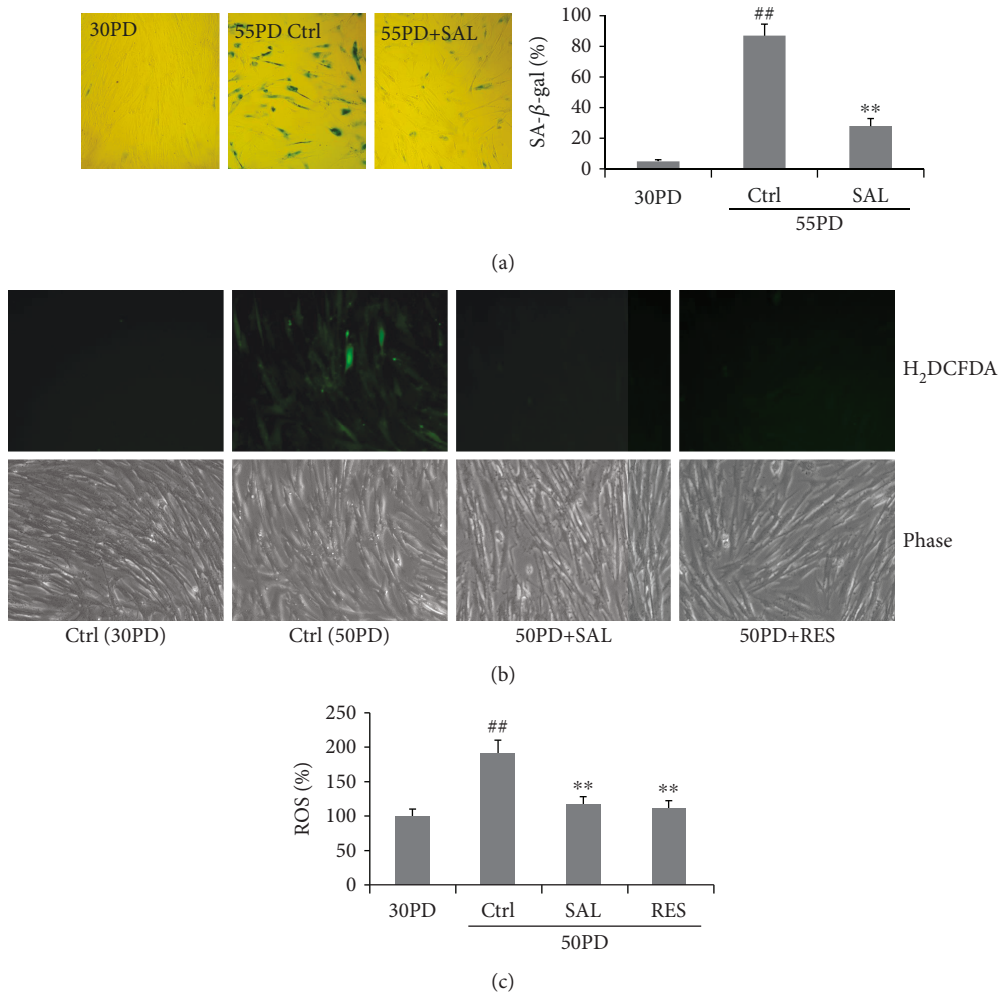


Figure 1: Salidroside (SAL) delays the phenotypes of replicative senescence of human fibroblast 2BS cells. (a) SA-$\beta$-gal staining of 2BS fibroblasts grown from 30PD in DMEM supplemented with 10 $\mu$M salidroside (SAL). Control cells at 55PD became replicative senescence. Cells at 30PD were set as young control. Cells of a nonconfluent state were washed with PBS, fixed with 3% formaldehyde, and submitted for SA-$\beta$-gal staining. Cells were microphotographed at a magnification of $10 \times 10$. (b, c) Effect of SAL and resveratrol (RES) on the ROS level in near-senescent 50PD 2BS cells. Cells treated by SAL (10 $\mu$M) or RES (10 $\mu$M) for 24 h were stained by $H_2$DCFDA for detection of intracellular ROS production. (b) Images of cells stained by $H_2$DCFDA were obtained by using fluorescence microscopy. (c) Quantitative measurement of an intracellular ROS level was performed by flow cytometric analysis. $^{\#\#}P < 0.01$ versus 30PD control (Ctrl); $^{**}P < 0.01$ versus control (Ctrl) at 55PD or 50PD.

*3.5. Effect of SAL on the miR22 Expression in 2BS Fibroblasts and SAL Partly Rescued Overexpressing miR22-Induced Senescence.* To further explore the underlying mechanisms regarding the effect of SAL on delaying cellular senescence, we attempted to screen miRNAs that related to the cellular senescence in human fibroblasts. The change of the miRNA expression profile of 2BS fibroblasts treated by SAL was analyzed by miRNA microarray. Among the miRNAs with obvious alteration upon SAL treatment, miR-22 was increased in near-senescent 2BS cells (50PD) in comparison to that of young cells (30PD), which could be reversed by SAL treatment (Figure 7). The increased miR22 expression in senescent fibroblast was reported in previous studies by using MRC-5 and TIG fibroblastic cell lines, and miR22 was proved to mediate the cellular senescent process through targeting of SIRT1 and CDK6 [19]. To test the effect of miR-22 overexpression on senescence in current 2BS fibroblasts, young cells at 30PD were transfected with a Pre-miR-22 lentiviral (Lenti-Pre22) construct, which stably expresses miR-22 precursor in its native context. Lenti-Pre22-infected cells showed a fivefold increase of mature miR-22 compared with the young control cells (Figures 8(a) and 8(b)) and exhibited an enlarged senescence morphology and SA-$\beta$-gal-positive staining (Figures 8(c) and 8(d)), accompanied with an increased protein level of senescence-associated molecules p53, p21, and p16 (Figure 8(e)). As anticipated, a decreased SIRT1 protein expression was observed in the Lenti-Pre22-infected cells (Figure 8(e)). However, SAL could partly impede the senescence progression induced by lenti-Pre-miR-22. The increment of SA-$\beta$-gal activity induced by overexpression of miR-22 was prevented in part by SAL (Figures 8(c) and 8(d)). Besides, declined expression of SIRT1 and increased protein levels

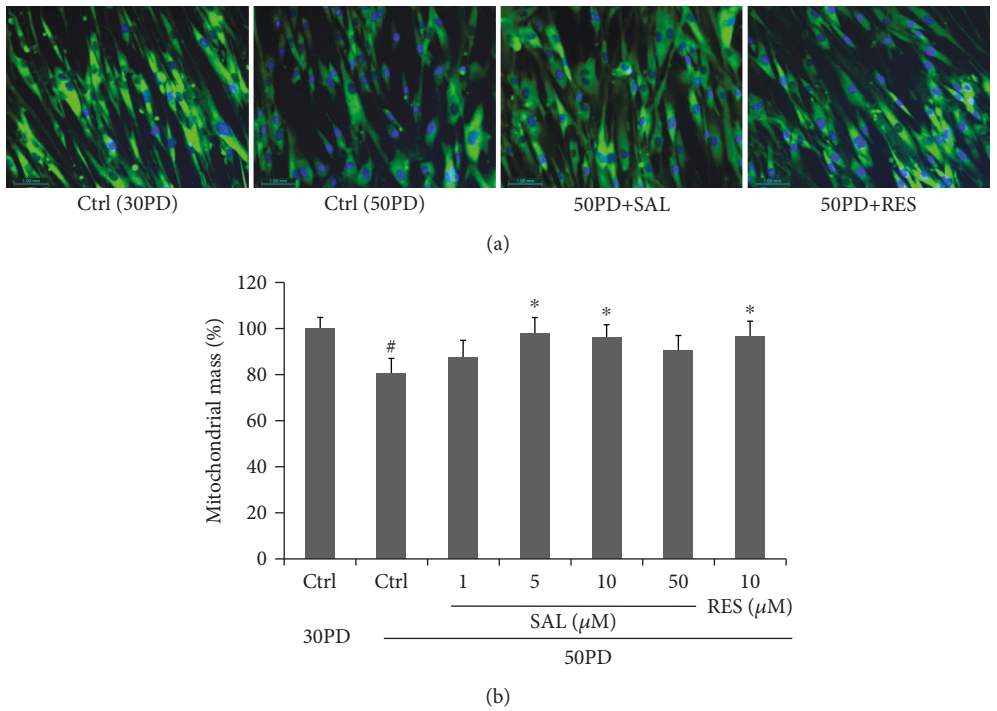


Figure 2: Effect of salidroside (SAL) on a mitochondrial mass. (a) Mitochondrial staining in 2BS cells incubated with SAL (10 $\mu$M) or resveratrol (RES) at 10 $\mu$M for 48 h. NAO signal in cells was visualized by confocal microscopy. Images were acquired by using a ×20 objective. DNA was visualized by DAPI. Pictures were shown as merged by two paired images from NAO staining and DAPI staining, respectively. (b) Mitochondrial mass in cells cultured after 48 h with SAL at different concentrations was quantified by flow cytometry by using NAO as indicated in Materials and Methods. Data indicate the relative mean of the MFI (mean fluorescence intensity) from three different experiments performed in duplicate. $^{\#}P < 0.05$ versus 30PD control (Ctrl); $^{*}P < 0.05$ versus control (Ctrl) at 50PD.

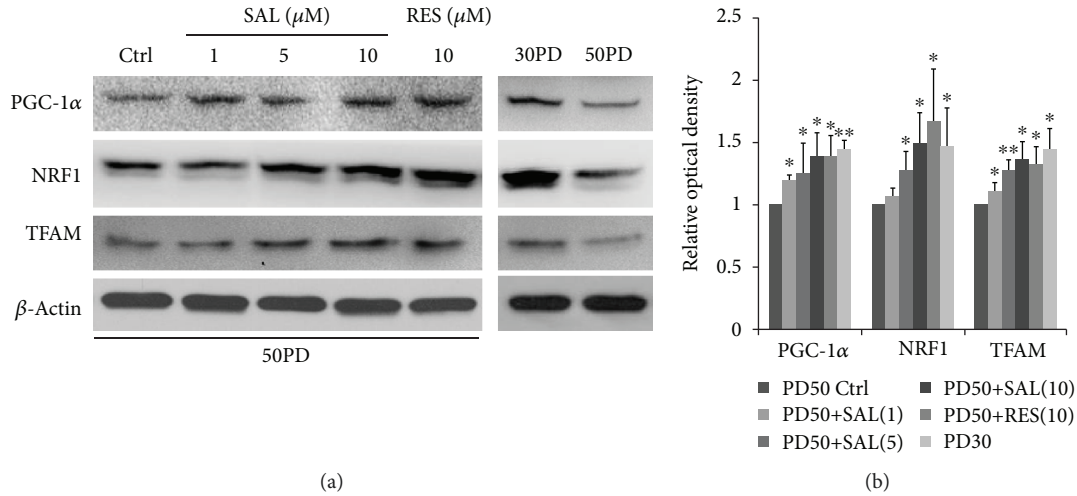


Figure 3: Effect of salidroside (SAL) on the mitochondrial biogenesis-associated PGC1$\alpha$-TFAM signaling pathway. 2BS cells at 50PD were treated by salidroside (SAL) at various dosages or resveratrol (RES) at 10 $\mu$M for 24 h and then were harvested for western blot analysis. (a) Representative images were acquired from three different experiments. (b) Quantitative analysis of the protein levels of PGC-1$\alpha$, NRF1, and TFAM. Bars represent relative protein levels counted as $D_1/D_0$ (the value for 50PD control was set as 1.0), where $D_0$ and $D_1$ stand for the optical density of $\beta$-actin ladder and sample ladder, respectively. The optical density for each ladder was calculated by the ImageJ software. Data were obtained from three independent experiments. $^{*}P < 0.05$ versus the 50PD control group.

of p53, p21, and p16 in Lenti-Pre22-infected cells were partly reversed by SAL treatment (Figure 8(e)). These results implied that SAL stimulates the SIRT1 partly through inhibition on miR-22.

## 4. Discussion

As a key mediator for the benefits of CR, SIRT1 was well accepted as a target for the drug discovery against aging

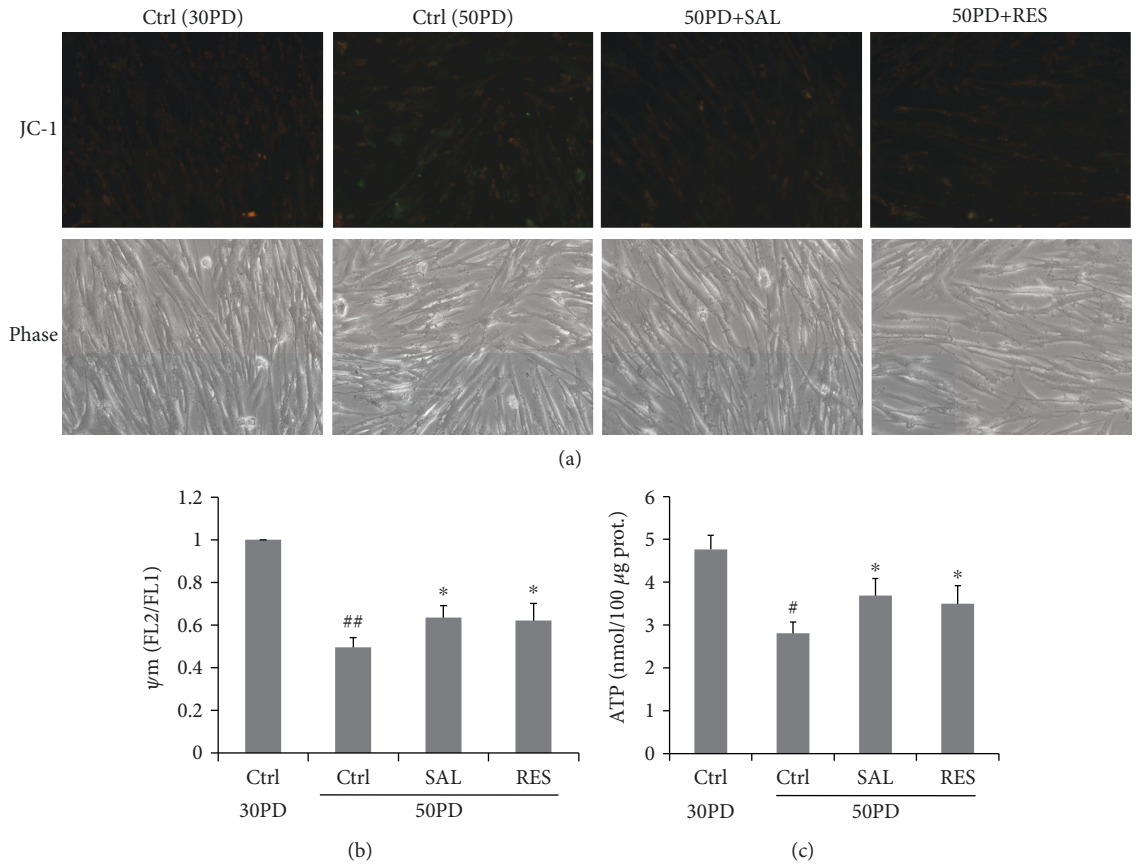


FIGURE 4: Effect of salidroside (SAL) on the mitochondrial potential ($\Delta\Psi$m) and ATP production. Cells treated by salidroside (SAL, 10 $\mu$M) and resveratrol (RES, 10 $\mu$M) for 24 h then were stained by JC-1 for $\Delta\Psi$m measurement. (a) Representative images of JC-1 staining were acquired by using fluorescence microscopy. (b) Quantitative measurement of $\Delta\Psi$m was performed by flow cytometric analysis. (c) ATP production was determined by using a commercial kit (ab83355). Cells were treated by salidroside (SAL, 10 $\mu$M) and resveratrol (RES, 10 $\mu$M) for 24 h and were harvested for ATP production. $^{\#\#}P < 0.01$ versus 30PD control (Ctrl); $^{\#}P < 0.05$ versus 30PD control (Ctrl); $^{*}P < 0.05$ versus control (Ctrl) at 50PD.

and aging-related degenerative disorders in recent decades. Resveratrol seems to be the first putative activator of SIRT1 [32]. Of all the natural SIRT1 activators discovered to date, RES is still the most potent. Resveratrol was initially identified in 1940 as a phenolic substance in the white hellebore, Veratrum grandiflorum, a flowering plant, and later in grape vines and the Japanese knotweed Polygonum sachalinense [33]. In recent years, SAL was found to exert health benefits such as cognitive improvement and inflammation amelioration probably through modulating SIRT1 [34–36]. However, the relationship of its activation on SIRT1 and replicative senescence still lacks direct evidences, and the detailed mechanism regarding its activation mode on SIRT1 remains elusive. In the current study, our findings suggested that SAL delays replicative senescence in human fibroblasts, which further solidified its antiaging effect based on our previous reports [20–22]. Its stimulatory role on mitochondrial biogenesis through upregulation on SIRT1 in human fibroblasts relates to its efficacy on delaying cellular senescence and antioxidative properties, which revealed a novel mechanistic mode for this naturally occurring compound regarding its beneficial effect against aging. Moreover, SAL delays cellular senescence partly through the miR-22/SIRT1 pathway. MicroRNA-22 (miR-22) has been predicted to potentially target SIRT1, and SAL seems to increase the SIRT1 expression by inhibition on miR-22.

Despite SIRT1, another important factor involved in the regulation of PGC-1$\alpha$ transcription is AMP-activated kinase (AMPK). AMPK activity appears to be one of the main factors associated with deficient mitochondrial biogenesis, insulin resistance, and impaired lipid metabolism observed in aged cells [37, 38]. Chronic AMPK inactivation is linked to a marked decrease in mitochondrial biogenesis in aged animals [37]. SAL was reported to exert its benefits through activating AMPK and its related pathways [39, 40]. In the current 2BS fibroblasts, we also found a SAL-induced increase of AMPK$\alpha$-Thr172 phosphorylation, and this activation of AMPK$\alpha$ could be blocked by 8-bromo-AMP (8Br-AMP), an AMPK inhibitor [41] (Figure S1 A). Meanwhile, SAL-induced mitochondrial mass increment and inhibitory on intracellular ROS production in 50PD cells were prevented by 8Br-AMP (Figure S1 B&C). Our data suggested that AMPK$\alpha$ activation is probably involved in SAL-induced mitochondrial biogenesis in 2BS cells. Furthermore, it was reported that resveratrol directly inhibits

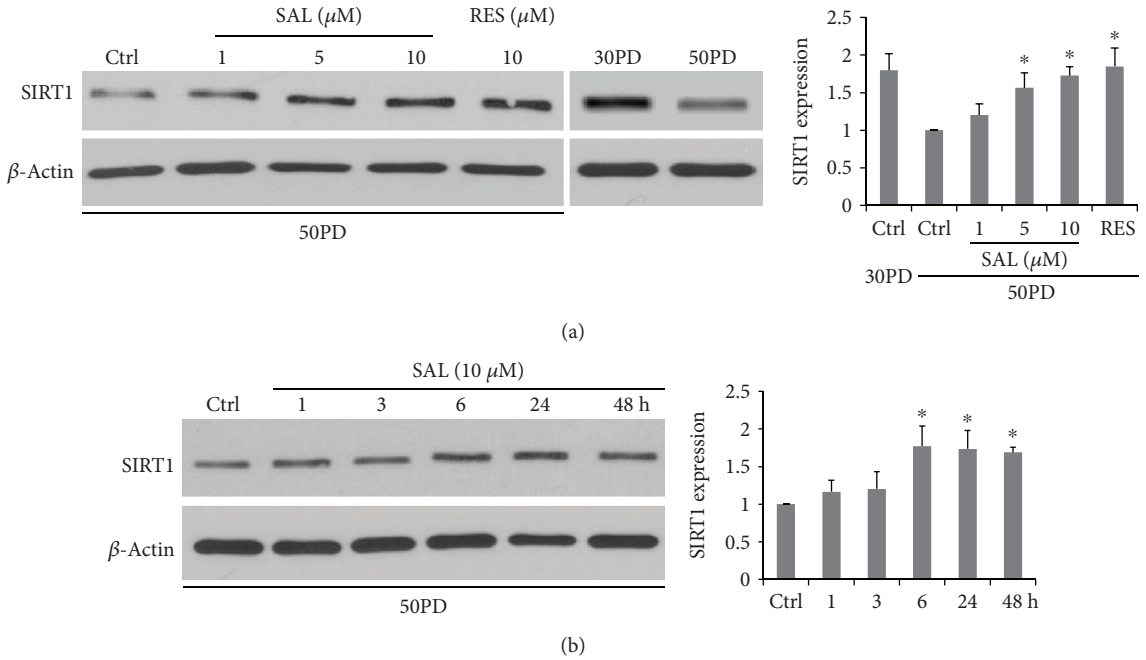


Figure 5: The dose dependence (a) and the time dependence (b) of salidroside (SAL) inducing an increment of SIRT1 expression in 2BS cells. (a) Cells at 50PD were treated by salidroside for 24 h. (b) Cells were exposed to SAL at 10 $\mu$M for different times and were harvested for western blot analysis. $^{*}P < 0.05$ versus control (Ctrl) at 50PD.

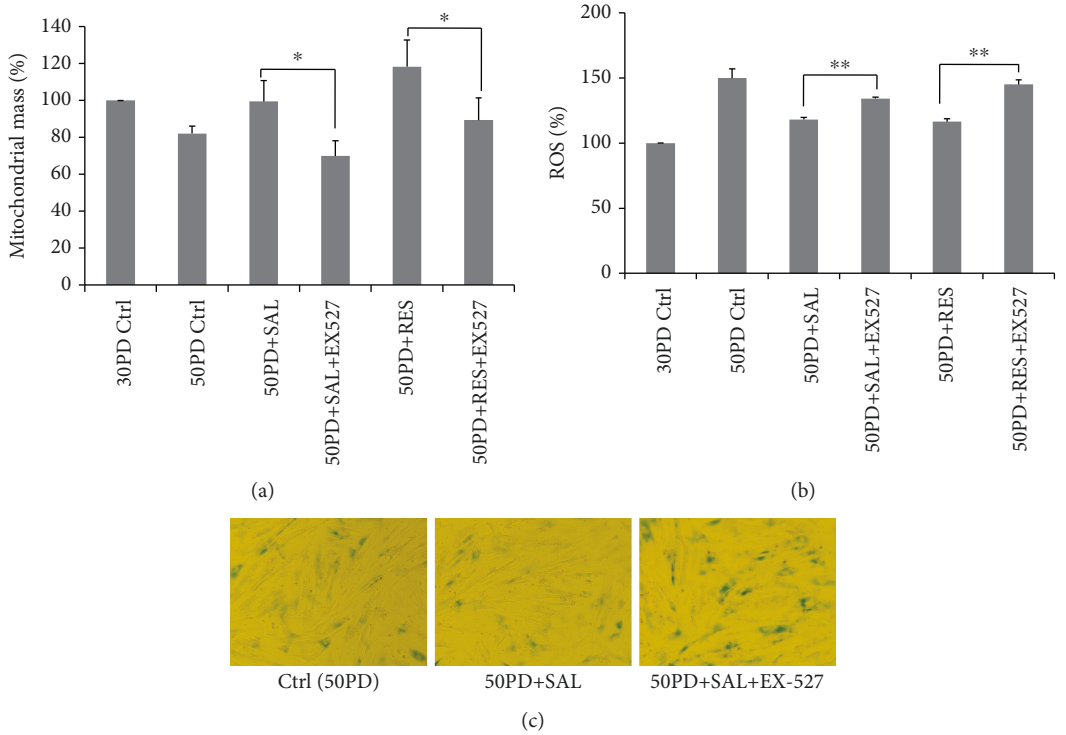


Figure 6: SIRT1 inhibitor EX-527 attenuates salidroside- (SAL-) or resveratrol- (RES-) induced increment of mitochondrial biogenesis (a) or decreased ROS production in 50PD 2BS cells (b) and induces an elevation of SA-$\beta$-gal activity in SAL-treated 50PD cells (c). EX-527 at 10 $\mu$M was added 2 hrs before SAL (10 $\mu$M) or RES (10 $\mu$M) supplementation in the culture medium and was present for 48 h before harvested. $^{*}P < 0.05$; $^{**}P < 0.01$.

cAMP-specific phosphodiesterases (PDE) and identified the cAMP effector protein Epac1 as a key mediator of the effects of resveratrol, which leads to the activation of AMPK and SIRT1 and contributes to the amelioration of aging-related metabolic phenotypes [42]. As a comparable effect of SAL and RES on inducing mitochondrial biogenesis as well as

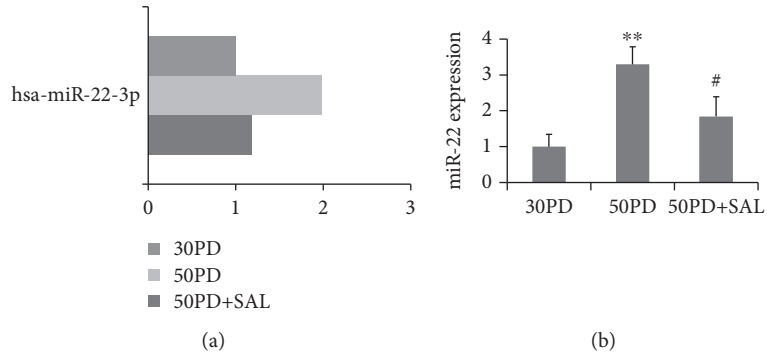


Figure 7: Effect of salidroside (SAL) on the miR-22 expression in near-senescent human fibroblasts. (a) The miR22 expression was analyzed by miRNA microarray, presented as fold changes in the miRNA expression. (b) Relative quantitation of the miR-22 expression in 2BS fibroblasts at 30PD, 50PD, or 50PD cells treated with SAL at 10 $\mu$M for 48 h was analyzed by qRT-PCR analysis. miR-22 expression levels were indicated relative to those in 30PD set at 1. U6 was used as an internal normalization control. $^{**}P < 0.05$ versus 30PD; $^{\#}P < 0.05$ versus 50PD.

ROS scavenging activity was observed according to our current work, they may share similar molecular mechanisms. Interestingly, according to a RNAseq assay in our recent work [43], SAL was shown to suppress the expression of PDE2A, a member of the PDE super family, which is a dual-substrate PDE towards both cAMP and cGMP. Moreover, according to a clinic trial in human and murine models of diabetes, treatment with a PDE5 inhibitor sildenafil induced increment of SIRT1 through a downregulation of the miR-22 expression, resulting in ameliorating visceral adipose tissue [44]. Thus, for the further detailed mechanisms regarding SAL on the modulation of the miR-22 expression, it seems to be related to the PDE inhibition.

Another important signaling pathway linked to mitochondrial biogenesis is related to eNOS activation [45]. It has been reported that resveratrol stimulates mitochondrial biogenesis in endothelial cells via activation of eNOS [5]. Indeed, a previous study indicated eNOS activation is involved in SAL-induced mitochondrial biogenesis in human umbilical vein endothelial cells (HUVECs) [46]. However, by using a mouse cardiac tissue sample as a positive control for the eNOS immune blotting, our data suggested that the eNOS protein was undetectable in young or near-senescent human 2BS fibroblasts, which were originally isolated from human fetal lung tissues (Figure S2 A). Consistently, the eNOS inhibitor NG-nitro-L-arginine methyl ester (L-NAME) did not affect the mitochondrial mass either the intracellular ROS production in 2BS cells under SAL or RES treatment in 50PD 2BS (Figure S2 B&C). Thus, the mechanisms of SAL on inducing mitochondrial biogenesis seem to be tissue specific. SAL induces mitochondrial biogenesis may be through different signaling pathways in different cell types, and it is a limitation for discovery of agents stimulating mitochondrial biogenesis through activation of eNOS in this cellular senescence model.

As the function of transfected mature miRNA may result from its supraphysiological level, we hereby used a stable miRNA vector that mimics miRNA biological processing. A Pre-miR-22 lentiviral construct (Lenti-Pre22), stably expressing miR-22 precursor in its native context, was used to study the effect of miR-22 on cellular senescence in 2BS fibroblasts. A fivefold increment of mature miR-22 was observed in young 2BS cells at 30PD after transfection with Lenti-Pre22 at MOI of 5, which was a bit higher than its normal level in presenescent 50PD cells (Figure 7) and was similar to the miR-22 level in replicative senescent MRC5 fibroblasts at 58PD reported previously [19]. Thus, Lenti-Pre22 induced cellular senescence in young 2BS cells through upregulation of miR-22, which subsequently suppressed the expression of SIRT1. SAL partly rescued this decline of SIRT1 and impeded the cellular senescence induced by Lenti-pre22. This may be explained due to the multifunction of this natural compound as follows: first, SAL may serve as a direct inhibitor on miR-22 formation, while the detailed mechanisms remain to be further explored. Second, miR-22 induces cellular senescence accompanied with oxidative stress and itself *per se* could mediate the intracellular oxidative stress [47–49], and SAL may directly prevent this process as it is a potent antioxidant according to our previous work and others' [21, 39]. Third, SAL could rescue the declined SIRT1 by other pathways. As described previously, SAL could activate the AMPK which may further stimulate SIRT1 or through a PDE inhibition way [42, 43]. Besides, SAL was reported to increase the expression level of the key protein NAMPT which synthesizes the NAD+, a coenzyme of SIRT1 [50]. In the current work, the enhanced mitochondrial biogenesis induced by SAL seems to be related to the SIRT1 activity, as it was blocked by EX-527, which inhibits SIRT1 activity and hampered the ability of other compounds, e.g., pyrroloquinoline quinone (PQQ), to stimulate mitochondrial biogenesis [29, 51].

## 5. Conclusions

In conclusion, to the best of our knowledge, our work is the first time to investigate the linkage of the natural occurring compound, salidroside, regarding its interventional effect on cellular senescence via modulation on the mitochondrial biogenesis and its regulation on microRNAs, specifically through the miR-22/SIRT1 pathway. Our findings further pave the way for the utilization of salidroside for delaying aging as well as for its clinical application against aging-related degenerative disorders in the future.

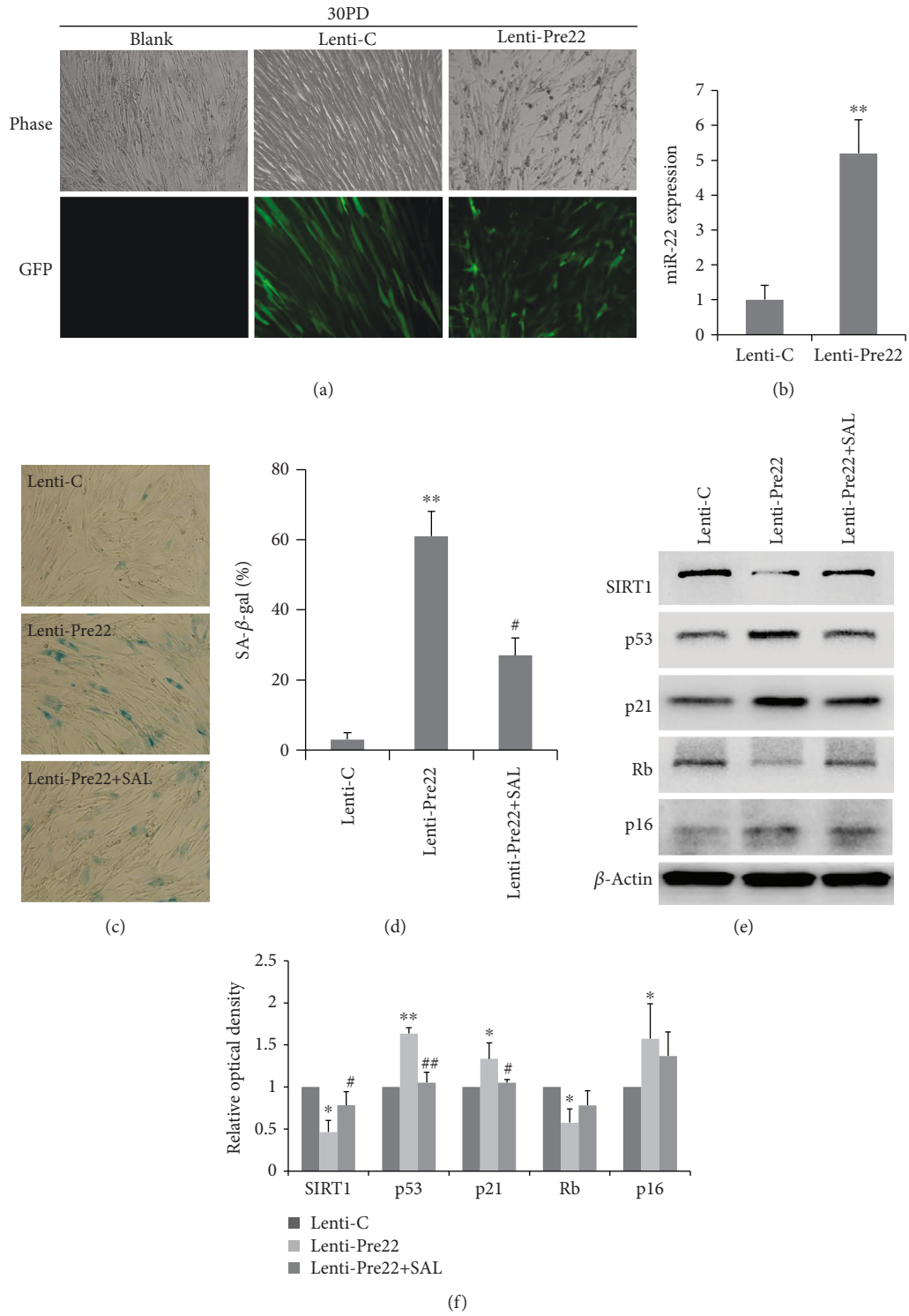


Figure 8: Overexpression of miR22 induces senescence in 30PD 2BS fibroblasts which is partially rescued by salidroside (SAL). (a) Cell morphology was analyzed with fluorescence microscopy at day 3 after infection. GFP-labeled cells indicate infected cells. (b) Relative quantitation of the miR-22 expression in 30PD 2BS cells transfected with Lenti-Pre22 (MOI of 5) was analyzed by qRT-PCR analysis, relative to that in control- (Lenti-C-) transfected cells set at 1. (c) SA-$\beta$-gal activity was analyzed by phase-contrast microscopy at day 4 after infection with control vector (Lenti-C) or Pre-miR-22 (Lenti-Pre22) and effect of SAL (10 $\mu$M) on SA-$\beta$-gal staining in Lenti-Pre22-transfected 2BS cells at 30PD. (d) The percentage of SA-$\beta$-gal-positive cells. (e) The protein expression of SIRT1 and cellular senescence molecules including p53, p21, p16, and Rb in 2BS cells transfected with control vector (Lenti-C) or Pre-miR-22 (Lenti-Pre22) and effect of SAL (10 $\mu$M) Lenti-Pre22-transfected 2BS cells at 30PD. Representative images were acquired from three repeated experiments. (f) Quantitative analysis of the protein levels of SIRT1, p53, p21, Rb, and p16. $^{*}P < 0.05$ versus Lenti-C; $^{**}P < 0.01$ versus Lenti-C; $^{\#}P < 0.05$ versus Lenti-Pre22; $^{\#\#}P < 0.01$ versus Lenti-Pre22.

## Data Availability

The data used to support the findings of this study are available from the corresponding authors upon request.

## Disclosure

Xiao-Gang Xu and San-Ying Wang are co-first authors.

## Conflicts of Interest

The authors declare that they have no conflicts of interest.

## Acknowledgments

This study was supported by the National Natural Science Foundation of China (81771520, 31201040, 31700307, and 31702144), the Science Technology Department of Zhejiang Province (2016C34002), the Natural Science Foundation of Zhejiang Province (LQ16H020006), and funds from the Health Bureau of Zhejiang Province (WKJ2011-2-014, 2015DTA001, 2015KYA001, 2019KY257, 2019RC091, 2019RC093, 2017KY188, and 2017KY189). Dr. Gen-Xiang Mao was an Irma and Paul Milstein Program for Senior Health fellow supported by the MMAAP Foundation (https://www.mmaapf.org/).

## Supplementary Materials

The figure legend for the two figures are as follows: Figure S1: AMPK inhibitor 8-bromo-AMP (8Br-AMP) blocks salidroside- (SAL-) induced increased AMPK$\alpha$-Thr172 phosphorylation (A) and abolished salidroside- (SAL-) or resveratrol- (RES-) induced increment of mitochondrial biogenesis (B) or decreased ROS production in 50PD 2BS cells (C). 8Br-AMP at 50 $\mu$M was added 2 h before SAL (10 $\mu$M) or RES (10 $\mu$M) supplementation in the culture medium and was present for 48 h before harvested. Figure S2: the protein expression of eNOS is undetectable in young 30PD or near-senescent 50PD 2BS fibroblasts when compared to an eNOS-positive expression sample, mouse cardiac tissue homogenate (A). The eNOS inhibitor NG-nitro-L-arginine methyl ester (L-NAME) does not influence the increment of mitochondrial biogenesis (B) or decreased ROS production induced by salidroside (SAL) or resveratrol (RES) in 50PD 2BS cells (C). L-NAME at 200 $\mu$M was added 2 h before SAL (10 $\mu$M) or RES (10 $\mu$M) supplementation in the culture medium and was present for 48 h before harvested. *(Supplementary Materials)*

## References

[1] D. Harman, "Aging: a theory based on free radical and radiation chemistry," *Journal of Gerontology*, vol. 11, no. 3, pp. 298–300, 1956.

[2] L. Guarente, "Mitochondria–a nexus for aging, calorie restriction, and sirtuins?," *Cell*, vol. 132, no. 2, pp. 171–176, 2008.

[3] G. López-Lluch, N. Hunt, B. Jones et al., "Calorie restriction induces mitochondrial biogenesis and bioenergetic efficiency," *Proceedings of the National Academy of Sciences*, vol. 103, no. 6, pp. 1768–1773, 2006.

[4] G. López-Lluch and P. Navas, "Calorie restriction as an intervention in ageing," *The Journal of physiology*, vol. 594, no. 8, pp. 2043–2060, 2016.

[5] A. Csiszar, N. Labinskyy, J. T. Pinto et al., "Resveratrol induces mitochondrial biogenesis in endothelial cells," *American Journal of Physiology Heart and Circulatory Physiology*, vol. 297, no. 1, pp. H13–H20, 2009.

[6] M. Lagouge, C. Argmann, Z. Gerhart-Hines et al., "Resveratrol improves mitochondrial function and protects against metabolic disease by activating SIRT1 and PGC-1alpha," *Cell*, vol. 127, no. 6, pp. 1109–1122, 2006.

[7] J. A. Baur, K. J. Pearson, N. L. Price et al., "Resveratrol improves health and survival of mice on a high-calorie diet," *Nature*, vol. 444, no. 7117, pp. 337–342, 2006.

[8] M. H. Muhammad and M. M. Allam, "Resveratrol and/or exercise training counteract aging-associated decline of physical endurance in aged mice; targeting mitochondrial biogenesis and function," *The Journal of Physiological Sciences*, vol. 68, no. 5, pp. 681–688, 2018.

[9] L. Giovannelli, V. Pitozzi, M. Jacomelli et al., "Protective effects of resveratrol against senescence-associated changes in cultured human fibroblasts," *The Journals of Gerontology: Series A*, vol. 66A, no. 1, pp. 9–18, 2011.

[10] M. Stefani, M. A. Markus, R. C. Y. Lin, M. Pinese, I. W. Dawes, and B. J. Morris, "The effect of resveratrol on a cell model of human aging," *Annals of the New York Academy of Sciences*, vol. 1114, no. 1, pp. 407–418, 2007.

[11] G. López-Lluch, P. M. Irusta, P. Navas, and R. de Cabo, "Mitochondrial biogenesis and healthy aging," *Experimental gerontology*, vol. 43, no. 9, pp. 813–819, 2008.

[12] J. J. Lehman, P. M. Barger, A. Kovacs, J. E. Saffitz, D. M. Medeiros, and D. P. Kelly, "Peroxisome proliferator-activated receptor gamma coactivator-1 promotes cardiac mitochondrial biogenesis," *The Journal of Clinical Investigation*, vol. 106, no. 7, pp. 847–856, 2000.

[13] T. Wenz, "Mitochondria and PGC-1$\alpha$ in aging and age-associated diseases," *Journal of Aging Research*, vol. 2011, Article ID 810619, 12 pages, 2011.

[14] R. C. Scarpulla, "Nuclear control of respiratory chain expression by nuclear respiratory factors and PGC-1-related coactivator," *Annals of the New York Academy of Sciences*, vol. 1147, no. 1, pp. 321–334, 2008.

[15] C. Kang, E. Chung, G. Diffee, and L. L. Ji, "Exercise training attenuates aging-associated mitochondrial dysfunction in rat skeletal muscle: role of PGC-1$\alpha$," *Experimental Gerontology*, vol. 48, no. 11, pp. 1343–1350, 2013.

[16] Y. Guo, P. Li, L. Gao et al., "Kallistatin reduces vascular senescence and aging by regulating microRNA-34a-SIRT1 pathway," *Aging Cell*, vol. 16, no. 4, pp. 837–846, 2017.

[17] J. Williams, F. Smith, S. Kumar, M. Vijayan, and P. H. Reddy, "Are microRNAs true sensors of ageing and cellular senescence?," *Ageing Research Reviews*, vol. 35, pp. 350–363, 2017.

[18] C. M. Gendron and S. D. Pletcher, "MicroRNAs mir-184 and let-7 alter Drosophila metabolism and longevity," *Aging Cell*, vol. 16, no. 6, pp. 1434–1438, 2017.

[19] D. Xu, F. Takeshita, Y. Hino et al., "miR-22 represses cancer progression by inducing cellular senescence," *The Journal of Cell Biology*, vol. 193, no. 2, pp. 409–424, 2011.

[20] G.-X. Mao, H.-B. Deng, L.-G. Yuan, D.-D. Li, Y.-Y. Yvonne Li, and Z. Wang, "Protective role of salidroside against aging in a mouse model induced by D-galactose," *Biomedical and Environmental Sciences*, vol. 23, no. 2, pp. 161–166, 2010.

[21] G.-X. Mao, Y. Wang, Q. Qiu et al., "Salidroside protects human fibroblast cells from premature senescence induced by $H_2O_2$ partly through modulating oxidative status," *Mechanisms of Ageing and Development*, vol. 131, no. 11-12, pp. 723–731, 2010.

[22] G. X. Mao, W. M. Xing, X. L. Wen et al., "Salidroside protects against premature senescence induced by ultraviolet B irradiation in human dermal fibroblasts," *International Journal of Cosmetic Science*, vol. 37, no. 3, pp. 321–328, 2015.

[23] Q. H. Zheng, L. W. Ma, W. G. Zhu, Z. Y. Zhang, and T. J. Tong, "p21Waf1/Cip1 plays a critical role in modulating senescence through changes of DNA methylation," *Journal of Cellular Biochemistry*, vol. 98, no. 5, pp. 1230–1248, 2006.

[24] G. X. Mao, L. D. Zheng, Y. B. Cao et al., "Antiaging effect of pine pollen in human diploid fibroblasts and in a mouse model induced by D-galactose," *Oxidative Medicine and Cellular Longevity*, vol. 2012, Article ID 750963, 10 pages, 2012.

[25] J. Li, Z. Zhang, and T. Tong, "The proliferative response and anti-oncogene expression in old 2BS cells after growth factor stimulation," *Mechanisms of Ageing and Development*, vol. 80, no. 1, pp. 25–34, 1995.

[26] G. P. Dimri, X. Lee, G. Basile et al., "A biomarker that identifies senescent human cells in culture and in aging skin in vivo," *Proceedings of the National Academy of Sciences*, vol. 92, no. 20, pp. 9363–9367, 1995.

[27] M. Reers, T. W. Smith, and L. B. Chen, "J-aggregate formation of a carbocyanine as a quantitative fluorescent indicator of membrane potential," *Biochemistry*, vol. 30, no. 18, pp. 4480–4486, 1991.

[28] K. Abdelmohsen, R. Pullmann Jr., A. Lal et al., "Phosphorylation of HuR by Chk2 regulates SIRT1 expression," *Molecular cell*, vol. 25, no. 4, pp. 543–557, 2007.

[29] A. D. Napper, J. Hixon, T. McDonagh et al., "Discovery of indoles as potent and selective inhibitors of the deacetylase SIRT1," *Journal of Medicinal Chemistry*, vol. 48, no. 25, pp. 8045–8054, 2005.

[30] X. Wang, N. L. Buechler, B. K. Yoza, C. E. McCall, and V. T. Vachharajani, "Resveratrol attenuates microvascular inflammation in sepsis via SIRT-1-induced modulation of adhesion molecules in *ob*/*ob* mice," *Obesity*, vol. 23, no. 6, pp. 1209–1217, 2015.

[31] P. Wang, C. Lv, T. Zhang et al., "FOXQ1 regulates senescence-associated inflammation via activation of SIRT1 expression," *Cell Death & Disease*, vol. 8, no. 7, article e2946, 2017.

[32] L. Guarente, "Sirtuins in aging and disease," *Cold Spring Harbor Symposia on Quantitative Biology*, vol. 72, no. 1, pp. 483–488, 2007.

[33] J. A. Baur and D. A. Sinclair, "Therapeutic potential of resveratrol: the in vivo evidence," *Nature Reviews Drug Discovery*, vol. 5, no. 6, pp. 493–506, 2006.

[34] K. Barhwal, S. K. Das, A. Kumar, S. K. Hota, and R. B. Srivastava, "Insulin receptor A and sirtuin 1 synergistically improve learning and spatial memory following chronic salidroside treatment during hypoxia," *Journal of Neurochemistry*, vol. 135, no. 2, pp. 332–346, 2015.

[35] Z. Qi, Y. Zhang, S. Qi et al., "Salidroside inhibits HMGB1 acetylation and release through upregulation of SirT1 during inflammation," *Oxidative Medicine and Cellular Longevity*, vol. 2017, Article ID 9821543, 11 pages, 2017.

[36] K. C. Lan, S. C. Chao, H. Y. Wu et al., "Salidroside ameliorates sepsis-induced acute lung injury and mortality *via* downregulating NF-$\kappa$B and HMGB1 pathways through the upregulation of SIRT1," *Scientific reports*, vol. 7, no. 1, article 12026, 2017.

[37] R. M. Reznick, H. Zong, J. Li et al., "Aging-associated reductions in AMP-activated protein kinase activity and mitochondrial biogenesis," *Cell Metabolism*, vol. 5, no. 2, pp. 151–156, 2007.

[38] W. Qiang, K. Weiqiang, Z. Qing, Z. Pengju, and L. Yi, "Aging impairs insulin-stimulated glucose uptake in rat skeletal muscle via suppressing AMPK$\alpha$," *Experimental & molecular medicine*, vol. 39, no. 4, pp. 535–543, 2007.

[39] L. Ju, X. Wen, C. Wang et al., "Salidroside, a natural antioxidant, improves $\beta$-cell survival and function via activating AMPK pathway," *Frontiers in Pharmacology*, vol. 8, p. 749, 2017.

[40] T. Zheng, X. Yang, D. Wu et al., "Salidroside ameliorates insulin resistance through activation of a mitochondria-associated AMPK/PI3K/Akt/GSK3$\beta$ pathway," *British Journal of Pharmacology*, vol. 172, no. 13, pp. 3284–3301, 2015.

[41] N. Musi, T. Hayashi, N. Fujii, M. F. Hirshman, L. A. Witters, and L. J. Goodyear, "AMP-activated protein kinase activity and glucose uptake in rat skeletal muscle," *American Journal of Physiology Endocrinology and Metabolism*, vol. 280, no. 5, pp. E677–E684, 2001.

[42] S. J. Park, F. Ahmad, A. Philp et al., "Resveratrol ameliorates aging-related metabolic phenotypes by inhibiting cAMP phosphodiesterases," *Cell*, vol. 148, no. 3, pp. 421–433, 2012.

[43] W. M. XING, S. S. CHEN, S. Y. WANG et al., "Salidroside reduces PDE2A expression by down-regulating p53 in human embryonic lung fibroblast," *Biomedical and environmental sciences*, vol. 32, no. 2, pp. 140–143, 2019.

[44] D. Fiore, D. Gianfrilli, E. Giannetta et al., "PDE5 inhibition ameliorates visceral adiposity targeting the miR-22/SIRT1 pathway: evidence from the CECSID trial," *The Journal of clinical endocrinology and metabolism*, vol. 101, no. 4, pp. 1525–1534, 2016.

[45] E. Nisoli, "Calorie restriction promotes mitochondrial biogenesis by inducing the expression of eNOS," *Science*, vol. 310, no. 5746, pp. 314–317, 2005.

[46] S. Xing, X. Yang, W. Li et al., "Salidroside stimulates mitochondrial biogenesis and protects against $H_2O_2$-induced endothelial dysfunction," *Oxidative Medicine and Cellular Longevity*, vol. 2014, Article ID 904834, 13 pages, 2014.

[47] V. Jazbutyte, J. Fiedler, S. Kneitz et al., "MicroRNA-22 increases senescence and activates cardiac fibroblasts in the aging heart," *Age*, vol. 35, no. 3, pp. 747–762, 2013.

[48] Z. Liu, T. Li, S.'n. Deng, S. Fu, X. Zhou, and Y. He, "Radiation induces apoptosis and osteogenic impairment through miR-22-mediated intracellular oxidative stress in bone marrow mesenchymal stem cells," *Stem Cells International*, vol. 2018, Article ID 5845402, 16 pages, 2018.

[49] L. Wang, Z. P. Tang, W. Zhao et al., "MiR-22/Sp-1 links estrogens with the up-regulation of cystathionine $\gamma$-lyase in myocardium, which contributes to estrogenic cardioprotection against oxidative stress," *Endocrinology*, vol. 156, no. 6, pp. 2124–2137, 2015.

[50] X. Huang, S. Xing, C. Chen, Z. Yu, and J. Chen, "Salidroside protects PC12 cells from A$\beta$1-40-induced cytotoxicity by regulating the nicotinamide phosphoribosyltransferase signaling pathway," *Molecular Medicine Reports*, vol. 16, no. 3, pp. 2700–2706, 2017.

[51] K. Saihara, R. Kamikubo, K. Ikemoto, K. Uchida, and M. Akagawa, "Pyrroloquinoline quinone, a redox-active o-quinone, stimulates mitochondrial biogenesis by activating the SIRT1/PGC-1$\alpha$ signaling pathway," *Biochemistry*, vol. 56, no. 50, pp. 6615–6625, 2017.

Hindawi
Oxidative Medicine and Cellular Longevity
Volume 2019, Article ID 6379493, 14 pages
https://doi.org/10.1155/2019/6379493

*Research Article*

# Effects of Lycium barbarum Polysaccharides on Health and Aging of *C. elegans* Depend on *daf-12/daf-16*

**Zhaokang Zhang,[1] Yannan Zhou,[1] Haitao Fan,[2] Kirunda John Billy,[1] Yunjie Zhao,[1] Xuan Zhan,[1] Lijian Yang,[1] and Ya Jia[1]**

[1]*Institute of Biophysics and Department of Physics, Central China Normal University, Wuhan 430079, China*
[2]*College of Bioengineering, Beijing Polytechnic, Beijing 100029, China*

Correspondence should be addressed to Lijian Yang; janeyang@mail.ccnu.edu.cn and Ya Jia; jiay@mail.ccnu.edu.cn

Received 25 April 2019; Revised 4 July 2019; Accepted 7 August 2019; Published 10 September 2019

Guest Editor: Myon-Hee Lee



As the global population ages, searching for drugs and functional foods which can slow down the aging process has attracted a number of researchers. In this paper, the Lycium barbarum polysaccharides (LBP) extracted from Lycium barbarum was characterized and the effects of LBP on the aging and health of *C. elegans* were studied. Results showed that LBP can prolong the lifespan, improve the abilities to withstand environmental stress, enhance reproductive potentials, and maintain muscle integrity of *C. elegans*. By using genetically mutated *C. elegans* strains, RNAi gene silencing, and measuring the mRNA expression level, it was demonstrated that the lifespan of *C. elegans* was extended by LBP mainly through *sir-2.1*, *daf-12*, and *daf-16*. The present study might provide a basis for further study of LBP as a food or drug to interfere with aging and reduce the incidence of age-related diseases.

## 1. Introduction

Aging is defined by the time-dependent functional decline of living organisms, during which the self-renewal and repair abilities of the organism are weakened [1]. Aging is often accompanied by a gradual decline in environmental adaptability, deterioration of physiological functions, and increase of vulnerability to diseases (such as hardening of the arteries, cancer, and Alzheimer's disease) [1, 2]. As the global population ages, searching for drugs, which can treat age-related diseases, slow down the normal aging process, and prolong lifespan, is an important aspect of current aging researches [3–5]. In addition, genetic pathways that regulate the lifespan have been shown to be evolutionarily conserved; therefore, revealing the molecular mechanism of using drugs to extend the lifespan of *C. elegans* can help to better understand the biological mechanisms related to lifespan [6].

As people pay more attention to the quality of life, it is more and more popular to choose drugs and functional foods which may reduce the risk of death. Therefore, a traditional Chinese herb, Lycium barbarum, has become the focus of many studies [7]. Lycium barbarum is widely grown in the western and northern regions of China (such as Gansu province, Ningxia province) [8]. It is generally used to improve vision, nourish the liver and kidneys, and delay aging [9, 10]. Due to its excellent health care function, it has been very popular not only in Asia but also in other continents [11, 12]. Recent medical research has shown that Lycium barbarum contains a variety of nutrients, with Lycium barbarum polysaccharides (LBP) as one of its main active ingredients [13].

The LBP can usually be obtained by water extraction and alcohol precipitation, ultrasonic assistance, or enzymatic hydrolysis [14]. It was reported that the main pharmacological effects of LBP include regulating immunity [15, 16], blood sugar, and lipids [17]; preventing tumors [18, 19]; and delaying aging [20–25]. By analyzing the expression levels of interleukin-2 and tumor necrosis factor-alpha-related mRNA and protein in human peripheral blood mononuclear cells, Gan et al. [15] showed that LBP can increase the activity of interleukin-2 and tumor necrosis

factor-alpha, which can induce the immune responses. Chen et al. [16] revealed that LBP can enhance the ability of dendritic cells to respond to Th1 and Th2 and then enhance hosts' immunity. By feeding mice with food of different fat contents and LBP, Ma et al. [17] found that LBP has no significant effect on the body weight of the mouse but significantly reduces blood lipids, lowers blood glucose, and inhibits lipid oxidation. Gan et al. [18] reported that feeding LBP to the mice inoculated with sarcoma S180 cells can inhibit the growth of the sarcoma S180, increase the immunity, improve the phagocytic function of macrophages, and proliferate spleen lymphocytes; thus, LBP can prevent tumors in the mouse. Luo et al. [19] demonstrated that LBP can induce apoptosis of prostate cancer cells (PC-3 and DU-145) in in vitro cell culture and inhibit the growth of prostate cancer in the nude mouse xenograft tumor model.

Up to now, the investigations on the effects of LBP on the aging process have been focused on eliminating free radicals and delaying skin aging [20–25]. In various antioxidant systems in vitro, Li et al. [20] indicated that LBP has the function of antioxidant remedies, such as inhibition of 1,1,2-diphenyl-2-picrylhydrazyl (DPPH) free radicals, superoxide scavenging ability, hydrogen peroxide-mediated erythrocyte hemolysis, and ferrous ion sequestration in mice. Lin et al. [21] showed that LBP can effectively scavenge DPPH and ABTS+ free radicals, superoxide anion, and hydroxyl radical. Tian et al. [22] reported that LBP can enhance the antioxidation capacity of chicken embryo liver cells, via resisting the decrease of the activity of chicken embryo liver cells induced by $H_2O_2$, reducing the ROS content and promoting the activity of antioxidant enzymes. Liang and Zhang [23] proved that LBP can delay skin aging through significantly increasing skin water content, skin thickness, subcutaneous thickness, and fibroblast count of the mice and improving the tissue of decayed skin. However, there is little direct evidence that the LBP can extend lifespan.

In this paper, the LBP used was extracted from Ningxia Lycium barbarum. First, we characterized the molecular weight distribution, monosaccharide composition, and infrared absorption spectrum of LBP. Then, the effects of LBP on lifespan and health of *C. elegans* were investigated and it was shown that LBP extends the lifespan, improves the abilities to withstand environmental stress, boosts reproductive potentials, and maintains muscle integrity. Finally, by using genetic mutated *C. elegans* strains, RNAi gene silencing, and examining mRNA expression level, our results revealed that the LBP extended lifespan mainly through *sir-2.1*, *daf-12*, and *daf-16*.

## 2. Materials and Methods

*2.1. Preparation of LBP.* The LBP from Ningxia Lycium barbarum was prepared by water extraction, alcohol precipitation, deproteinization, and recrystallization. In brief, the fruits of Ningxia Lycium barbarum were vacuum dried in a vacuum drying oven at 60°C, taken out, and placed in a desiccator for 24 h. We took 10 g of the crushed element and placed it in a normal reflux device, then added 20 ml chloroform+methanol in the ratio of 2 : 1 each time. We degreased twice at 60°C. Filtration was done, the liquid was discarded, and the residue was vacuum dried. Then, 20 ml of 80% ethanol was added and the mixture was refluxed twice at 60°C to recover ethanol. After that, the mixture was extracted twice with water at 60°C, with the liquid-solid ratio being 1 : 20. The resultant compound was concentrated, precipitated 4 times with 95% ethanol, and kept in the oven for 24 hours. Filtration was then done by suction. The product was washed with 95% ethanol, absolute ethanol, and acetone, then vacuum dried (50°C) to obtain a crude powder of LBP. Finally, the product was deproteinized and recrystallized.

*2.2. Characterization of LBP*

*2.2.1. Chemical Composition Analysis.* We measured the carbohydrate content of LBP by phenol-sulfuric acid method [26], determined the content of uronic acid by m-hydroxydiphenyl method [27], and then detected the protein content by BCA method. The retention time (RT) of the dextran standard was determined by HPLC-GPC, and a standard curve was drawn. The HPLC-GPC was then used to detect the molecular weight distribution of the LBP.

*2.2.2. Determination of the Composition of LBP Monosaccharides.* 5 mg of LBP was dissolved in 2 mol/L TFA, hydrolyzed at 99°C for 5 h, removed with acid by rotary distillation, and then added 0.5 ml of 4% sodium borohydride solution. The resultant solution was placed at room temperature for 1.5 h and added acetic acid dropwise until no bubbles were generated, and then, the concentration process was repeated. Next, the concentrated sample was vacuum dried, 1 ml of pyridine and n-propylamine was added, and the mixture was placed in a water bath at 55°C for 30 min. The mixture was vacuum dried, 0.5 ml of pyridine and acetic anhydride was added followed by heating at 95°C for 1 h, blown dried with nitrogen, and vacuum dried. The mixture was then dissolved in chloroform for GC-MS analysis.

*2.2.3. Determination of FT-IR Spectra.* The LBP was mixed with potassium bromide powder and pressed into millimeter-sized sheets, and the FT-IR spectrum of LBP was recorded by using the Fourier transform infrared spectrometer in the frequency range of 4000-500 $cm^{-1}$.

*2.3. Strains and Culture. C. elegans* strains (N2 (wild type), BA17 (fem-1(hc17) IV.), VC199 (sir-2.1(ok434) IV.), GR1307 (daf-16(mgDf50) I.), CF1038 (daf-16(mu86) I.), and DR1407 (daf-12(m583) X.)) were obtained from the Caenorhabditis Genetics Center which is supported by the National Institutes of Health and from Professor Huairong Luo, Southwest Medical University. *E. coli* OP50 was provided by Professor Zhengxing Wu, Huazhong University of Science and Technology. The other bacterial strains were obtained from Professor Ge Shan, University of Science and Technology of China, and from Professor Huairong Luo. Strains were kept at 25°C according to standard methods, cultured on NGM plates, and seeded with *E. coli* OP50 [28].

*2.4. Lifespan Analysis.* The worms synchronized to the L4 stage were picked and provided with enough *E. coli* OP50 as food on ordinary NGM plates with different concentrations

of LBP. These NGM plates had 25 $\mu$M 5-fluoro-2′-deoxyuridine (FUdR), and we replaced any NGM plate when eggs were found during the experimental process. Worms were observed every 24 hours until all of them were dead. Worms were scored dead if they did not move when gently touched by the worm picker. Those that disappeared from the plate and died prematurely from internal hatching or vulval rapture were excluded from the analysis.

For lifespan experiments involving RNAi, HT115 bacteria containing an empty vector L4440 or RNAi plasmid were used instead of *E. coli* OP50 on NGM plates (these NGM plates contained carbenicillin (25 mg/ml) and IPTG (1 mM), excluding FUdR) and the other operations were the same as mentioned above. The bacteria for RNAi were from the Ahringer library.

*2.5. Lifespan under Different Stressors.* Worm culture for the following assays was the same as in the previous ordinary lifespan assay. After 5 days, respective stress analyses were done as follows: (a) For the heat stress assay, worms were transferred to new corresponding NGM plates. Then, their survival at 37°C was monitored every 2 hours until they were all dead. (b) For the osmotic, metal, and oxidative stress analysis, worms were transferred to S-buffer solutions (0.5 M $KH_2PO_4$, 0.5 M $K_2HPO_4$, and 0.1 M NaCl) containing 300 mM NaCl (for osmotic stress), 50 $\mu$M $CdCl_2$ (for metal stress), and 30 mM $H_2O_2$ (for oxidative stress). Then, the survival was monitored hourly until all of worms died.

*2.6. Self-Brood Size and Egg Production Rate.* After bleaching, L1 stage worms were placed on the NGM plates seeded with enough *E. coli* OP50 and with different concentrations of LBP. After worms developed to the L4 stage, they were transferred to their new corresponding NGM plate every day until the cessation of egg production. A single worm was cultured on an individual NGM plate. The number of eggs produced was determined by the progeny size.

*2.7. Motility Measurement.* Worm culturing was the same as in the ordinary lifespan assay. Motility was measured on day 1 (L4 stage), day 6, day 11, and day 16. The animal's motile ability is divided into three categories A, B, or C [29]. Worms which can spontaneously move sinusoidally are put in Class A. On stimulation, worms that are unable to move sinusoidally but can still move belong to Class B. Worms that can only move the head or the tail on stimulation are placed in Class C.

*2.8. Determination of Antioxidant Enzyme Activity and ROS Content.* Worm culturing was the same as in the ordinary lifespan assay (all the NGM plates had 150 $\mu$M FUdR). On day 5, the NGM plates were washed with S-buffer and the worms were collected in an EP tube. The worms were washed 3 times with sterile physiological saline, and sterile physiological saline was added. The mixture was homogenized on ice and centrifuged, and the supernatant was taken for use. A portion of the product was mixed with a DCFDA probe solution or according to the SOD/CAT kit instructions, and the fluorescence was measured using a fluorescent plate reader. Simultaneously, the other portion of the product was used for determining protein concentration with the BCA method. The relative values of the control and test groups were determined by calculating the fluorescence values of the unit protein concentration.

Table 1: qPCR primer sequence.

| Primer name | | Primer sequence |
|---|---|---|
| act-1 | F | 5′-CTACGAACTTCCTGACGGACAAG-3′ |
| | R | 5′-CCGGCGGACTCCATACC-3′ |
| sir-2.1 | F | 5′-GCAACGATTCAGAAGTTGCG-3′ |
| | R | 5′-TGTGCATAGAACCGATTTCTGG-3′ |
| daf-16 | F | 5′-ATCGTGTGCTCAGAATCC-3′ |
| | R | 5′-ATGAATAGCTGCCCTCC-3′ |
| daf-12 | F | 5′-AAACGAAGAACAACTGCGGC-3′ |
| | R | 5′-TGTGGTGACTGCTGATTCCC-3′ |

Table 2: Chemical compositions of LBP.

| No. | Compositions | Percentage of quality (%) |
|---|---|---|
| 1 | Carbohydrate | 79.24 ± 1.75 |
| 2 | Uronic acid | 1.33 ± 0.16 |
| 3 | Protein content | 1.37 ± 0.11 |
| 4 | Starch | (-) |

*2.9. Relative Expression of mRNA Analysis.* Worms were cultured in the same way as in the ordinary lifespan assay. On day 5, the NGM plates were washed with S-buffer and the worms were collected in an EP tube. We washed the worms 3 times with S-buffer, and RNA was extracted by the rapid freeze-thaw lysis and TRIzol/chloroform method. Then, RNA was reverse transcribed into cDNA. The relative expression levels of the genes were detected using the real-time PCR according to the SYBR green Mix instructions. *act-1* gene was used as the internal reference gene. There were three setups for each gene to be tested, and the entire experiment was repeated three or more times. The primers used for PCR are shown in Table 1.

*2.10. Statistical Analysis.* All tests were repeated at least three times. Mean lifespan was defined as the average lifespan, and the error was the standard deviation from multiple results. Log-rank test was used to obtain the mean lifespan and the corresponding $P$ values. Maximum lifespan was the average lifespan of 10% longest worms, and the error was the standard deviation of multiple results. The number of eggs was the average of multiple outcomes with an error of the standard deviation from each individual. Others were multiple experimental means and standard deviations. Softwares Origin8, SPSS-22, and GraphPad Prism 8.1.2 were used for statistical analysis and plotting of the experimental data. $P < 0.05$ for significant differences, and $P < 0.01$ for extremely significant differences in hypothesis test analysis.

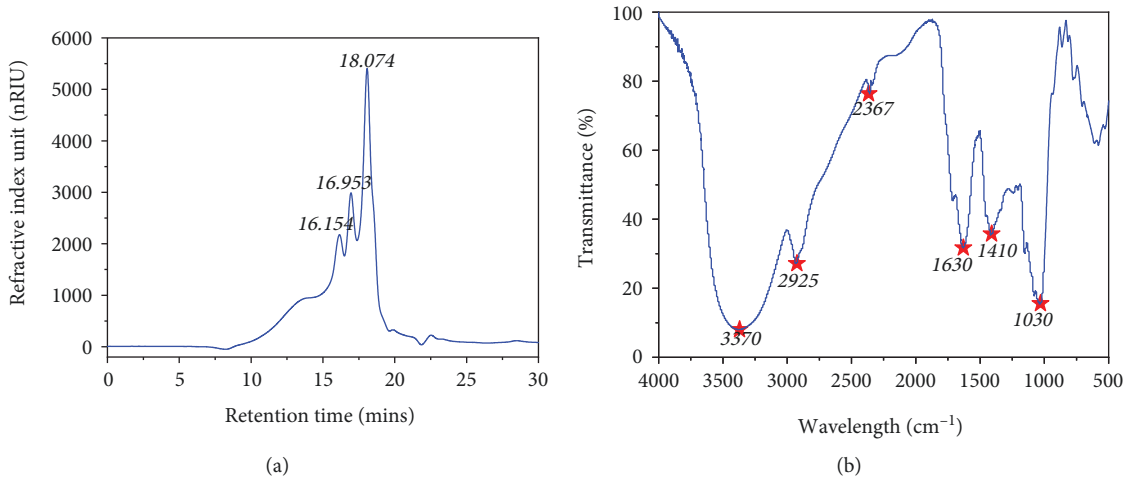


Figure 1: Characterization of LBP. (a) HPLC-GPC detection chromatogram of LBP. (b) Infrared spectra of LBP.

Table 3: Mw of main component peaks of LBP.

| No. | Retention times (mins) | Mw (Da) |
|---|---|---|
| 1 | 16.15 | 4.31*E*+03 |
| 2 | 16.95 | 1.91*E*+03 |
| 3 | 18.07 | <1000 |

## 3. Results

*3.1. Chemical Composition of LBP.* LBP had a carbohydrate content of 79.24% ± 1.75%, a protein content of 1.37% ± 0.11%, uronic acid content of 1.33 ± 0.16, and iodization reaction without starch (Table 2). After hydrolysis, it is found by GC-MS analysis that the monosaccharide composition of LBP consisted of mannose, glucose, and galactose in a molar ratio of 1.5 : 118 : 1. The HPLC-GPC chromatogram of LBP revealed that the molecular weight of LBP is composed of 4310 Da, 1910 Da, and less than 1000 Da, with a respective retention time of 16.15, 16.95, and 18.07 minutes (Figure 1(a), Table 3).

The FT-IR spectra of LBP demonstrate that LBP has a predominant carbohydrate composition (Figure 1(b)). Among the spectra, one peak (gently broad) approximately at 3370 cm$^{-1}$ may be a characteristic vibration peak of the hydroxyl group. There is a peak caused by C-H vibration at about 2930 cm$^{-1}$. A weak peak at around 2400 cm$^{-1}$ is caused by $CO_2$ in the air. 1630 cm$^{-1}$ has a relatively sharp peak caused by carboxyl groups. A weak peak at around 1410 cm$^{-1}$ is caused by C-H. A series of peaks in the range of 1000-1250 cm$^{-1}$ might be the (C-O-C) glycosidic band vibrations and ring vibrations overlapped with the C-OH. There are a series of peaks in the range of 820-950 cm$^{-1}$ that can be the small amount of $\beta$-configuration sugar, small amount of mannose, and $\alpha$-D-glucose.

*3.2. LBP Can Extend the Lifespan of C. elegans.* Lifespan is a very important indicator for measuring aging. Our study shows that for wild-type (N2) and BA17 worm strains, 300 $\mu$g/ml LBP is the best concentration for lifespan extension which is temperature independent (Figures 2(a)–2(d), Table 4). At 25°C, the mean lifespan of N2 (control group) was 14.38 ± 0.30 days and the maximum lifespan was 19.64 ± 0.54 days, while the mean lifespan of N2 cultured with 300 $\mu$g/ml LBP was 17.36 ± 0.24 days and the maximum lifespan was 21.99 ± 0.94 days. The results (Figures 2(a) and 2(b)) show that when feeding 300 $\mu$g/ml LBP, the average lifespan expectancy and maximum lifespan of N2 are significantly extended by 20.72% and 21.69%, respectively. Under different concentrations of LBP, it can be seen that the best concentration for extending lifespan was 300 $\mu$g/ml, while the extensions were not linearly related to the concentration (Figure 2(a)). BA17 worms were temperature-sensitive mutant, and they will develop into sterile adults at 25°C. Since egg production complicates survival analysis, sterile BA17 worms are also used here. Survival curves of BA17 worms cultured with or without LBP were displayed in Figure 2(c). It is shown that 300 $\mu$g/ml LBP can prolong the lifespan of BA17 worms significantly (Table 4). Therefore, LBP can extend lifespan regardless whether reproductive function is minimized or not. Temperature is important for the survival of organisms; therefore, worms were also cultured with 300 $\mu$g/ml LBP at 20°C (Figure 2(d), Table 4). Regardless of varying temperatures at 20°C or 25°C, cultures with 300 $\mu$g/ml LBP significantly extended lifespan, so this suggests that the effect of LBP on extending lifespan is independent of temperature.

The F1 offspring of N2 from plates with 300 $\mu$g/ml LBP was transferred to new NGM plates without LBP, and their lifespan is compared with that of control N2. As shown in Figures 3(a) and 3(b), their lifespans were essentially the same and this implies that the effects of LBP lifespan extension cannot be inherited. In order to investigate whether LBP affects the lifespan on a particular stage of development, worms were divided into four groups (Figure 3(c), Table 4). We found that no matter whether the N2 worms were grown on plates with or without LBP before L4, there was no significant effect on the lifespan (Figures 3(c) and 3(d), Table 4).

*3.3. LBP Can Improve the Health of C. elegans.* Animals are considered to be healthy if they have the ability to withstand

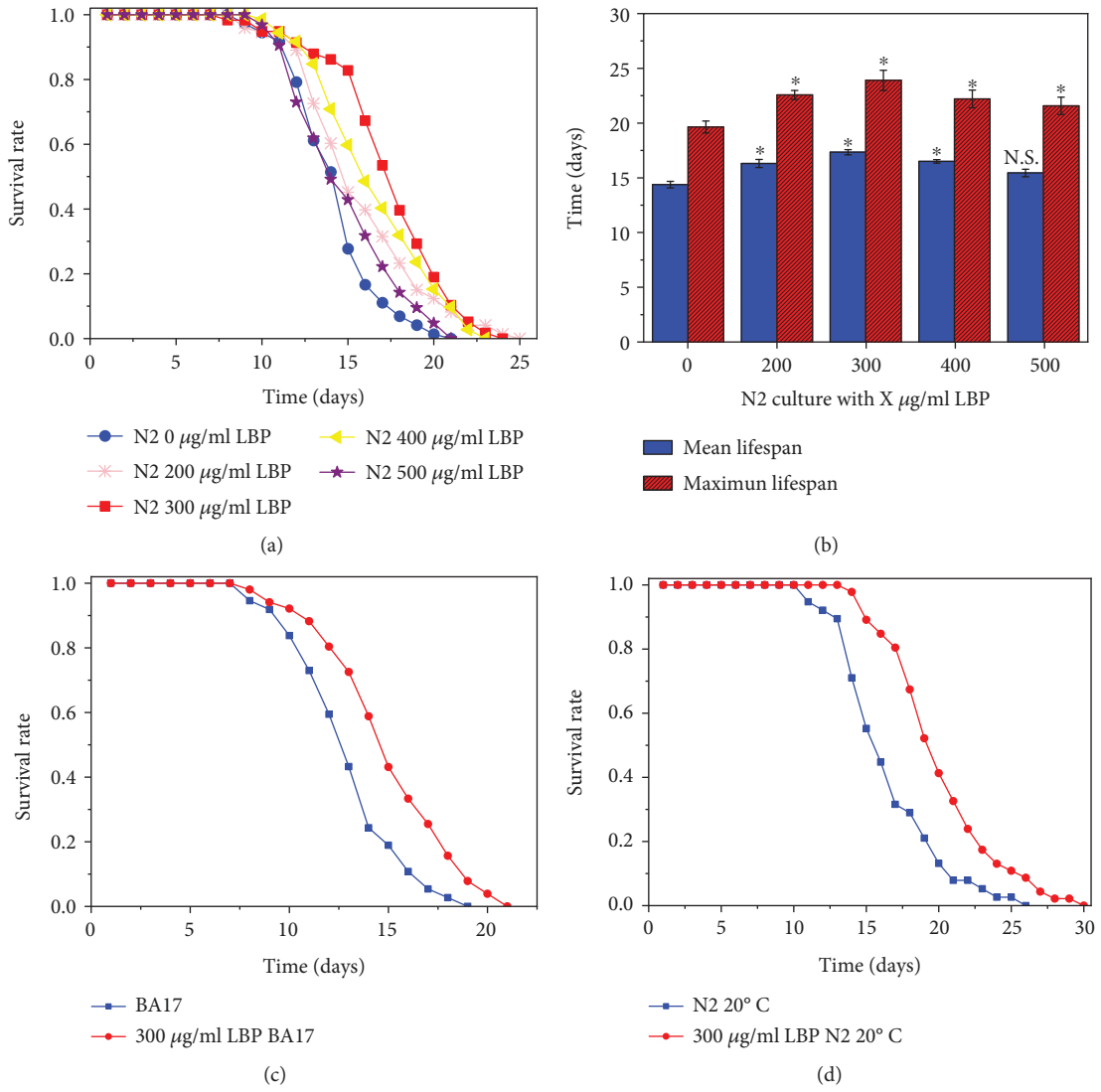


Figure 2: LBP can extend the lifespan of *C. elegans*. (a) At 25°C, *C. elegans* longevity was cultured at different concentrations of LBP and survival was monitored. (b) At 25°C, the mean lifespan and maximum lifespan of *C. elegans* were cultured at different concentrations of LBP. (c) At 25°C, BA17 mutant longevity was cultured with or without LBP and survival was monitored. (d) At 20°C, the survival of *C. elegans* was cultured with or without LBP. Not significant was abbreviated as N.S., $^*P < 0.05$.

environmental stresses. As can be seen from Figure 4, the lifespan of N2 cultured with 300 $\mu$g/ml LBP was longer than that of the control group in heat stress, oxidative stress, and heavy metal stress, while it was almost the same as that of the control group under osmotic stress. In other words, LBP can improve the ability of *C. elegans* to resist high environmental temperature, enhance antioxidation responses, and boost heavy metal stress resistance, but with no impact on osmotic stress. We also measured the ROS, SOD, and CAT levels in the worm, and the consistent results suggested that LBP can enhance antioxidation responses of *C. elegans*. ROS is the most important factor causing oxidative damage, so the lower the total ROS level in the body, the stronger the antioxidant activity. As the main antioxidant in the body, the enzyme SOD mainly removes excess superoxide radicals from the body. CAT acts as a major peroxidase to promote the breakdown of $H_2O_2$ into molecular oxygen and water and get rid of hydrogen peroxide from the body, thereby protecting cells from $H_2O_2$ toxicity. Levels of both CAT and SOD represent the antioxidative capacities of the organism, i.e., the higher their levels, the stronger the antioxidation capacity. We found that N2 cultured with 300 $\mu$g/ml LBP had lower ROS levels and higher levels of SOD and CAT (Figure 4(e)). These results were consistent with earlier results that revealed enhanced resistant to different environmental stresses.

Self-brood size and egg production rate are the embodiments of reproductive ability which is a key parameter to quantify health. We evaluated the progeny size and egg production rate of the worms at 25°C and 20°C. We found that N2 cultured with 300 $\mu$g/ml LBP had a higher egg production rate than those of the control group at 25°C and 20°C (Figures 5(a) and 5(b)). At 25°C, the self-brood size was $121.81 \pm 20.40$ against $108.77 \pm 19.17$ for the control group,

Table 4: Summary of all lifespan experiments shown in this work.

| No. | Strains | Bacteria | LBP ($\mu$g/ml) | Temperature (°C) | Mean lifespan (days) | Max. lifespan (days) | Compared with no. | $P$ (log-rank test) |
|---|---|---|---|---|---|---|---|---|
| 1 | N2 | *E. coli* OP50 | 0 | 25 | 14.38 ± 0.30 | 19.64 ± 0.54 | / | / |
| 2 | N2 | *E. coli* OP50 | 50 | 25 | 15.30 ± 0.30 | 20.98 ± 0.29 | 1 | 0.1393 |
| 3 | N2 | *E. coli* OP50 | 100 | 25 | 15.84 ± 0.39 | 21.99 ± 0.94 | 1 | 0.0368 |
| 4 | N2 | *E. coli* OP50 | 200 | 25 | 16.31 ± 0.37 | 22.57 ± 0.41 | 1 | 0.0013 |
| 5 | N2 | *E. coli* OP50 | 300 | 25 | 17.34 ± 0.24 | 23.90 ± 0.92 | 1 | <0.0001 |
| 6 | N2 | *E. coli* OP50 | 400 | 25 | 16.50 ± 0.16 | 22.20 ± 0.81 | 1 | <0.0001 |
| 7 | N2 | *E. coli* OP50 | 500 | 25 | 15.44 ± 0.34 | 21.57 ± 0.79 | 1 | 0.1592 |
| 8 | BA17 | *E. coli* OP50 | 0 | 25 | 12.89 ± 0.36 | 17.73 ± 0.48 | / | / |
| 9 | BA17 | *E. coli* OP50 | 300 | 25 | 15.18 ± 0.23 | 19.82 ± 0.41 | 8 | 0.0006 |
| 10 | N2 | *E. coli* OP50 | 0 | 20 | 16.98 ± 0.52 | 24.60 ± 0.73 | / | / |
| 11 | N2 | *E. coli* OP50 | 300 | 20 | 19.83 ± 0.35 | 27.33 ± 0.94 | 10 | <0.0001 |
| 12 | N2 | *E. coli* OP50 | 0 (mother worms: 0) | 25 | 14.10 ± 0.27 | 20.15 ± 0.72 | / | / |
| 13 | N2 | *E. coli* OP50 | 0 (mother worms: 300) | 25 | 13.92 ± 0.30 | 19.92 ± 0.92 | 12 | 0.6266 |
| 14 | N2 | *E. coli* OP50 | 0 | 25 | 14.21 ± 0.47 | 19.33 ± 1.09 | / | / |
| 15 | N2 | *E. coli* OP50 | L1-L4: 300<br>L4: 0 | 25 | 14.02 ± 0.70 | 18.91 ± 0.84 | 14 | 0.9505 |
| 16 | N2 | *E. coli* OP50 | L1-L4: 0<br>L4: 300 | 25 | 17.22 ± 0.30 | 23.64 ± 0.94 | 14 | <0.0001 |
| 17 | N2 | *E. coli* OP50 | 300 | 25 | 17.15 ± 0.47 | 23.57 ± 0.66 | 16 | 0.8412 |
| 18 | *sir-2.1* | *E. coli* OP50 | 0 | 25 | 11.64 ± 0.41 | 16.78 ± 0.35 | / | / |
| 19 | *sir-2.1* | *E. coli* OP50 | 300 | 25 | 13.18 ± 0.92 | 18.21 ± 0.46 | 18 | <0.0001 |
| 20 | *daf-16* (mu86) | *E. coli* OP50 | 0 | 25 | 9.79 ± 0.85 | 14.11 ± 0.51 | / | / |
| 21 | *daf-16* (mu86) | *E. coli* OP50 | 300 | 25 | 10.98 ± 0.08 | 15.33 ± 0.67 | 20 | 0.0126 |
| 22 | *daf-16* (Df50) | *E. coli* OP50 | 0 | 25 | 9.45 ± 0.66 | 13.67 ± 0.34 | / | / |
| 23 | *daf-16* (Df50) | *E. coli* OP50 | 300 | 25 | 11.16 ± 0.66 | 15.80 ± 0.50 | 22 | 0.001 |
| 24 | N2 | *daf-16* RNAi | 0 | 25 | 9.78 ± 0.51 | 14.95 ± 0.63 | / | / |
| 25 | N2 | *daf-16* RNAi | 300 | 25 | 10.99 ± 0.21 | 16.11 ± 0.51 | 24 | 0.0095 |
| 26 | *sir-2.1* | *daf-16* RNAi | 300 | 25 | 10.89 ± 0.66 | 15.81 ± 1.17 | 25 | 0.4269 |
| 27 | *daf-12* | *E. coli* OP50 | 0 | 25 | 12.54 ± 0.51 | 18.05 ± 0.54 | / | / |
| 28 | *daf-12* | *E. coli* OP50 | 300 | 25 | 13.86 ± 0.78 | 20.82 ± 0.50 | 27 | 0.0033 |
| 29 | *daf-16* | *daf-12* RNAi | 0 | 25 | 9.47 ± 0.46 | 13.64 ± 0.13 | / | / |
| 30 | *daf-16* | *daf-12* RNAi | 300 | 25 | 9.73 ± 0.40 | 14.75 ± 1.54 | 29 | 0.7915 |
| 31 | *daf-12* | *daf-16* RNAi | 0 | 25 | 9.37 ± 0.66 | 13.56 ± 0.51 | / | / |
| 32 | *daf-12* | *daf-16* RNAi | 300 | 25 | 9.40 ± 0.47 | 13.92 ± 0.74 | 31 | 0.1554 |

while at 20°C, the self-brood size was 220.65 ± 27.11 against 192.98 ± 22.43 for the control group, reflecting an improvement by 11.99% and 14.34%, respectively. Motility is a measure of muscle integrity, and its measurement has a direct implication on quality living. We found that N2 cultured with 300 $\mu$g/ml LBP were able to maintain a better motile state than the control group (Figure 5(c)). At day 16, there were still 46.5% of N2 cultured with 300 $\mu$g/ml LBP that belong to Class A but only 18.6% of the control group was still in Class A. All these results indicate that LBP can enhance the worms' ability to reproduce and maintain considerably high muscle integrity.

*3.4. LBP Lifespan Extension Requires daf-16 and sir-2.1.* The insulin/IGF-1 signaling (IIS) pathway is undoubtedly a key regulator of longevity in a variety of animals, where the genes *daf-16* and *sir-2.1* play cardinal roles [30]. Our study showed that VC199 (ok434) mutants for *sir-2.1* deletion exhibited a significantly longer lifespan when cultured with 300 $\mu$g/ml LBP but the proportion of prolonged lifespan was significantly shorter than that of the wild-type N2 (Figure 6(a), Table 4). At 25°C, the mean and maximum lifespans of worms on NGM with 25 $\mu$M FUdR were 11.64 ± 0.41 days and 16.78 ± 0.35 days, respectively, for the VC199 mutants. However, when cultured with 300 $\mu$g/ml, the mean and

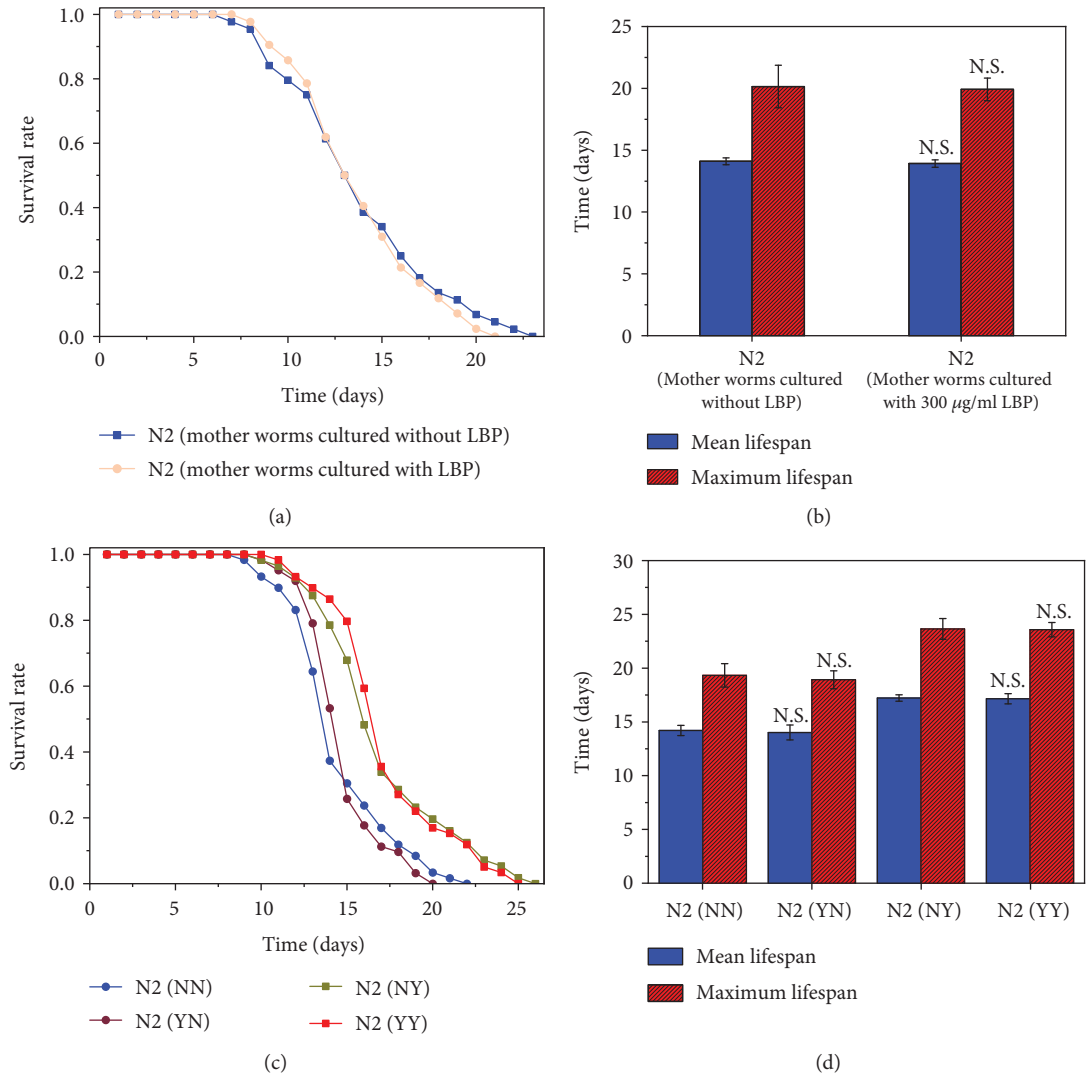


FIGURE 3: In *C. elegans*, LBP lifespan extension effects are not inheritable and do not depend on a particular stage of development. (a) Survival of offspring of N2 produced on plates with 300 $\mu$g/ml LBP to standard NGM plates without LBP and the control. (b) The mean lifespan and maximum lifespan of F1 offspring of N2 produced on plates with 300 $\mu$g/ml LBP to standard NGM plates without LBP and the control. (c) Survival of the worms before or after L4 as they were fed or not with LBP. (d) The mean lifespan and maximum lifespan of the worms before or after L4 as they were fed or not with LBP. Not significant was abbreviated as N.S. N2 (NN): culture without LBP; N2 (YN): culture with 300 $\mu$g/ml LBP before the L4 stage but without LBP after the L4 stage; N2 (NY): culture without LBP before the L4 stage but with 300 $\mu$g/ml LBP after the L4 stage; N2 (YY): culture with 300 $\mu$g/ml.

maximum lifespans were $13.18 \pm 0.92$ days and $18.21 \pm 0.46$ days, respectively. It implies that the mean and maximum lifespans were extended by 13.23% and 8.52%, respectively. LBP cannot cause such a tremendous effect on the proportion of extended lifespan in VC199 mutants compared with the N2, so LBP-induced lifespan extension requires *sir-2.1*. By RT-PCR in Figure 6(f), we obtained a *sir-2.1* fold expression of $2.43 \pm 0.22$ of N2 cultured with 300 $\mu$g/ml LBP relative to the control group, which further proves this result.

Similarly, at 25°C, we cultured two different worm mutants, in which *daf-16* has been deleted, GR1307 (Df50) and CF1038 (mu86) (Figures 6(b) and 6(c)). We found that the lifespan of these strains cultured with 300 $\mu$g/ml LBP was longer than that of the control group, but still, the proportion of the extended lifespan was significantly shorter than that of the N2, therefore implying that *daf-16* is vital in LBP lifespan extension. We also obtained similar results through *daf-16* RNAi gene silencing experiment as shown in Figure 6(d). To further confirm the importance of daf-16 expression, we performed RT-PCR of daf-16 (Figure 6(f)). We found that 300 $\mu$g/ml LBP treatment significantly upregulates this gene in C. elegans, confirming that the lifespan-extending effect of LBP is mediated by the DAF-16 pathway.

In 2006, Berdichevsky et al. [31] reported that *sir-2.1* can activate *daf-16* to prolong the lifespan, which means *sir-2.1* plays a role dependent on *daf-16*. The *daf-16* RNAi experiments were performed on N2 and VC199 worm strains. We found that the results of the *daf-16* RNAi

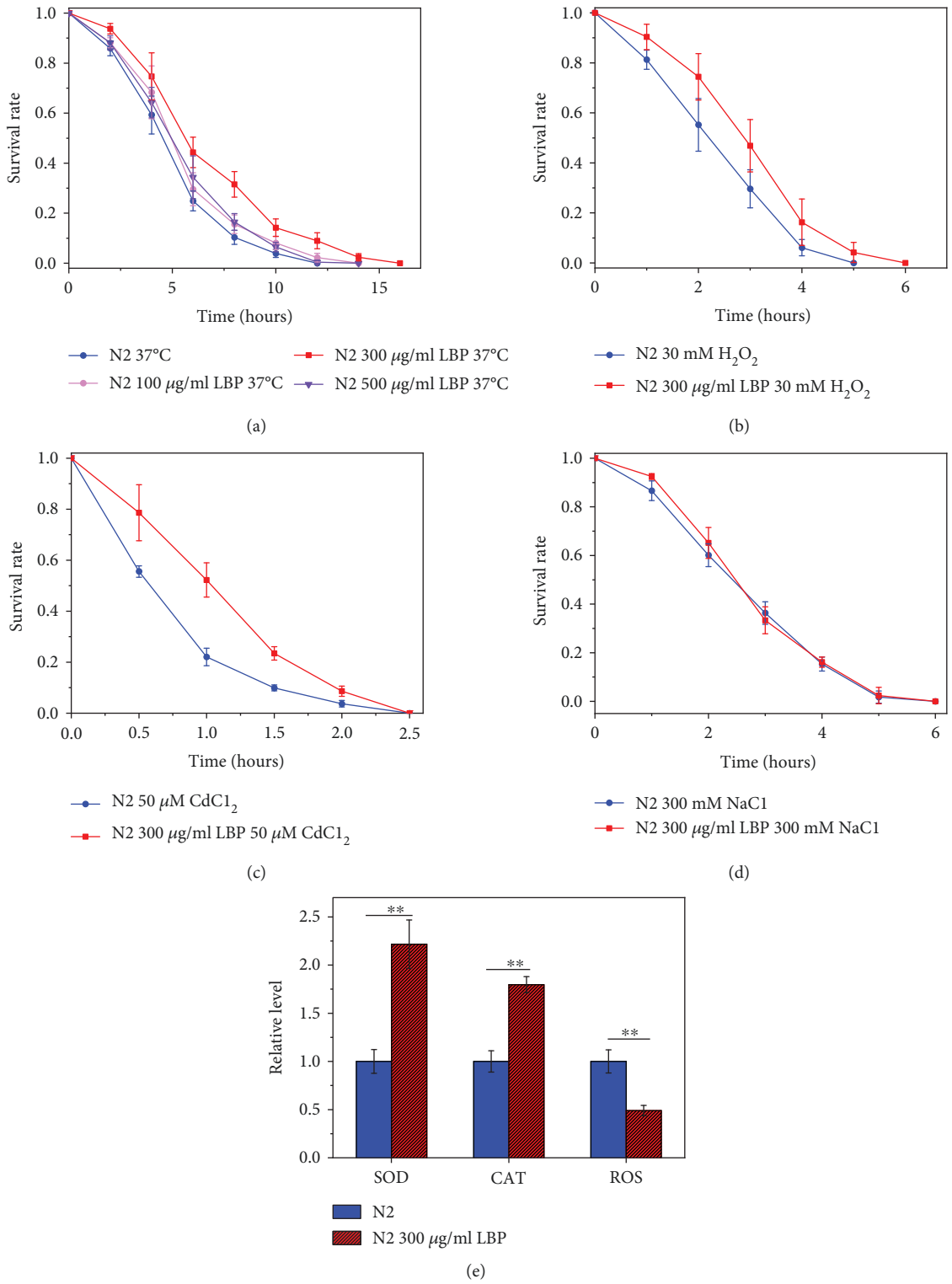


Figure 4: LBP improved the health of *C. elegans*. (a) Survival curves of N2 at 37°C for heat stress at different concentrations of LBP. (b) Survival of N2 cultured with or without LBP in S-buffer containing 30 mM $H_2O_2$ for oxidative stress. (c) Survival of N2 cultured with or without LBP in S-buffer containing 50 mM $CdCl_2$ for metal stress. (d) Survival of N2 cultured with or without LBP in S-buffer containing 300 mM NaCl for osmotic stress. (e) The relative fluorescence values of SOD, CAT, and ROS in the unit protein concentration of worms. Not significant was abbreviated as N.S., $^{**}P < 0.01$.

experiment were basically the same for the N2 and VC199 worm strains in cultures with 300 μg/ml LBP. In the case of *daf-16* RNAi, LBP does not promote longevity of N2 or VC199 worm strains (Figure 6(e)). This suggests that the LBP's ability to extend the lifespan is through *sir-2.1* whose effect can be dependent of *daf-16*.

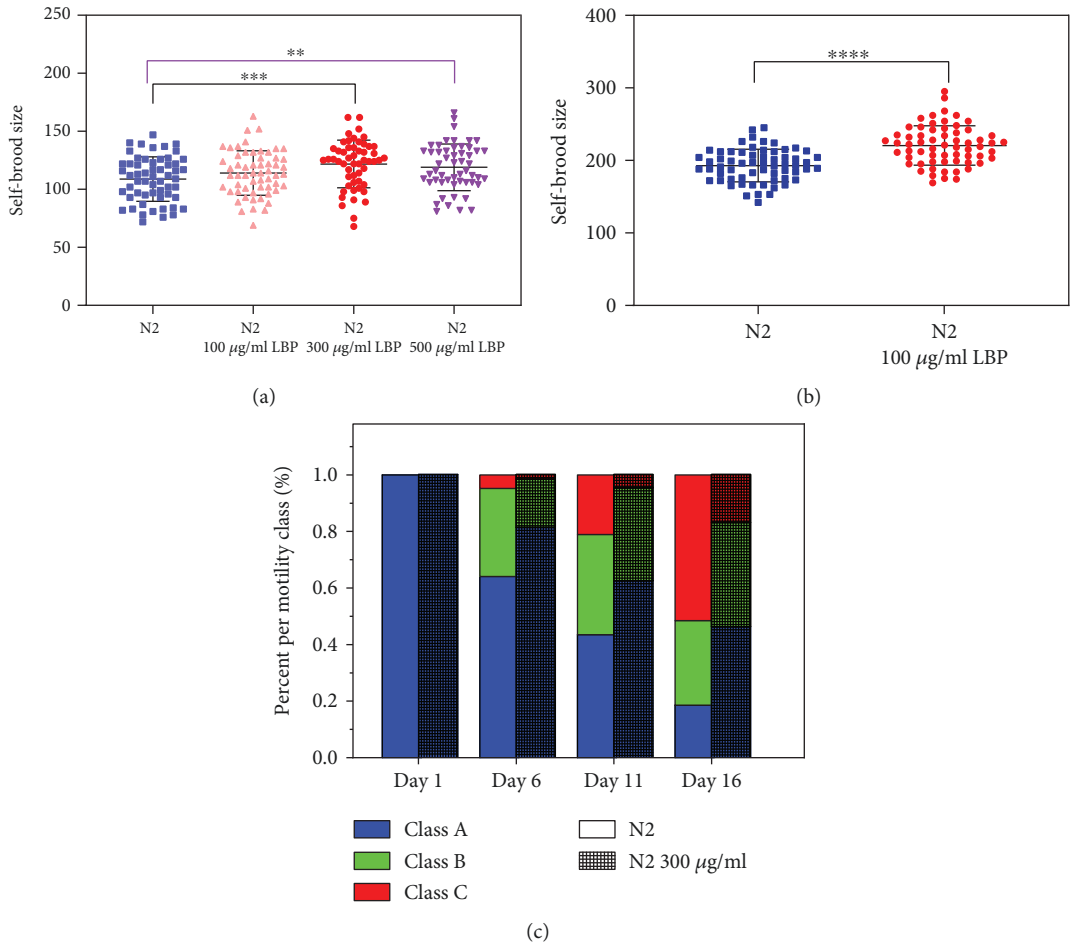


Figure 5: LBP enhances the worms' ability to reproduce and maintain a considerably high muscle integrity. (a) At 25°C, the progeny size and egg production rate of N2 cultured at different concentrations of LBP. (b) At 20°C, the progeny size and egg production rate of N2 cultured with or without LBP. (c) Percent of per motility class of N2 cultured with or without LBP on day 1, day 6, day 11, and day 16. $^{**}P < 0.01$, $^{***}P < 0.001$, and $^{****}P < 0.0001$.

*3.5. LBP Lifespan Extension Requires daf-12.* The *daf-12* gene plays an important role in regulating somatic and reproductive development, fat metabolism, and prolonging survival [32]. The function of *daf-12* in the process of extending lifespan relies on *daf-16* or acts independently [32]. Our study shows that DR1407 (m583) mutants for *daf-12* deletion cultured with 300 $\mu$g/ml LBP lived significantly longer but the proportion of extended lifespan was remarkably shorter than that of N2 (Figure 7(a), Table 4). At 25°C, the mean and maximum lifespans of DR1407 mutants were $12.54 \pm 0.51$ days and $18.05 \pm 0.54$ days, respectively. When cultured with 300 $\mu$g/ml LBP, the mean and maximum lifespans of DR1407 were $13.86 \pm 0.78$ days and $20.82 \pm 0.50$ days, respectively, thereby exhibiting a 10.53% increase and a 15.35% increase, respectively, in lifespan. The role of LBP in prolonging the lifespan of worms of DR1407 strain is not as significant as that in N2, which indicates that the LBF lifespan extension effect requires *daf-12*. RT-PCR results in Figure 7(b) show that there was an increase in the *daf-12* mRNA level in the 300 $\mu$g/ml LBP-treated N2 worms when compared to the control, which further proves the formidable role of *daf-12* in LBP lifespan extension.

*3.6. LBP Extend Lifespan by daf-12/daf-16.* The effects of LBP on extended lifespan require *daf-16* and *daf-12*. To understand the relationship between *daf-16* and *daf-12* in the extended lifespan by LBP, we performed the RNAi treatment to silence *daf-16* in the DR1407 mutants and *daf-12* in the GR1307 mutants. We found that strains cultured with 300 $\mu$g/ml LBP had almost the same lifespan as the control and there was no significant difference in lifespan between the RNAi groups (Figure 8). LBP cannot have impact on the lifespan of worms in which *daf-12* and *daf-16* were not expressed; therefore, LBP extends lifespan by *daf-12*/*daf-16*. The corresponding relationship among daf-12/daf-16 and other genes with lifespan is shown in Figure 8(c).

## 4. Discussion and Conclusions

Aging is a process regulated by many factors and is characterized by a gradual impairment of the body's response to stress and general deterioration of the main metabolic pathways [33]. Studies in various animal models, including worms, mice, and monkeys, have found that many factors, such as limiting food intake, slowing mitochondrial

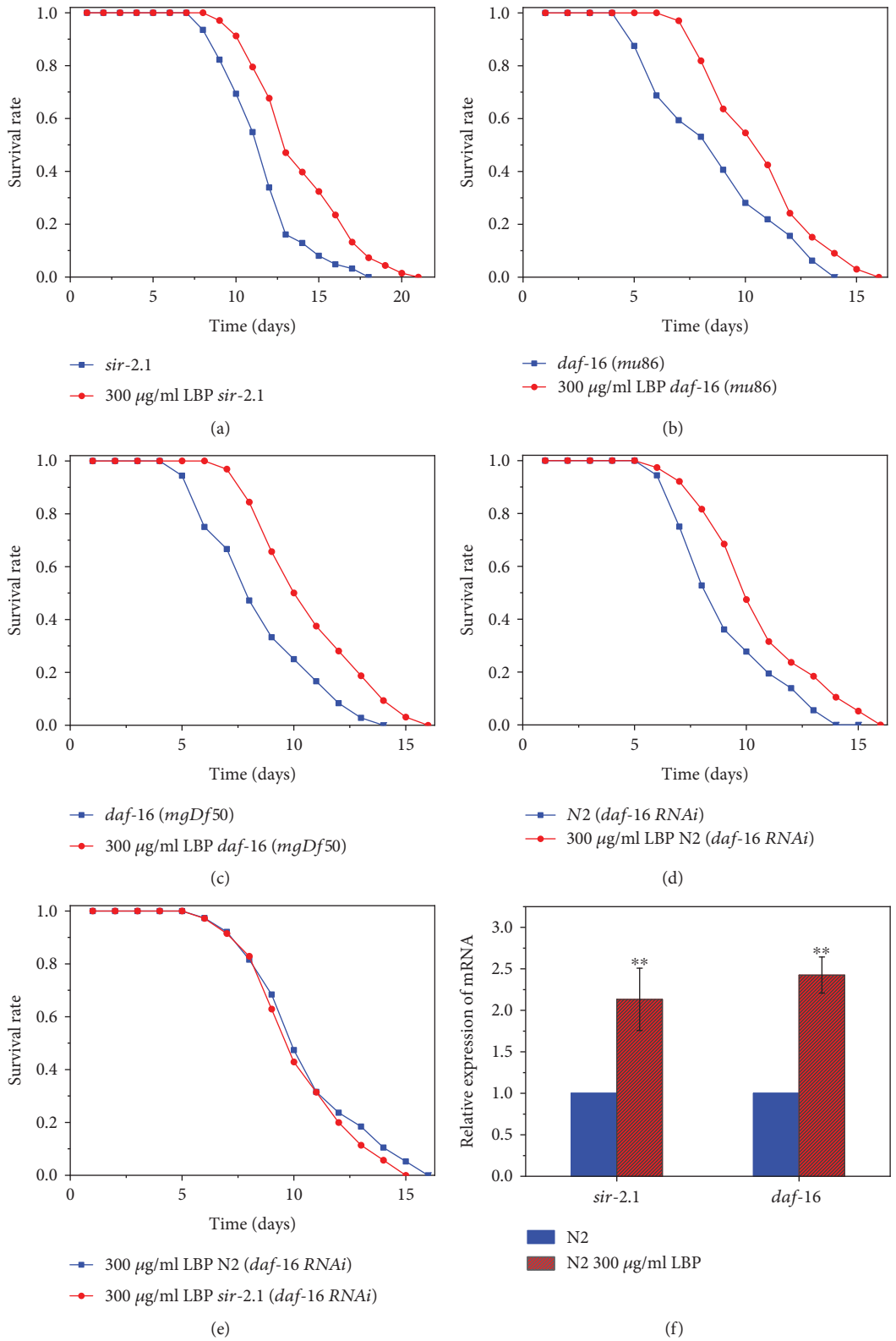


Figure 6: LBP lifespan extension requires *daf-16* and *sir-2.1*. (a) Survival of *sir-2.1* mutants cultured with or without LBP. (b) Survival of *daf-16* (*mu86*) mutants cultured with or without LBP. (c) Survival of *daf-16* (*mgDf50*) mutants cultured with or without LBP. (d) Survival of N2 (*daf-16* RNAi) cultured with or without LBP. (e) Survival of N2 (*daf-16* RNAi) and *sir-2.1* (*daf-16* RNAi) cultured with LBP. (f) The relative expression of *sir-2.1* and *daf-16* in N2 cultured with LBP to that of N2 cultured without LBP. $^{**}P < 0.01$.

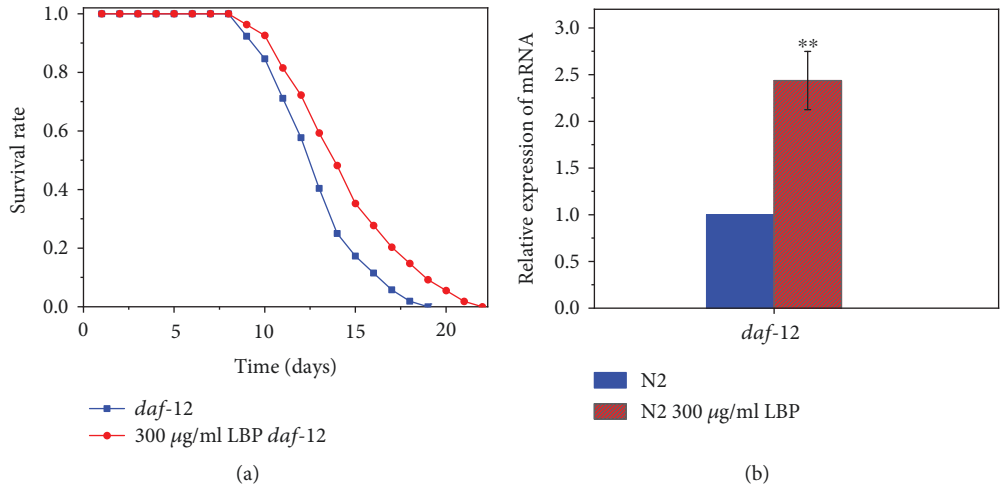


Figure 7: LBP lifespan extension requires *daf-12*. (a) Survival of *daf-12* mutants cultured with or without LBP. (b) The relative expression of *daf-12* in N2 cultured with LBP to that of N2 cultured without LBP. $^{**}P < 0.01$.

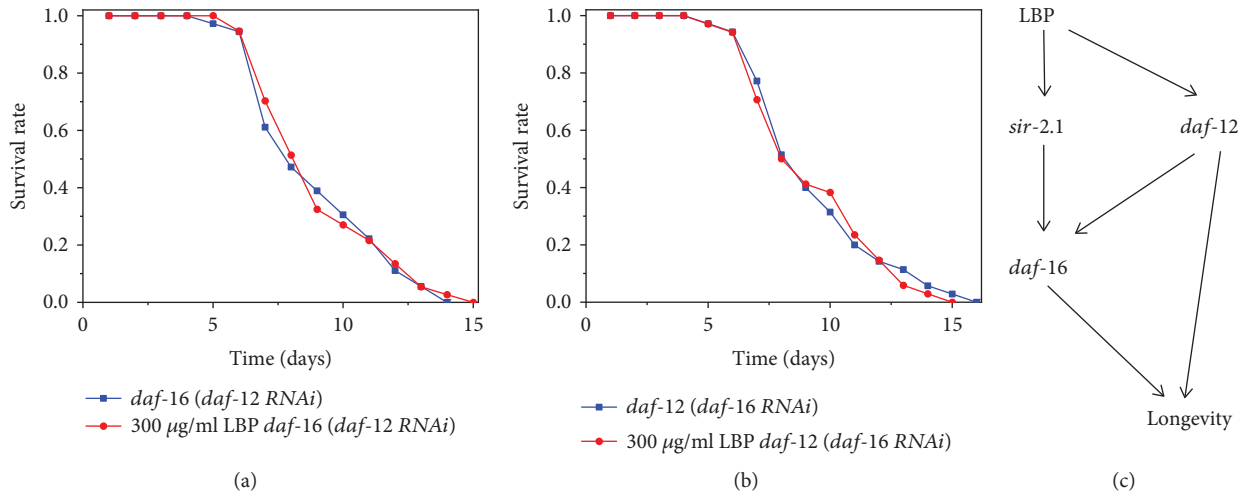


Figure 8: LBP lifespan extension requires *daf-16* and *daf-12*. (a) Survival of *daf-16* (*daf-12* RNAi) mutants cultured with or without LBP. (b) Survival of *daf-12* (*daf-16* RNAi) mutants cultured with or without LBP. (c) Pathway of LBP lifespan extension.

respiration, reducing germ cell function, or lowering temperature, can extend lifespan [34–39]. As the global aging population increases, it is one of the current research hotspots to find drugs or foods that can safely and effectively delay aging [40, 41]. We extracted a polysaccharide with a relatively stable composition from the Ningxia Lycium barbarum. LBP mainly consists of carbohydrates, most of which being glucose obtained after hydrolysis. We used *C. elegans* to examine the function of LBP in extending lifespan and maintaining health.

We studied the lifespan of *C. elegans* cultured at different concentrations of LBP and found that LBP can extend lifespan. The extended lifespan was not simply linearly dependent on the dose of LBP, and it was very interesting that there was an optimal concentration of 300 $\mu$g/ml. The lifespan extension effect of LBP on worms was independent of temperature and nonheritable. LBP was also found to enhance the viability of N2 under high temperature, strong oxidation, and heavy metals. LBP promotes the antioxidant capacity of the worms, significantly increases the activity of CAT and SOD to scavenge oxidative free radicals, and suppresses the detrimental effect of ROS, thereby reducing oxidative damage of cells and improving the health. LBP can also enhance the reproductive potentials and muscle integrity of *C. elegans*. In a word, LBP did not only extend the lifespan but also improved the health status of the nematodes.

Reproduction of C. elegans was also significantly increased when worms were cultured with 300 $\mu$g/ml LBP. This result seems somewhat contradictory to previous studies, which suggest that there is a tradeoff between longevity and reproduction. It has been found that long-lived C. elegans (caused by genetic mutations or nutritional disturbances) can reduce egg production. For example, reduced fertility of mutant animals, such as *age-1*, *eat-2*, and *daf-2*, is accompanied by the extension of the lifespan [42–44]. Hsin and Kenyon showed that the lifespan of germlineless C. elegans will be 60% longer than that of the wild-type animals [45]. The tradeoff relationship between longevity and

reproduction may result from the energy competition between these two processes. Energy and resources used for one process come at the cost of another. However, there may be other tradeoff relationships for longevity, such as the tradeoff between lifespan extension and the decline of the pharyngeal pumping rate [46] when worms were cultured with blueberry polyphenols. In addition, recent works by Sang-Kyu Park's group [47, 48] show that N-acetyl-L-cysteine and extracts from Tenebrio molitor can extend the lifespan and increase the fertility of C. elegans at the same time. Therefore, it seems reasonable that LBP extend C. elegans lifespan without reducing fertility. There can be other tradeoffs that need further examination in future studies.

Many genetic pathways have been shown to be conserved, and it is necessary to elucidate the molecular mechanisms by which LBP extends lifespan [49–52]. *sir-2.1* and *daf-16* are extremely outstanding genes in the IIS pathway; as well, DAF-16/FOXO transcription factors are also key components of the IIS pathway associating with aging and metabolism [30, 31]. We found that LBP has a shorter extending lifespan effect on mutants of *sir-2.1* and *daf-16* than on N2. This means that the LBP-extended lifespan effect requires *sir-2.1* and *daf-16*. For *daf-16* RNAi, there is no difference in the effect of LBP on N2 and *sir-2.1* mutants, which implies that *sir-2.1* may play a role dependent on *daf-16*. The *daf-12* gene plays an important role in aging, immunity, and antioxidation [32]. We found that LBP had a shorter lifespan extension effect on *daf-12* mutants than on N2, implying that the LBP-extended lifespan requires *daf-12*. *daf-16* RNAi was done to the *daf-12* mutants, and *daf-12* RNAi was done to the *daf-16* mutants, and it was shown that LBP lost the function of prolonging the lifespan, which suggests the effects of LBP on the aging of *C. elegans* depend on *daf-12* and *daf-16*.

In summary, a polysaccharide was obtained from Lycium barbarum, which has the functions of prolonging the lifespan and maintaining the environmental adaptability, reproductive capacity, and motility of *C. elegans*. The effects of LBP on the health and aging of *C. elegans* are regulated by *sir-2.1*, *daf-12*, and *daf-16*. Our study presented the preparation, basic chemical properties, and composition of LBP; its role in aging and health; and its molecular mechanism. It also provided a basis for further research on LBP and LBP as a food or drug for intervention of aging.

## Data Availability

The data used to support the findings of this study are available from the corresponding author upon request.

## Conflicts of Interest

The authors have no potential competing interests and conflicts to declare.

## Authors' Contributions

Z.Z., L.Y., and Y.J. designed the research, contributed to the interpretation of the results, drafted the manuscript, and approved the final version. Z.Z., Y.Z., H.F., K.J.B., X.Z., Y.Z., L.Y., and Y.J. contributed to the conducted the research, performed the statistical analysis, reviewed the manuscript, and approved the final version.

## Acknowledgments

We are very grateful to Professor Ruohuai Luo, Professor Ge Shan, Professor Zhengxing Wu, and the CGC which is funded by NIH Office of Research Infrastructure Programs (P40 OD010440) for their support and help in worm strains and bacteria. We are also very grateful to Professor Zhiyong Gong from Wuhan Polytechnic University and his support in real-time PCR. This study was supported by the National Natural Science Foundation of China under Grant nos. 11775091 (Y.J.), 11474117 (Y.J.), and 11704140 (Y.Z.); the Natural Science Foundation of Hubei Province under no. 2017CFB116 (Y.Z.); in part by the Thousand Talents Plan under no. 31103201603 (Y.Z.); and the self-determined research funds of CCNU from the colleges' basic research and operation of MOE under nos. CCNU18TS032 (X.Z.) and CCNU18QN035 (L.Y.).

## References

[1] J. Tigges, J. Krutmann, E. Fritsche et al., "The hallmarks of fibroblast ageing," *Mechanisms of Ageing and Development*, vol. 138, no. 1, pp. 26–44, 2014.

[2] T. Flatt, "A new definition of aging?," *Frontiers in Genetics*, vol. 3, no. 3, p. 148, 2012.

[3] A. J. Ding, S. Q. Zheng, X. B. Huang et al., "Current perspective in the discovery of anti-aging agents from natural products," *Natural Products and Bioprospecting*, vol. 7, no. 5, pp. 335–404, 2017.

[4] E. L. Greer, T. J. Maures, A. G. Hauswirth et al., "Members of the H3K4 trimethylation complex regulate lifespan in a germline-dependent manner in *C. elegans*," *Nature*, vol. 466, no. 7304, pp. 383–387, 2010.

[5] L. Wu, B. Zhou, N. Oshiro-Rapley et al., "An ancient, unified mechanism for metformin growth inhibition in *C. elegans* and cancer," *Cell*, vol. 167, no. 7, pp. 1705–1718.e13, 2016.

[6] Q. L. Wan, X. Shi, J. Liu et al., "Metabolomic signature associated with reproduction-regulated aging in *Caenorhabditis elegans*," *Aging*, vol. 9, no. 2, pp. 447–474, 2017.

[7] A. Masci, S. Carradori, M. A. Casadei et al., "*Lycium barbarum* polysaccharides: extraction, purification, structural characterisation and evidence about hypoglycaemic and hypolipidaemic effects. A review," *Food Chemistry*, vol. 254, pp. 377–389, 2018.

[8] J. Z. Dong, J. J. Yang, and Y. Wang, "Resources of Lycium species and related research progress," *China Journal of Chinese Materia Medica*, vol. 33, no. 18, pp. 2020–2027, 2008.

[9] H. Amagase and N. R. Farnsworth, "A review of botanical characteristics, phytochemistry, clinical relevance in efficacy and safety of *Lycium barbarum* fruit (Goji)," *Food Research International*, vol. 44, no. 7, pp. 1702–1717, 2011.

[10] R. Bo, S. Zheng, J. Xing et al., "The immunological activity of *Lycium barbarum* polysaccharides liposome in vitro and adjuvanticity against PCV2 in vivo," *International Journal of Biological Macromolecules*, vol. 85, pp. 294–301, 2016.

[11] I. Bondia-Pons, O. Savolainen, R. Törrönen, J. A. Martinez, K. Poutanen, and K. Hanhineva, "Metabolic profiling of Goji

berry extracts for discrimination of geographical origin by non-targeted liquid chromatography coupled to quadrupole time-of-flight mass spectrometry," *Food Research International*, vol. 63, pp. 132–138, 2014.

[12] S. J. Wu, L. T. Ng, and C. C. Lin, "Antioxidant activities of some common ingredients of traditional Chinese medicine, *Angelica sinensis*, *Lycium barbarum* and *Poria cocos*," *Phytotherapy Research*, vol. 18, no. 12, pp. 1008–1012, 2004.

[13] R. C.-C. Chang and K.-F. So, "Use of anti-aging herbal medicine, *Lycium barbarum*, against aging-associated diseases. What do we know so far?," *Cellular and Molecular Neurobiology*, vol. 28, no. 5, pp. 643–652, 2008.

[14] G. Yin and Y. Dang, "Optimization of extraction technology of the *Lycium barbarum* polysaccharides by Box–Behnken statistical design," *Carbohydrate Polymers*, vol. 74, no. 3, pp. 603–610, 2008.

[15] L. Gan, S. H. Zhang, Q. Liu, and H. B. Xu, "A polysaccharide-protein complex from *Lycium barbarum* upregulates cytokine expression in human peripheral blood mononuclear cells," *European Journal of Pharmacology*, vol. 471, no. 3, pp. 217–222, 2003.

[16] Z. Chen, J. Lu, N. Srinivasan, B. K. H. Tan, and S. H. Chan, "Polysaccharide-protein complex from *Lycium barbarum* L. is a novel stimulus of dendritic cell immunogenicity," *The Journal of Immunology*, vol. 182, no. 6, pp. 3503–3509, 2009.

[17] M. Ming, L. Guanhua, Y. Zhanhai, C. Guang, and Z. Xuan, "Effect of the *Lycium barbarum* polysaccharides administration on blood lipid metabolism and oxidative stress of mice fed high-fat diet in vivo," *Food Chemistry*, vol. 113, no. 4, pp. 872–877, 2009.

[18] L. Gan, S. Hua Zhang, X. Liang Yang, and H. Bi Xu, "Immunomodulation and antitumor activity by a polysaccharide–protein complex from *Lycium barbarum*," *International Immunopharmacology*, vol. 4, no. 4, pp. 563–569, 2004.

[19] Q. Luo, Z. Li, J. Yan, F. Zhu, R. J. Xu, and Y. Z. Cai, "*Lycium barbarum* polysaccharides induce apoptosis in human prostate cancer cells and inhibits prostate cancer growth in a xenograft mouse model of human prostate cancer," *Journal of Medicinal Food*, vol. 12, no. 4, pp. 695–703, 2009.

[20] X. M. Li, X. L. Li, and A. G. Zhou, "Evaluation of antioxidant activity of the polysaccharides extracted from *Lycium barbarum* fruits in vitro," *European Polymer Journal*, vol. 43, no. 2, pp. 488–497, 2007.

[21] C. L. Lin, C. C. Wang, S. C. Chang, B. S. Inbaraj, and B. H. Chen, "Antioxidative activity of polysaccharide fractions isolated from *Lycium barbarum* Linnaeus," *International Journal of Biological Macromolecules*, vol. 45, no. 2, pp. 146–151, 2009.

[22] W. J. Tian, J. L. Qin, C. J. Yue, R. R. Hou, K. H. Liu, and Y. L. Hu, "Effects of three kinds of polysaccharides on antioxidative ability of chicken embryo liver cells," *Acta Veterinaria et Zootechnica Sinica*, vol. 49, no. 7, pp. 1517–1523, 2018.

[23] G. E. Liang and C. W. Zhang, "Experimental research on the skin aging function of Lycium barbarum polysaccharides," *Chinese Journal of Aesthetic Medicine*, vol. 6, pp. 734–736, 2007.

[24] R. Yi, X. Liu, and Q. Dong, "A study of Lycium barbarum polysaccharides (LBP) extraction technology and its anti-aging effect," *African Journal of Traditional, Complementary and Alternative Medicines*, vol. 10, no. 4, 2013.

[25] T. Tang and B. He, "Treatment of D-galactose induced mouse aging with *Lycium barbarum* polysaccharides and its mechanism study," *African Journal of Traditional, Complementary and Alternative Medicines*, vol. 10, no. 4, 2013.

[26] M. Dubois, K. A. Gilles, J. K. Hamilton, P. A. Rebers, and F. Smith, "Colorimetric method for determination of sugars and related substances," *Analytical Chemistry*, vol. 28, no. 3, pp. 350–356, 1956.

[27] N. Blumenkrantz and G. Asboe-Hansen, "New method for quantitative determination of uronic acids," *Analytical Biochemistry*, vol. 54, no. 2, pp. 484–489, 1973.

[28] T. Stiernagle, "Maintenance of C. elegans," in *WormBook*, pp. 1–11, University of Minnesota, 1999.

[29] L. A. Herndon, P. J. Schmeissner, J. M. Dudaronek et al., "Stochastic and genetic factors influence tissue-specific decline in ageing *C. elegans*," *Nature*, vol. 419, no. 6909, pp. 808–814, 2002.

[30] M. Viswanathan and L. Guarente, "Regulation of *Caenorhabditis elegans* lifespan by *sir-2.1* transgenes," *Nature*, vol. 477, no. 7365, pp. E1–E2, 2011.

[31] A. Berdichevsky, M. Viswanathan, H. R. Horvitz, and L. Guarente, "*C. elegans* SIR-2.1 interacts with 14-3-3 proteins to activate DAF-16 and extend life span," *Cell*, vol. 125, no. 6, pp. 1165–1177, 2006.

[32] D. L. Motola, C. L. Cummins, V. Rottiers et al., "Identification of ligands for DAF-12 that govern dauer formation and reproduction in *C. elegans*," *Cell*, vol. 124, no. 6, pp. 1209–1223, 2006.

[33] M. H. Lee, B. Hook, L. B. Lamont, M. Wickens, and J. Kimble, "LIP-1 phosphatase controls the extent of germline proliferation in *Caenorhabditis elegans*," *The EMBO Journal*, vol. 25, no. 1, pp. 88–96, 2006.

[34] A. Ghazi, S. Henis-Korenblit, and C. Kenyon, "A transcription elongation factor that links signals from the reproductive system to lifespan extension in *Caenorhabditis elegans*," *PLoS Genetics*, vol. 5, no. 9, article e1000639, 2009.

[35] S. H. Bae, S. H. Sung, S. Y. Oh et al., "Sestrins activate Nrf2 by promoting p62-dependent autophagic degradation of Keap1 and prevent oxidative liver damage," *Cell Metabolism*, vol. 17, no. 1, pp. 73–84, 2013.

[36] D. E. Harrison, R. Strong, Z. D. Sharp et al., "Rapamycin fed late in life extends lifespan in genetically heterogeneous mice," *Nature*, vol. 460, no. 7253, pp. 392–395, 2009.

[37] A. San-Miguel, P. T. Kurshan, M. M. Crane et al., "Deep phenotyping unveils hidden traits and genetic relations in subtle mutants," *Nature Communications*, vol. 7, no. 1, article 12990, 2016.

[38] D. S. Williams, A. Cash, L. Hamadani, and T. Diemer, "Oxaloacetate supplementation increases lifespan in *Caenorhabditis elegans* through an AMPK/FOXO-dependent pathway," *Aging Cell*, vol. 8, no. 6, pp. 765–768, 2009.

[39] N. A. Bishop and L. Guarente, "Genetic links between diet and lifespan: shared mechanisms from yeast to humans," *Nature Reviews Genetics*, vol. 8, no. 11, pp. 835–844, 2007.

[40] N. Sudharsanan, M. K. Ali, N. K. Mehta, and K. M. V. Narayan, "Population aging, macroeconomic changes, and global diabetes prevalence, 1990–2008," *Population Health Metrics*, vol. 13, no. 1, 2015.

[41] R. W. Powers III, M. Kaeberlein, S. D. Caldwell, B. K. Kennedy, and S. Fields, "Extension of chronological life span in yeast by decreased TOR pathway signaling," *Genes & Development*, vol. 20, no. 2, pp. 174–184, 2006.

[42] S. Yanase, K. Yasuda, and N. Ishii, "Adaptive responses to oxidative damage in three mutants of *Caenorhabditis elegans*

(*age-1*, *mev-1* and *daf-16*) that affect life span," *Mechanisms of Ageing and Development*, vol. 123, no. 12, pp. 1579–1587, 2002.

[43] J. M. van Raamsdonk and S. Hekimi, "Deletion of the mitochondrial superoxide dismutase *sod-2* extends lifespan in *Caenorhabditis elegans*," *PLoS Genetics*, vol. 5, no. 2, article e1000361, 2009.

[44] J. M. Van Raamsdonk and S. Hekimi, "Reactive oxygen species and aging in *Caenorhabditis elegans*: causal or casual relationship?," *Antioxidants & Redox Signaling*, vol. 13, no. 12, pp. 1911–1953, 2010.

[45] H. Hsin and C. Kenyon, "Signals from the reproductive system regulate the lifespan of *C. elegans*," *Nature*, vol. 399, no. 6734, pp. 362–366, 1999.

[46] J. A. Joseph, B. Shukitt-Hale, N. A. Denisova et al., "Reversals of age-related declines in neuronal signal transduction, cognitive, and motor behavioral deficits with blueberry, spinach, or strawberry dietary supplementation," *The Journal of Neuroscience*, vol. 19, no. 18, pp. 8114–8121, 1999.

[47] S.-M. Won, H.-U. Cha, S. S. Yi, S.-J. Kim, and S.-K. Park, "*Tenebrio molitor* extracts modulate the response to environmental stressors and extend lifespan in *Caenorhabditis elegans*," *Journal of Medicinal Food*, vol. 19, no. 10, pp. 938–944, 2016.

[48] S. I. Oh, J. K. Park, and S. K. Park, "Lifespan extension and increased resistance to environmental stressors by N-acetyl-L-cysteine in Caenorhabditis elegans," *Clinics*, vol. 70, no. 5, pp. 380–386, 2015.

[49] S. Q. Zheng, X. B. Huang, T. K. Xing, A. J. Ding, G. S. Wu, and H. R. Luo, "Chlorogenic acid extends the lifespan of *Caenorhabditis elegans* via insulin/IGF-1 signaling pathway," *The Journals of Gerontology Series A: Biological Sciences and Medical Sciences*, vol. 72, no. 4, pp. 464–472, 2017.

[50] H. A. Tissenbaum and L. Guarente, "Increased dosage of a *sir-2* gene extends lifespan in *Caenorhabditis elegans*," *Nature*, vol. 410, no. 6825, pp. 227–230, 2001.

[51] G. Kwon, J. Lee, J. H. Koh, and Y. H. Lim, "Lifespan extension of *Caenorhabditis elegans* by *Butyricicoccus pullicaecorum* and *Megasphaera elsdenii* with probiotic potential," *Current Microbiology*, vol. 75, no. 5, pp. 557–564, 2018.

[52] A. Bansal, E. S. Kwon, D. Conte et al., "Transcriptional regulation of *Caenorhabditis elegans* FOXO/DAF-16 modulates lifespan," *Longevity & Healthspan*, vol. 3, no. 1, p. 5, 2014.

Hindawi
Oxidative Medicine and Cellular Longevity
Volume 2019, Article ID 8030697, 8 pages
https://doi.org/10.1155/2019/8030697

*Research Article*

# Abnormal Meiosis Initiation in Germ Cell Caused by Aberrant Differentiation of Gonad Somatic Cell

**Min Chen,[1] Min Chen,[1,2] Suren Chen,[1,2] Jingjing Zhou,[1,2] Fangfang Dong,[1,2] Zhiming Shen,[1,2] Haowei Wu,[1,2] Xiuhong Cui,[1] and Fei Gao [1,2]**

[1]*State Key Laboratory of Stem cell and Reproductive Biology, Institute of Zoology, Chinese Academy of Sciences, Beijing 100101, China*
[2]*University of Chinese Academy of Sciences, Beijing 100049, China*

Correspondence should be addressed to Fei Gao; gaof@ioz.ac.cn

Received 3 May 2019; Revised 27 July 2019; Accepted 8 August 2019; Published 5 September 2019

Guest Editor: Huai-Rong Luo



The interaction between germ cell and somatic cell plays important roles in germ cell development. However, the exact function of gonad somatic cell in germ cell differentiation is unclear. In the present study, the function of gonad somatic cell in germ cell meiosis was examined by using mouse models with aberrant somatic cell differentiation. In $Wt1^{R394W/R394W}$ mice, the genital ridge is absent due to the apoptosis of coelomic epithelial cells. Interestingly, in both male and female $Wt1^{R394W/R394W}$ germ cells, STRA8 was detected at E12.5 and the scattered SYCP3 foci were observed at E13.5 which was consistent with control females. In $Wt1^{-/flox}$; $Cre\text{-}ER^{TM}$ mice, *Wt1* was inactivated by the injection of tamoxifen at E9.5 and the differentiation of Sertoli and granulosa cells was completely blocked. We found that most germ cells were located outside of genital ridge after *Wt1* inactivation. STRA8, SYCP3, and γH2AX proteins were detected in germ cells of both male and female $Wt1^{-/flox}$; $Cre\text{-}ER^{TM}$ gonads, whereas no thread-like SYCP3 signal was observed. Our study demonstrates that aberrant development of gonad somatic cells leads to ectopic expression of meiosis-associated genes in germ cells, but meiosis was arrested before prophase I. These results suggest that the proper differentiation of gonad somatic cells is essential for germ cell meiosis.

## 1. Introduction

In mice, primordial germ cells (PGCs) arise from extraembryonic ectoderm at approximately E6.25 and migrate to the developing genital ridge at E10.5 [1]. After several rounds of mitosis, the germ cells in male gonads enter G0/G1 arrest between E12.5 and E14.5 until initiating meiosis after birth. The female germ cells start meiosis right after sex determination at approximately E12.5, then arrest at diplotene stage of prophase I until ovulation and the meiosis is completed after fertilization [2]. The different fates of germ cells in male and female gonads are not determined by the sex chromosome constitution but by the somatic cells in the gonad [3].

Retinoic acid (RA) is the most important extrinsic factor which is indispensable for germ cell meiosis initiation. RA is synthesized in mesonephros and diffuses into adjacent gonad to induce the expression of *Stra8* in germ cells of female gonads [4–7]. In male gonads, the germ cells are surrounded by Sertoli cells in testicular cords. Cytochrome P450, family 26, subfamily b, polypeptide 1 (*Cyp26b1*), is highly expressed in Sertoli cells during embryonic stages, which catalyzes the oxidization of RA to inactive metabolites. Therefore, the germ cells in male gonad could not access RA and initiate meiosis during embryonic stage.

As a nuclear transcription factor, Wilms tumor gene 1 (*Wt1*) is abundantly expressed in the coelomic epithelium of the urogenital ridge and the underlying mesenchymal cells before sex determination [8]. In sex-committed gonads, *Wt1* is specifically expressed in both Sertoli cells and granulosa cells. *WT1* is originally identified as a tumor suppressor gene associated with the development of Wilms' tumors and is subsequently found to be mutated in patients with Denys-Drash syndrome (DDS) [9]. $Wt1^{R394W/R394W}$ mice are embryonic lethal and the genital ridge can not

develop [10]. Our previous study demonstrates that in $Wt1^{R394W/R394W}$ mice, the directional migration of PGCs is not affected and most PGCs reach the mesenchyme under the coelomic epithelium at E10.5 which is consistent with control embryos [11]. We also find that when *Wt1* is deleted at approximately E9.5 using *Cre-ER*$^{TM}$, the development of genital ridge is not affected, whereas the differentiation of both Sertoli and granulosa cells is blocked and most genital ridge somatic cells differentiate into steroidogenic cells in both male and female gonads [12].

It has been proposed that the differentiation of gonad somatic cell plays important roles in germ cell development. However, the exact functions of somatic cells are still unclear. In this study, the function of somatic cell on germ cell meiosis is examined by using genital agenesis ($Wt1^{R394W/R394W}$) and somatic aberrantly differentiated ($Wt1^{-/flox}$; *Cre-ER*$^{TM}$) mouse models. We find both male and female germ cells start to express STRA8, but no germ cells at prophase I are observed. Our study demonstrates that the meiosis initiation of germ cell is accurately regulated by somatic factors.

## 2. Materials and Methods

*2.1. Mice.* All animal work was carried out in accordance with institutional animal care and the use committee regulations of Institute of Zoology, CAS. All mice were maintained in a C57BL/6;129/SvEv mixed background. The mouse strain carrying the $Wt1^{R394W}$ point mutation was generated in Dr. Vicki Huff's laboratory [10]. $Wt1^{R394W/R394W}$ mice were obtained by crossing male and female $Wt1^{+/R394W}$ mice. $Wt1^{-/flox}$; *Cre-ER*$^{TM}$ offspring were obtained by crossing $Wt1^{flox/flox}$ mice with $Wt1^{+/-}$ and *Cre-ER*$^{TM}$ transgenic mice. DNA isolated from adult tails and fetal tissues was used for genotyping. Pregnant $Wt1^{flox/flox}$ females were injected with Tamoxifen (Sigma-Aldrich) intraperitoneally at a dose of 6 mg/40 g body weight at E9.5 to induce Cre activity as described previously [12]. $Wt1^{flox/flox}$ and $Wt1^{-/flox}$ embryos were used as controls.

*2.2. Organ Culture.* The experiment of organ culture was performed as described previously [13, 14]. In brief, pregnant $Wt1^{flox/flox}$ females were injected with tamoxifen at E9.5. The gonads with mesonephroi were dissected from control and $Wt1^{-/flox}$; *Cre-ER*$^{TM}$ embryos at E13.5, placed on agarose stands (1.5% *w*/*v*, in 24-well plates), and cultured at 37°C and 5% $CO_2$. After 3 days of culture, the gonads were fixed in 4% PFA for further analysis.

*2.3. Tissue Collection and Histological Analysis.* Control and *Wt1*-inactivated embryos were collected immediately following euthanasia of pregnant mice. Gonads with mesonephroi were dissected in PBS, fixed in 4% paraformaldehyde for up to 24 hrs, stored in 70% ethanol, and embedded in paraffin. Then, tissue sections of 5 $\mu$m thickness were cut and mounted on glass slides.

*2.4. Immunofluorescence Analysis and TUNEL Assay.* Tissue sections were deparaffinized, rehydrated, and subjected to antigen retrieval. After blocking in 5% donkey serum in 0.3% Triton X-100 for 1 hr, the sections were incubated with primary antibodies for 1.5 hrs and the corresponding FITC-conjugated and Cy$^{TM}$3-conjugated secondary antibodies (1 : 150 and 1 : 300, respectively, Jackson) for 1 hr at room temperature. The following dilutions of primary antibodies were used: STELLA (1 : 200, Santa Cruz, sc-67249), GATA4 (1 : 300, Santa Cruz, sc-1237), STRA8 (1 : 200, Abcam, ab49405), SYCP3 (1 : 200, Abcam, ab15093), $\gamma$H2AX (1 : 200, Millipore, 05-636), DAZL (1 : 100, AbD Serotec, MCA2336), and MVH (1 : 500, Abcam, ab13840). After three washes in PBS, the sections were counterstained with DAPI to label the nuclei. The images were captured with a confocal laser scanning microscope (Carl Zeiss Inc., Thornwood, NY). TUNEL assay was conducted using the DeadEnd Fluorometric TUNEL system (Promega, G3250) as recommended.

*2.5. Quantitative Reverse Transcription PCR.* Gonads of E13.5 embryos were used to extract total RNA using a Qiagen RNeasy kit following manufacturer's instructions. The relative expression level was calculated using the formula $2^{-\Delta\Delta CT}$. *Hprt1* was used as an endogenous control. The primers used were listed as follows: *Stra8* sense, CTCCTC CTCCACTCTGTTGC, antisense, GCGGCAGAGACAAT AGGAAG; *Sycp3* sense, AGAAATGTATACCAAAGCTTC TTTCAA, antisense, TTAGATAGTTTTTCTCCTTGTTCC TCA; *Rec8* sense, CTACCTAGCTTGCTTCTTCCCA, antisense, GCCTCTAAAAGGTGTCGAATCTG; and *Dmc1* sense, CCCTCTGTGTGACAGCTCAAC, antisense, GGTC AGCAATGTCCCGAAG.

*2.6. Chromosome Spread and Immunofluorescence.* After culture for three days, the gonads were incubated in hypotonic extraction buffer (30 mM Tris, pH 8.2; 50 mM sucrose; 17 mM trisodium citrate dihydrate; 5 mM EDTA; 0.5 mM DTT; and 0.5 mM PMSF) for 45 mins at room temperature. After hypotonic treatment, 100 $\mu$l sucrose (100 mM) was added and cell suspension was pipetted up and down for several times. APES treated slides were coated with 1% paraformaldehyde containing 0.15% Triton X. 10 $\mu$l cell suspension was dispersed to the slide containing a layer of paraformaldehyde. Slides were placed in a humid chamber for at least 6 hrs at room temperature, then allowed to air dry and stored at −80°C until use.

The slides were washed in 0.4% Kodak Photo-Flo 200 for 4 min and 0.1% Triton X-100 in PBS for three times, blocked in 200 $\mu$l blocking buffer (3% nonfat milk in PBST) for 1 hr at room temperature, followed by an overnight incubation with primary antibody at 4°C and the corresponding FITC-conjugated and Cy$^{TM}$3-conjugated secondary antibodies for 1 hr. After three washes in PBS, the sections were analyzed with a confocal laser scanning microscope (Carl Zeiss Inc., Thornwood, NY).

*2.7. Statistical Analysis.* Experiments were repeated at least three times. Three to five control, *Wt1*-mutant or *Wt1*-deficient male or female embryos at each time point were used for immunostaining. For gonad culture, at least 4 pairs of male or female gonads of each genotype were used. For real-time PCR, 3 pairs of gonads of the same genotype were pooled and three independent pools were used for RNA

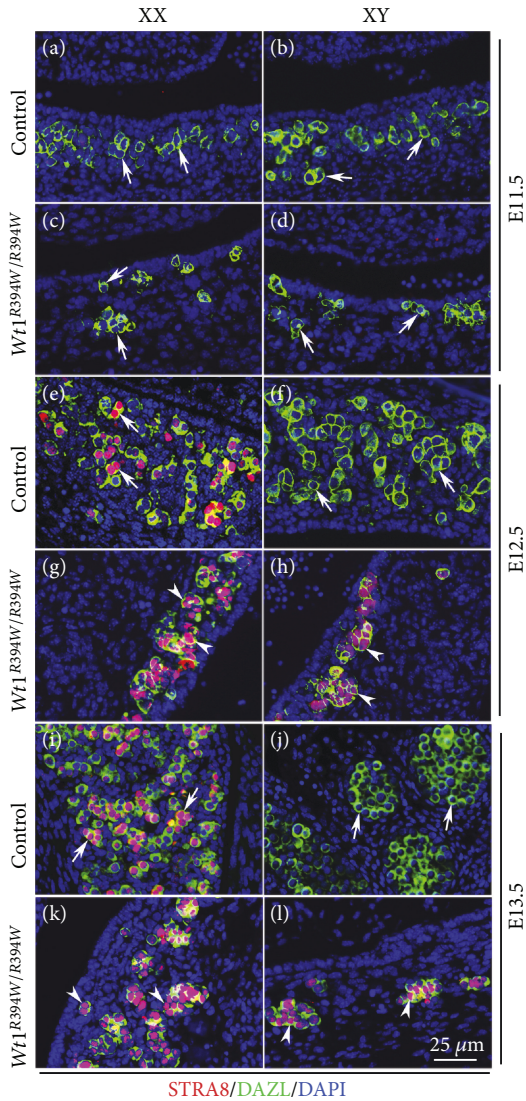


Figure 1: STRA8 was expressed in germ cells of both male and female $Wt1^{R394W/R394W}$ mice at E12.5 and E13.5. STRA8/DAZL double-staining experiment was performed with control ($Wt1^{+/R394W}$) and $Wt1^{R394W/R394W}$ embryos at E11.5 (A–D), E12.5 (E–H), and E13.5 (I–L). Germ cells were labeled with DAZL (green). DAPI (blue) was used to stain the nuclei. The arrowheads point to STRA8-positive germ cells in $Wt1^{R394W/R394W}$ gonads. The gender of the embryos was confirmed with PCR using *Sry* primers.

preparation. The results are presented as the mean ± SEM. Student's *t*-test was used to analyze the data. Probability values of <0.05 were considered as significant.

## 3. Results and Discussion

*3.1. STRA8 Was Expressed in Both Male and Female Germ Cells of $Wt1^{R394W/R394W}$ Mice.* Our previous study demonstrates that the genital ridge is absent in $Wt1^{R394W/R394W}$ mice due to the apoptosis of coelomic epithelial cells. However, the migration of PGCs is not affected and most germ cells arrive at position where genital ridge is formed [11]. To examine whether the differentiation of germ cells is affected in the

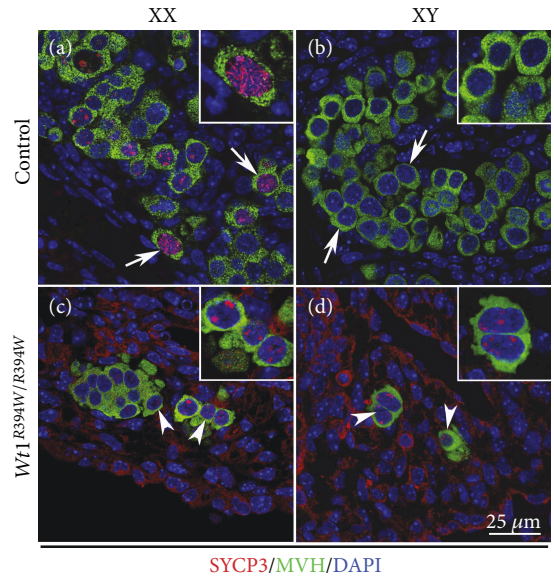


Figure 2: SYCP3 was expressed in germ cells of both male and female $Wt1^{R394W/R394W}$ gonads at E13.5. SYCP3/MVH double-staining experiment was performed with control $Wt1^{+/R394W}$ (A, B) and $Wt1^{R394W/R394W}$ (C, D) embryos at E13.5. Germ cells were labeled with MVH (green). DAPI (blue) was used to stain the nuclei. The arrowheads point to SYCP3-positive germ cells in $Wt1^{R394W/R394W}$ gonads. The gender of the embryos was confirmed with PCR using *Sry* primers.

absence of gonad somatic cells in $Wt1^{R394W/R394W}$ mice, the expression of meiotic genes STRA8 and SYCP3 was analyzed by immunofluorescence. As shown in Figure 1, STRA8 was expressed in germ cells of control ovaries at E12.5 (Figure 1A), and more positive germ cells were observed at E13.5 (Figure 1I). No STRA8 protein was detected in germ cells of control testes at E12.5 and E13.5 (Figure 1B, F, and J). In $Wt1^{R394W/R394W}$ mice, STRA8-positive germ cells were observed in both female (Figure 1G and K) and male gonads (Figure 1H and L) at E12.5 and E13.5. SYCP3 (synaptonemal complex protein 3), a lateral component of the synaptonemal complex, was first detected in control female germ cells at E13.5 (Figure 2A), but not in control male germ cells (Figure 2B). A few MVH/SYCP3 double-positive germ cells were noted in both male (Figure 2D) and female (Figure 2C) $Wt1^{R394W/R394W}$ gonads. In mammals, the timing of germ cell entry into meiosis is different between male and female. Female germ cell initiates meiosis right after sex determination. By contrast, male germ cell will not start meiosis during embryonic stage. Retinoic acid (RA) is a major extrinsic factor for germ cells to enter meiosis [15, 16]. *Stra8* is a gatekeeper gene for meiosis initiation which is expressed in germ cells in response to RA induction [3, 17]. In male gonad, meiosis is suppressed by RA-degrading enzyme CYP26b1 secreted from Sertoli cells during embryonic stage. In the present study, STRA8 and SYCP3 proteins were expressed in germ cells of both male and female $Wt1^{R394W/R394W}$ mice. These results indicated that RA is sufficient to induce STRA8 and SYCP3 expression in the absence of gonad somatic cells in both male and female gonads.

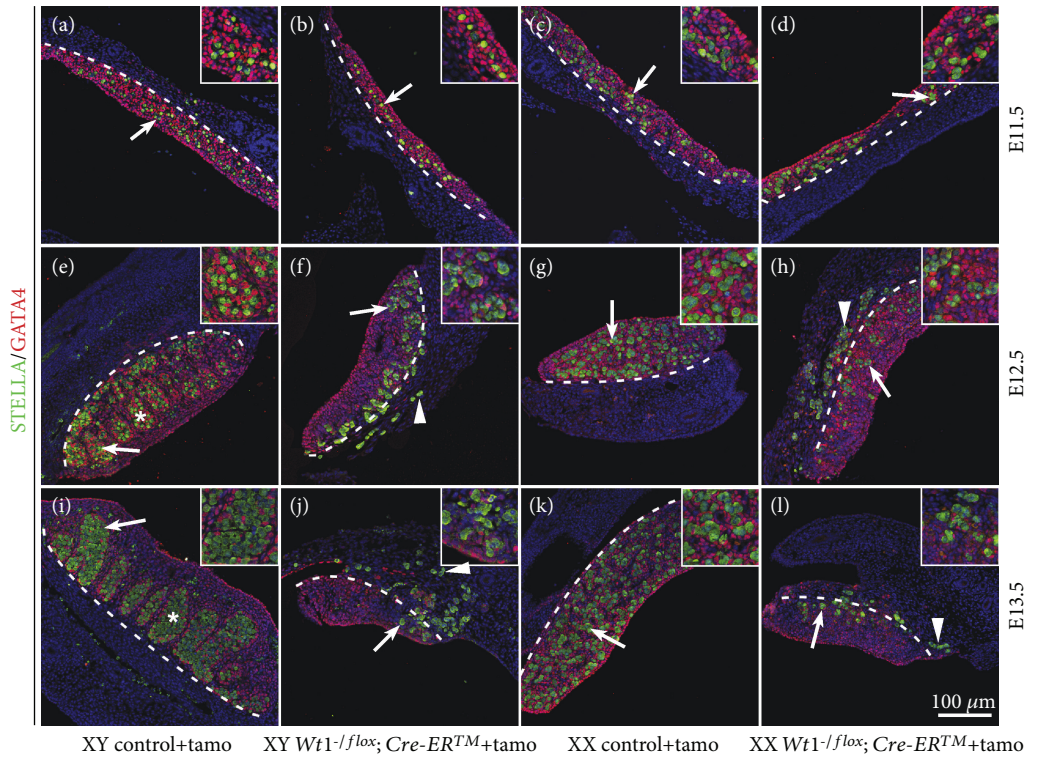


Figure 3: The location of germ cells was disrupted in *Wt1*$^{-/flox}$*; Cre-ER*$^{TM}$ gonads. *Wt1*$^{flox/flox}$ females were crossed with *Wt1*$^{-/flox}$*; Cre-ER*$^{TM}$ mice and the pregnant females were injected with tamoxifen at E9.5 to induce Cre activity. *Wt1*$^{flox/flox}$ and *Wt1*$^{-/flox}$ embryos were used as controls. Germ cells were labeled with STELLA (green, white arrows), and gonad somatic cells were labeled with GATA4 (red). The nuclei were stained in blue using DAPI. The dotted line denotes the border between the gonads and mesonephros. The arrowheads point to germ cells at the boundary between gonads and mesonephros. The gender of the embryos was confirmed with PCR using *Sry* primers. *Testicular cords.

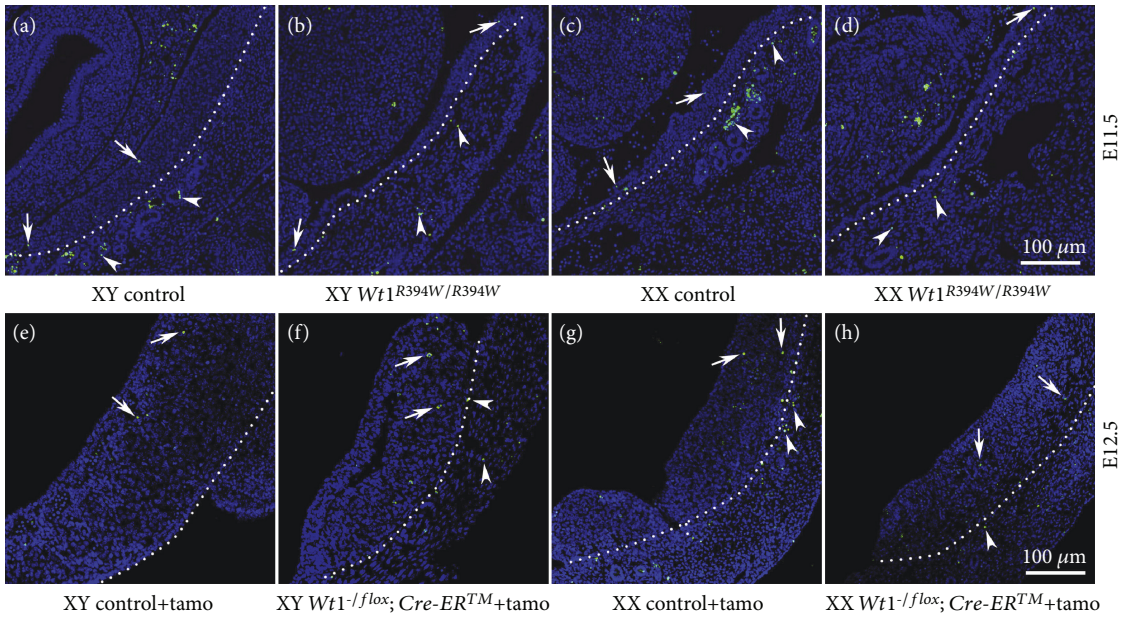


Figure 4: The number of apoptotic cells was not increased in *Wt1*-inactivated gonads. TUNEL assay was conducted in gonads of *Wt1* mutant (A, C: *Wt1*$^{+/R394W}$; B, D: *Wt1*$^{R394W/R394W}$) and *Wt1* knockout (E, G: *Wt1*$^{flox/flox}$ or *Wt1*$^{-/flox}$; F, H: *Wt1*$^{-/flox}$*; Cre-ER*$^{TM}$) mice. Arrows and arrowheads point to apoptotic cells (green) in gonads and mesonephros, respectively. The nuclei were stained in blue using DAPI. The dotted line denotes the border between the gonads and mesonephros. The gender of the embryos was confirmed with PCR using *Sry* primers.

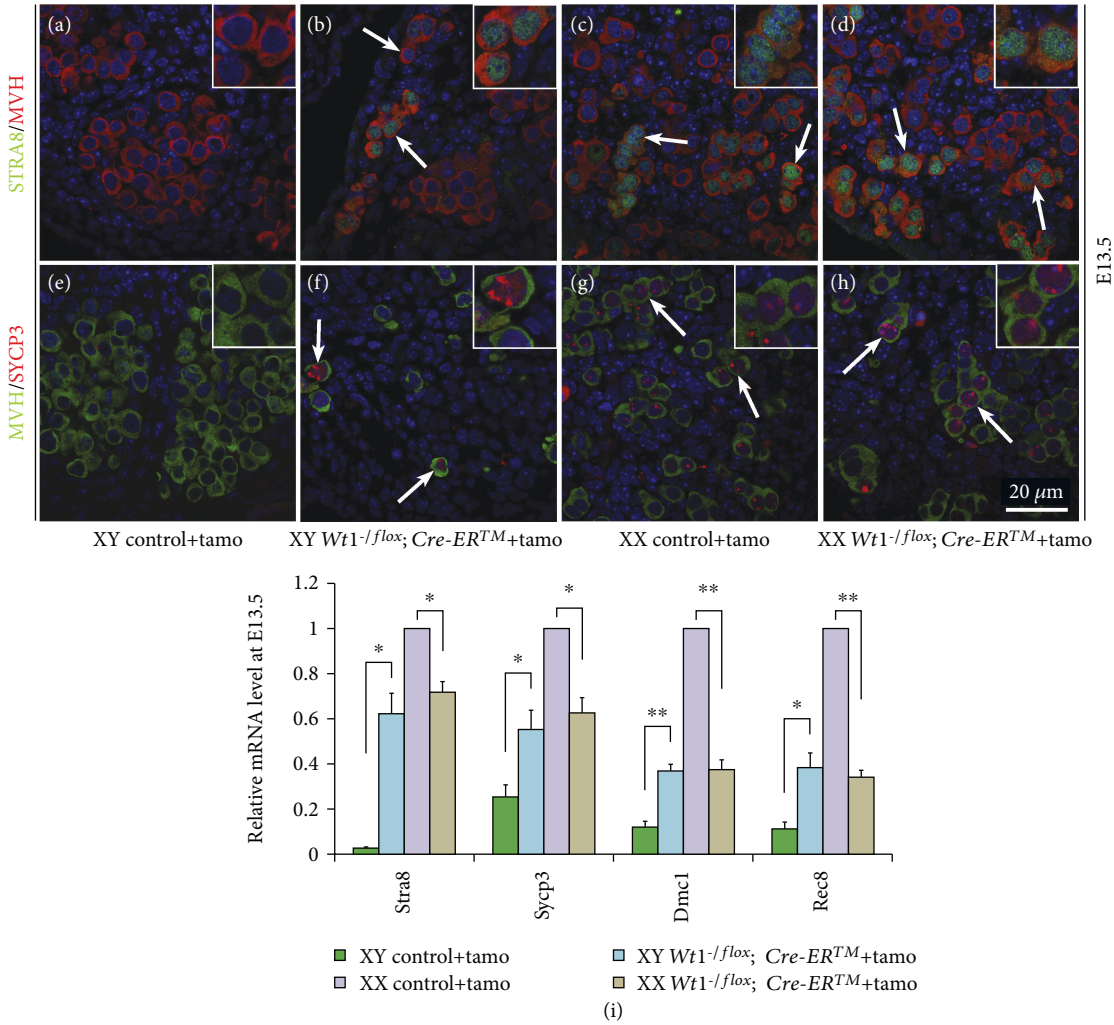


Figure 5: The meiotic genes were expressed in germ cells of both male and female *Wt1*$^{-/flox}$; *Cre-ER*$^{TM}$ mice after tamoxifen induction. *Wt1*$^{flox/flox}$ females were crossed with *Wt1*$^{-/flox}$; *Cre-ER*$^{TM}$ mice, and the pregnant females were injected with tamoxifen at E9.5 to induce Cre activity. *Wt1*$^{flox/flox}$ and *Wt1*$^{-/flox}$ embryos were used as controls. A–H: immunofluorescence analysis of STRA8/MVH (A–D) and SYCP3/MVH (E–H) in control and *Wt1*$^{-/flox}$; *Cre-ER*$^{TM}$ embryos at E13.5. Germ cells were labeled with MVH. DAPI (blue) was used to stain the nuclei. The arrows point to double-positive germ cells. I: real-time PCR analysis of *Stra8*, *Sycp3*, *Dmc1*, and *Rec8* in control and *Wt1*$^{-/flox}$; *Cre-ER*$^{TM}$ embryos at E13.5. *Hprt1* was used as an endogenous control. The data are presented as mean ± SEM. $^{*}P < 0.05$; $^{**}P < 0.01$.

*3.2. The Location of Germ Cells in Genital Ridge Was Disrupted when Wt1 Was Inactivated at E9.5.* To further investigate the functions of somatic cells in germ cell development, *Wt1* was deleted at later stage using a tamoxifen-inducible Cre (*Cre-ER*$^{TM}$) mice. *Wt1*$^{flox/flox}$ females were crossed with *Wt1*$^{-/flox}$; *Cre-ER*$^{TM}$ males, and the pregnant females were injected with tamoxifen at E9.5 and the embryos were collected from E11.5 to E13.5. STELLA and GATA4 were used to label germ cells and somatic cells, respectively. As shown in Figure 3, the size of *Wt1*-deficient gonads (F, H, J, and L) was smaller than control gonads (E, G, I, K) at E12.5 and E13.5. In control males, the testicular cords were well organized at E12.5 and E13.5 (Figure 3E and I, asterisks). By contrast, no testicular cords were observed in *Wt1*$^{-/flox}$; *Cre-ER*$^{TM}$ male gonads (Figure 3F and J), suggesting that *Wt1* is required for the testicular formation which is consistent with our previous study [18]. In control female gonads, germ cells were scattered inside the genital ridge (Figure 3G and K, white arrows). Interestingly, only a small portion of the germ cells were located inside the genital ridge of *Wt1*$^{-/flox}$; *Cre-ER*$^{TM}$ mice at E12.5 and E13.5, and most germ cells were observed at the boundary between gonads and mesonephros (white dotted line). Our previous study has demonstrated that *Wt1* directs the lineage specification of Sertoli and granulosa cells. Without *Wt1* expression, the somatic cells differentiate into steroidogenic cells instead of supporting cells [12]. In this mouse model, *Wt1* was deleted at E10.5 approximately. The abnormal differentiation of supporting cells became evident after E11.5[12] and the mislocation of germ cells in *Wt1*$^{-/flox}$; *Cre-ER™* mice was observed at E12.5 and E13.5. Based on these results, we speculated that structure support or paracrine signals released from somatic cells are indispensable for the precise location of germ cells in the gonads. However, the detailed regulatory mechanism

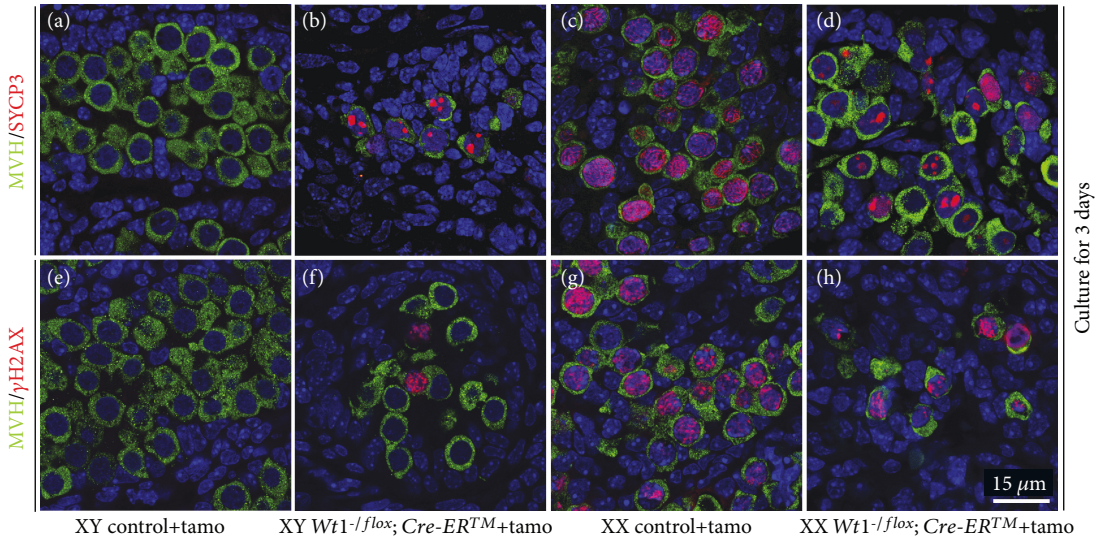


Figure 6: The meiosis was blocked in germ cells of $Wt1^{-/flox}$; $Cre\text{-}ER^{TM}$ gonads. $Wt1^{flox/flox}$ females were crossed with $Wt1^{-/flox}$; $Cre\text{-}ER^{TM}$ mice, and the pregnant females were injected with tamoxifen at E9.5 to induce Cre activity. Control ($Wt1^{flox/flox}$ and $Wt1^{-/flox}$) and $Wt1^{-/flox}$; $Cre\text{-}ER^{TM}$ gonads were dissected at E13.5 and cultured in vitro for 3 days. MVH/SYCP3 (A–D) and MVH/γH2AX (E–H) double-staining experiment was performed, and germ cells were labeled with MVH (green). DAPI (blue) was used to stain the nuclei. The gender of the embryos was confirmed with PCR using *Sry* primers.

needs further investigation. To further examine whether abnormal differentiation of gonad somatic cell causes germ cell death, TUNEL assay was performed. As shown in Figure 4, a small number of TUNEL-positive cells (green) were observed in both control and *Wt1*-inactivated gonads, and no significant difference was noted between control and $Wt1^{R394W/R394W}$ gonads (A–D) or control and $Wt1^{-/flox}$; $Cre\text{-}ER^{TM}$ gonads (E–H). These results indicated that aberrant differentiation of gonad somatic cells does not cause germ cell death.

*3.3. The Expression of Meiosis-Associated Genes in Both Male and Female Germ Cells of Wt1-Inactivated Gonads.* To test whether the differentiation of germ cells is affected in $Wt1^{-/flox}$; $Cre\text{-}ER^{TM}$ gonads, the expression of STRA8 and SYCP3 was examined by immunofluorescence. As shown in Figure 5, STRA8 (A) and SYCP3 (E) proteins were not expressed in germ cells of control males at E13.5. However, both STRA8 (Figure 5B and D) and SYCP3 (Figure 5F and H) signal were detected in germ cells of $Wt1^{-/flox}$; $Cre\text{-}ER^{TM}$ male and female gonads at E13.5. The expression pattern resembled that of the control female germ cells (Figure 5C and G). The mRNA level of meiosis-associated genes was also analyzed by real-time PCR. The expression of *Stra8*, *Sycp3*, *Dmc1* (a meiosis specific recombinase), and *Rec8* (a meiotic cohesin) was similar between male and female $Wt1^{-/flox}$; $Cre\text{-}ER^{TM}$ gonads at E13.5, and it was significantly increased compared to the control male gonads (Figure 5I).

Because most $Wt1^{-/flox}$; $Cre\text{-}ER^{TM}$ embryos died at E14.5 after tamoxifen induction, to examine the meiosis of germ cells at later developmental stage, control and $Wt1^{-/flox}$; $Cre\text{-}ER^{TM}$ gonads with mesonephroi were dissected at E13.5 and cultured in vitro for 3 days. The expression of SYCP3 and γH2AX (phospho-H2AX histone) was examined by immunofluorescence. As shown in Figure 6, thread-like SYCP3 signal was observed in germ cells of the control ovaries and no SYCP3 signal was detected in germ cell of the control testes. The expression of SYCP3 was also detected in germ cells of both $Wt1^{-/flox}$; $Cre\text{-}ER^{TM}$ male and female gonads. However, only scattered SYCP3 foci were noted. The expression of γH2AX protein which marks DNA double-strand breaks was also detected in germ cells of both *Wt1*-deficient male and female gonads, but the number of γH2AX-positive germ cells was significantly reduced compared to the control females.

To further confirm the results, the gonads with mesonephroi of control and $Wt1^{R394W/R394W}$ mice were also dissected at E12.5, cultured in vitro for 3 days, and then subjected to chromosome spreads and immunofluorescence of SYCP3 and γH2AX. In the control female ovaries, most germ cells have progressed to zygotene stage (Figure 7D–F) and a few germ cells were in leptotene (Figure 7A–C). However, in both male (Figure 7M–O) and female (Figure 7G–I) $Wt1^{R394W/R394W}$ germ cells, meiosis cannot progress beyond leptotene stage.

SYCP3 is a lateral element of synaptonemal complex that forms between two homologous chromosomes. Its localization pattern during meiosis is used to identify cells at different stages of meiotic prophase I. SYCP3 first appears diffusely in the leptotene stage. As meiosis progresses to the zygotene stage, SYCP3 forms line-shaped structure. In late zygotene and pachytene, prominent synapsis marked by SYCP3 is observed [19]. Although SYCP3 protein were expressed in the germ cells of *Wt1*-inactivated mice, only diffuse signal was observed, suggesting the meiosis is not properly initiated.

In this study, we found that STRA8 and SYCP3 were expressed in the male germ cells of both $Wt1^{R394W/R394W}$ and $Wt1^{-/flox}$; $Cre\text{-}ER^{TM}$ mouse models. A possible reason for this phenomenon is that the Sertoli cell differentiation

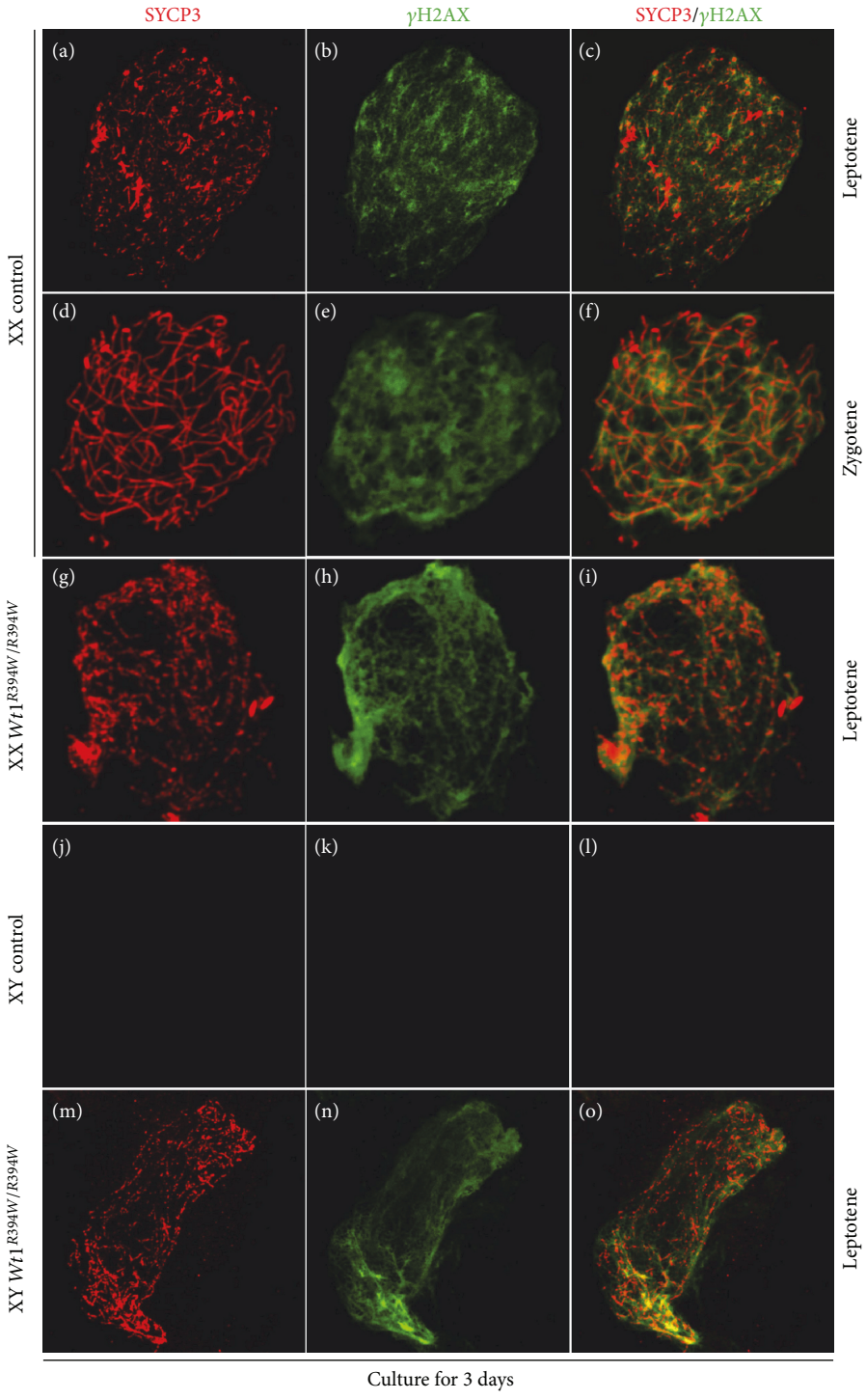


Figure 7: Meiosis was blocked at leptotene stage in both male and female germ cells of $Wt1^{R394W/R394W}$ gonads. Immunofluorescent staining of SYCP3 (red) and γH2AX (green) were performed on chromosome spreads of control ($Wt1^{+/R394W}$; A–F: female; J–L: male) and $Wt1^{R394W/R394W}$ (G–I: female; M–O: male) gonads which were dissected at E12.5 and cultured in vitro for 3 days. The gender of the embryos was confirmed with PCR using *Sry* primers.

was blocked and no testicular cords were formed in these mouse models. Therefore, the expression of CYP26b1 was decreased and the germ cells would access mesonephros-derived RA, which in turn induced the expression of STRA8 and SYCP3. It has been demonstrated that primordial germ cells at E11.5 are bipotential and they enter meiosis or not depending on the somatic cells [20]. Interestingly, only scattered SYCP3 signals were observed in both male and female germ cells of *Wt1*-deficient gonads. These results indicate that RA is not sufficient to induce germ cell meiosis initiation and somatic cell environment is also essential for normal meiosis process.

## 4. Conclusions

Our study demonstrates that aberrant differentiation of somatic cells leads to abnormal meiosis in both male and female germ cells. RA is not sufficient to induce germ cell meiosis initiation, and somatic cell environment is also essential for normal meiosis process.

## Data Availability

The data used to support the findings of this study are included within the article.

## Conflicts of Interest

The authors declare that there is no conflict of interest regarding the publication of this paper.

## Authors' Contributions

Min Chen and Min Chen are co-first authors. In the author list, the two names "Min Chen" reflect two different authors.

## Acknowledgments

This work was supported by the National Key R&D Program of China (2018YFA0107702); National Science Fund for Distinguished Young Scholars (81525011); Strategic Priority Research Program of the Chinese Academy of Sciences (XDB19000000); and the National Natural Science Foundation of China (31601193 and 31671496).

## References

[1] A. McLaren, "Primordial germ cells in the mouse," *Developmental Biology*, vol. 262, no. 1, pp. 1–15, 2003.

[2] A. McLaren, "Meiosis and differentiation of mouse germ cells," *Symposia of the Society for Experimental Biology*, vol. 38, pp. 7–23, 1984.

[3] M. E. Gill, Y. C. Hu, Y. Lin, and D. C. Page, "Licensing of gametogenesis, dependent on RNA binding protein DAZL, as a gateway to sexual differentiation of fetal germ cells," *Proceedings of the National Academy of Sciences of the United States of America*, vol. 108, no. 18, pp. 7443–7448, 2011.

[4] K. Niederreither, V. Fraulob, J. M. Garnier, P. Chambon, and P. Dolle, "Differential expression of retinoic acid-synthesizing (RALDH) enzymes during fetal development and organ differentiation in the mouse," *Mechanisms of Development*, vol. 110, no. 1-2, pp. 165–171, 2002.

[5] J. Bowles, D. Knight, C. Smith et al., "Retinoid signaling determines germ cell fate in mice," *Science*, vol. 312, no. 5773, pp. 596–600, 2006.

[6] C. W. Feng, J. Bowles, and P. Koopman, "Control of mammalian germ cell entry into meiosis," *Molecular and Cellular Endocrinology*, vol. 382, no. 1, pp. 488–497, 2014.

[7] J. Koubova, D. B. Menke, Q. Zhou, B. Capel, M. D. Griswold, and D. C. Page, "Retinoic acid regulates sex-specific timing of meiotic initiation in mice," *Proceedings of the National Academy of Sciences of the United States of America*, vol. 103, no. 8, pp. 2474–2479, 2006.

[8] J. F. Armstrong, K. Pritchard-Jones, W. A. Bickmore, N. D. Hastie, and J. B. L. Bard, "The expression of the Wilms' tumour gene, WT1, in the developing mammalian embryo," *Mechanisms of Development*, vol. 40, no. 1-2, pp. 85–97, 1993.

[9] J. A. Kreidberg, H. Sariola, J. M. Loring et al., "WT-1 is required for early kidney development," *Cell*, vol. 74, no. 4, pp. 679–691, 1993.

[10] F. Gao, S. Maiti, G. Sun et al., "The $Wt1^{+/R394W}$ mouse displays glomerulosclerosis and early-onset renal failure characteristic of human Denys-Drash syndrome," *Molecular and Cellular Biology*, vol. 24, no. 22, pp. 9899–9910, 2004.

[11] S. R. Chen, Q. S. Zheng, Y. Zhang, F. Gao, and Y. X. Liu, "Disruption of genital ridge development causes aberrant primordial germ cell proliferation but does not affect their directional migration," *BMC Biology*, vol. 11, no. 1, p. 22, 2013.

[12] M. Chen, L. Zhang, X. Cui et al., "*Wt1* directs the lineage specification of sertoli and granulosa cells by repressing *Sf1* expression," *Development*, vol. 144, no. 1, pp. 44–53, 2017.

[13] J. Martineau, K. Nordqvist, C. Tilmann, R. Lovell-Badge, and B. Capel, "Male-specific cell migration into the developing gonad," *Current Biology*, vol. 7, no. 12, pp. 958–968, 1997.

[14] T. Sato, K. Katagiri, Y. Kubota, and T. Ogawa, "In vitro sperm production from mouse spermatogonial stem cell lines using an organ culture method," *Nature Protocols*, vol. 8, no. 11, pp. 2098–2104, 2013.

[15] Q. Zhou, R. Nie, Y. Li et al., "Expression of stimulated by retinoic acid gene 8 (Stra8) in spermatogenic cells induced by retinoic acid: an in vivo study in vitamin A-sufficient postnatal murine testes," *Biology of Reproduction*, vol. 79, no. 1, pp. 35–42, 2008.

[16] X. Mu, J. Wen, M. Guo et al., "Retinoic acid derived from the fetal ovary initiates meiosis in mouse germ cells," *Journal of Cellular Physiology*, vol. 228, no. 3, pp. 627–639, 2013.

[17] Y. Lin, M. E. Gill, J. Koubova, and D. C. Page, "Germ cell-intrinsic and -extrinsic factors govern meiotic initiation in mouse embryos," *Science*, vol. 322, no. 5908, pp. 1685–1687, 2008.

[18] F. Gao, S. Maiti, N. Alam et al., "The Wilms tumor gene, *Wt1*, is required for *Sox9* expression and maintenance of tubular architecture in the developing testis," *Proceedings of the National Academy of Sciences of the United States of America*, vol. 103, no. 32, pp. 11987–11992, 2006.

[19] Y. H. Chi, L. I. Cheng, T. Myers et al., "Requirement for Sun1 in the expression of meiotic reproductive genes and piRNA," *Development*, vol. 136, no. 6, pp. 965–973, 2009.

[20] N. Nakatsuji and S. Chuma, "Differentiation of mouse primordial germ cells into female or male germ cells," *The International Journal of Developmental Biology*, vol. 45, pp. 541–548, 2001.

Hindawi
Oxidative Medicine and Cellular Longevity
Volume 2019, Article ID 2860642, 14 pages
https://doi.org/10.1155/2019/2860642

*Research Article*

# Phosphatidylcholine Extends Lifespan via DAF-16 and Reduces Amyloid-Beta-Induced Toxicity in *Caenorhabditis elegans*

**So-Hyeon Kim, Bo-Kyoung Kim, Suhyeon Park, and Sang-Kyu Park**

*Department of Medical Biotechnology, Soonchunhyang University, Asan 31538, Republic of Korea*

Correspondence should be addressed to Sang-Kyu Park; skpark@sch.ac.kr

Received 28 February 2019; Revised 16 May 2019; Accepted 27 May 2019; Published 11 July 2019

Guest Editor: Myon-Hee Lee



Phosphatidylcholine is one of the major phospholipids comprising cellular membrane and is known to have several health-promoting activities, including the improvement of brain function and liver repair. In this paper, we examine the *in vivo* effect of dietary supplementation with phosphatidylcholine on the response to environmental stressors and aging in *C. elegans*. Treatment with phosphatidylcholine significantly increased the survival of worms under oxidative stress conditions. However, there was no significant difference in response to stresses caused by heat shock or ultraviolet irradiation. Oxidative stress is believed to be one of the major causal factors of aging. Then, we examined the effect of phosphatidylcholine on lifespan and age-related physiological changes. Phosphatidylcholine showed a lifespan-extending effect and a reduction in fertility, possibly as a tradeoff for long lifespan. Age-related decline of motility was also significantly delayed by supplementation with phosphatidylcholine. Interestingly, the expressions of well-known longevity-assuring genes, *hsp-16.2* and *sod-3*, were significantly upregulated by dietary intervention with phosphatidylcholine. DAF-16, a transcription factor modulating stress response genes, was accumulated in the nucleus by phosphatidylcholine treatment. Increase of the ROS level with phosphatidylcholine suggests that the antioxidant and lifespan-extending effects are due to the hormetic effect of phosphatidylcholine. Phosphatidylcholine also showed a protective effect against amyloid beta-induced toxicity in Alzheimer's disease model animals. Experiments with long-lived mutants revealed that the lifespan-extending effect of phosphatidylcholine specifically overlapped with that of reduced insulin/IGF-1-like signaling and required DAF-16. These findings showed the antioxidant and antiaging activities of phosphatidylcholine for the first time *in vivo*. Further studies focusing on the identification of underlying cellular mechanisms involved in the antiaging effect will increase the possibility of using phosphatidylcholine for the development of antiaging therapeutics.

## 1. Introduction

Aging is one of the most complex biological processes. During aging, the structure and cellular function of the body gradually decline, while susceptibility to disease and death rapidly increases [1]. To explain the aging process, numerous theories of aging have been suggested. The free radical theory suggests that various free radicals present in the surrounding environment cause cellular damage and accumulation of this damage eventually leads to aging in the organism [2]. Major free radicals are the reactive oxygen species (ROS) produced as a byproduct of mitochondrial electron transport chain reaction. There is a positive correlation between cellular ROS levels and an organism's lifespan [3]. The other related theory of aging is the mitochondrial decline theory of aging, which emphasizes the role of age-related decrease in mitochondrial function in the normal aging process [4]. As cells age, mutations are accumulated in the mitochondrial genome and the efficiency of the mitochondrial electron transport chain reaction declines, producing less ATP and more ROS [5]. Some theories of aging focus on the importance of genomic stability [6]. For example, the telomere theory of aging suggests that the attrition of telomere sequences at chromosome ends as cell replicates play a key role in cellular senescence [6]. Faster attrition of telomere sequences was observed in the genomes of a Werner syndrome patient, which is an adult progeria showing accelerating aging phenotypes [7]. However, there is no single theory of aging that can

explain the complex aging process as a whole and people believe that many aging theories are interlinked with each other.

Based on the free radical theory of aging supported by the majority, many genetic and nutritional interventions modulating the cellular antioxidant system have been studied so far. Genetic knockout of antioxidant genes, including catalase (CAT) and superoxide dismutase (SOD), shortened the lifespan of many model organisms, while overexpression of those genes extended the lifespan [8]. However, some studies have reported that additional copy of antioxidant genes had no effect on lifespan [9]. The role of antioxidant genes in lifespan determination is still elusive. Nutritional interventions with antioxidants include dietary supplementation with resveratrol and vitamin E. Resveratrol is a polyphenol compound found in many plants, including grapes, raspberries, cranberries, and other berries. Resveratrol has a variety of beneficial bioactivities, such as antioxidant, anticancer, and anti-inflammatory effects [10]. Supplementation with resveratrol increased lifespan in yeast, *C. elegans*, and *Drosophila melanogaster* [11–13]. The lifespan-extending effect of resveratrol involves the activation of the SIRT1 gene, which inhibits apoptosis [14]. Recent studies have shown that cysteine derivatives have both antioxidant and antiaging effect *in vivo*. N-Acetyl-L-cysteine increased the resistance to environmental stresses and lifespan, mimicking dietary restriction [15]. Supplementation with selenocysteine conferred longevity phenotype and ameliorated age-related pathophysiological changes [16]. Extracts from *Acanthopanax sessiliflorus*, a plant used as a traditional treatment for many diseases, or *Tenebrio molitor*, an insect whose extracts have antibacterial, antifungal, and anticancer activities, also showed antioxidant and antiaging effect in *C. elegans* [17, 18].

Phosphatidylcholine is one of the most abundant phospholipids found in all cell membranes. Recent studies have identified various beneficial health effects of phosphatidylcholine. Impaired biosynthesis of phosphatidylcholine is associated with fatty liver disease and lowered liver regeneration [19]. Phosphatidylcholine also modulates brain function and brain disease. In the aged human, the plasma level of phosphatidylcholine was positively correlated with cognitive flexibility within the prefrontal cortex and the decreased plasma level of phosphatidylcholine was observed in Alzheimer's disease (AD) patients [20]. Dietary supplementation with phosphatidylcholine improved brain function, such as learning and memory, and conferred increased resistance to oxidative stress by modulating the activity of SOD in mice [21]. In rat adrenal pheochromocytoma cells, treatment with phosphatidylcholine hydroperoxides enhanced the activities of antioxidant genes, including CAT, SOD, and glutathione peroxidase [22]. Nanoparticles based on phosphatidylcholine, vitamins, and melatonin showed wrinkle-reducing and antiaging effects in skin [23].

In this study, we investigated the antistress and antiaging effects of phosphatidylcholine in *C. elegans*. We also investigated the effect of phosphatidylcholine on age-related physiological and genetic markers and age-related disease. Finally, we determined the underlying mechanisms involved in the lifespan-extending effect of phosphatidylcholine. This study will broaden the understanding of the aging process itself and provide novel biomolecules having antiaging activity *in vivo*.

## 2. Materials and Method

*2.1. Worm Strains and Culture Conditions.* N2 was used as the wild-type control in all experiments. The long-lived mutants, *age-1* (*hx546*), *clk-1* (*e2519*), and *eat-2* (*ad465*), and the green fluorescent protein- (GFP-) expressing strains, CL2070 (dvIs70 [*Phsp-16.2::GFP, rol-6*]), CF1553 (muIs84 [*Psod-3::GFP, rol-6*]), and TJ356 (zls356 IV [*daf-16p::daf-16a/b::GFP, rol-6*]), were purchased from the *C. elegans* Genetics Center (CGC, Minneapolis/St. Paul, MN, USA). The CL4176 expressing muscle-specific human amyloid beta $(A\beta)_{1\text{-}42}$ (dvls27 [*myo-3/Aβ1-42/let UTR, rol-6*]) was used for $A\beta$-induced toxicity assay. Worms were cultured at 20°C on solid Nematode Growth Medium (NGM) plates (25 mM NaCl, 1.7% agar, 2.5 mg/ml peptone, 50 mM KH2PO4 (pH 6.0), 5 $\mu$g/ml cholesterol, 1 mM $CaCl_2$, and 1 mM $MgSO_4$) spotted with *Escherichia coli* OP50 as food source.

*2.2. Resistance to Oxidative Stress.* Five young adult worms were transferred to a fresh NGM plate and permitted to lay eggs for 6 h. Then, the five adult worms were removed from the plate. The remaining eggs were hatched and grown on NGM plates for 3 days at 20°C. Thirty age-synchronized worms were transferred to fresh NGM plates containing different concentrations (1, 10, and 100 mg/l) of phosphatidylcholine and adapted for 24 h in 20°C. Then, worms were placed in 96-well plates (5 worms/well) containing 2 mM hydrogen peroxide ($H_2O_2$) in S-basal without cholesterol (5.85 g sodium chloride, 1 g potassium phosphate dibasic, and 6 g potassium phosphate monobasic for 1 l sterilized distilled water). The survival of worms was recorded. A worm not responding to any mechanical stimuli was considered as dead. For statistical analysis, the log-rank test was used [24].

*2.3. Thermotolerance Assay.* Sixty age-synchronized worms were transferred to fresh NGM plates pretreated with different concentrations of phosphatidylcholine (1, 10, and 100 mg/l) and incubated at 20°C for 24 h. Then, worms were exposed to 35°C heat shock for 7 h. After heat shock, worms were transferred back to a 20°C incubator. On the next day, the survival of worms was monitored every day, until all worms were dead.

*2.4. Survival after Ultraviolet (UV) Irradiation.* Sixty age-synchronized young adult worms were transferred to fresh NGM plates containing different concentrations of phosphatidylcholine (1, 10, and 100 mg/l). After 24 h at 20°C, worms were irradiated with 20 J/cm$^2$/min of UV for 1 min in a UV crosslinker (BLX-254, Vilber Lourmat Co., Torcy, France). Then, worms were transferred to fresh NGM plates treated with different concentrations of phosphatidylcholine. Living and dead worms were scored daily, until all worms were dead.

*2.5. Lifespan Assay.* To prevent internal hatching during the assay, 5-fluoro-2′-deoxyruridine (12.5 mg/l) was added to NGM plates. With sixty age-synchronized worms, the numbers of live and dead worms were recorded every day. Worms lost, killed, or having internal hatching were excluded from the assay. The log-rank test was employed for statistical comparison of survival curves [24]. A $P$ value lower than 0.05 was considered to be a significant difference between two survival curves.

*2.6. Fertility Assay.* Five L4/young adult stage worms were transferred to a fresh NGM plate containing different concentrations of phosphatidylcholine (10 and 100 mg/l) and permitted to lay eggs for 5 h. The eggs were maintained at 20°C for 2 d. Ten 2-day-old worms were transferred to 10 fresh NGM plates individually containing different concentrations of phosphatidylcholine every day. Eggs spawned each day by an individual worm were incubated at 20°C for 48 h, and the number of progeny produced was recorded, until the worm no longer produced eggs.

*2.7. Motility Assay.* Age-synchronized young adult worms were grown on NGM plates containing different concentrations of phosphatidylcholine (10 and 100 mg/l) at 20°C. On 5, 10, 15, 20, and 25 days after laying eggs, worms were classified according to their motility: phase 1, a worm moving without any mechanical stimulation, phase 2, a worm that moves in response to mechanical stimuli, and phase 3, a worm that can move only the head part with a mechanical stimulus. The relative distributions of each phase and dead worms among 100 age-synchronized worms were compared between the untreated control and phosphatidylcholine-treated groups. For quantitative analysis, thrashing assay was performed. After treating phosphatidylcholine to age-synchronized worms, fifteen worms were randomly selected and placed on NGM plates individually for 2 min. Then, a single worm was transferred to M9 buffer and adapted for 1 min. The number of trashing per 1 min was counted for each worm.

*2.8. Subcellular Localization of DAF-16.* Sixty age-synchronized TJ356 worms were transferred to NGM plates with or without 100 mg/l of phosphatidylcholine. After 5, 7, and 9 days, worms were anesthetized with 1 M sodium azide on a slide glass and the cellular distribution of DAF-16 was monitored using a fluorescence microscope.

*2.9. Expression of Longevity Assurance Genes.* Age-synchronized CL2070 and CF1553 worms ($n = 20$) were grown on NGM plates containing 10 or 100 mg/l of phosphatidylcholine for 5, 7, and 9 days. Then, a single worm was mounted on a slide glass coated with 2% agarose, anesthetized with 1 M sodium azide, and covered with cover slide glass and the expression level of GFP was monitored with a confocal microscope (Olympus FV10i, Olympus, Tokyo, Japan). The quantification of GFP expression was determined with a fluorescence multireader (Infinite F200, Tecan, Grodig, Austria).

*2.10. Cellular ROS Levels.* Age-synchronized young-adult worms were treated with or without phosphatidylcholine for 5 and 7 days at 20°C. Then, worms were transferred to a 96-well black plate containing 190 $\mu$l of PBST individually ($n = 20$). Incubate worms for 3 h with 10 $\mu$l of H2DCF-DA (Sigma-Aldrich, St. Louis, USA), and fluorescence intensity was measured with a fluorescence multireader (Infinite F200, Tecan, Grodig, Austria).

*2.11. Aβ-Induced Toxicity Assay.* Thirty young adult CL4176 worms grown at 15°C were transferred to NGM plates pretreated with 10 or 100 mg/l of phosphatidylcholine and permitted to lay eggs for 2 h at 15°C. Then, all adult worms were removed from the plate and the progeny were grown for 24 h at 15°C. Then, sixty randomly selected worms were incubated in 25°C incubator for 24 h to induce human Aβ expression. The number of paralyzed worms was counted every hour.

*2.12. RNA Interference (RNAi).* For the gene knockdown of *daf-16*, *E. coli* clones harboring *daf-16* gene for RNAi were obtained from the Ahringer RNAi library [25]. The expression of double-stranded RNA was induced by 0.4 mM isopropyl-β-D-thiogalactoside (IPTG) (Sigma-Aldrich, St. Louis, MO, USA) for 4 h after OD600 reached 0.4. Then, cultured bacteria were used as food source for RNAi experiment. *E. coli* clone transformed with empty vector was used as a negative control for RNAi.

## 3. Results

*3.1. Phosphatidylcholine Increased Resistance to Oxidative Stress and Lifespan.* In order to investigate the effect of phosphatidylcholine on the response to environmental stresses, we examined the effect of phosphatidylcholine on resistance to oxidative stress, heat shock, and UV irradiation. $H_2O_2$ was used to induce oxidative stress in *C. elegans*. A significant increase in survival under oxidative stress conditions was observed in worms supplemented with phosphatidylcholine (Figure 1(a)). The mean survival time was 3.6 h in the untreated control. Pretreatment of phosphatidylcholine increased the mean survival time under oxidative stress condition up to 6.3 ($P = 0.256$), 7.0 ($P = 0.027$), and 6.9 h ($P = 0.032$) with 1, 10, and 10 mg/l of concentration. However, lower concentration of phosphatidylcholine than 1 mg/l failed to show a significant change in resistance to oxidative stress (data not shown). Then, we determined the effect of dietary supplementation with phosphatidylcholine on other environmental stresses. However, unlike the results obtained with oxidative stress, there was no significant difference in resistance to either heat shock or UV irradiation. The survival curve after 7 h of heat shock was not altered by any concentration of phosphatidylcholine tested (Figure 1(b)). Dietary supplementation with phosphatidylcholine failed to increase the time course survival rate after UV irradiation (Figure 1(c)). Taken together, we concluded that phosphatidylcholine positively regulates resistance to oxidative stress but has no effect on the response to heat shock or UV irradiation. The free radical theory of aging suggests that the age-related accumulation of cellular damages caused by oxidative stress is one of the major causal factors of aging [2, 3]. Based

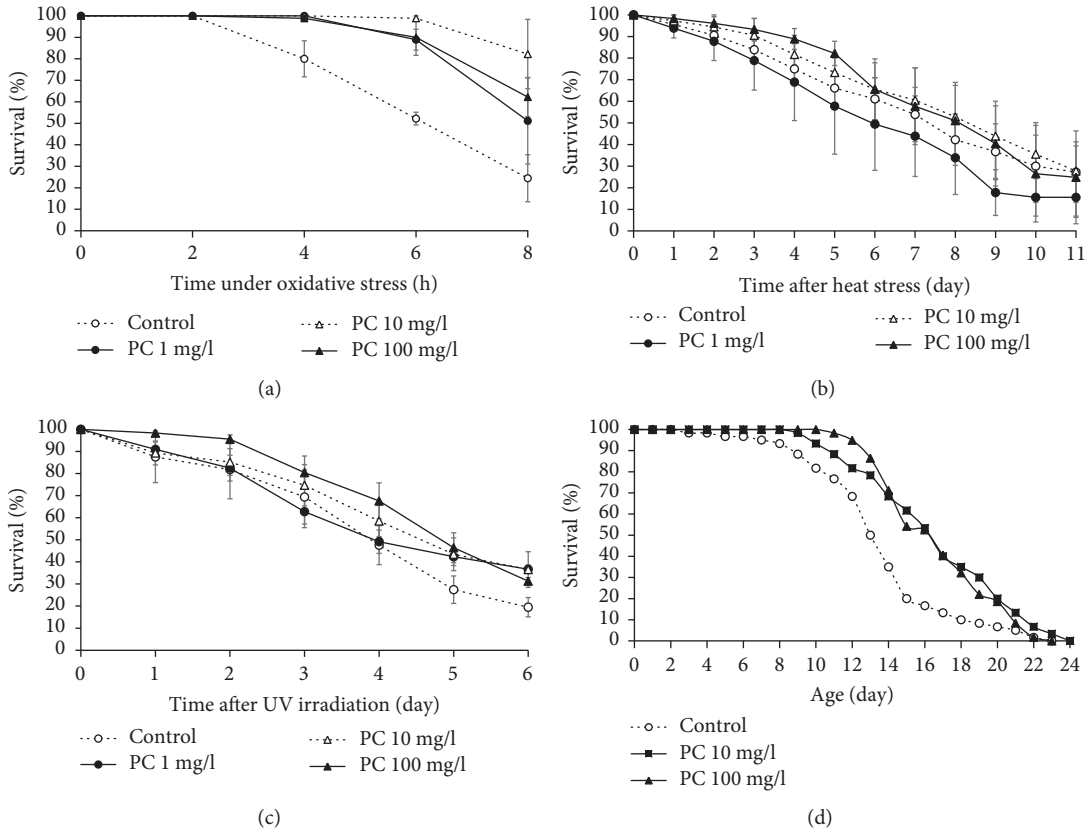


Figure 1: Effect of phosphatidylcholine on resistance to oxidative stress and lifespan. Sixty age-synchronized worms pretreated with phosphatidylcholine were placed under (a) oxidative stress, (b) heat shock, and (c) UV irradiation conditions. Survival of worms was monitored at indicated times after stress. (d) Lifespan was compared between the untreated control and worms treated with phosphatidylcholine. Error bar indicates standard error. PC: phosphatidylcholine.

on the previous finding that phosphatidylcholine can increase the resistance to oxidative stress, we asked whether dietary supplementation with phosphatidylcholine can modulate lifespan in *C. elegans*. As shown in Figure 1(d), the lifespan of *C. elegans* was significantly increased by phosphatidylcholine. The mean lifespan of wild-type N2 was 13.8 days. Animals treated with 10 mg/l of phosphatidylcholine showed a 28.8% increase in mean lifespan (17.7 d, $P < 0.001$). There was also a significant increase of mean lifespan in 100 mg/l of phosphatidylcholine-treated worms: the mean lifespan was 16.8 days (22.2% increase, $P < 0.001$) (Figure 1(d)). Independent repetitive experiments also showed a significant increase in lifespan by supplementation with phosphatidylcholine (Table 1). To discern whether this effect of phosphatidylcholine is caused directly by phosphatidylcholine or indirectly by bacteria with phosphatidylcholine treatment, we performed the lifespan assay with dead bacteria. The same significant lifespan-extending effect was observed by phosphatidylcholine in worms fed with dead bacteria, suggesting that the longevity phenotype was induced directly from phosphatidylcholine (Figure S1).

*3.2. Fertility Was Reduced by Supplementation with Phosphatidylcholine.* Many lifespan-extending genetic/dietary interventions have shown reduced fertility as a tradeoff [12, 26]. We examined the effect of phosphatidylcholine on the reproduction of *C. elegans*. The total number of progeny produced during a gravid period significantly decreased by supplementation with phosphatidylcholine (Figure 2(a)). In wild-type N2 worms, 243.0 ± 8.41 progeny were produced. However, the number of total progeny was reduced to 208.4 ± 9.43 ($P = 0.012$) in the 10 mg/l phosphatidylcholine-treated group and 195.3 ± 12.25 ($P = 0.005$) in the 100 mg/l phosphatidylcholine-treated group. The time course distribution of progeny produced during a gravid period revealed that there were decreases in the number of progeny on the 3rd day and 4th day after laying eggs (Figure 2(b)). Independent replicative experiment also showed the same reduced fertility by dietary intervention with phosphatidylcholine (data not shown). We also examined effect of phosphatidylcholine on fertility in *age-1* mutants, which is known to have reduced fertility as cost for extended lifespan [26]. Interestingly, there was no significant change in fertility by supplementation with phosphatidylcholine in *age-1* mutants (Figure S2). Our results indicate that the longevity phenotype conferred by supplementation with phosphatidylcholine accompanies reduced fertility as a tradeoff for long lifespan.

*3.3. Age-Related Decline in Motility Was Delayed by Phosphatidylcholine.* One of the obvious physiological changes happening with aging in almost all organisms is muscle atrophy and reduced motility [27]. In *C. elegans*,

Table 1: Effect of phosphatidylcholine on lifespan of *C. elegans*.

| | PC (mg/l) | Mean lifespan (day) | *P* value[1] | % effect[2] |
|---|---|---|---|---|
| 1st experiment | 0 | 13.8 | | |
| | 10 | 17.7 | <0.001 | 28.8 |
| | 100 | 16.8 | <0.001 | 22.2 |
| 2nd experiment | 0 | 18.6 | | |
| | 10 | 21.8 | <0.001 | 17.3 |
| | 100 | 20.3 | 0.021 | 9.2 |
| 3rd experiment | 0 | 18.7 | | |
| | 10 | 20.1 | 0.078 | 7.2 |
| | 100 | 21.3 | 0.001 | 13.6 |

[1]*P* value was calculated using the log-rank test by comparing the survival rate of the untreated control group (0 mg/l phosphatidylcholine) to that of the phosphatidylcholine-treated group (10 or 100 mg/L phosphatidylcholine). [2]% effects were calculated by $(C - p)/C^*100$, where $p$ is the mean lifespan of the phosphatidylcholine-treated group and $C$ is the mean lifespan of the untreated control group. PC: phosphatidylcholine.

locomotive behavior declines with aging. Then, we investigated the role of dietary intervention with phosphatidylcholine on the age-related decline of motility in *C. elegans*. We could observe the delayed decline of locomotive activity with aging in worms treated with phosphatidylcholine (Figure 3(a)). There were no clear differences in locomotive activity between the untreated control and phosphatidylcholine-treated groups in young worms (5- and 10-day-old worms). In 15-day-old worms, we could detect a slight increase in the number of worms categorized as phases 1 and 2, which are worms moving spontaneously without any mechanical stimuli and worms moving after mechanical stimuli, respectively. In contrast, more worms were classified as phase 3 (worms could move only the head part after mechanical stimuli) in the untreated control, compared to the phosphatidylcholine-treated groups. These differences were not statistically significant ($P > 0.05$). However, a significant difference between the untreated control and phosphatidylcholine-treated groups was detected in 20- and 25-day-old worms. On the 20th day, the number of worms categorized as phase 1 increased from $7.5 \pm 1.13\%$ in the untreated control to $24.0 \pm 3.46\%$ ($P = 0.011$) with 10 mg/l phosphatidylcholine treatment and $22.3 \pm 4.91\%$ ($P = 0.043$) with 100 mg/l phosphatidylcholine treatment. The worms classified as phase 2 also significantly increased by supplementation with phosphatidylcholine: $6.1 \pm 0.55$, $23.3 \pm 3.84$ ($P = 0.011$), and $20.6 \pm 3.71\%$ ($P = 0.018$) in the untreated control, 10 mg/l phosphatidylcholine-treated group, and 100 mg/l phosphatidylcholine-treated group, respectively (Figure 3(a)). The same significant delay of decline in motility was observed in 25-day-old worms (Table 2). We also examined effect of phosphatidylcholine on thrashing activity. There was no significant difference in the number of thrashing between the untreated control and phosphatidylcholine-treated groups in 5-day-old young animals. However, in aged worms, the number of thrashing was significantly increased by supplementation with phosphatidylcholine (Figure 3(b)). The number of thrashing per min was increased from $75.1 \pm 4.45$ in the untreated control to $95.1 \pm 4.05$ ($P = 0.002$) and $90.3 \pm 7.06$ ($P = 0.079$) in 10 mg/l and 100 mg/l phosphatidylcholine-treated groups, respectively, on 10 days after laying eggs. In 15-day-old control worms, the number of thrashing per min was decreased to $7.9 \pm 1.66$. However, supplementation with phosphatidylcholine significantly enhanced thrashing activity. The numbers of thrashing per min were $20.3 \pm 3.86$ ($P = 0.016$) with 10 mg/l of phosphatidylcholine and $17.7 \pm 2.50$ ($P = 0.008$) with 100 mg/l of phosphatidylcholine (Figure 3(b)).

*3.4. Phosphatidylcholine Induced Nuclear Localization of DAF-16 and Expression of Longevity Assurance Genes.* DAF-16 localizes to the nucleus in response to various stresses and modulates the expression of stress response genes [28]. Here, we determined the subcellular distribution of DAF-16 with or without dietary supplementation with phosphatidylcholine (Figure 4(a)). As shown in Figure 4(b), supplementation with phosphatidylcholine induced rapid nuclear localization of DAF-16. In 7-day-old worms, the percentage of worms showing intermediate localization were $19.4 \pm 10.56$ in the untreated control group and $32.8 \pm 11.07$ in the phosphatidylcholine-treated group. In the phosphatidylcholine-treated group, $2.8 \pm 2.78\%$ of worms showed nuclear localization, while no worm showed nuclear localization of DAF-16 in the untreated control. The differences observed on day 7 were not statistically significant ($P > 0.05$). However, there were significant differences in the subcellular distribution of DAF-16 between the untreated control and the phosphatidylcholine-treated groups on day 9. No worm showed cytosolic distribution of DAF-16 by supplementation with phosphatidylcholine, but $5.0 \pm 2.55\%$ of the untreated worms still showed cytosolic distribution of DAF-16. The percent of worms showing intermediate distribution decreased from $35.0 \pm 2.55\%$ in the untreated control to $13.3 \pm 5.09\%$ in the phosphatidylcholine-treated group ($P = 0.019$). In contrast, more worms showed nuclear localization by supplementation with phosphatidylcholine: $60.0 \pm 5.00\%$ in the untreated control and $86.7 \pm 5.09\%$ in the phosphatidylcholine-treated group ($P = 0.020$) (Figure 4(b)). Previous studies have shown that the expressions of downstream targets of DAF-16, *hsp-16.2* and *sod-3*, were positively correlated with the individual's lifespan in *C. elegans* [29, 30]. Having observed increased nuclear localization of DAF-16 by phosphatidylcholine, we next analyzed the expression of longevity assurance genes, *hsp-16.2* and *sod-3*, quantitatively. As shown in Figure 4(c), we could detect brighter fluorescence derived by *hsp-16.2* in worms treated with phosphatidylcholine. Quantification of fluorescence using multireader revealed that there was a significant increase in phosphatidylcholine-treated worms compared to the untreated control (Figure 4(d)). Relative expressions were $100.0 \pm 5.01$ in the 7-day-old untreated control, $148.2 \pm 5.74$ with 10 mg/l of phosphatidylcholine ($P < 0.001$), and $192.0 \pm 10.49$ with 100 mg/l of phosphatidylcholine ($P < 0.001$). The expression of *sod-3* was also significantly upregulated by supplementation with phosphatidylcholine (Figure 4(c)). There was a $55.3 \pm 7.99\%$ increase in relative expression with 10 mg/l of phosphatidylcholine ($P < 0.001$) and $105.1 \pm 8.97$

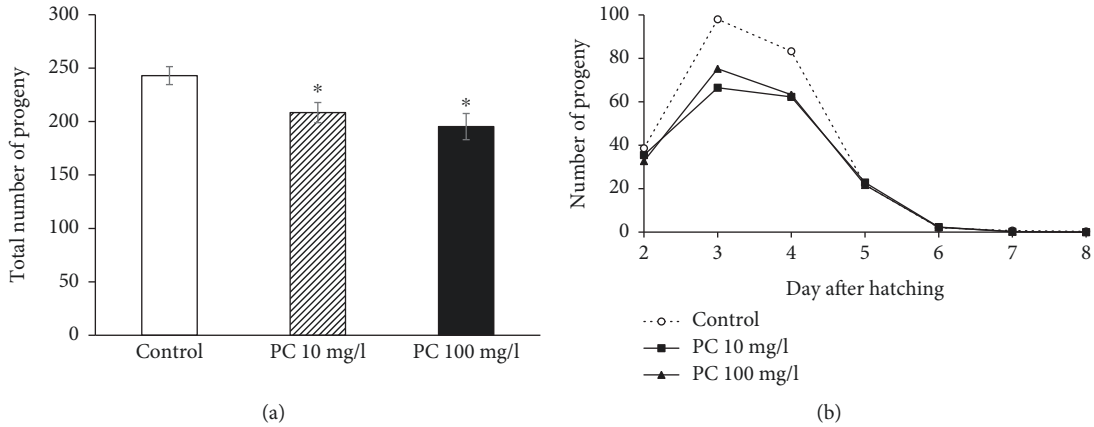


Figure 2: Effect of phosphatidylcholine on reproduction. (a) Total number of progeny produced during a gravid period was compared between the untreated control and phosphatidylcholine-treated groups. (b) Time course distribution of progeny produced during a gravid period. Number of progeny was recorded every day until there was no progeny produced. Data indicate a mean of 10 individual worms. Error bar indicates standard error. PC: phosphatidylcholine; *statistically significant ($P < 0.05$).

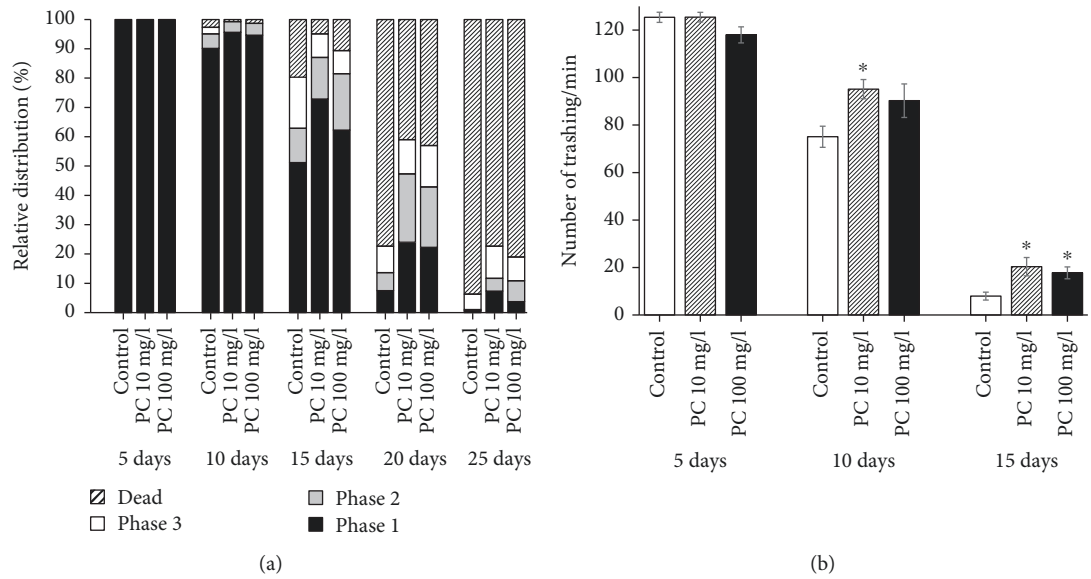


Figure 3: Effect of phosphatidylcholine on age-related decline in motility. (a) Relative distribution of worms in different locomotive phases was calculated in the untreated control and phosphatidylcholine-treated groups at indicated days. Phase 1, worms moving spontaneously without any stimuli; Phase 2, worms moving the whole body in response to mechanical stimuli; Phase 3, worms moving only the head part in response to mechanical stimuli; (b) the number of trashing was counted individually ($n = 15$) at indicated days after laying eggs. PC: phosphatidylcholine; *statistically significant ($P < 0.05$).

% increase with 100 mg/l of phosphatidylcholine ($P < 0.001$) in 7-day-old worms (Figure 4(d)). We could also observe a significant induction of *hsp-16.2* and *sod-3* by supplementation with phosphatidylcholine in 5- and 9-day-old worms (data not shown). This suggests that dietary supplementation with phosphatidylcholine may extend the lifespan of *C. elegans* through an induction of longevity assurance genes.

*3.5. The Cellular ROS Level Was Increased by Supplementation with Phosphatidylcholine.* Having observed increased resistance to oxidative stress and induction of oxidative stress response genes, we, next, tested the effect of phosphatidylcholine on the cellular ROS level. Surprisingly, the cellular ROS level was rather increased by supplementation with phosphatidylcholine (Figure 5). In 5-day-old worms, fluorescence intensity observed in the untreated control was $9322.4 \pm 1298.85$, which was increased up to $18295.7 \pm 1770.11$ with 10 mg/l of phosphatidylcholine ($P < 0.001$) and $28105.3 \pm 2342.10$ with 100 mg/l of phosphatidylcholine ($P < 0.001$). There was an increase in cellular ROS levels in 7-day-old worms, compared to 5-day-old worms in all experimental groups. We could observe the similar increase in the ROS level with phosphatidylcholine in 7-day-old worms. Fluorescence intensities were $25033.1 \pm 2092.52$, $30217.5 \pm 1643.30$ ($P = 0.059$), and $35329.4 \pm$

Table 2: Effect of phosphatidylcholine on age-related decline of motility.

| Age (day) | Phase | Control (%) | 10 mg/l PC (%) | 100 mg/l PC (%) |
|---|---|---|---|---|
| 5 | 1 | 100 | 100 | 100 |
| | 2 | 0 | 0 | 0 |
| | 3 | 0 | 0 | 0 |
| | Dead | 0 | 0 | 0 |
| 10 | 1 | 90.1 ± 3.33 | 95.6 ± 1.41 | 94.7 ± 3.53 |
| | 2 | 5.0 ± 1.64 | 3.7 ± 2.03 | 4.0 ± 2.31 |
| | 3 | 2.0 ± 1.10 | 0 | 0 |
| | Dead | 2.7 ± 1.80 | 0.7 ± 0.72 | 1.3 ± 1.33 |
| 15 | 1 | 51.2 ± 10.32 | 72.8 ± 22.29 | 62.3 ± 18.23 |
| | 2 | 11.7 ± 4.47 | 14.2 ± 4.79 | 19.2 ± 9.88 |
| | 3 | 17.4 ± 2.27 | 8.1 ± 5.00 | 7.9 ± 4.90 |
| | Dead | 19.7 ± 5.13 | 4.9 ± 2.79 | 10.6 ± 3.56 |
| 20 | 1 | 7.5 ± 1.13 | 24.0 ± 3.46* | 22.3 ± 4.91* |
| | 2 | 6.1 ± 0.55 | 23.3 ± 3.84* | 20.6 ± 3.71* |
| | 3 | 9.1 ± 1.15 | 11.7 ± 1.76 | 14.1 ± 2.88 |
| | Dead | 77.3 ± 2.60 | 41.0 ± 3.21* | 43.0 ± 5.25* |
| 25 | 1 | 0.67 ± 0.67 | 7.3 ± 1.86* | 3.7 ± 0.30* |
| | 2 | 0.33 ± 0.33 | 4.3 ± 2.60 | 7.2 ± 1.84* |
| | 3 | 5.29 ± 2.09 | 11.0 ± 3.79 | 8.1 ± 1.47 |
| | Dead | 93.7 ± 3.02 | 77.3 ± 2.03* | 81.0 ± 1.11* |

PC: phosphatidylcholine; *statistically significant compared to control ($P < 0.05$).

1806.83 ($P < 0.001$) in the untreated control, 10 mg/l phosphatidylcholine-treated, and 100 mg/l phosphatidylcholine-treated groups, respectively.

*3.6. Phosphatidylcholine Alleviated Aβ-Induced Toxicity, Which Is Independent of DAF-16.* Next, we examined the effect of phosphatidylcholine on AD, the age-related neurodegenerative disease. Using the *C. elegans* genetic model of AD, in which human Aβ transgene can be induced in muscle tissues, we determined the rate of paralysis caused by the accumulation of Aβ in muscle [31]. The rate of paralysis was significantly reduced by dietary supplementation with phosphatidylcholine (Figure 6(a)). In the untreated control, the time when 50% of worms were paralyzed was 4.1 h. However, treatment with phosphatidylcholine extended the time when 50% of worms were paralyzed up to 6.3 h with 10 mg/l phosphatidylcholine ($P < 0.001$) and 7.0 h with 100 mg/l phosphatidylcholine ($P < 0.001$). The protective effect by phosphatidylcholine against Aβ-induced paralysis was 55.7 and 71.3% with 10 and 100 mg/l of phosphatidylcholine, respectively. Independent replicative experiments also showed the significant protective effect of phosphatidylcholine on Aβ-induced toxicity (Table 3). It was reported that DAF-16, the FOXO transcription factor involved in insulin/IGF-1-like signaling, can delay the onset of Aβ-induced toxicity [32]. However, we observed the same significant delayed paralysis by supplementation with phosphatidylcholine with *daf-16* knockdown genetic background (Figure 6(b)). These findings suggest that phosphatidylcholine has a protective effect against Aβ-induced toxicity, which is independent of DAF-16.

*3.7. Effect of Phosphatidylcholine on Lifespan Specifically Overlapped with That of Age-1 Mutation and Requires DAF-16.* In order to identify the underlying mechanisms involved in phosphatidylcholine-induced longevity, we tested the effect of phosphatidylcholine on the lifespan of long-lived mutants. The lifespan of *age-1*, in which lifespan was extended due to reduced insulin/IGF-1-like signaling, was not altered by phosphatidylcholine treatment (Figure 7(a)). Interestingly, supplementation with phosphatidylcholine significantly increased the lifespan of *clk-1* and *eat-2*. The *clk-1* (*e2519*) mutant has defect in the ubiquinone biosynthesis required for the mitochondrial electron transport system and, as a result, produces less ROS [33]. The *eat-2* (*ad465*) mutation causes a reduced food pumping rate and leads to dietary restriction as a consequence [34]. There was a 14.7% increase in the mean lifespan of *clk-1* (*e2519*) by supplementation with phosphatidylcholine: 22.2 days in the untreated control and 25.4 days in the phosphatidylcholine-treated group ($P = 0.013$) (Figure 7(b)). The long lifespan of the genetic model of dietary restriction, *eat-2* (ad465), was further extended by phosphatidylcholine treatment. The mean lifespan was increased from 21.0 to 25.8 days by phosphatidylcholine ($P = 0.001$, 18.3% increase) (Figure 7(c)). A repetitive experiment showed the same effect of phosphatidylcholine on long-lived mutants (Table 4). Overall, our data indicate that the lifespan-extending effect of phosphatidylcholine overlaps with that of *age-1* mutation, but not with that of *clk-1* or *eat-2* mutation. The longevity phenotype conferred by reduced insulin/IGF-1-like signaling requires DAF-16 [26]. Based on our finding that the effect of phosphatidylcholine on lifespan overlapped with that of *age-1* mutation, we examined the effect of *daf-16* knockdown on the lifespan extension induced by supplementation with phosphatidylcholine. Unlike the results observed in worms treated with empty vector, dietary supplementation with phosphatidylcholine failed to increase lifespan when the expression of *daf-16* was inhibited using RNAi (Figure 7(d)). Mean lifespan was increased from 17.9 to 21.1 days by supplementation with phosphatidylcholine in worms treated with empty vector RNAi ($P < 0.001$). In contrast, there was no significant difference between the control and the phosphatidylcholine-treated groups in worms treated with *daf-16* RNAi: mean lifespans were 15.5 and 15.6 days in the control and phosphatidylcholine-treated groups, respectively ($P = 0.622$). A replicative experiment showed the same results (Table 5). These results indicate that DAF-16 is required for the effect of phosphatidylcholine on lifespan and support our previous finding that the longevity phenotype conferred by supplementation with phosphatidylcholine is mediated by reduced insulin/IGF-1-like signaling.

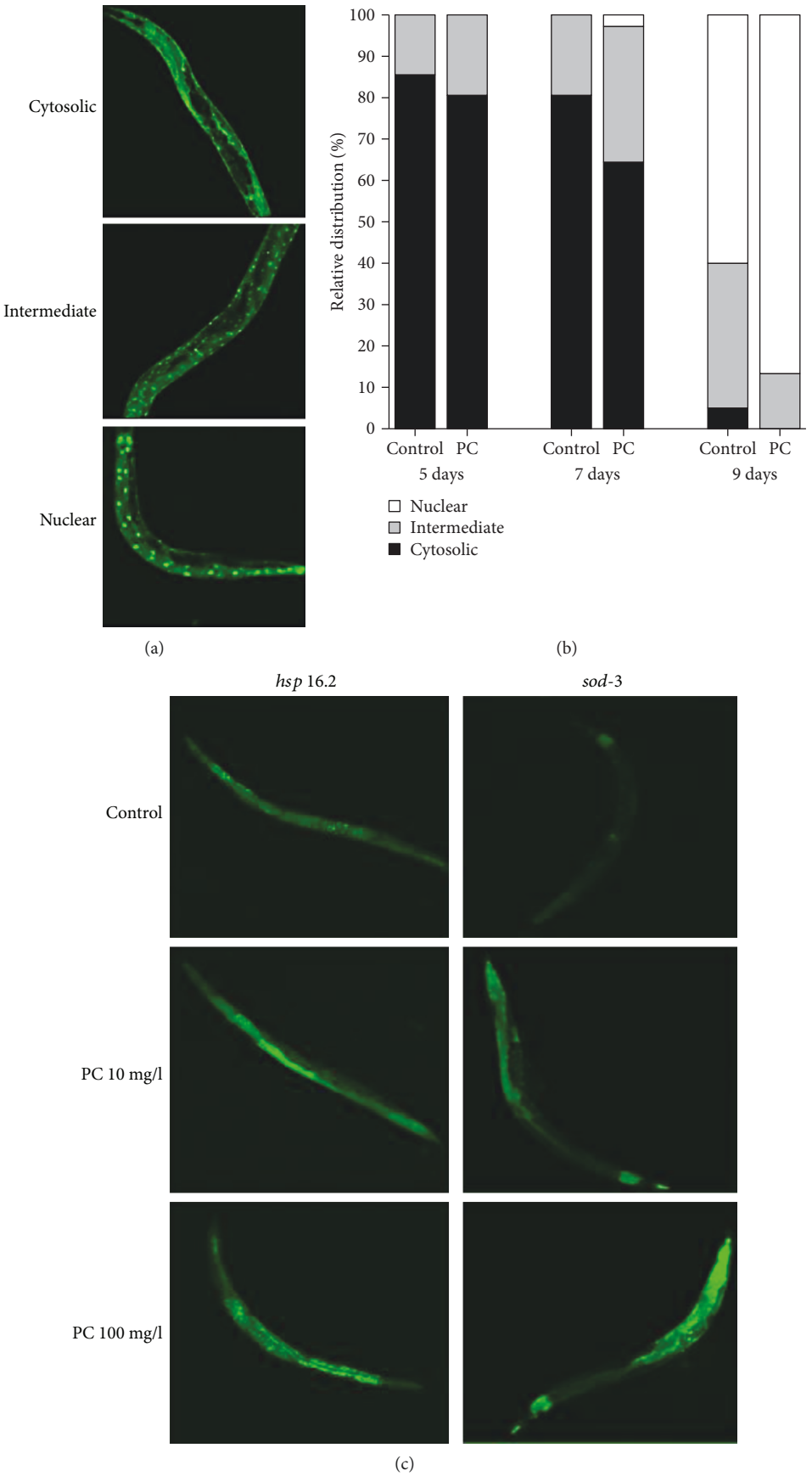


Figure 4: Continued.

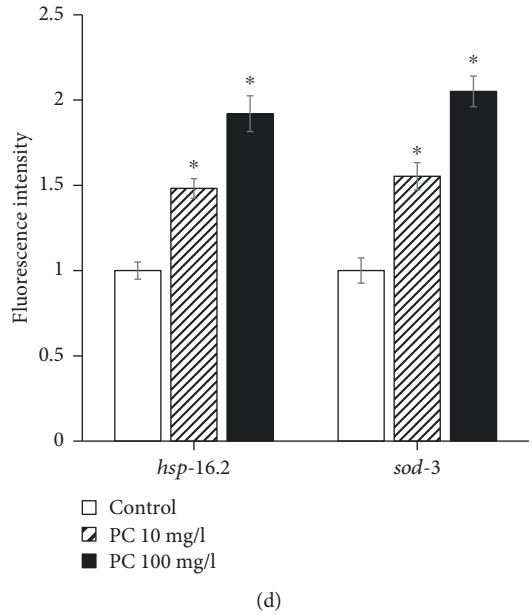


Figure 4: Cellular distribution of DAF-16 and GFP expressions of downstream targets of DAF-16. (a) Subcellular localization was classified as three categories: cytosolic, fluorescence was spread in cytosol; intermediate, GFP can be found both in cytosol and nucleus; and nucleus, clear localization of GFP into the nucleus. (b) Relative distribution of DAF-16 was compared between the untreated control and 100 mg/l phosphatidylcholine-treated groups. (c) Age-synchronized 3-day-old worms were treated with each concentration of phosphatidylcholine for 7 d. Then, worms were observed on confocal microscopy. (d) Change in the expression level was determined using a fluorescence multireader. Fluorescence intensity of PC-treated worms is expressed as the ratio of fluorescence intensity determined in the untreated control. Error bar indicates standard error. PC: phosphatidylcholine; *statistically significant ($P < 0.05$).

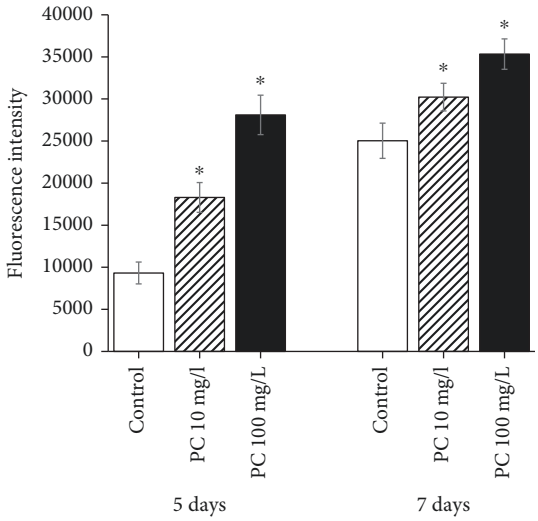


Figure 5: Effect of phosphatidylcholine on the cellular ROS level. The cellular ROS level was measured in an individual worm at indicated days after laying eggs. Error bar indicates standard error. PC: phosphatidylcholine; *statistically significant ($P < 0.05$).

## 4. Discussion

Based on the free radical theory of aging emphasizing the role of oxidative damages accumulated with time in normal aging, numerous studies have reported the effect of supplementation with antioxidant on aging. Resveratrol, a polyphenol compound rich in red wine, has been shown to have strong antioxidant and lifespan-extending effects on various model organisms [35]. Recent studies reported that amino acid derivatives, including N-acetyl-L-cysteine, S-allylcysteine, and selenocysteine, increase resistance to oxidative stress and extend lifespan in *C. elegans* [15, 16, 36]. In the present study, we showed that phosphatidylcholine, a phospholipid composing cellular membrane, had an antioxidant activity *in vivo* and conferred the longevity phenotype in *C. elegans* for the first time. Our findings support the free radical theory of aging and provide a scientific background for the use of phospholipid as a novel antioxidant and antiaging biomolecule. There is another well-known theory of aging, named "the membrane theory of aging" by Dr. ImreZs-Nagy [37]. According to the membrane theory of aging, age-related decline in membrane function leads to inefficient communication through membrane and accumulation of toxic compound in the cellular membrane and eventually causes the aging of cells [37]. The amount of phosphatidylcholine in membrane decreases with aging, which results in decreased membrane function for nutrient uptake and toxin excretion and solidification of membrane filled with cholesterol and toxic deposits, called lipofuscin [38]. Since we observed the positive effect of phosphatidylcholine on lifespan, it is also suggestive that supplementation with phosphatidylcholine might reverse the aging process, possibly through the avoidance of age-related depletion of phosphatidylcholine and maintenance of membrane integrity.

The disposable soma theory states that limited cellular resources should be allocated to cell maintenance, repair, and reproduction and that there is a tradeoff between

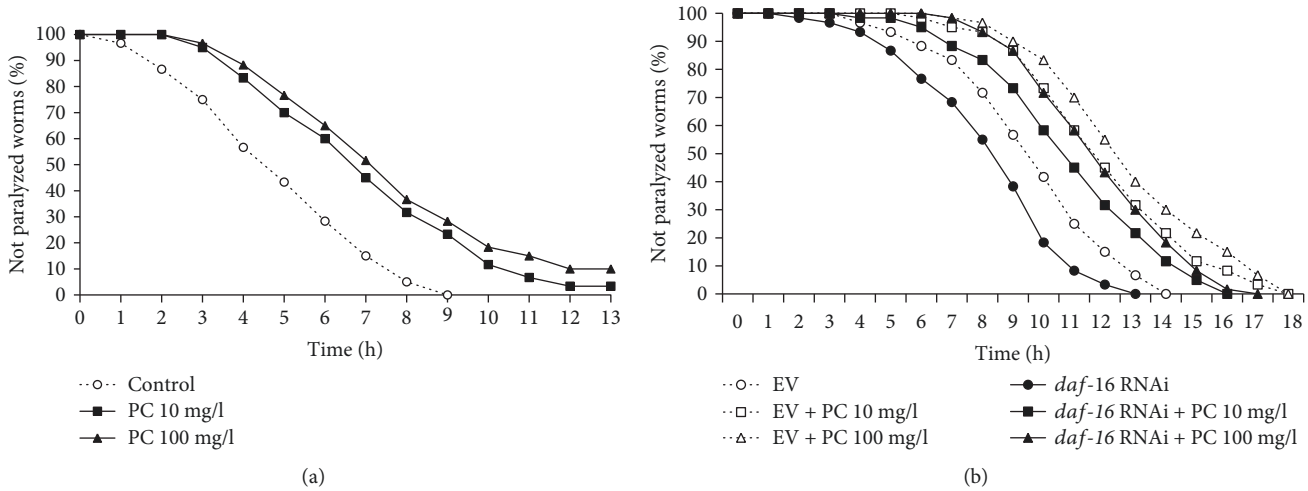


Figure 6: Effect of phosphatidylcholine on A$\beta$-induced toxicity. (a) Paralyzed worms were counted every hour after human A$\beta$ induction in muscle tissues. (b) Effect of *daf-16* knockdown on reduced susceptibility to A$\beta$-induced toxicity was determined using RNAi. PC: phosphatidylcholine; EV: empty vector.

Table 3: Effect of phosphatidylcholine on A$\beta$-induced toxicity in *C. elegans*.

| | PC (mg/l) | Time when 50% of worms were paralyzed (h) | $P$ value[1] | % effect[2] |
|---|---|---|---|---|
| 1st experiment | 0 | 4.1 | | |
| | 10 | 6.3 | <0.001 | 55.7 |
| | 100 | 7.0 | <0.001 | 71.3 |
| 2nd experiment | 0 | 4.1 | | |
| | 10 | 7.1 | <0.001 | 71.8 |
| | 100 | 7.4 | <0.001 | 77.8 |
| 3rd experiment | 0 | 3.3 | | |
| | 10 | 6.7 | <0.001 | 106.1 |
| | 100 | 8.4 | <0.001 | 157.7 |

[1] $P$ value was calculated using the log-rank test by comparing the rate of paralysis in the untreated control group (0 mg/l phosphatidylcholine) to that in the phosphatidylcholine-treated group (10 or 100 mg/l phosphatidylcholine). [2]% effects were calculated by $(C - p)/C^* 100$, where $p$ is the time when 50% of worms were paralyzed in the phosphatidylcholine-treated group and $C$ is the time when 50% of worms were paralyzed in the untreated control group. PC: phosphatidylcholine.

increased lifespan and reduced fertility [39]. We observed a significant decrease in the number of progeny produced in worms treated with phosphatidylcholine, compared to the untreated control, which supports the disposable soma theory of aging. Long-lived *age-1* mutants showed reduced fertility, and knockout of germ cells increased lifespan in *C. elegans* [26]. Lifespan extension by dietary interventions with resveratrol also accompanied decreased reproduction [12]. The other widely used phenotypic marker of aging is the age-related decline of motility. Decreased motility with aging is associated with muscle atrophy and dysfunction [40]. Recent studies have shown that genetic intervention with antioxidant genes, such as *cat* and *sod-1*, or nutritional intervention with antioxidants, such as silymarin and selenocysteine, can modulate age-related muscle dysfunction [16, 41, 42]. Here, we showed that phosphatidylcholine also has a preventive effect against the age-related decline of motility. Since muscle tissues are one of the high energy-demanding tissues and have many mitochondria producing ROS as a byproduct of ATP generation, the effect of phosphatidylcholine on muscle aging seems to be due to its antioxidant activity. In addition to phenotypic age-related markers, we also examined the effect of phosphatidylcholine on the genetic markers of aging. Rea *et al.* found that the variability observed in lifespan among animals with the same genetic and environmental backgrounds was due to the differential expression of *hsp-16.2* [29]. Another study reported that *sod-3* could be a transcriptional marker of long lifespan [30]. The expressions of both *hsp-16.2* and *sod-3* were significantly upregulated by supplementation with phosphatidylcholine. Additionally, we observed increased nuclear localization of DAF-16, a transcription factor-regulating expression of many stress-responsive genes, including *hsp-16.2* and *sod-3* [28]. Taken together, we concluded that dietary supplementation with phosphatidylcholine can modulate the physiological and molecular markers of aging, as well as the organism's lifespan. Since there was an increase in the cellular ROS level with supplementation with phosphatidylcholine, it is suggestive that phosphatidylcholine may be a ROS generator *in vivo* and the antioxidant and anti-aging effects of phosphatidylcholine may be due to its hormetic effect. A previous study also showed that a ROS generator, juglone, induced expressions of *hsp-16.2* and hormesis [43].

AD is a neurodegenerative disease whose incidence is associated with aging. One of the molecular markers positively correlated with the incidence of AD is A$\beta$ accumulation in the brain [44]. The Amyloid precursor protein (APP) is degraded by $\alpha$-secretase and produces nonamyloidogenic fragment, but proteolysis of APP by $\gamma$-secretase produces A$\beta$. The accumulation of A$\beta$ is found in the brain of AD patients [45]. Lifespan-extending amino acid derivatives,

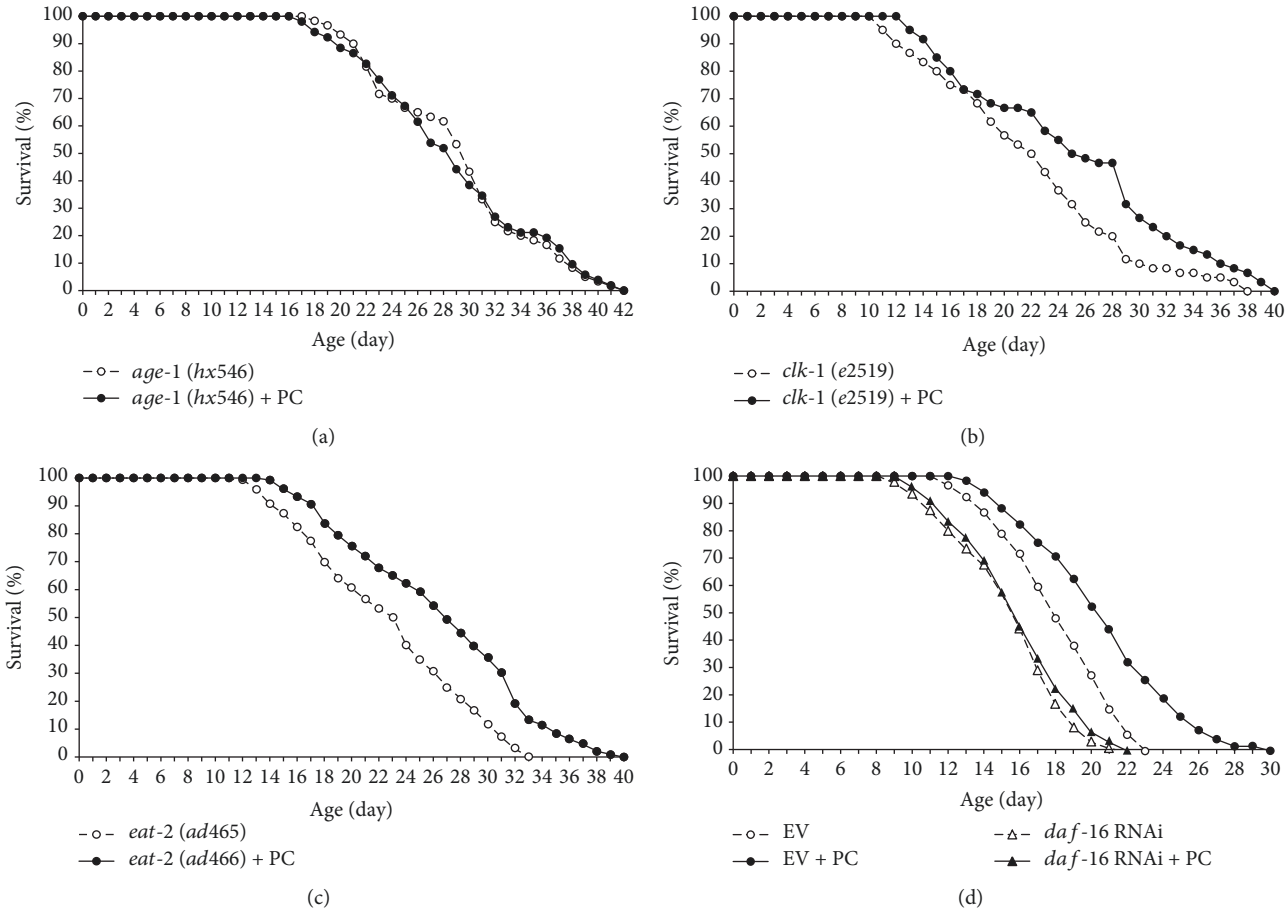


Figure 7: The underlying mechanism involved in the lifespan-extending effect of phosphatidylcholine. Survival curve was compared between the untreated control and phosphatidylcholine-treated groups in three long-lived mutants, (a) *age-1*, (b) *clk-1*, and (c) *eat-2*. (d) Requirement of DAF-16 on lifespan extension by phosphatidylcholine. EV: empty vector; PC: 100 mg/l of phosphatidylcholine.

Table 4: Effect of phosphatidylcholine on lifespan of wild-type N2 and long-lived mutants.

| | | Mean lifespan (day) | | $P$ value[1] | % effect[2] |
|---|---|---|---|---|---|
| | | Control | 100 mg/l PC | | |
| N2 | 1st experiment | 17.5 | 20.6 | <0.001 | 17.6 |
| | 2nd experiment | 21.6 | 24.9 | <0.001 | 15.4 |
| *age-1* (*hx546*) | 1st experiment | 29.2 | 28.9 | 0.970 | -1.0 |
| | 2nd experiment | 33.8 | 30.4 | 0.090 | -10.1 |
| *clk-1* (*e2519*) | 1st experiment | 22.2 | 25.4 | 0.013 | 14.7 |
| | 2nd experiment | 22.0 | 25.8 | <0.001 | 17.2 |
| *eat-2* (*ad465*) | 1st experiment | 21.9 | 25.8 | 0.001 | 18.3 |
| | 2nd experiment | 23.7 | 27.4 | 0.002 | 15.6 |

[1]$P$ value was calculated using the log-rank test by comparing the survival of the untreated control group to that of the phosphatidylcholine-treated group. [2]% effects were calculated by $(C-p)/C^*100$, where $p$ is the mean lifespan of the phosphatidylcholine-treated group and $C$ is the mean lifespan of the untreated control group. PC: phosphatidylcholine.

N-acetyl-L-cysteine and selenocysteine, reduced A$\beta$-induced toxicity in *C. elegans* [15, 16]. DAF-16 is necessary for protection against A$\beta$-induced toxicity and selenocysteine induced nuclear localization of DAF-16 [16, 32]. We observed that dietary supplementation with phosphatidylcholine can delay paralysis caused by A$\beta$ induction and the effect was not affected by DAF-16. These findings suggest that phosphatidylcholine can modulate A$\beta$-induced toxicity, which is independent of DAF-16, and can be a strong candidate for the development of functional food for the treatment of AD.

Genetic screenings have identified several lifespan-extending mechanisms in *C. elegans*. The first long-lived mutant reported was *age-1* mutant [46]. The *age-1* gene encodes phosphoinositide 3-kinase, which mediates

Table 5: Effect of *daf-16* knockdown on lifespan extension with phosphatidylcholine.

| | RNAi | Mean lifespan (day) | | $P$ value[1] |
|---|---|---|---|---|
| | | Control | 100 mg/l PC | |
| 1st experiment | EV | 17.9 | 21.1 | <0.001 |
| | *daf-16* | 15.5 | 15.6 | 0.622 |
| 2nd experiment | EV | 18.5 | 20.2 | 0.005 |
| | *daf-16* | 15.7 | 16.4 | 0.255 |

[1] $P$ value was calculated using the log-rank test by comparing the survival rate of the untreated control group to that of the phosphatidylcholine-treated group. PC: phosphatidylcholine; EV: empty vector.

insulin/IGF-1-like signaling. Mutations in *daf-2*, the upstream receptor gene for the insulin/IGF-1-like signaling pathway, also resulted in increased lifespan [47]. The longevity phenotype conferred by reduced insulin/IGF-1-like signaling is common in various organisms [48]. The other lifespan-extending mutations found in *C. elegans* include mutations in genes causing lowered mitochondrial electron transport chain reaction and decreased production of harmful ROS as a result. For example, mutations in *clk-1* (gene required for the biosynthesis of ubiquinone) or *isp-1* (subunit of mitochondrial complex III) significantly increased lifespan and genome-wide RNAi screening revealed mutations in many genes involved in mitochondrial electron transport chain reaction that led to lifespan extension [33, 49]. The only intervention that showed consistent lifespan-extending effect on all experimental organisms from yeast to monkeys is dietary restriction [50]. The *eat-2* mutant is a well-known genetic model of dietary restriction in *C. elegans* [51]. We tested the effect of supplementation with phosphatidylcholine on the lifespan of *age-1*, *clk-1*, and *eat-2* mutants. Interestingly, only the lifespan of *age-1* was not affected by supplementation with phosphatidylcholine. In addition, phosphatidylcholine did not affect the fertility of *age-1*, while it significantly reduced the fertility of wild-type control. These results indicate that the lifespan-extending mechanism regulated by supplementation with phosphatidylcholine overlaps specifically with reduced insulin/IGF-1-like signaling. The complete disappearance of the longevity phenotype conferred by supplementation with phosphatidylcholine by RNAi knockdown of *daf-16*, the downstream effector of reduced insulin/IGF-1-like signaling, further supports our conclusion.

## 5. Conclusions

In the present study, we report the antioxidant and antiaging activities of phosphatidylcholine for the first time. Phosphatidylcholine also showed a positive effect on the physiological and molecular markers of aging and a protective effect against A$\beta$-induced toxicity. Finally, we identify the cellular mechanisms underlying the lifespan-extending effect of phosphatidylcholine. Our data reveal the novel bioactivities of phosphatidylcholine and provide a scientific rationale for additional aging research with other phospholipid molecules. The results of the study can also be useful for the development of pharmaceutical or dietary supplement having antiaging effect. Further studies focusing on the antiaging effect of phosphatidylcholine on higher model organisms, such as mice, should follow in the near future.

## Data Availability

The data used to support the results of this study are included within the article (and its supplementary materials). Requests for material should be made to the corresponding author.

## Conflicts of Interest

The authors declare that they have no conflicts of interest.

## Acknowledgments

This work was supported by the Soonchunhyang University Research Fund and the Basic Science Research Program through the National Research Foundation of Korea funded by the Ministry of Education (2018R1D1A1B07043414).

## Supplementary Materials

Supplementary Figures: (1) effect of phosphatidylcholine on lifespan measured with dead bacteria; (2) effect of phosphatidylcholine on reproduction of *age-1*. *(Supplementary Materials)*

## References

[1] R. J. Pignolo, "Exceptional human longevity," *Mayo Clinic Proceedings*, vol. 94, no. 1, pp. 110–124, 2019.

[2] D. Harman, "Aging: a theory based on free radical and radiation chemistry," *Journal of Gerontology*, vol. 11, no. 3, pp. 298–300, 1956.

[3] K. B. Beckman and B. N. Ames, "The free radical theory of aging matures," *Physiological Reviews*, vol. 78, no. 2, pp. 547–581, 1998.

[4] M. E. Harper, L. Bevilacqua, K. Hagopian, R. Weindruch, and J. J. Ramsey, "Ageing, oxidative stress, and mitochondrial uncoupling," *Acta Physiologica Scandinavica*, vol. 182, no. 4, pp. 321–331, 2004.

[5] M. K. Shigenaga, T. M. Hagen, and B. N. Ames, "Oxidative damage and mitochondrial decay in aging," *Proceedings of the National Academy of Sciences of the United States of America*, vol. 91, no. 23, pp. 10771–10778, 1994.

[6] M. Fossel, "Telomerase and the aging cell: implications for human health," *Journal of the American Medical Association*, vol. 279, no. 21, pp. 1732–1735, 1998.

[7] R. A. Shamanna, D. L. Croteau, J. H. Lee, and V. A. Bohr, "Recent advances in understanding Werner syndrome," *F1000 Research*, vol. 6, p. 1779, 2017.

[8] R. S. Sohal, A. Agarwal, S. Agarwal, and W. C. Orr, "Simultaneous overexpression of copper- and zinc-containing superoxide dismutase and catalase retards age-related oxidative damage and increases metabolic potential in *Drosophila melanogaster*," *The Journal of Biological Chemistry*, vol. 270, no. 26, pp. 15671–15674, 1995.

[9] V. I. Pérez, A. Bokov, H. V. Remmen et al., "Is the oxidative stress theory of aging dead?," *Biochimica et Biophysica Acta*

*(BBA) - General Subjects*, vol. 1790, no. 10, pp. 1005–1014, 2009.

[10] M. Jang, L. Cai, G. O. Udeani et al., "Cancer chemopreventive activity of resveratrol, a natural product derived from grapes," *Science*, vol. 275, no. 5297, pp. 218–220, 1997.

[11] K. T. Howitz, K. J. Bitterman, H. Y. Cohen et al., "Small molecule activators of sirtuins extend *Saccharomyces cerevisiae* lifespan," *Nature*, vol. 425, no. 6954, pp. 191–196, 2003.

[12] J. Gruber, S. Y. Tang, and B. Halliwell, "Evidence for a trade-off between survival and fitness caused by resveratrol treatment of *Caenorhabditis elegans*," *Annals of the New York Academy of Sciences*, vol. 1100, no. 1, pp. 530–542, 2007.

[13] J. Long, H. Gao, L. Sun, J. Liu, and X. Zhao-Wilson, "Grape extract protects mitochondria from oxidative damage and improves locomotor dysfunction and extends lifespan in a Drosophila Parkinson's disease model," *Rejuvenation Research*, vol. 12, no. 5, pp. 321–331, 2009.

[14] E. Marzetti, R. Calvani, R. Bernabei, and C. Leeuwenburgh, "Apoptosis in skeletal myocytes: a potential target for interventions against sarcopenia and physical frailty - a mini-review," *Gerontology*, vol. 58, no. 2, pp. 99–106, 2012.

[15] S. I. Oh and S. K. Park, "N-Acetyl-L-cysteine mimics the effect of dietary restriction on lifespan and reduces amyloid beta-induced toxicity in *Caenorhabditis elegans*," *Food Science and Biotechnology*, vol. 26, no. 3, pp. 783–790, 2017.

[16] S.-H. Kim, B.-K. Kim, and S.-K. Park, "Selenocysteine mimics the effect of dietary restriction on lifespan via SKN-1 and retards age-associated pathophysiological changes in Caenorhabditis elegans," *Molecular Medicine Reports*, vol. 18, no. 6, pp. 5389–5398, 2018.

[17] J. K. Park, C. K. Kim, S. K. Gong, A. R. Yu, M. Y. Lee, and S. K. Park, "Acanthopanax sessiliflorus stem confers increased resistance to environmental stresses and lifespan extension in Caenorhabditis elegans," *Nutrition Research and Practice*, vol. 8, no. 5, pp. 526–532, 2014.

[18] S. M. Won, H. U. Cha, S. S. Yi, S. J. Kim, and S. K. Park, "*Tenebrio molitor* extracts modulate the response to environmental stressors and extend lifespan in *Caenorhabditis elegans*," *Journal of Medicinal Food*, vol. 19, no. 10, pp. 938–944, 2016.

[19] J. N. van der Veen, J. P. Kennelly, S. Wan, J. E. Vance, D. E. Vance, and R. L. Jacobs, "The critical role of phosphatidylcholine and phosphatidylethanolamine metabolism in health and disease," *Biochimica et Biophysica Acta (BBA) - Biomembranes*, vol. 1859, no. 9, pp. 1558–1572, 2017.

[20] M. Kim, A. Nevado-Holgado, L. Whiley et al., "Association between plasma ceramides and phosphatidylcholines and hippocampal brain volume in late onset Alzheimer's disease," *Journal of Alzheimer's Disease*, vol. 60, no. 3, pp. 809–817, 2017.

[21] M. M. Zhou, Y. Xue, S. H. Sun et al., "Effects of different fatty acids composition of phosphatidylcholine on brain function of dementia mice induced by scopolamine," *Lipids in Health and Disease*, vol. 15, no. 1, p. 135, 2016.

[22] Y. Yamanaka, S. Yoshida-Yamamoto, and H. Doi, "Microtubule formation and activities of antioxidative enzymes in PC12 cells exposed to phosphatidylcholine hydroperoxides," *International Journal of Molecular Sciences*, vol. 13, no. 12, pp. 15510–15522, 2012.

[23] P. Morganti, Guevara, Palombo et al., "A phosphatidylcholine hyaluronic acid chitin–nanofibrils complex for a fast skin remodeling and a rejuvenating look," *Clinical, Cosmetic and Investigational Dermatology*, vol. 5, pp. 213–220, 2012.

[24] R. Peto and J. Peto, "Asymptotically efficient rank invariant test procedures," *Journal of the Royal Statistical Society. Series A (General)*, vol. 135, no. 2, pp. 185–207, 1972.

[25] R. S. Kamath, A. G. Fraser, Y. Dong et al., "Systematic functional analysis of the Caenorhabditis elegans genome using RNAi," *Nature*, vol. 421, no. 6920, pp. 231–237, 2003.

[26] T. E. Johnson, "Increased life-span of age-1 mutants in Caenorhabditis elegans and lower Gompertz rate of aging," *Science*, vol. 249, no. 4971, pp. 908–912, 1990.

[27] M. J. Gomes, P. F. Martinez, L. U. Pagan et al., "Skeletal muscle aging: influence of oxidative stress and physical exercise," *Oncotarget*, vol. 8, no. 12, pp. 20428–20440, 2017.

[28] C. T. Murphy, "The search for DAF-16/FOXO transcriptional targets: approaches and discoveries," *Experimental Gerontology*, vol. 41, no. 10, pp. 910–921, 2006.

[29] S. L. Rea, D. Wu, J. R. Cypser, J. W. Vaupel, and T. E. Johnson, "A stress-sensitive reporter predicts longevity in isogenic populations of Caenorhabditis elegans," *Nature Genetics*, vol. 37, no. 8, pp. 894–898, 2005.

[30] A. Sanchez-Blanco and S. K. Kim, "Variable pathogenicity determines individual lifespan in *Caenorhabditis elegans*," *PLoS Genetics*, vol. 7, no. 4, article e1002047, 2011.

[31] C. D. Link, "*C. elegans* models of age-associated neurodegenerative disease: lessons from transgenic worm models of Alzheimer's disease," *Experimental Gerontology*, vol. 41, no. 10, pp. 1007–1013, 2006.

[32] E. Cohen and A. Dillin, "The insulin paradox: aging, proteotoxicity and neurodegeneration," *Nature Reviews Neuroscience*, vol. 9, no. 10, pp. 759–767, 2008.

[33] A. Wong, P. Boutis, and S. Hekimi, "Mutations in the clk-1 gene of Caenorhabditis elegans affect developmental and behavioral timing," *Genetics*, vol. 139, no. 3, pp. 1247–1259, 1995.

[34] B. Lakowski and S. Hekimi, "The genetics of caloric restriction in Caenorhabditis elegans," *Proceedings of the National Academy of Sciences of the United States of America*, vol. 95, no. 22, pp. 13091–13096, 1998.

[35] J. G. Wood, B. Rogina, S. Lavu et al., "Sirtuin activators mimic caloric restriction and delay ageing in metazoans," *Nature*, vol. 430, no. 7000, pp. 686–689, 2004.

[36] T. Ogawa, Y. Kodera, D. Hirata, T. K. Blackwell, and M. Mizunuma, "Natural thioallyl compounds increase oxidative stress resistance and lifespan in *Caenorhabditis elegans* by modulating SKN-1/Nrf," *Scientific Reports*, vol. 6, no. 1, article 21611, 2016.

[37] A. W. Pathath, "Theories of aging," *International Journal of Indian Psychology*, vol. 4, no. 4, pp. 15–22, 2017.

[38] W. K. Martins, A. B. Gomide, É. T. Costa et al., "Membrane damage by betulinic acid provides insights into cellular aging," *Biochimica et Biophysica Acta (BBA) - General Subjects*, vol. 1861, no. 1, Part A, pp. 3129–3143, 2017.

[39] T. B. L. Kirkwood, "Evolution of ageing," *Nature*, vol. 270, no. 5635, pp. 301–304, 1977.

[40] A. del Campo, E. Jaimovich, and M. F. Tevy, "Mitochondria in the aging muscles of flies and mice: new perspectives for old characters," *Oxidative Medicine and Cellular Longevity*, vol. 2016, Article ID 9057593, 10 pages, 2016.

[41] F. L. Muller, W. Song, Y. Liu et al., "Absence of CuZn superoxide dismutase leads to elevated oxidative stress and

acceleration of age-dependent skeletal muscle atrophy," *Free Radical Biology and Medicine*, vol. 40, no. 11, pp. 1993–2004, 2006.

[42] J. Kumar, K. C. Park, A. Awasthi, and B. Prasad, "Silymarin extends lifespan and reduces proteotoxicity in C. elegans Alzheimer's model," *CNS & Neurological Disorders - Drug Targets*, vol. 14, no. 2, pp. 295–302, 2015.

[43] K. Hartwig, T. Heidler, J. Moch, H. Daniel, and U. Wenzel, "Feeding a ROS-generator to Caenorhabditis elegans leads to increased expression of small heat shock protein HSP-16.2 and hormesis," *Genes & Nutrition*, vol. 4, no. 1, pp. 59–67, 2009.

[44] X. Zhang, Z. Fu, L. Meng, M. He, and Z. Zhang, "The early events that initiate $\beta$-amyloid aggregation in Alzheimer's disease," *Frontiers in Aging Neuroscience*, vol. 10, p. 359, 2018.

[45] J. Rasmussen, J. Mahler, N. Beschorner et al., "Amyloid polymorphisms constitute distinct clouds of conformational variants in different etiological subtypes of Alzheimer's disease," *Proceedings of the National Academy of Sciences of the United States of America*, vol. 114, no. 49, pp. 13018–13023, 2017.

[46] D. B. Friedman and T. E. Johnson, "Three mutants that extend both mean and maximum life span of the nematode, Caenorhabditis elegans, define the age-1 gene," *Journal of Gerontology*, vol. 43, no. 4, pp. B102–B109, 1988.

[47] C. Kenyon, J. Chang, E. Gensch, A. Rudner, and R. Tabtiang, "A C. elegans mutant that lives twice as long as wild type," *Nature*, vol. 366, no. 6454, pp. 461–464, 1993.

[48] M. Tatar, A. Bartke, and A. Antebi, "The endocrine regulation of aging by insulin-like signals," *Science*, vol. 299, no. 5611, pp. 1346–1351, 2003.

[49] A. Dillin, A. L. Hsu, N. Arantes-Oliveira et al., "Rates of behavior and aging specified by mitochondrial function during development," *Science*, vol. 298, no. 5602, pp. 2398–2401, 2002.

[50] R. J. Colman, R. M. Anderson, S. C. Johnson et al., "Caloric restriction delays disease onset and mortality in rhesus monkeys," *Science*, vol. 325, no. 5937, pp. 201–204, 2009.

[51] W. Mair and A. Dillin, "Aging and survival: the genetics of life span extension by dietary restriction," *Annual Review of Biochemistry*, vol. 77, no. 1, pp. 727–754, 2008.

Hindawi
Oxidative Medicine and Cellular Longevity
Volume 2019, Article ID 2818415, 11 pages
https://doi.org/10.1155/2019/2818415

*Research Article*

# New Insights into Chronological Mobility of Retrotransposons In Vivo

**Amr. R. Ghanam, Jun Cao, Xuan Ouyang, and Xiaoyuan Song**

*Hefei National Laboratory for Physical Sciences at the Microscale, CAS Key Laboratory of Brain Function and Disease, Neurodegenerative Disorder Research Center, School of Life Sciences, Division of Life Sciences and Medicine, University of Science and Technology of China, Hefei, Anhui 230026, China*

Correspondence should be addressed to Xiaoyuan Song; songxy5@ustc.edu.cn

Received 18 April 2019; Accepted 3 June 2019; Published 26 June 2019

Guest Editor: Huai-Rong Luo



Tissue aging is the gradual decline of physiological homeostasis accompanied with accumulation of senescent cells, decreased clearance of unwanted biological compounds, and depletion of stem cells. Senescent cells were cell cycle arrested in response to various stimuli and identified using distinct phenotypes and changes in gene expression. Senescent cells that accumulate with aging can compromise normal tissue function and inhibit or stop repair and regeneration. Selective removal of senescent cells can slow the aging process and inhibits age-associated diseases leading to extended lifespans in mice and thus provides a possibility for developing antiaging therapy. To monitor the appearance of senescent cells *in vivo* and target them, a clearer understanding of senescent cell expression markers is needed. We investigated the age-associated expression of three molecular hallmarks of aging: SA-$\beta$-gal, $P16^{INK4a}$, and retrotransposable elements (RTEs), in different mouse tissues during chronological aging. Our data showed that the expression of these markers is variable with aging in the different tissues. $P16^{INK4a}$ showed consistent increases with age in most tissues, while expression of RTEs was variable among different tissues examined. These data suggest that biological changes occurring with physiological aging may be useful in choosing the appropriate timing of therapeutic interventions to slow the aging process or keep more susceptible organs healthier in the aging process.

## 1. Introduction

Aging is a time-dependent decline of normal physiological processes. It is a phenomenon shared by almost all living organisms and results from the consequences of accumulations of or decreased clearance of biological compounds in senescent cells. Aging at the organism level increases an individual's susceptibility to disease, including cancers, metabolic disorders, diabetes, cardiovascular diseases, and neurodegenerative diseases [1–5]. On the other hand, replicative senescence, described by Hayflick as a permanent state of cell cycle arrest [6], is a process by which cells lose their proliferative potential and can serve as an endogenous anticancer strategy, resulting in irreversible growth arrest in response to potentially oncogenic stimuli [7]. Thus, senescence is a double-edged sword that has both beneficial and adverse effects.

Different research groups have identified several aging markers (reviewed in detail in [8]), including increased $\beta$-galactosidase ($\beta$-gal) reflecting the accumulation of lysosomes with aging [9]. Traditionally, tissue aging has been assessed by measuring the fraction of $\beta$-gal-positive cells [10].

$P16^{INK4a}$ is one of the cyclin-dependent kinase inhibitors that drive the aging process, and it is considered another marker of aging. $P16^{INK4a}$ activates the tumor suppressor, retinoblastoma (Rb), which enforces cell cycle arrest and induces senescence. Aged cells that do not express $P16^{INK4a}$ may resume growth after inactivation of the tumor suppressor, P53 [11]. Accumulation of $P16^{INK4a}$-positive senescent

cells can induce tissue degeneration and cataracts in mice, while clearance of $P16^{INK4a}$ senescent cells delayed aging and increased the average lifespan of mice [12, 13].

Transposable elements (TEs) are highly expressed in eukaryotic cells, representing nearly half of eukaryotic genomes, and persist through independent replication of their sequences. They move in the genome via RNA intermediates (retrotransposons) or direct cutting and pasting of their DNA sequences (DNA transposons), through the action of transposase, which is encoded in the sequence. Retrotransposons can be subdivided into two subgroups: those with long terminal repeats (LTRs) and those without LTRs (non-LTRs). LTR retrotransposons are widely found in eukaryotes and make up nearly 8% of the human genome [14]. The most abundant TEs in mammals are non-LTR retrotransposons, including long and short interspersed nuclear elements (LINEs and SINEs, respectively), both of which are widespread in eukaryotic genomes. LINE-1 (Long Interspersed Element 1) and Alu elements are two non-LTR retrotransposons that account for approximately one-quarter of the human genome. Retrotransposons can mobilize themselves through an element-derived RNA intermediate, which is converted into complementary DNA (cDNA) by reverse transcription. This is followed by integrating into a new genomic locus that generates a second copy of the TE, which is referred to as a copy-and-paste mechanism.

Organisms counteract transposition of retrotransposable elements (RTEs) by preventing their transcription through heterochromatinization of the genomic regions where they are inserted, thus repressing their activity [15], or by posttranscriptional actions of the Piwi-piRNA system that effectively silences TEs in germ cells and tumor cells. The piRNA pathway also can repress TE activity at the transcriptional level through RNA-mediated chromatin modification, which is referred to as RNA-mediated epigenetic silencing [16].

Based on studies from several model organisms, TEs can be highly active in the genome, raising the possibility that these mobile elements promote genomic instability and contribute to loss of cellular function with age. Furthermore, epigenetic studies of diverse aging models have revealed that TEs are associated with extensive relaxation of heterochromatin, decreased core histone content, altered posttranslational modifications, and genomic insatiability [17]. These observations led to a theory of aging through transposition [18]. TE misregulation also has been associated with specific diseases and disorders, such as cancers, aging [19], neurological disorders [20], and autoimmunity [21].

The extent of senescent cell accumulation in different organs of mammals in the aging process and the functional outcome of such accumulation are not very clear. In the current study, we examined three aging hallmarks, $\beta$-gal, $P16^{INK4a}$, and RTEs, to verify the sequential order of aging in different mouse tissues throughout the aging process. Upon identification of age-susceptible organs, further studies will be able to direct to understand the underlying molecular mechanism(s) and potentially lead to the development of preventive therapies that target tissue-specific senescent cells.

## 2. Materials and Methods

*2.1. Experimental Animals.* The present work was carried out using healthy male BALB/c mice purchased from Vital River Laboratories (Beijing, China). We used young (1 mo), middle-aged (12 mo), and old mice (24 mo) that were maintained in specific-pathogen-free and humidity- and temperature-controlled microisolator cages with a 12-h light/dark cycle. Food and water were given *ad libitum*. The mice were anesthetized using chloral hydrate 8%, followed by cardiac infusion of phosphate-buffered saline (PBS), then different organs were dissected in cold PBS.

*2.2. Ethics Committee Statement.* All animal manipulations were conducted in strict accordance with the guidelines and regulations set forth by the University of Science and Technology of China (USTC) Animal Resources Center and University Animal Care and Use Committee. The protocol was approved by the Committee on the Ethics of Animal Experiments of the USTC (Permit Number: PXHG-SXY201510183) for mouse experiments.

*2.3. MEF Cell Isolation.* Following the methods of Ahmed et al. [22], uteri from pregnant female mice (Balb/C) at 14 days post coitum were dissected and washed with PBS and the embryos were collected into sterile Petri dishes with PBS. The fetal liver, heart, and head were removed, minced, and incubated at 37°C for 15 min in 0.25% trypsin EDTA (Gibco®, Grand Island, NY, USA) with gentle shaking as previously described [23]. Trypsin was neutralized with an equal amount of Dulbecco's modified Eagle's medium (DMEM), and the cells were collected by centrifugation (1000 rpm for 7 min). The isolated cells were resuspended and cultured on growth medium containing high glucose DMEM (11995-065, Gibco®) mixed with 10% fetal bovine serum (FBS, HyClone), 4 mM L-glutamine (25030-081, Gibco®), and 1 : 100 penicillin–streptomycin and incubated at 37°C with 5% $CO_2$. We examined the cells daily using an inverted microscope (Olympus IX73, Japan).

*2.4. $\beta$-Gal Assay.* Tissue staining was performed as described previously [24]. Briefly, mouse tissues were rapidly dissected, immersed in OCT, then flash frozen using liquid nitrogen and sectioned at 5 $\mu$M thickness using a cryostat (Leica CM1950). Sections were mounted on glass microscope slides, dried, rinsed with PBS, then fixed with 1% formaldehyde in PBS for 1 min at room temperature, followed by three PBS washes. The sections were stained overnight in $\beta$-gal solution (Beyotime C0602) at 37°C. Blue-stained cells were examined using an inverted microscope (Olympus IX73, Japan). Images were acquired using cellSens standard imaging software, followed by deconvolution and maximum protection under the default settings provided by the program software.

*2.5. Western Blot Analysis.* All steps were done according to the manufacturer's protocol, using a Bio-Rad system (Bio-Rad, USA). Briefly, each organ was cut into small pieces using scissors and homogenized in RIPA lysis buffer (150 mM NaCl, 1.0% NP40, 0.5% sodium deoxycholate, 0.1% SDS, 50 mM Tris-HCl, and pH 8.0 with protease

inhibitors). The homogenized samples were slowly rotated at 4°C for 2 h followed by sonification for 5 min, then centrifuged at 12,000 g at 4°C for 10 min. The supernatant was collected, and the protein concentration was determined using a BCA protein assay kit (Beyotime, China). Protein samples were heated for 10 min at 95°C, then separated using 10% sodium dodecyl sulfate polyacrylamide gel electrophoresis (SDS–PAGE) (20 $\mu$g protein/lane). Afterward, the samples were blotted onto polyvinylidene fluoride (PVDF) membranes (Solarbio, China) using a Trans-Blot SD system (Bio-Rad). The membranes with target proteins were blocked with BSA blocking buffer (CW2143S, CWBIO, China) for 2 hrs at room temperature, then incubated overnight with the primary antibody $P16^{INK4a}$ (Proteintech, #10883-1-AP) and beta tubulin antibody (Proteintech, #66240-1-Ig) (1 : 2000) at 4°C. After three washes, the appropriate secondary antibody HRP labeled goat anti-mouse IgG or anti-rabbit IgG (Proteintech, #SA00001-1 and #SA00002-1) at a dilution of 1 : 5000. The membranes were incubated at room temperature for 2 hrs then washed using TBST (CW0043S, CWBIO, China). Bands were visualized using the enhanced chemiluminescence method (ECL) western blot kits (CW0048 M, CWBIO, China) and the FluorChem Q system (ProteinSimple, USA). Protein band intensity was quantified using the ImageJ program (National Institutes of Health, Bethesda, MD, USA).

*2.6. Real-Time PCR Assessment of RTEs.* Total RNA was extracted from the different mouse organs using TRIzol Reagent (Ambion, Cat. #: 15596) following the manufacturers' instructions. RNase-Free DNase (Promega, Cat. #: M6101) was used to eliminate DNA contamination. Reverse transcription was performed using the reverse transcription system (Promega, Cat. #: A5001). RT-qPCR was performed using 10 $\mu$l aliquots and AceQ qPCR SYBR Green Master Mix (Vazyme # Q111-03) on a Bio-Rad detection instrument (CFX Connect), according to the manufacturer's specifications. Primers used for detection of different kinds of RTEs were previously described [25]. Real-time PCR primers for $P16^{INK4a}$ and Mki67 were as follows: $P16^{INK4a}$-F, 5′CGCA GGTTCTTGGTCACTGT3′; $P16^{INK4a}$-R, 5′TGTTCACG AAAGCCAGAGCG3′; Mki67-F, 5′ATCATTGACCGCT CCTTTAGGT3′; Mki67-R, 5′GCTCGCCTTGATGGTTC CT3′; GAPDH-F, 5′ACATCATCCCTGCATCCACTG3′, GAPDH-R, 5′CCTGCTTCACCACCTTCTTG3′.

*2.7. Statistical Analysis.* Statistical differences among groups were analyzed using one-way ANOVA and the post hoc Tukey's test. If two groups were analyzed, the significance was determined by Student's $t$-test. Statistical significance was established at 0.05 ($^{*}P \leq 0.05$, $^{**}P \leq 0.01$, and $^{***}P \leq 0.001$) using SPSS® software V.21 (Chicago, IL). GraphPad Prism 7.0 was used to prepare the statistical illustrations (GraphPad Software, La Jolla, CA, USA).

## 3. Results

*3.1. Confirming Aging Markers in Replicative Senescence in Mouse Embryonic Fibroblasts.* Before testing the three aging markers *in vivo*, we examined them in replicative senescence. Mouse embryonic fibroblasts (MEFs) were isolated and grown to senescence *in vitro*. We found that P7-MEFs (MEFs at the $7^{th}$ passage) exhibited an enlarged phenotype with significantly increased $\beta$-gal staining (Figures 1(a)–1(c)). Furthermore, RT-qPCR showed that Mki67, a marker for cell proliferation, was significantly decreased, while $P16^{INK4a}$ mRNA and protein levels were significantly increased in senescent MEFs (Figures 1(d) and 1(e)). In addition, RNA-Seq was performed on these cells, and we identified a number of lncRNAs and mRNAs that were differentially expressed in senescent MEFs compared to young MEFs (data not shown). We further examined the expression levels of different classes of RTEs (IAP, LINEs, 3 ′UTR of LINEs (L3UTR), and 5′ UTR of LINEs (L5UTR)) and observed they were significantly upregulated in senescent MEFs (Figure 1(f)). These observations suggested that replicative senescence in MEFs was associated with increased expression of $P16^{INK4a}$, RTEs, and $\beta$-gal and could serve as positive controls for these three senescence markers we proposed to use in the *in vivo* tissues.

*3.2. Aging Brain Revealed Marked Regional Specific Expression of Aging Markers.* Efforts have been carried out to reveal molecular changes in brain regions that are susceptible to age-associated diseases, including the hippocampus and substantia nigra. For example, Purkinje and cortical hippocampus neurons were positively stained with $\beta$-gal in aged mice [26]. However, other brain regions are less studied. In the current study, we found that Purkinje cells (Figure 2(a) A, E, I) and hippocampus-specific CA3 region neurons (Figure 2(a) B, F, J) were strongly stained in aged mouse brains compared to young mouse brains. $\beta$-Gal staining increased with age in the choroid plexus of the lateral ventricles (LV) (Figure 2(a) G, K), substantia nigra (SN) (Figure 2(a) J), and a few scattered cells in the frontal cortex. For RTEs, we found that LINEs were upregulated, which was similar to other studies [27, 28], and all different classes of RTEs were significantly upregulated in the aged mouse brain (Figure 3(a)). In addition, both $P16^{INK4a}$ mRNA (Figure 4(a)) and protein (Figure 4(b)) levels were upregulated in the aged mouse brain. These findings suggested that age-associated brain senescent cells were $P16^{INK4a}$ positive and exhibited increased RTE activity.

*3.3. Aging Markers Occurred in the Kidney as Early as 1 Month of Age.* Aged kidneys are associated with decreased glomerular filtration rate, which is due to the reductions in glomerular capillary plasma flow rate and glomerular capillary ultrafiltration coefficient, and decreased renal blood flow, resulting from the reduction in afferent arteriolar resistance [29]. Mortuza et al. reported that diabetic kidneys showed increased $\beta$-gal staining and decreased *Sirt1* mRNA levels [30]. We found that the $\beta$-gal-positive cells were predominantly restricted to the renal cortex, in line with a previous report showing that the renal cortex was more sensitive than the renal medulla [31], and showed high expression of $\beta$-gal as early as 1 month of age (Figure 2(a) D). The staining intensity increased further with age at 12 months and 24 months (Figure 2(a) H, L), but the renal medulla did not show any

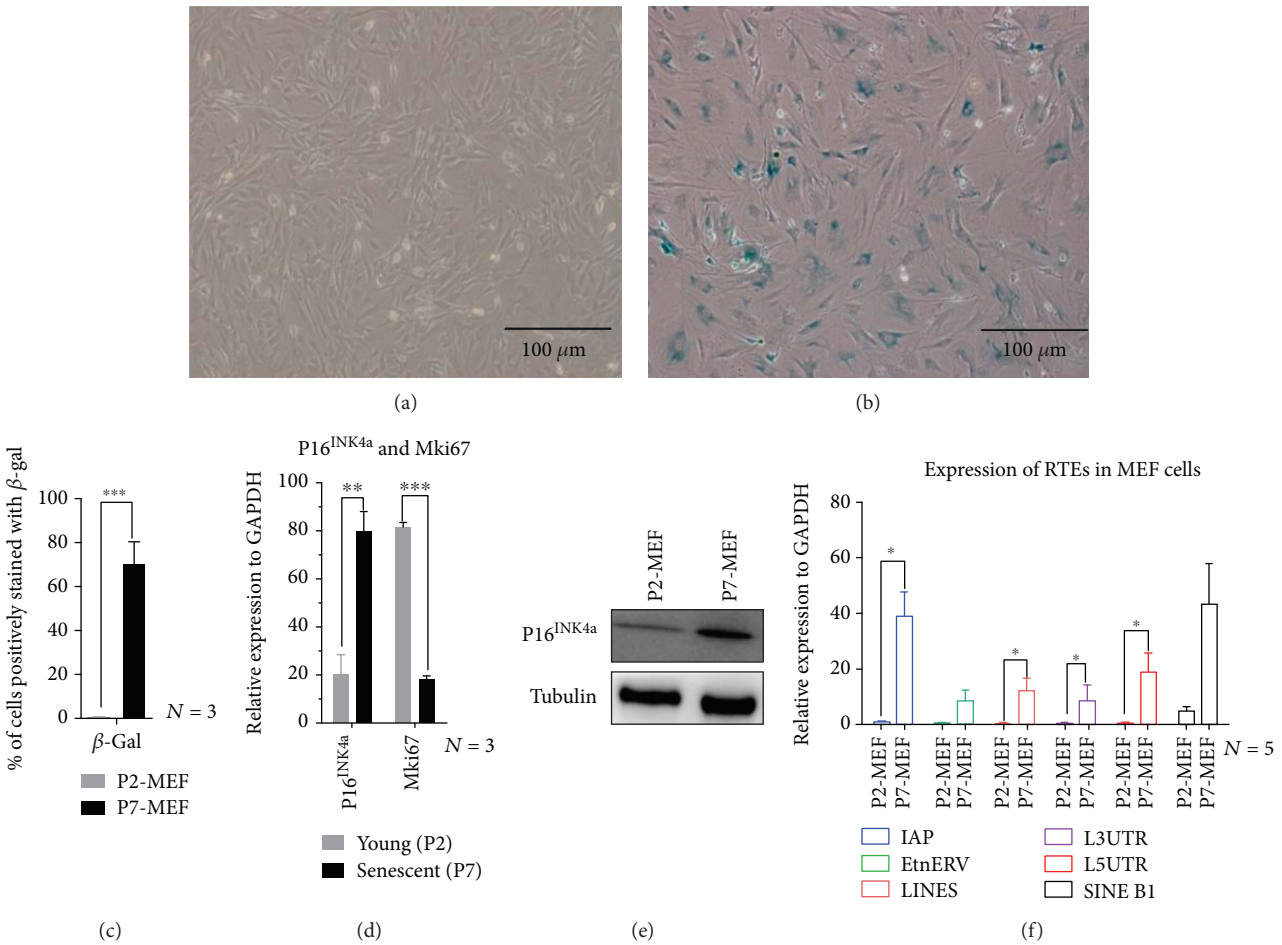


Figure 1: Replicative senescence of MEFs. (a, b) SA-$\beta$-gal staining of MEFs, comparing young (P2-MEF, in (a)) and senescent (P7-MEF, in (b)). (c) Quantification of $\beta$-gal-positive (blue stained) MEFs. (d) mRNA expression level of Mki67 and $P16^{INK4a}$ examined by RT-qPCR. (e) $P16^{INK4a}$ protein level in young and senescent MEFs. $\beta$-Tubulin was used as the loading control. (f) RT-qPCR analysis of different classes of RTEs. $^{*}P \leq 0.05$, $^{**}P \leq 0.01$, and $^{***}P \leq 0.001$.

staining even at 24 months of age (Figure 2(a) L). As seen in the mouse brain, the kidney showed upregulation of both RTEs (Figure 3(b)) and $P16^{INK4a}$ mRNA (Figure 4(a)) and protein (Figure 4(c)) levels with increasing age. These data indicated that the kidney might be susceptible to aging earlier than the brain and the renal cortex was much more sensitive to aging than the renal medulla.

*3.4. Changes in Aging Lungs Were Restricted to Bronchioles.* There are many age-associated changes in the human respiratory system including shrinkage of the lung volume, reduced pulmonary reserve, and increased susceptibility to pulmonary infectious diseases [32]. Cellular senescence is known to be involved in the pathogenesis of some lung diseases, including idiopathic pulmonary fibrosis (IPF) and chronic pulmonary disease. Fibroblast cells isolated from IPF patients showed upregulation of senescence marker $P16^{INK4a}$, P21, and $\beta$-gal [33, 34]. We stained lung tissue sections for $\beta$-gal at 1 month, 12 months, and 24 months. We observed positively stained lung sections in 24-month-old mice, mainly around bronchioles and a few scattered positive cells in the lung alveolar epithelium (Figure 2(b) I), whereas middle-aged mice at 12 months showed only a small amount of low-intensity signal around the bronchioles (Figure 2(b) E). Young mouse lung tissue sections showed very little positive $\beta$-gal staining (Figure 2(b) A). We quantified mRNA expression levels for several different RTEs and observed significantly decreased expression with age except for LINEs, which increased at 12 months of age, followed by a significant decrease at 24 months of age (Figure 3(c)). Similar to previous reports [31], $P16^{INK4a}$ mRNA did not increase significantly with age (Figure 4(a)) in the lung. Even though others failed to detect the $P16^{INK4a}$ protein level either by IHC or by western blotting [31], our results showed that the $P16^{INK4a}$ protein was significantly upregulated with age (Figure 4(d)). These observations suggested that aging lung tissue was associated with upregulation of $P16^{INK4a}$, positive $\beta$-gal-stained bronchioles, and decreased expression of RTEs.

*3.5. Aging Heart Did Not Stain with β-Gal but Had Increased $P16^{INK4a}$.* Induced cardiac hypertrophy in rats showed increased $\beta$-gal stain, accumulation of lipofuscin, and high levels of cyclin-dependent kinase inhibitors [35]. Our heart

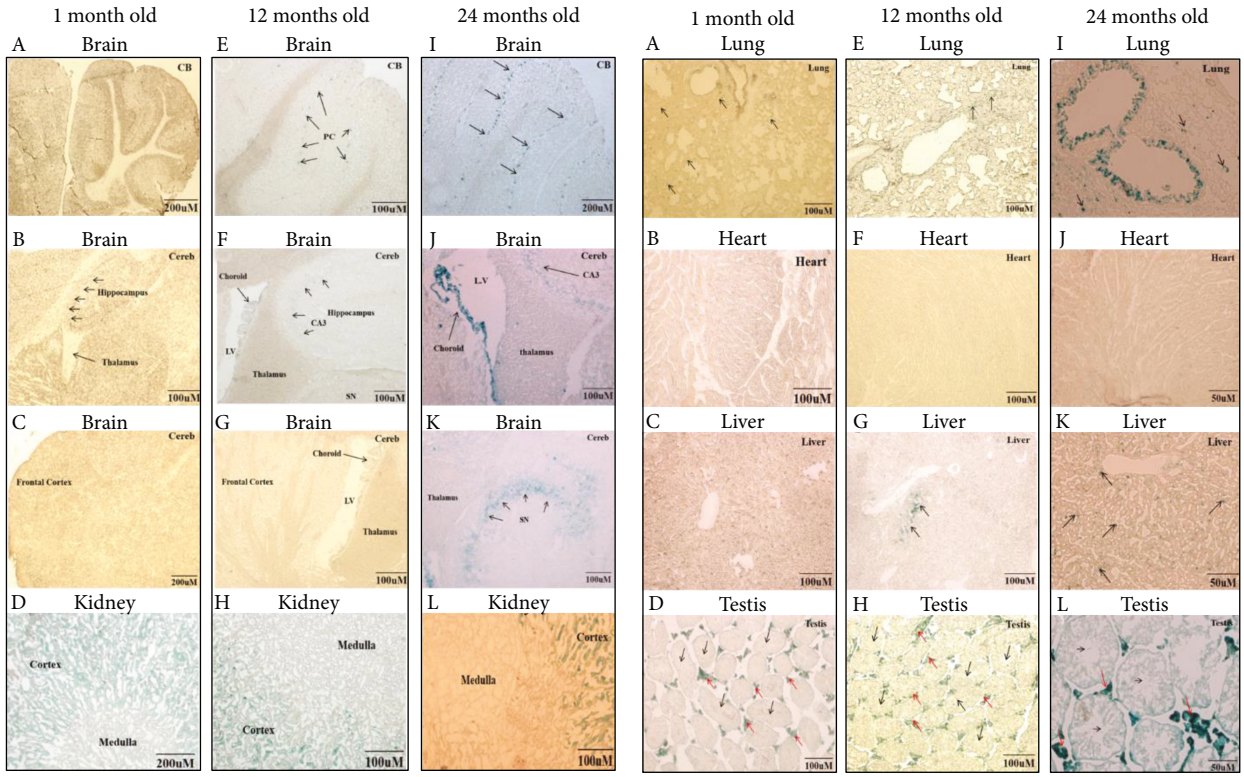


Figure 2: Chronological expression of $\beta$-gal in the brain, kidney, lung, liver, heart, and testis. (a) The brain and kidney. A–C: sagittal brain sections at 1 month did not show any positive staining signal. E–G: 12 months showed a few positively stained cells within the cerebellum (CB), where PC indicates Purkinje cells (E), and faintly stained cerebrum (Cereb), CA3 of the hippocampus, and choroid plexus (Choroid) (F). I–K: 24-month-old brain sections showed positive $\beta$-gal staining in the cerebellar folia, specifically in Purkinje cells (PC) (I), choroid plexus of the lateral ventricle (LV) (J), and CA3 (J) and substantia nigra (SN) (K). D, H, L: Photomicrographs of kidney cross-sections at different ages (1 month of age in D, 12 months of age in H, and 24 months of age in L) stained with $\beta$-gal showed strong signal in the renal cortex at 1 month, 12 months, and 24 months of age, while renal medulla remained unstained. (b) Photomicrographs of lung, liver, heart, and testis sections at different ages (1 month of age in A–D, 12 months of age in E–H, and 24 months of age in I–L) stained with $\beta$-gal. A, E, and I showed a few scattered positively stained lung cells that were observed in 1-month-old and 12-month-old lungs (arrows), and a strong signal was detected in old mouse lung bronchi (24 months of age), with a few scattered positive cells located in the alveolar epithelium (arrows). B, E, and J showed that no $\beta$-gal-positive staining was observed at any age examined in the heart. C, G, and K showed a few $\beta$-gal-positive stained cells in the liver at 12 months and 24 months of age (arrows). D, H, L: Interstitial cells of the testis were strongly positively stained for $\beta$-gal (red arrows).

sections stained for $\beta$-gal however did not reveal any positively stained cells in any of the ages tested (Figure 2(b) B, F, J). Additionally, among the tested RTEs, only IAP was significantly upregulated with aging, while LINEs and SINE B1 were increased at 12 months of age followed by significant downregulation (Figure 3(d)). On the other hand, $P16^{INK4a}$ mRNA was significantly increased in the aged heart (Figure 4(a)). For technical reasons, we could not examine the protein level of the $P16^{INK4a}$. These findings indicated that the mouse heart showed different patterns of aging markers in the aging process.

*3.6. Aging Liver Was Accompanied by Decreased Accumulation of $P16^{INK4a}$-Positive Cells and Decreased RTEs.* In spite of the regenerative properties of liver hepatocytes, aging enhances the vulnerability of the liver to various diseases and advanced age is associated with a poorer prognosis in general. Hepatic steatosis has been associated with increased expression of the senescence marker P21 and telomere-associated DNA damage foci [36]. We found that at 1 month, mouse livers did not show any positive $\beta$-gal staining (Figure 2(b) C), while 12-month-old mouse (Figure 2(b) G) and 24-month-old mouse (Figure 2(b) K) livers showed a few focally distributed $\beta$-gal-positive cells. In addition, liver RTEs showed increased expression of IAP and LINEs at the age of 12 months followed by a significant decrease at 24 months of age (Figure 3(e)). Consistent with the observed RTE expression, both $P16^{INK4a}$ mRNA and protein were significantly downregulated in aged liver at 24 months (Figures 4(a) and 4(e)). These observations suggested that the liver might effectively eliminate $P16^{INK4a}$ senescent cells and thus showed no aging phenotype until very old age.

*3.7. Aging Testes Showed Increased $\beta$-Gal Staining and $16^{INK4a}$ Expression.* Testicular aging is associated with

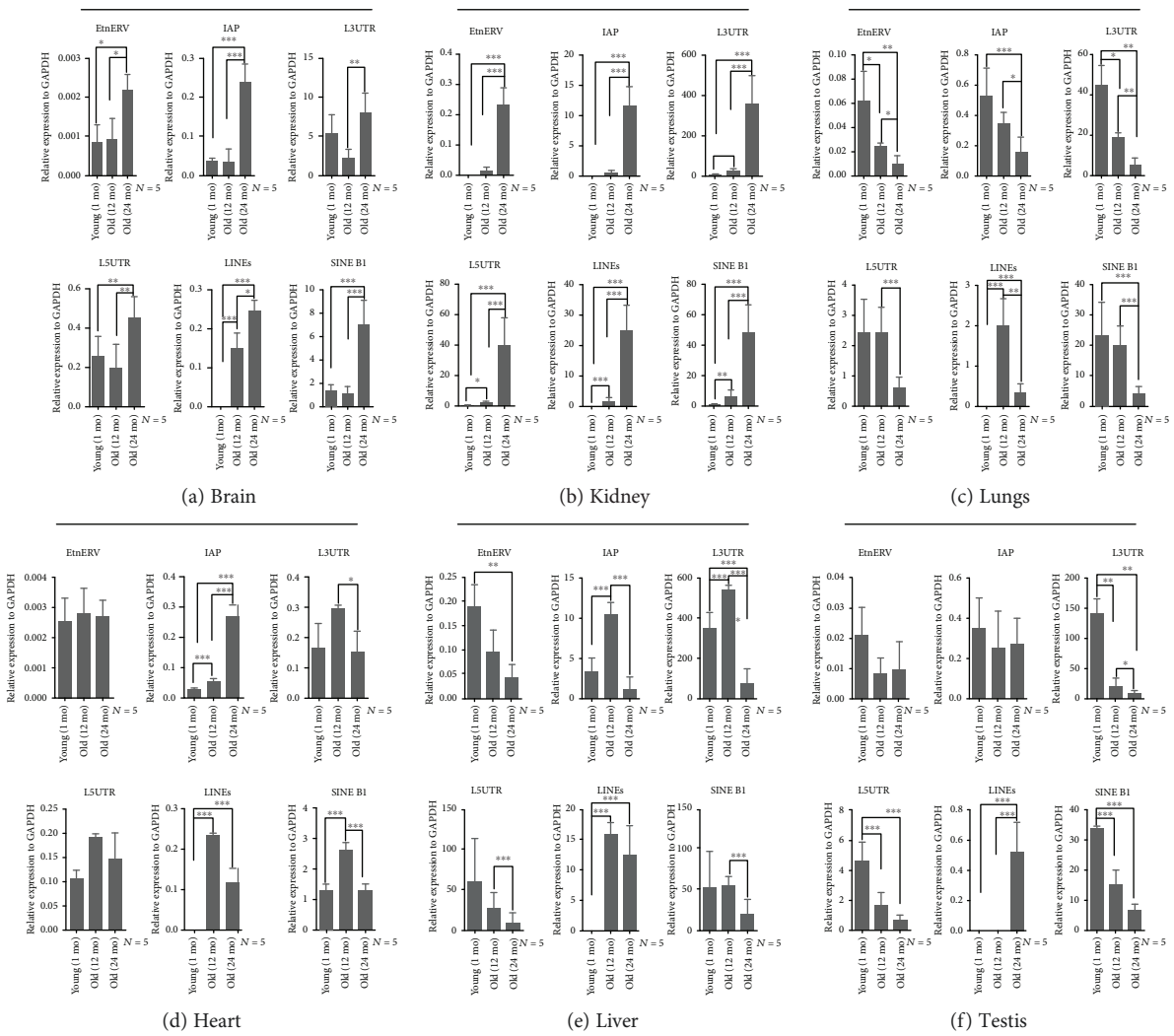


Figure 3: Chronological expression of RTEs (IAP, ERV, L3UTR, L5UTR, LINEs, and SINE B1) in the brain, kidney, lung, liver, heart, and testis. (a) RT-qPCR analysis indicated that all RTEs were significantly upregulated in the aged mouse brain. (b) RT-qPCR analysis of RTEs showing that they were significantly upregulated in aged mouse kidneys. (c) RT-qPCR analysis showed that the RTE expression was significantly downregulated in aged mouse lungs. (d) RT-qPCR analysis of RTEs in the heart showed that only IAP was upregulated, while L3UTR, LINEs, and SINE B1 were downregulated. (e) RT-qPCR analysis of liver RTEs showed that the majority of them were significantly decreased with age. (f) RT-qPCR analysis of RTEs in the testis showed that the majority of them were significantly decreased in aged testes (24 months of age). $^{*}P \leq 0.05$, $^{**}P \leq 0.01$, and $^{***}P \leq 0.001$.

decreased testosterone levels, which is projected to be 1% every year after 30 years of age in humans [37]. Similarly, the SAMP8 mouse showed age-related decrease in serum testosterone level to 71% at the age of 4 and 12 months of age, compared to a 26% decrease in R1 mice of the same age [38]. Our results showed strong positive $\beta$-gal staining in testicular interstitial cells, which was increased with age (Figure 2(b) D, H, L). We did not observe any positive $\beta$-gal staining in the seminiferous tubules (Figure 2(b) D, H, L). Meanwhile, RTEs were significantly decreased with aging with the exception of LINEs, which were significantly increased (Figure 3(f)). In line with what Krishnamurthy et al. has reported [31], $P16^{INK4a}$ mRNA was significantly decreased with aging (Figure 4(a)). However, $p16^{INK4a}$ protein levels were significantly upregulated (Figure 4(f)).

## 4. Discussion

Data accumulated in the last 30 years have helped us to identify different environmental and genetic factors, as well as chemical substances that affect lifespan in many different eukaryotic species [32, 33]. However, understanding the molecular mechanisms of the aging process remains an unsolved question in biology.

Despite multiple theories proposed to explain the aging process, it is still not clear how aging begins and what influence aging exerts on different organs. Therefore, we assessed the response of different mouse organs (brain, liver, lung, kidney, heart, and testis) to three possible mechanisms involved in aging. We examined the expression of $\beta$-gal staining, $P16^{INK4a}$, and RTEs at three different stages in the

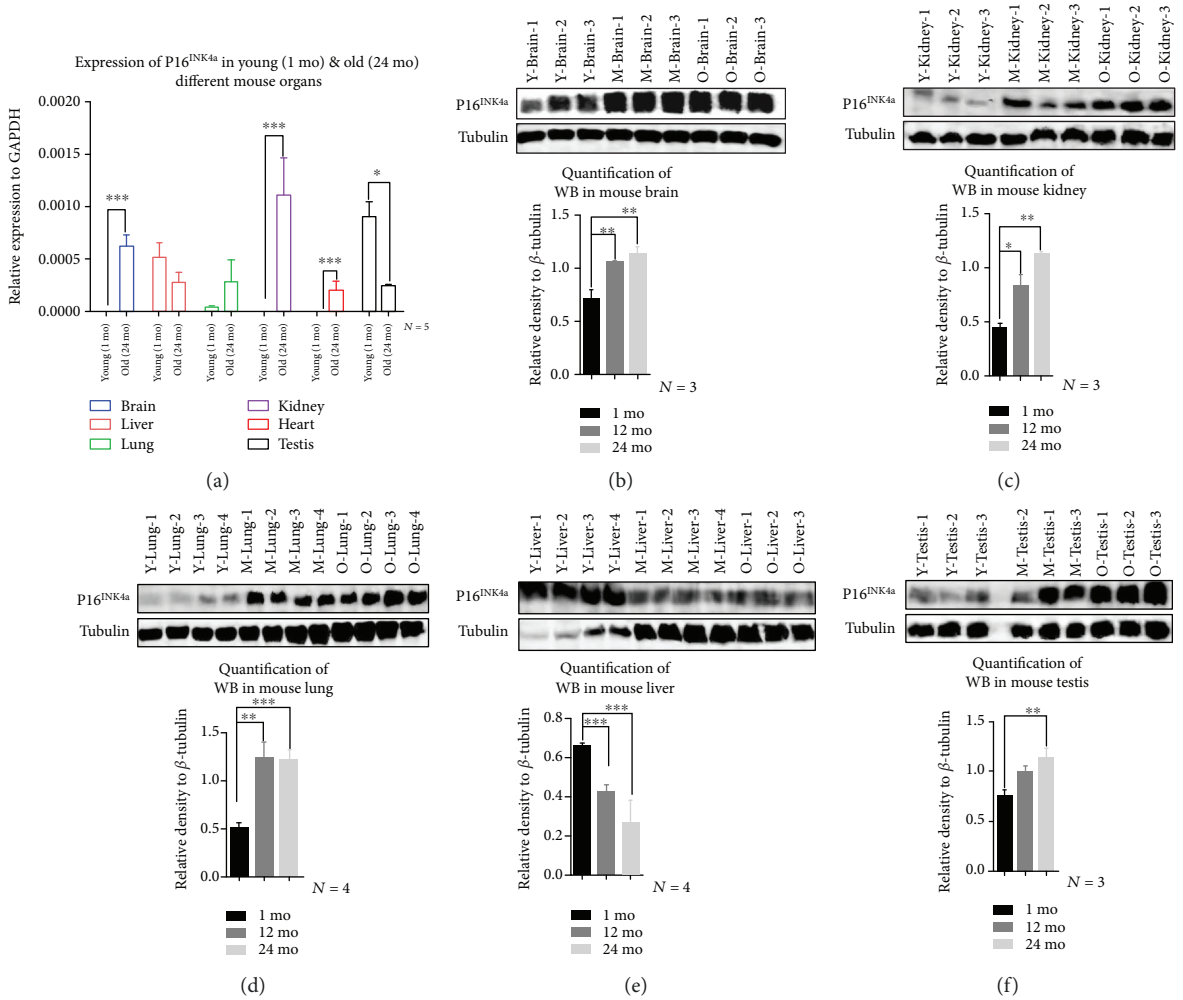


FIGURE 4: Chronological expression of $P16^{INK4a}$ in different organs. (a) RT-qPCR, of $P16^{INK4a}$ mRNA, in different mouse organs. Significant upregulation was observed in the mouse brain, kidney, and heart. Significant downregulation was observed in testes. No significant changes were observed in the liver or lungs (b–f): $P16^{INK4a}$ protein expression at 1 month (Y), 12 months (M), and 24 months (O) (b) in the brain showed upregulation at M and O compared to Y, (c) in the kidney showed upregulation at M and O compared to Y, (d) in the lungs showed upregulation at M and O compared to Y, (e) in the liver showed downregulation in M and O compared to Y, and (f) in the testis showed upregulation in O compared to Y. The histograms below the panels showed the densitometric mean ± SD normalized to the corresponding level of the loading control protein, $\beta$-tubulin ($^{*}P \leq 0.05$, $^{**}P \leq 0.01$, and $^{***}P \leq 0.001$).

aging process (1 month, 12 months, and 24 months). As organisms age, gradual accumulation of unrepaired cellular damage can drive the aging process and determine the incidence of age-related disease [39, 40].

Moreover, jumping of TEs into functional (coding or regulatory) DNA regions can produce loss of function and increase genome instability, resulting in the death of affected cells. The occurrence of transposition events also can lead to various degenerative processes [41]. In spite of the tight regulation of TEs, either epigenetically or posttranscriptionally, the mobility of LINE-1 has been previously reported in the nervous system [19, 42]. Age-related gross morphometric measurements of mouse organs revealed age-associated increase in body weight and percentage of body fat and decreased testicular weights [43]. However, more detailed responses of various body organs to various aging markers have not been carried out before.

Aged mouse brain showed upregulation of the three tested aging markers used in our study. Increased $\beta$-gal staining in cerebellar Purkinje neurons might reflect locomotor incoordination that is often associated with aged individuals. Increased $\beta$-gal staining also was observed in the hippocampus and substantia nigra, which are major brain regions associated with neurodegenerative diseases such as Alzheimer and Parkinson diseases, respectively. In addition, human aging is associated with reduced amounts of cerebrospinal fluid (CSF) and increased protein concentrations [23], which might be attributed to an aged choroid plexus. Thus, specific brain regions appear to be highly sensitive to an aging phenotype, which suggested that further investigations are warranted, especially for the choroid plexus and for the unique functions of CSF in healthy people and patients.

Whole genome bisulfide sequencing in the aged human brain revealed that DNA has significant lower methylation

Table 1: Summary of RTEs in different mouse organs.

| Organ | LINES | L3UTR | L5UTR | IAP | SINE B1 | EtnERV |
|---|---|---|---|---|---|---|
| Brain | +++ | +++ | +++ | +++ | +++ | +++ |
| Kidneys | +++ | +++ | +++ | +++ | +++ | +++ |
| Lungs | +(12 mo) - (24 mo) | — | — | — | — | — |
| Heart | +(12 mo) - (24 mo) | — | Ns | ++ | +(12 mo) - (24 mo) | Ns |
| Liver | +(12 mo) - (24 mo) | +(12 mo) - (24 mo) | — | +(12 mo) - (24 mo) | — | – |
| Testes | +++ | — | — | Ns | — | Ns |

(+) indicates upregulation; (-) indicates downregulation; Ns indicates no significant changes were observed.

compared with that of newborn DNA [24]. In line with previous studies showing that upregulation of IAP-RTEs with aging is due to promoter hypomethylation [25], we observed generalized and significant increases in tested RTEs with and without LTR. In addition, a significant accumulation of $p16^{INK4a}$ mRNA and protein was observed. Together, these observations revealed that the brain is highly sensitive to physiological aging at the molecular level, influencing both morphology and function.

Similar to the brain, mouse kidneys demonstrated significant upregulation of the aging markers used in this study, especially in the renal cortex. It was surprising that the kidneys expressed a senescent phenotype earlier than any of the other organs included in this study. These findings might reflect the essential role of the kidney in the aging process. Previous studies have not focused on this relationship. The kidney is important in maintaining homeostasis of the body, suggesting that aging of the kidney is more likely to occur earlier than other organs and possibly the age-related decline of other organs might be a consequence of failure of the kidney to effectively eliminate circulating age-inducing molecules. Since elderly humans have less renal functional reserve and are more susceptible to chronic renal diseases [44], actions to preserve renal function might help to delay or alleviate aging-related consequences in the whole body.

Since previous studies did not test the lung and the liver for $\beta$-gal staining and protein expression levels of $P16^{INK4a}$ [31], we demonstrated that $\beta$-gal staining of bronchioles was associated with aging in the mouse lungs along with upregulation of $P16^{INK4a}$ protein and significant decrease in RTE expression at 24 months of age. Similarly, we observed a few scattered $\beta$-gal-positive cells in the mouse liver along with significant downregulation of RTEs. These findings suggested that lungs and livers were less influenced by aging or their aging may be a consequence of aging in the kidney. These observations raised a question concerning the theory of aging through retrotransposition. Generalized age-associated declines are thought to affect all organs, but the increased expression of RTEs was observed only in the brain and kidney. This may be due to the fact that the mobility of RTEs is a functional necessity in the brain and kidney and not a function of the aging process. In contrast to the lung, the liver showed downregulation of the $P16^{INK4a}$ protein. Further investigations are required to determine how the mouse liver might eliminate $P16^{INK4a}$-positive cells.

We observed that the aged mouse heart did not present any $\beta$-gal-positive cells, while IAP was significantly increased with aging. In addition, LINEs and SINE B1 were significantly increased at 12 months of age, followed by a significant decrease at 24 months of age. In line with the observations in the brain and lungs, the mouse heart showed increased expression of $P16^{INK4a}$ mRNA. A greater understanding of the processes involved in cardiac aging may lead to identification of novel and more specific cardiac aging biomarkers.

Similar to kidneys, the interstitial cells of the testes were positively stained for $\beta$-gal as early as 1 month of age, and the staining presented significant increases with aging. This might attribute to the early development of both organs from intermediate mesoderm through formation of urogenital ridge. However, cells in the seminiferous tubules did not show any positive staining for $\beta$-gal. This could be associated with the decline of testosterone levels that is associated with aging in males. Additionally, testicular RTEs and $P16^{INK4a}$ mRNA were significantly decreased with aging.

This work provided the *in vivo* chronological aging profiling in different organs in mice using three aging biomarkers. We demonstrated that aging significantly influenced specific brain regions, the renal cortex, pulmonary bronchioles, and interstitial cells of the testes but had little or no effect on lung parenchyma, the liver, heart, and testicular seminiferous tubules (summarized in Table 1). In conclusion, the gradual functional decline of peripheral organs might be a consequence of the aging brain or kidneys either through aging of neurons that influence these organs or through failure of the kidneys to eliminate age-associated molecules that occur due to environmental and genetic causes (Figure 5). Additionally, the age-dependent changes in RTE expression may be related to changes in function rather than directly associated with the aging process. The upregulation of RTEs in the mouse brain and kidneys might positively enhance the clearance of $P16^{INK4a}$-positive cells. We think that measuring the expression of these aging markers might provide evidence for the process of aging, as upregulation of the three aging markers ($P16^{INK4a}$, $\beta$-gal, and RTEs) indicated higher aging susceptibility as seen in the brain and kidneys, yet upregulation of $P16^{INK4a}$ and $\beta$-gal with down- or various regulations of RTEs indicated a moderate aging progress as seen in the lungs and testes, while downregulation of the one or two markers and with less or no $\beta$-gal staining represent longevity as seen in the liver and heart.

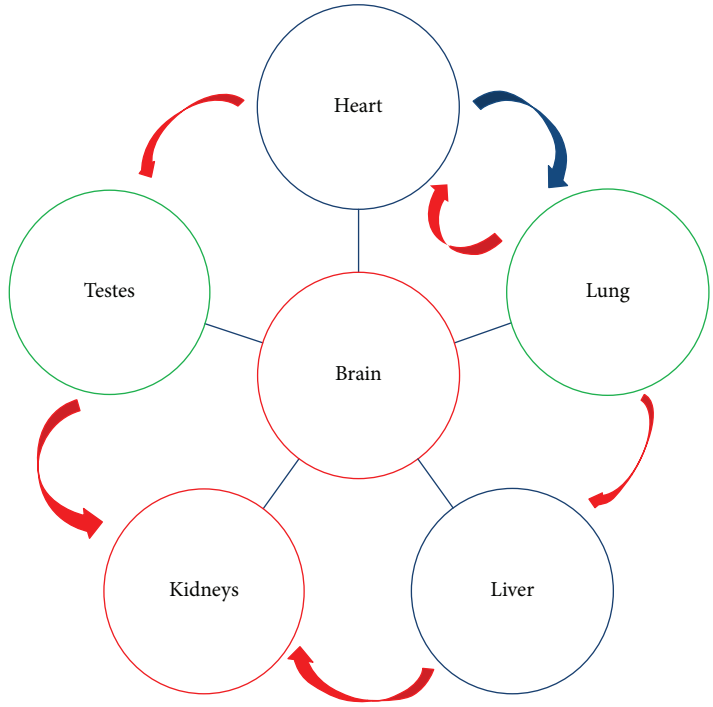


Figure 5: Model of organ aging. The model illustrates the center of aging that might be due to changes in the brain and kidney, then followed by the lung and testis. The heart and liver were the least affected organs. Red arrows represent circulating blood, which is filtered by the kidneys. The blue lines represent neurons that connect organs with the brain.

In summary, $P16^{INK4a}$ expression was upregulated with age in all mouse tissues tested except for the liver, thus reinforcing the importance of $P16^{INK4a}$ as a biomarker of *in vivo* aging. However, recent studies demonstrated that $P16^{INK4a}$ is not exclusively expressed in senescent cells [45, 46], which might raise a question about the future use of $P16^{INK4a}$ senolytics and encourage research on more specific aging biomarkers.

The information provided in this study may be useful for consideration of age-associated diseases including neurodegenerative diseases such as Alzheimer disease and Parkinson disease, kidney-associated diseases such as chronic renal failure, pulmonary-associated diseases such as chronic pulmonary diseases, cardiovascular disease, and reproductive diseases associated with the decline of testosterone levels. This study provides a foundation for other aging research groups to use the mouse as an animal model and identify specific organs to elucidate molecular mechanisms underlying the aging process. Taken together, these observations could lead to development of tissue-specific senolytics that enhance senescent cell clearance and/or decrease accumulation in the brain and kidney, which would allow the kidney and brain to remain healthier and sustain function longer with positive effects on later life in people.

The remaining challenge will be to answer the following questions: First, is derepression of RTEs a major driving force for aging or is it merely a consequence of existing pathogenesis? Second, it is important to identify ideal aging biomarkers to be able to better predict the functional capacity and assess the biological process of aging *in vivo*.

## Data Availability

The authors confirm that the data supporting the findings of this study are available within the article.

## Conflicts of Interest

The authors declare no conflicts of interest to disclose.

## Authors' Contributions

ARG, JC, and XS designed the experiments and analyzed the data. XO contributed to raising the mice. ARG performed all the experiments. ARG, JC, and XS wrote the manuscript. Amr. R. Ghanam and Jun Cao are contributed equally.

## Acknowledgments

We are grateful to Dr. Louise C. Abbott from Texas A&M University, for the kind help and suggestions during preparation of the manuscript. This work was funded by the National Key Scientific Program of China (2016YFA0100502) and National Natural Science Foundation of China (91540107). A.R.G. is a recipient of the Chinese Scholarship Council (CSC) fellowship.

## References

[1] D. J. Baker, C. Perez-Terzic, F. Jin et al., "Opposing roles for $p16^{Ink4a}$ and $p19^{Arf}$ in senescence and ageing caused by BubR1 insufficiency," *Nature Cell Biology*, vol. 10, no. 7, pp. 825–836, 2008.

[2] J. Feser and J. Tyler, "Chromatin structure as a mediator of aging," *FEBS Letters*, vol. 585, no. 13, pp. 2041–2048, 2011.

[3] A. Brunet and S. L. Berger, "Epigenetics of aging and aging-related disease," *The Journals of Gerontology Series A: Biological Sciences and Medical Sciences*, vol. 69, Supplement 1, pp. S17–S20, 2014.

[4] B. K. Kennedy, S. L. Berger, A. Brunet et al., "Geroscience: linking aging to chronic disease," *Cell*, vol. 159, no. 4, pp. 709–713, 2014.

[5] A. Moskalev, A. Aliper, Z. Smit-McBride, A. Buzdin, and A. Zhavoronkov, "Genetics and epigenetics of aging and longevity," *Cell Cycle*, vol. 13, no. 7, pp. 1063–1077, 2014.

[6] L. Hayflick, "The limited in vitro lifetime of human diploid cell strains," *Experimental Cell Research*, vol. 37, no. 3, pp. 614–636, 1965.

[7] J. Campisi, "Aging, cellular senescence, and cancer," *Annual Review of Physiology*, vol. 75, no. 1, pp. 685–705, 2013.

[8] A. R. Ghanam, Q. Xu, S. Ke, M. Azhar, Q. Cheng, and X. Song, "Shining the light on senescence associated LncRNAs," *Aging and Disease*, vol. 8, no. 2, pp. 149–161, 2017.

[9] D. J. Kurz, S. Decary, Y. Hong, and J. D. Erusalimsky, "Senescence-associated (beta)-galactosidase reflects an increase in lysosomal mass during replicative ageing of human endothelial cells," *Journal of Cell Science*, vol. 113, pp. 3613–3622, 2000.

[10] R. T. Bree, C. Stenson-Cox, M. Grealy, L. Byrnes, A. M. Gorman, and A. Samali, "Cellular longevity: role of apoptosis and replicative senescence," *Biogerontology*, vol. 3, no. 4, pp. 195–206, 2002.

[11] C. M. Beauséjour, A. Krtolica, F. Galimi et al., "Reversal of human cellular senescence: roles of the p53 and p16 pathways," *The EMBO Journal*, vol. 22, no. 16, pp. 4212–4222, 2003.

[12] D. J. Baker, T. Wijshake, T. Tchkonia et al., "Clearance of $p16^{Ink4a}$-positive senescent cells delays ageing-associated disorders," *Nature*, vol. 479, no. 7372, pp. 232–236, 2011.

[13] D. J. Baker, B. G. Childs, M. Durik et al., "Naturally occurring $p16^{Ink4a}$-positive cells shorten healthy lifespan," *Nature*, vol. 530, no. 7589, pp. 184–189, 2016.

[14] R. Cordaux and M. A. Batzer, "The impact of retrotransposons on human genome evolution," *Nature Reviews Genetics*, vol. 10, no. 10, pp. 691–703, 2009.

[15] H. L. Levin and J. V. Moran, "Dynamic interactions between transposable elements and their hosts," *Nature Reviews Genetics*, vol. 12, no. 9, pp. 615–627, 2011.

[16] K. H. Burns and J. D. Boeke, "Human transposon tectonics," *Cell*, vol. 149, no. 4, pp. 740–752, 2012.

[17] S. Pal and J. K. Tyler, "Epigenetics and aging," *Science Advances*, vol. 2, no. 7, article e1600584, 2016.

[18] J. M. Sedivy, J. A. Kreiling, N. Neretti et al., "Death by transposition - the enemy within?," *BioEssays*, vol. 35, no. 12, pp. 1035–1043, 2013.

[19] M. De Cecco, S. W. Criscione, E. J. Peckham et al., "Genomes of replicatively senescent cells undergo global epigenetic changes leading to gene silencing and activation of transposable elements," *Aging Cell*, vol. 12, no. 2, pp. 247–256, 2013.

[20] M. T. Reilly, G. J. Faulkner, J. Dubnau, I. Ponomarev, and F. H. Gage, "The role of transposable elements in health and diseases of the central nervous system," *The Journal of Neuroscience*, vol. 33, no. 45, pp. 17577–17586, 2013.

[21] H. E. Volkman and D. B. Stetson, "The enemy within: endogenous retroelements and autoimmune disease," *Nature Immunology*, vol. 15, no. 5, pp. 415–422, 2014.

[22] M. F. Ahmed, A. K. el-Sayed, H. Chen et al., "Direct conversion of mouse embryonic fibroblast to osteoblast cells using hLMP-3 with Yamanaka factors," *The International Journal of Biochemistry & Cell Biology*, vol. 106, pp. 84–95, 2019.

[23] C. P. C. Chen, R. L. Chen, and J. E. Preston, "The influence of ageing in the cerebrospinal fluid concentrations of proteins that are derived from the choroid plexus, brain, and plasma," *Experimental Gerontology*, vol. 47, no. 4, pp. 323–328, 2012.

[24] H. Heyn, N. Li, H. J. Ferreira et al., "Distinct DNA methylomes of newborns and centenarians," *Proceedings of the National Academy of Sciences of the United States of America*, vol. 109, no. 26, pp. 10522–10527, 2012.

[25] W. Barbot, A. Dupressoir, V. Lazar, and T. Heidmann, "Epigenetic regulation of an IAP retrotransposon in the aging mouse: progressive demethylation and de-silencing of the element by its repetitive induction," *Nucleic Acids Research*, vol. 30, no. 11, pp. 2365–2373, 2002.

[26] D. Jurk, C. Wang, S. Miwa et al., "Postmitotic neurons develop a p21-dependent senescence-like phenotype driven by a DNA damage response," *Aging Cell*, vol. 11, no. 6, pp. 996–1004, 2012.

[27] N. G. Coufal, J. L. Garcia-Perez, G. E. Peng et al., "L1 retrotransposition in human neural progenitor cells," *Nature*, vol. 460, no. 7259, pp. 1127–1131, 2009.

[28] C. A. Thomas, A. C. M. Paquola, and A. R. Muotri, "LINE-1 retrotransposition in the nervous system," *Annual Review of Cell and Developmental Biology*, vol. 28, no. 1, pp. 555–573, 2012.

[29] J. R. Weinstein and S. Anderson, "The aging kidney: physiological changes," *Advances in Chronic Kidney Disease*, vol. 17, no. 4, pp. 302–307, 2010.

[30] R. Mortuza, S. Chen, B. Feng, S. Sen, and S. Chakrabarti, "High glucose induced alteration of SIRTs in endothelial cells causes rapid aging in a p300 and FOXO regulated pathway," *PLoS One*, vol. 8, no. 1, article e54514, 2013.

[31] J. Krishnamurthy, C. Torrice, M. R. Ramsey et al., "*Ink4a*/*Arf* expression is a biomarker of aging," *The Journal of Clinical Investigation*, vol. 114, no. 9, pp. 1299–1307, 2004.

[32] E. M. Lowery, A. L. Brubaker, E. Kuhlmann, and E. J. Kovacs, "The aging lung," *Clinical Interventions in Aging*, vol. 8, pp. 1489–1496, 2013.

[33] M. J. Schafer, T. A. White, K. Iijima et al., "Cellular senescence mediates fibrotic pulmonary disease," *Nature Communications*, vol. 8, no. 1, article 14532, 2017.

[34] A. D. Hudgins, C. Tazearslan, A. Tare, Y. Zhu, D. Huffman, and Y. Suh, "Age- and tissue-specific expression of senescence biomarkers in mice," *Frontiers in Genetics*, vol. 9, p. 59, 2018.

[35] R. Sun, B. Zhu, K. Xiong et al., "Senescence as a novel mechanism involved in $\beta$-adrenergic receptor mediated cardiac hypertrophy," *PLoS One*, vol. 12, no. 8, article e0182668, 2017.

[36] M. Ogrodnik, S. Miwa, T. Tchkonia et al., "Cellular senescence drives age-dependent hepatic steatosis," *Nature Communications*, vol. 8, no. 1, article 15691, 2017.

[37] J. Rajfer, "Decreased testosterone in the aging male: summary and conclusions," *Revista de Urología*, vol. 5, Supplement 1, pp. S49–S50, 2003.

[38] J. F. Flood, S. A. Farr, F. E. Kaiser, M. la Regina, and J. E. Morley, "Age-related decrease of plasma testosterone in

Samp8 mice - replacement improves age-related impairment of learning and memory," *Physiology & Behavior*, vol. 57, no. 4, pp. 669–673, 1995.

[39] J. Koubova and L. Guarente, "How does calorie restriction work?," *Genes & Development*, vol. 17, no. 3, pp. 313–321, 2003.

[40] T. B. L. Kirkwood, "A systematic look at an old problem," *Nature*, vol. 451, no. 7179, pp. 644–647, 2008.

[41] K. A. O'Donnell and K. H. Burns, "Mobilizing diversity: transposable element insertions in genetic variation and disease," *Mobile DNA*, vol. 1, no. 1, p. 21, 2010.

[42] J. K. Baillie, M. W. Barnett, K. R. Upton et al., "Somatic retrotransposition alters the genetic landscape of the human brain," *Nature*, vol. 479, no. 7374, pp. 534–537, 2011.

[43] M. Lessard-Beaudoin, M. Laroche, M. J. Demers, G. Grenier, and R. K. Graham, "Characterization of age-associated changes in peripheral organ and brain region weights in C57BL/6 mice," *Experimental Gerontology*, vol. 63, pp. 27–34, 2015.

[44] C. G. Musso, J. Reynaldi, B. Martinez, A. Pierángelo, M. Vilas, and L. Algranati, "Renal reserve in the oldest old," *International Urology and Nephrology*, vol. 43, no. 1, pp. 253–256, 2011.

[45] N. E. Sharpless and C. J. Sherr, "Forging a signature of in vivo senescence," *Nature Reviews Cancer*, vol. 15, no. 7, pp. 397–408, 2015.

[46] B. M. Hall, V. Balan, A. S. Gleiberman et al., "Aging of mice is associated with p16(Ink4a)- and $\beta$-galactosidase-positive macrophage accumulation that can be induced in young mice by senescent cells," *Aging*, vol. 8, no. 7, pp. 1294–1315, 2016.

Hindawi
Oxidative Medicine and Cellular Longevity
Volume 2019, Article ID 5768953, 14 pages
https://doi.org/10.1155/2019/5768953

*Research Article*

# The Effects of Age and Reproduction on the Lipidome of *Caenorhabditis elegans*

**Qin-Li Wan,[1] Zhong-Lin Yang,[2,3] Xiao-Gang Zhou,[1] Ai-Jun Ding,[1] Yuan-Zhu Pu,[1] Huai-Rong Luo,[1,2] and Gui-Sheng Wu[1]**

[1]*Key Laboratory for Aging and Regenerative Medicine, Department of Pharmacology, School of Pharmacy, Southwest Medical University, Luzhou, Sichuan 646000, China*
[2]*State Key Laboratory of Phytochemistry and Plant Resources in West China, Yunnan Key Laboratory of Natural Medicinal Chemistry, Kunming Institute of Botany, Chinese Academy of Sciences, Kunming, Yunnan 650201, China*
[3]*University of Chinese Academy of Sciences, Beijing 100039, China*

Correspondence should be addressed to Gui-Sheng Wu; wgs@swmu.edu.cn

Received 30 December 2018; Accepted 25 February 2019; Published 9 May 2019

Academic Editor: Consuelo Borrás



Aging is a complex life process, and a unified view is that metabolism plays key roles in all biological processes. Here, we determined the lipidomic profile of *Caenorhabditis elegans* (*C. elegans*) using ultraperformance liquid chromatography high-resolution mass spectrometry (UPLC-HRMS). Using a nontargeted approach, we detected approximately 3000 species. Analysis of the lipid metabolic profiles at young adult and ten-day-old ages among wild-type N2, *glp-1* defective mutant, and double mutant *daf-16;glp-1* uncovered significant age-related differences in the total amount of phosphatidylcholines (PC), sphingomyelins (SM), ceramides (Cer), diglycerides (DG), and triglycerides (TG). In addition, the age-associated lipid profiles were characterized by ratio of polyunsaturated (PUFA) over monounsaturated (MUFA) lipid species. Lipid metabolism modulation plays an important role in reproduction-regulated aging; to identify the variations of lipid metabolites during germ line loss-induced longevity, we investigated the lipidomic profiles of long-lived *glp-1*/notch receptor mutants, which have reproductive deficiency when grown at nonpermissive temperature. The results showed that there was some age-related lipid variation, including TG 40:2, TG 40:1, and TG 41:1, which contributed to the long-life phenotype. The longevity of *glp-1* mutant was *daf-16*-dependent; the lipidome analysis of *daf-16;glp-1* double mutant revealed that the changes of some metabolites in the *glp-1* mutant were *daf-16*-dependent, while other metabolites displayed more complex epistatic patterns. We first conducted a comprehensive lipidome analysis to provide novel insights into the relationships between longevity and lipid metabolism regulated by germ line signals in *C. elegans*.

## 1. Introduction

Life expectancy in humans has dramatically increased worldwide [1]. Aging is often accompanied by diseases and disabilities, including cardiovascular diseases, neurodegenerative diseases, infectious diseases, and cancers [2, 3]. Thus, understanding the physiological characteristics of aging is of extreme importance to enable populations to grow old in good health and without disease.

Several pathways involved in aging mechanisms (e.g., mitochondrial health, DNA damage, proteostasis imbalance, systemic inflammation, epigenetic modifications, and nutrient-sensing pathways) have been associated with undesirable metabolic alterations [4, 5]. Without exception, metabolism changes also occur during reproduction-regulated aging. Using comprehensive nontargeted metabolomics, we previously demonstrated that aging is a process of metabolome remodeling and that long-lived germ line-less *glp-1* mutants regulated the levels of many age-variant metabolites to attenuate aging, including pyrimidine metabolism, purine metabolism, citric acid cycle, glycerophospholipid metabolism, and starch and sucrose metabolism [6]. These findings elucidated the mechanism of reproduction-regulated aging based on the metabolism of small molecules

of endogenous water. Undoubtedly, the metabolism of non-water-soluble molecules is also involved in reproduction-regulated aging.

Previous studies have reported that sacrificing fertility to induce lifespan extension is evolutionarily conserved [7, 8]. In *C. elegans*, germ line removal not only lengthens lifespan but also increases fat accumulation, as observed using lipid-labeling dyes and gas chromatography (GC) [9, 10]. Notably, a reproductive deficiency leading to enhanced fat accumulation has been observed in many other organisms, including both invertebrates (e.g., drosophila) [11, 12] and vertebrates (e.g., mice, rats, and monkeys) [13–15].

In *C. elegans*, a RNA-Seq study demonstrated that upon GSC removal the genes associated with lipid metabolism were upregulated by DAF-16/FOXO3A and/or TCER-1/TCERG1 [16]. These genes included enzymes that initiate *de novo* fatty acid synthesis (including *pod-2* (encodes acetyl CoA carboxylase, ACC), *mlcd-1* (malonyl CoA decarboxylase 1, MLCD), and *fasn-1* (encodes fatty-acid synthase, FAS)) and the genes encoding diacylglycerol acyltransferase (DGAT) enzymes, which catalyze the final step in triglyceride (TAG) production (including *dgat-2*, *acs-22*, *mboa-2*, *Y53G8B.2*, and *K07B1.4*). In addition, in *glp-1* mutants, expression of desaturase enzymes, which catalyze the conversion of saturated fatty acids (SFAs) into unsaturated fatty acids (UFAs), was enhanced in a NHR-49/PPAR$\alpha$- and NHR-80/HNF4-dependent manner, thereby increasing the monounsaturated fatty acid MUFA and reducing SFA levels. Furthermore, expression of *fat-6* and *fat-7*, encoding stearoyl-CoA 9-desaturase (SCD) enzymes, which transform stearic acid (SA, a SFA) to oleic acid (OA, a MUFA), was obviously altered in *glp-1* mutants. Additionally, in *glp-1* mutants, expression of genes involved in $\beta$-oxidation was upregulated in an NHR-49/PPAR$\alpha$-dependent manner [17]. Moreover, following GSC loss, upregulation of the expression of the genes encoding lipase and lipase-like protein (i.e., *lipl-4*, orthologous to the human lipase LIPA) was mediated by DAF-16/FOXO3A, TCER-1/TCERG1, or SKN-1/NRF2 [16, 18, 19]. These studies illustrated that in germ line loss animals, lipid catabolism and anabolism are simultaneously elevated, and germ line loss animals show fat accumulation phenotypes. Expectedly, in *glp-1* mutants, lipid staining and gas chromatography/mass spectrometry (GC/MS) analyses displayed increased levels of TAG and some fatty acids, including C 16:0, C 16:1n7, C 18:0, C 18:1n7, and C 18:3 [9, 10, 16]. However, these studies only highlighted changes in the levels of overall lipids and fatty acids in *glp-1* mutants, barely elucidating the role of individual intact lipid molecules in the regulation of aging by reproduction. Therefore, the aim of the present study was to clarify the role of lipid metabolism in the regulation of aging by reproduction based on lipidomics to obtain intact lipid information and lipid metabolic profiles.

Lipidomics, a branch of metabolomics, refers to the characterization and analysis of the lipid complement of biological systems. Lipidomics can be achieved through comprehensive measurement of the lipid metabolic profiles based on analytical chemistry principles and technological tools, particularly mass spectrometry [20, 21]. In recent years, reflecting the development of MS, lipidomic technology has been widely used in many fields, such as organic biofluids with environmental, pathological, or toxicological stress [22–25]. Furthermore, the lipidome has been used in aging studies. For example, the Leiden Longevity Study demonstrated that specific lipids are associated with familial longevity [26]. Additional lipidomic analyses revealed that some lipids containing phosphatidylethanolamines, phosphatidylcholines, and sphingomyelins are associated with aging in humans [27]. Other studies have revealed that phospho/sphingolipids may represent putative markers and biological modulators of healthy aging in humans [28]. Furthermore, studies have illustrated that PC(O-34:1) and PC(O-34:3) are positively associated with longevity and negatively associated with diabetes [29, 30].

The objectives of the present study were to characterize the lipid metabolic profiles of *C. elegans* hermaphrodites during aging and identify germ line signals that regulate aging. Here, we assessed the lipid metabolic phenotype of whole *C. elegans* between two physiological ages among different mutants (e.g., wild type, *glp-1* mutants, and *daf-16;glp-1* double mutants) using ultraperformance liquid chromatography high-resolution mass spectrometry (UPLC-HRMS), with multivariate statistics analysis, including unsupervised principal component analysis (PCA) as well as hierarchical and supervised orthogonal projection to latent structure with discriminant analysis (OPLS-DA). These results demonstrated that reproductive signals affect lifespan by regulating metabolic changes, and some of these metabolic controls were mediated by FOXO/DAF-16.

## 2. Materials and Methods

*2.1. Culture of Nematodes.* Wild-type N2, CF1903 *glp-1(e2144)III*, and CF1880 *daf-16(mu86)I;glp-1(e2144)III* were obtained from the Caenorhabditis Genetics Center (CGC) and maintained under standard conditions on nematode growth media (NGM) with *Escherichia coli* OP50 as previously described, unless otherwise stated [31].

*2.2. Sample Preparation for Metabolomic Analysis.* The strains were cultured for 2-3 generations prior to collection. To eliminate germ cells of the *glp-1(e2144)* and *daf-16(mu86);glp-1(e2144)* alleles, all strains were synchronized and incubated at 20°C for 12 h, shifted to 25°C, grown to the L4 stage, and subsequently shifted back to 20°C, followed by harvest. The samples were prepared as previously described [6]. Briefly, a large sample of young adult (YA) or day-10 adult (10A) worms (~8000) was pooled and washed with M9 buffer and subsequently collected. All samples were snap frozen in liquid nitrogen and dried overnight *in vacuo* at a low temperature, weighed, and stored at -80°C until extraction. For samples of old worms, 10 $\mu$M 5-fluoro-2′-deoxyuridine (FUdR, Sigma) was used to prevent self-fertilization. It is known that FUdR influences metabolism of worms [32], but the biomass of worms required for lipidomic analysis cannot be collected without using FUdR or a similar intervention. While in order to reduce the influence

of FUdR, all strains were maintained on the same condition, as previously described [6].

Lipid metabolites from *C. elegans* samples were extracted three times with 600 $\mu$L of precooled $CH_2Cl_2$/MeOH (2 : 1) using a TissueLyser at 55 Hz for 90 s. All extracts were subjected to centrifugation (12000 rpm for 10 min at 4°C), subsequently stored at -80°C until further analysis.

*2.3. Lipidomic Analysis Using UPLC-HRMS*

*2.3.1. Sample Preparation.* The samples were thawed at room temperature, centrifuged at 12,000 rpm for 10 min at 4°C, and analyzed using UPLC-HRMS.

*2.3.2. Apparatus and Analytical Conditions.* According to Witting et al. [33], liquid chromatography was performed using a reversed-phase C18 column (CORTECS UPLC C18, waters, 1.6 $\mu$m 150 × 2.1 mm diameter column) with a flow rate of 300 $\mu$L/min at 35°C, and 5 $\mu$L of sample was injected. The mobile phase comprised ACN/H2O (3 : 2, *v*/*v*) (A) and iPrOH/ACN (9 : 1, *v*/*v*) (B), and both A and B contained 0.1% formic acid and 5 mM ammonium formate. The initial eluent comprised 32% solvent B, which was held for 2 min; the percent of buffer B was then gradually increased to 97% in 30 min, was held for 5 min, and was then returned to the initial condition in 0.1 min. The column was reequilibrated for 4.9 min, and the total run time was 40 min.

Analyses were conducted using the Agilent 1290 UPLC System (Agilent, Santa Clara, CA) connected to an Agilent 6500 Q-TOF Mass Spectrometer (Agilent, Santa Clara, CA). The parameter of mass spectrometry analyses in positive ion mode was set previously described, with some modifications [6].

*2.3.3. Data Processing.* Raw files from UPLC-MS were converted to the mzData format using Masshunter Qualitative Software (Agilent, Santa Clara, CA). Peak detection, alignment, and integration were performed using the open-source software XCMS and CAMERA implemented with the freely available R statistical language (version 3.2.2). The procedures and parameters were conducted according to previous studies, with some modifications [34]. Identification of metabolites was performed based on their molecular ion masses and $MS^n$ fragmentation compared with the literature and metabolomic library entries of purified standards, such as LIPID MAPS [35], LIPID BANK [36], the HMDB [37], Lipidhome [38], and LIPIDAT [39]. Subsequently, the putative identifications were verified through comparisons of the retention time matches to those of authentic standard compounds. In addition, we also purchased some commercially available purified standard compounds from Avanti Polar Lipids (Alabaster, AL, USA) to identify metabolites. These standard compounds include heptadecasphing-4-enine, heptadecasphinganine, C17 Sphingosine-1-phosphate, C17 Sphinganine-1-phosphate, SM(d18:1/12:0), Cer(d18:1/12:0), CerP(d18:1/12:0), Cer(d18:1/25:0), d5-DG(14:0/0:0/14:0), d5-DG(15:0/0:0/15:0), d5-DG(16:0/0:0/16:0), d5-DG(17:0/0:0/17:0), d5-DG(19:0/0:0/19:0), d5-TG(20:0/20:1/20:0), d5-TG(20:2/18:3/20:2), d5-TG(20:4/18:2/20:4), d5-DG(20:5/0:0/20:5), d5-TG(14:0/16:1/14:0), d5-TG(20:5/22:6/20:5), d5-TG(15:0/18:1/15:0), d5-TG(16:0/18:0/16:0), d5-TG(17:0/17:1/17:0), d5-TG(19:0/12:0/19:0), d5-TG(20:0/20:1/20:0), d5-TG(20:2/18:3/20:2), d5-TG(20:4/18:2/20:4), PE(17:0/14:1), and PC(17:0/14:1).

*2.4. Bioinformatics and Statistical Analyses.* Nontargeted lipidomic analyses were performed as previously described, with some modifications [6]. For the UPLC-MS data, after normalizing against the dry weights, the resolved data sets were subjected to statistical analysis. The algorithm for significance analysis of microarray (SAM) data (the false discovery rate FDR ≤ 0.05 unless otherwise noted) and unsupervised hierarchical clustering was performed using the web-based metabolomic data processing tool metaboAnalyst [40]. PCA and OPLS-DA were performed using SIMCA-P11.5. Other statistical calculations were conducted using PASW Statistics 20 (SPSS, Chicago, USA), and a $p$ value of 0.05 or less was considered significant in every comparison.

MUFA-to-PUFA ratios were calculated as previously described [26]. Briefly, adding levels of all MUFA lipids (lipids with one double bond in any acyl chain), resulting value was divided by the sum of all PUFA lipids (species with three or more double bonds in their acyl chains).

## 3. Results

*3.1. Lipidomic Profile Associated with Aging in C. elegans.* The first aim of the present study was to characterize changes in the lipidomic profile during aging in *C. elegans* to identify novel lipids or groups of lipids as biomarkers of aging. To this end, we acquired the nontargeted UPLC-HRMS lipidomic profiles of wild-type N2 in young adults (YA) (egg laying has not commenced) and day 10 adults (10A) (aging, egg laying has ceased). Selecting these two time points diminished interference from the egg laying and stochastic components of aging in *C. elegans*. Using these samples (approximately 3000 molecules), multivariate statistical analyses were performed, including unsupervised PCA [41] and supervised OPLS-DA [42] models. PCA and OPLS-DA score plots showed precise separation when the two groups were compared (Figures 1 and 2(b)). In addition, detailed lipid analysis suggested that in old worms the concentrations of DG, PC, and SM significantly decreased, while that of Cer increased (Figure S1). These results suggested that aging included the reprogramming of lipid metabolism.

*3.2. Identification of a Lipid Set with respect to Age.* We displayed the top 40 different lipids for 10A worms compared with YA worms using heat mapping. The resulting heat map displayed a clear variation in the concentrations of metabolites with respect to age. Subsequently, to assess the individual discriminant of each component of the signature, $t$-test (2-tailed) or Mann-Whitney $U$ tests basing on checking for normal distribution were performed (data not shown).

Compared with YA worms, the concentration of long-chain glycerol lipids (such as TG 57:3, TG 59:1, TG 58:3, and DG 42:3) increased in 10A worms, while the concentration of short-chain glycerol lipids (such as DG 30:0, TG 51:4, and DG 28:0) decreased. Additionally, glycerophospholipid

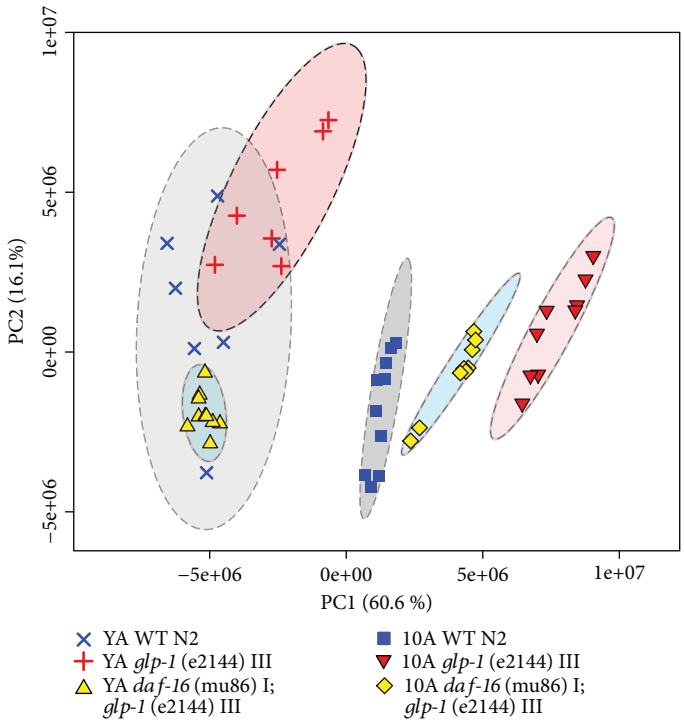


Figure 1: Lipid metabolic variations in WT, *glp-1(e2142)*, and *daf-16(mu86);glp-1(e2141)* worms. PCA included young adults and 10-day adults WT, *glp-1*, and *daf-16;glp-1*. PC1 and PC2 represent the first and second principal components, respectively.

levels changed for selected species with advanced age, and the concentration of most PCs was decreased in aged worms (such as PC 29:5, PC 34:1, PC 29:1, and PC 28:2), and the concentrations of SM 32:0 and SM 34:2 were also decreased in aged animals (Figure 2(a)). In addition, consistent with a previous study on the lipidomics of familial longevity, these results showed that the concentrations of TG 57:2 and TG 56:7 significantly increased in aged animals (Figures 2(c) and 2(d)), although TG 56:6 did not (Figure 2(e)) [26].

Content differences in polyunsaturated (PUFA) and monounsaturated (MUFA) lipids determine membrane peroxidation, and the MUFA-to-PUFA ratio has been suggested to be a marker of longevity [43, 44]. Therefore, we determined differences in the MUFA-to-PUFA ratio between YA and 10A worms. 10A worms displayed a lower MUFA-to-PUFA ratio compared with young worms (Figure 2(f)).

*3.3. Lipidomic Characterization of Long-Lived glp-1 Mutants according to Longevity.* Germ line elimination, leading to lifespan extension in *C. elegans*, is successfully simulated by mutations that cause GSC loss and sterility. One such temperature-sensitive mutant, *glp-1(e2144ts)*, has been widely used as a model for lifespan extension resulting from germ line elimination. Fat metabolism, reproduction, and aging are intertwined regulatory axes, and previous studies have demonstrated that the longevity phenotype of the *glp-1* mutant is associated with the regulation of lipid metabolism and lipid homeostasis using fat staining and GC to detect the fat content [10, 16, 18]. However, the specific lipids regulated by *glp-1* to extend lifespan remain unknown. To demonstrate the relationship between lipid metabolism and aging in the *glp-1* mutant, we detected the intact lipid profiles in the *glp-1* mutant using a comprehensive lipidomic analysis method. Unsupervised PCA analysis showed that the *glp-1* mutant and wild-type samples have distinct lipid metabolic profiles at either the YA or 10A stage, albeit with little overlap at the young adult stage, which also indicated that aging increases metabolic differences (Figure 1). Further supervised OPLS-DA analysis revealed dramatic changes in the lipid metabolism of the *glp-1* mutant compared with the wild type at either the YA or 10A stage (Figures 3(a) and 3(b)).

Furthermore, the top 40 significantly different lipids of the YA and 10A *glp-1* mutants compared with wild-type worms were identified using heat mapping, and the results are listed in Figures 3(c) and 3(d). In addition, fat alterations associated with longevity primarily reflected the accumulation of short-chain lipids (such as TG 40:2, TG 40:1, and TG 41:1), which decreased in aged wild-type worms compared with young worms (Figures 3(c) and 3(d)). These finding suggested that the *glp-1* mutant regulated lipid metabolism to younger profiles compared with wild type.

Additionally, we used RF™ and univariate analyses to identify biomarkers associated with the long-lived phenotype and observed that *glp-1* dysregulated some age-variation lipids (such as PC 44:2, TG 48:4, and TG 50:1) to extend lifespan (Figure 4(c)), although some lipids were not changed (such as DG 34:1, DG 42:3, PC 33:4, and TG 60:3). These results indicated that not all aspects of aging were reset in long-living *glp-1* mutants. More detailed information regarding the significant metabolite changes in *glp-1* mutants compared with wild-type worms are listed in the supplemental information, Tables S1 and S2. In addition, the age-variation MUFA-to-PUFA ratio was obviously increased in *glp-1* mutants compared with wild type at either the YA or 10A stage (Figures 5(b) and 5(c)).

*3.4. FOXO/DAF-16 Mediate Lipid Metabolism Reprogramming in glp-1 Mutants.* Previous studies have demonstrated that the transcription regulators DAF-16/FOXO are essential for the longevity of germ line-less adults, enhancing the expression of multiple genes involved in lipid metabolism and gene classes that promote longevity [16, 18]. Here, we used lipidomic analysis to reveal how germ line loss mutants depend on DAF-16 to regulate lipid metabolism to achieve the longevity phenotype. The results of multivariate analysis, including PCA and OPLS-DA, revealed that the lipid metabolism profiles of *daf-16;glp-1* mutants were different from those of wild type and the *glp-1* mutant (data not shown). Further univariate analysis indicated that some age-related metabolites regulated by germ line loss signals were *daf-16*-dependent (such as DG 34:3; TG 49:2, and TG 51:3) (Figure 5(a)), while other metabolites showed more complex epistatic patterns, such as TG 46:5, TG 40:1, and PC 38:3. More detailed information is provided in the supplemental information, Tables S1 and S2. In addition, the age-related MUFA-to-PUFA ratio was upregulated in the *glp-1* mutant, while no variation was observed in the *daf-16;glp-1* mutant, which may indicate that the age-related MUFA-to-

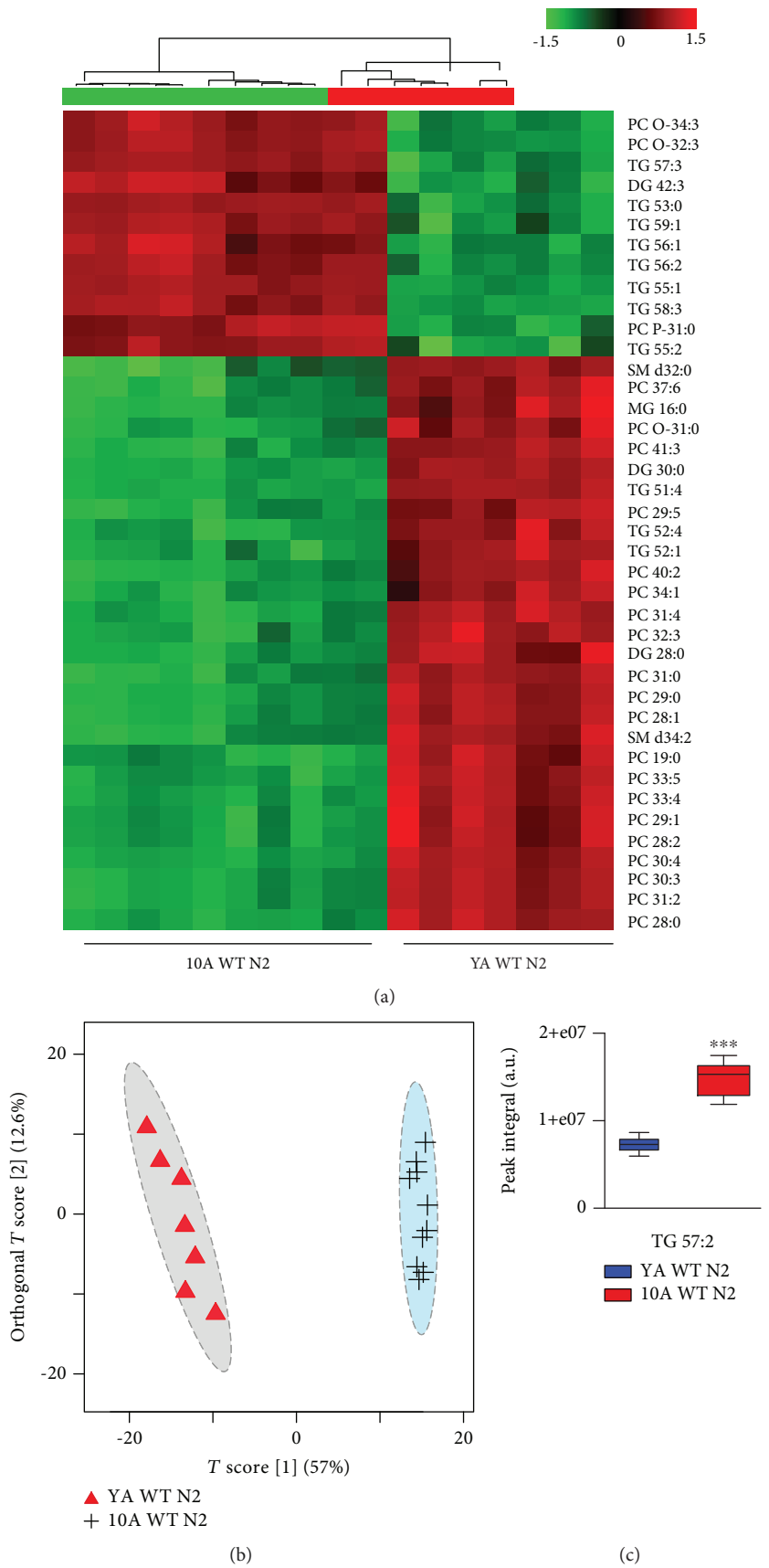


Figure 2: Continued.

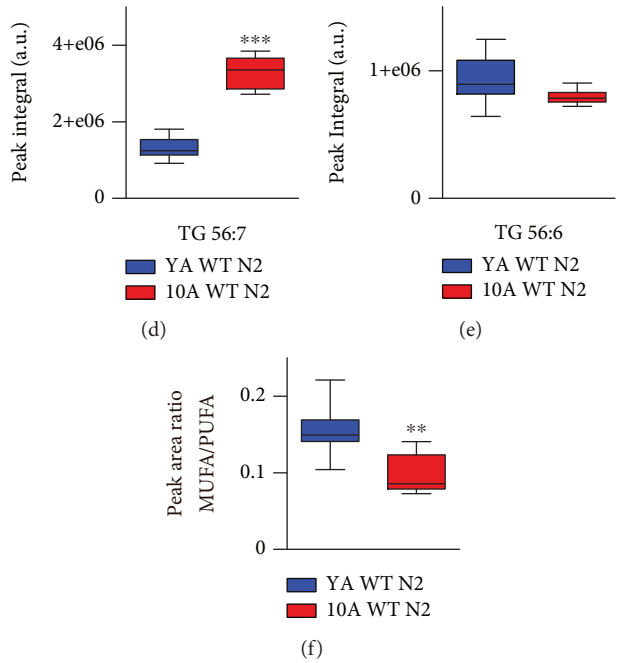


Figure 2: Age-related comprehensive lipidomic analysis in wild-type *C. elegans* (a) lipidomic analysis for YA (young adult) and 10A (10 days of adulthood) wild-type N2. Heat map plot showing the 40 most important different metabolites from the samples according to their aging status. Data are presented using hierarchical clustering (Pearson's correlation coefficient). Metabolite abundance levels were reflected in the heat maps using colors, with blue representing lower and red representing higher levels when comparing the mean metabolite abundance values. The distance function 1-correlation was used in hierarchical clustering to determine the order of metabolites and animals. (b) Scores from OPLS-DA model for YA and 10A wild-type N2. The peak integral (a.u.) of (c) TG 57:2, (d) TG 56:7, and (e) TG 56:6 in YA N2 and 10A N2. (f) MUFA-to-PUFA ratio differences in YA N2 and 10A N2. The $p$ values were calculated using the Mann-Whitney $U$ test, and 0.05 or less was considered significant. All statistical analyses were conducted using SPSS package.

PUFA ratio regulation in *glp-1* was mediated by *daf-16* (Figures 5(b), 5(c)–5(e)).

## 4. Discussion

Untargeted lipidomics enables the comprehensive investigation of endogenous lipids in complex biological systems and has the potential to identify modifications in metabolic pathways and networks in response to biological effects [45, 46]. The role of lipids in aging diseases and human longevity has been widely acknowledged, and the metabolic changes of several lipids associated with age-related diseases, such as hypertension, diabetes type 2, and cardiovascular disease, have been identified [47–49]. Therefore, we investigated the aging-related lipid metabolic variation in *C. elegans*. Analysis of the age-variation lipid profiles in aged worms revealed that the levels of DG, PC, and SM were significantly decreased, while that of Cer was increased. In addition, these results showed that accumulation of long-chain lipid and deleterious short-chain lipids in aged worms might contribute to aging. The aging-related lipid profile was also characterized by a lower MUFA-to-PUFA ratio. The present study is the first to report the age-related lipidomic profiles in *C. elegans*. The lipid profile, representative of healthy aging in *C. elegans*, comprised higher levels of ether PC and SM species and lower levels of PE and long-chain TG species.

In the present study, we observed that the levels of some SM significantly decreased, while those of Cer increased in aged worms compared with young animals. Sphingomyelin species are important components of tissue membranes and cellular messengers and are particularly abundant in neuronal cells. Low levels of SM species have been associated with aging-related diseases, including Alzheimer's, Parkinson's, Huntington's [50], diabetes [30], subclinical atherosclerosis [51], and cardiovascular disease [52]. Sphingomyelinase (SMase) is an enzyme that hydrolyzes SM species into ceramides, whose activity tends to increase with age, thereby decreasing SM levels and increasing ceramide levels [53, 54]. In addition, consistent with the results of the present study, a recent lipidomic study of familial longevity and aging kidney uncovered that the levels of SM species decreased in aged individuals [26, 27]. Thus, alterations in ceramide metabolism may directly influence aging.

We also detected decreasing levels of PC species. PC species prevent the oxidation of polyunsaturated fatty acids in lipoproteins [55]. In addition, upregulation of ether phospholipids is associated with a lower risk for hypertension, diabetes, and aging kidney [27, 30]. In addition, consistent with the results of the present study, a familial longevity study revealed that a higher level of PC represents a younger lipid profile [26]. Thus, PC species were present at lower levels in aged worms, consistent with the decreased antioxidant capacity of these molecules.

Long-chain triglycerides undergo beta-oxidation or peroxisomes, whose enzymatic capacity decreases with age

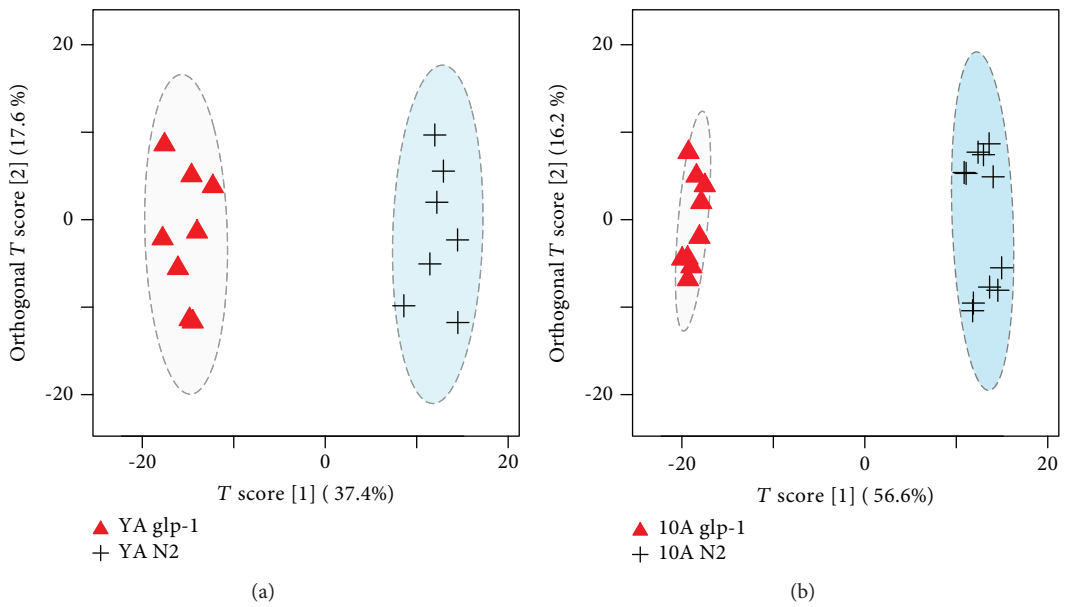


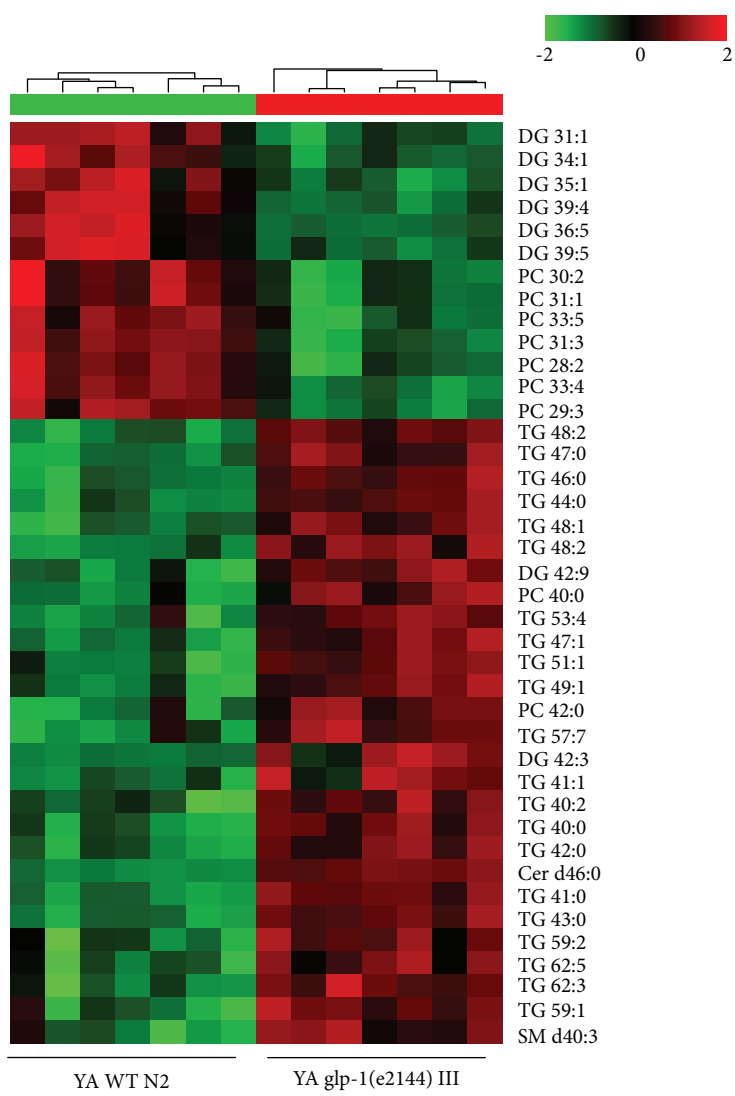


Figure 3: Continued.

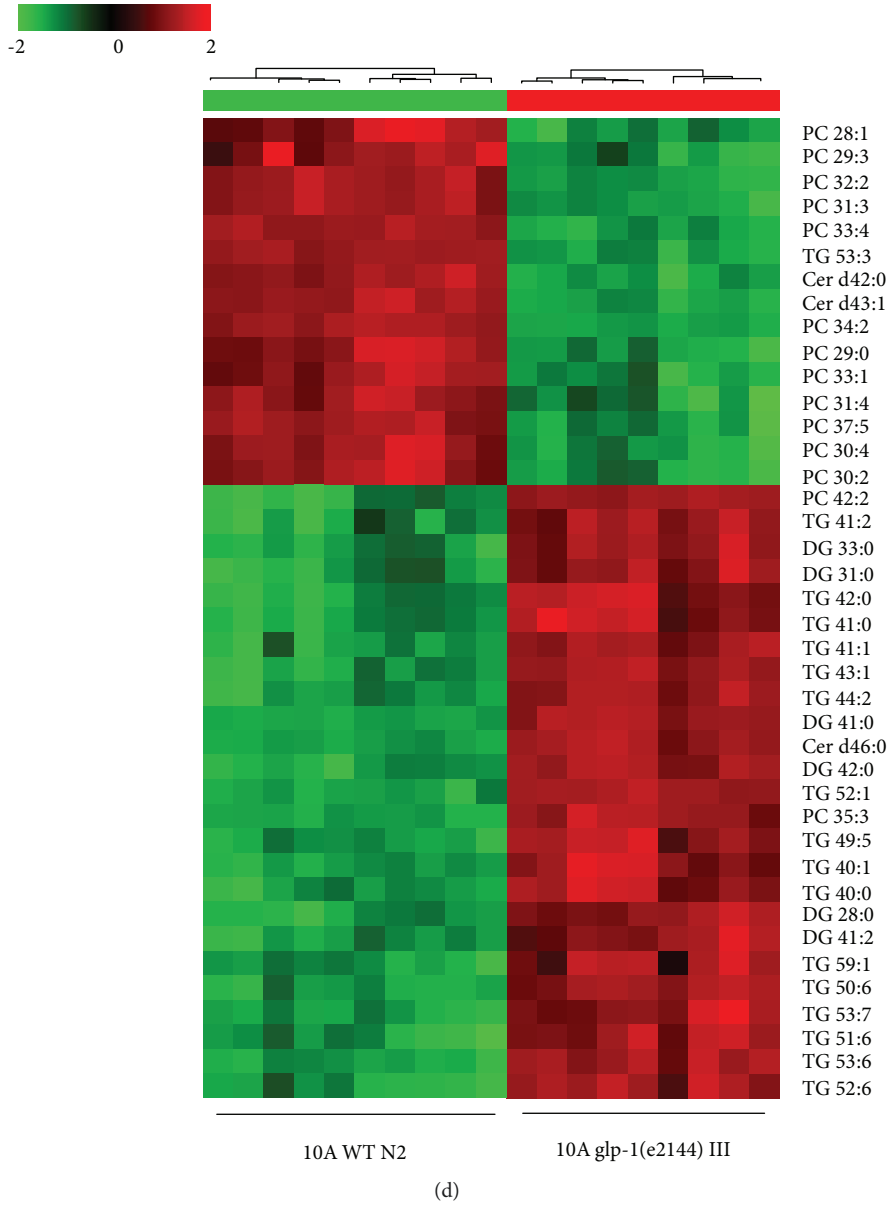


(d)

Figure 3: The long-lived *glp-1(e2144)* mutant has a distinctive lipid metabolic profile. (a) Scores from the OPLS-DA model for *glp-1* and wild-type N2 at (a) young adult stage and (b) 10 days of adulthood. Heat map plot showed the top 40 most important different metabolites from *glp-1* against N2 at (c) young adult stage and (d) 10 days of adulthood.

[26]. Therefore, in aged worms, higher levels of long-chain TG and lower level of short-chain TG may reflect a declined beta-oxidation function compared to younger worms.

The fact that the MUFA-to-PUFA ratio is a longevity biomarker is consistent with reports showing a negative correlation between the membrane double bond content and longevity in mammals [56, 57]. SFA and MUFA are more essentially resistant to peroxidation than PUFA; thus, higher PUFA levels may increase lipid peroxidation and oxidative damage [56, 58]. Thus, in aged worms, a lower MUFA-to-PUFA ratio may be more prone to lipid peroxidation and oxidative damage. Altogether, the lipidome of aged worms, with a lower PC and higher polyunsaturated TG species, may reflect the accumulation of oxidative damage in aged animals.

A previous study reported that *glp-1* mutants showed increased fat storage at the nonpermissive temperature relative to the wild type (N2) by using oil red O staining [16]. Other transcriptomic studies revealed that many aspects of lipid metabolism were altered in *glp-1* mutants, including fatty acid (FA) oxidation, FA desaturation, and triglyceride lipase [16, 18]. Another study showed that some FA (i.e., C16:0, C16:1n7, C18:0, and C18:3) changed in *glp-1* mutant through GC analysis [16, 18]. However, these studies did not determine which intact lipids were regulated by *glp-1* to achieve lifespan extension (Figures 4(a) and 4(b)), although total fatty acid analysis can provide insight into fatty acid metabolism. Extending upon previous studies, we analyzed the lipidome of *glp-1* mutants. Consistent with the results of a previous study, these results demonstrated that fat

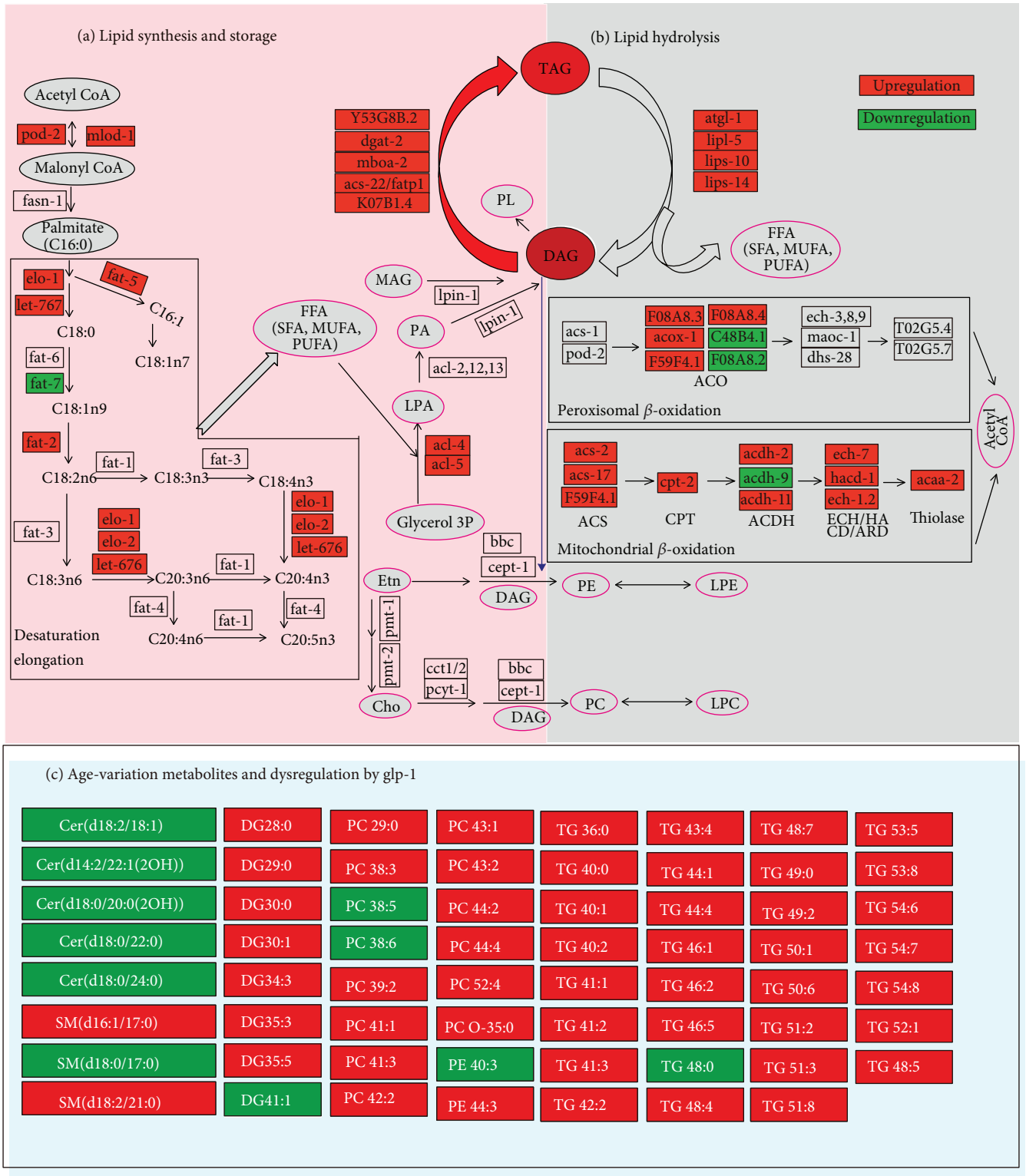


Figure 4: *glp-1* regulated age-variation lipid to achieve the longevity phenotype. (a, b) *glp-1* regulated the key genes involved in lipid anabolism and catabolism, which was modified from Amrit et al., *PLoS Genetics* 2016 [16]. (c) *glp-1* regulated age-variation lipid, and the colors reflect lipid changes, with yellow representing lower and red representing higher values when comparing *glp-1* mutants vs. N2.

storage elevated in *glp-1* mutants. Compared to previous studies, we observed more special intact lipid molecule information regulated by *glp-1*. We observed that *glp-1* regulated some age-related lipids to extend lifespan, including PC 44:2, TG 48:4, and TG50:1 (Figures 4(c) and 5(a)). Furthermore, analysis of the lipidomics of the *daf-16;glp-1* double


Figure 5: The age-related metabolic variation regulated by *glp-1* partly depends on FOXO/DAF-16. (a) Metabolite variation with age in *glp-1(e2144)* and *daf-16(mu86);glp-1(e2144)* double mutants in young adults and 10-day-old adults. Metabolite abundance levels were reflected using colors, increase (green) or decrease (purple) in metabolite concentrations, gray represents no significant difference, when mutants vs. N2. MUFA-to-PUFA ratio differences when *glp-1* vs. N2 at (b) young adult stage or (c) 10-day-old adult stage, or when *daf-16;glp-1* vs. N2 at (d) young adult stage or (e) 10-day-old adult. $p$ values that were calculated using the Mann-Whitney $U$ test of 0.05 or less was considered significant. All statistical analyses were calculated using SPSS package. $p$ values were calculated using the Mann-Whitney $U$ test, and the $p$ value of 0.05 or less was considered significant. All statistical analyses were calculated using SPSS package.

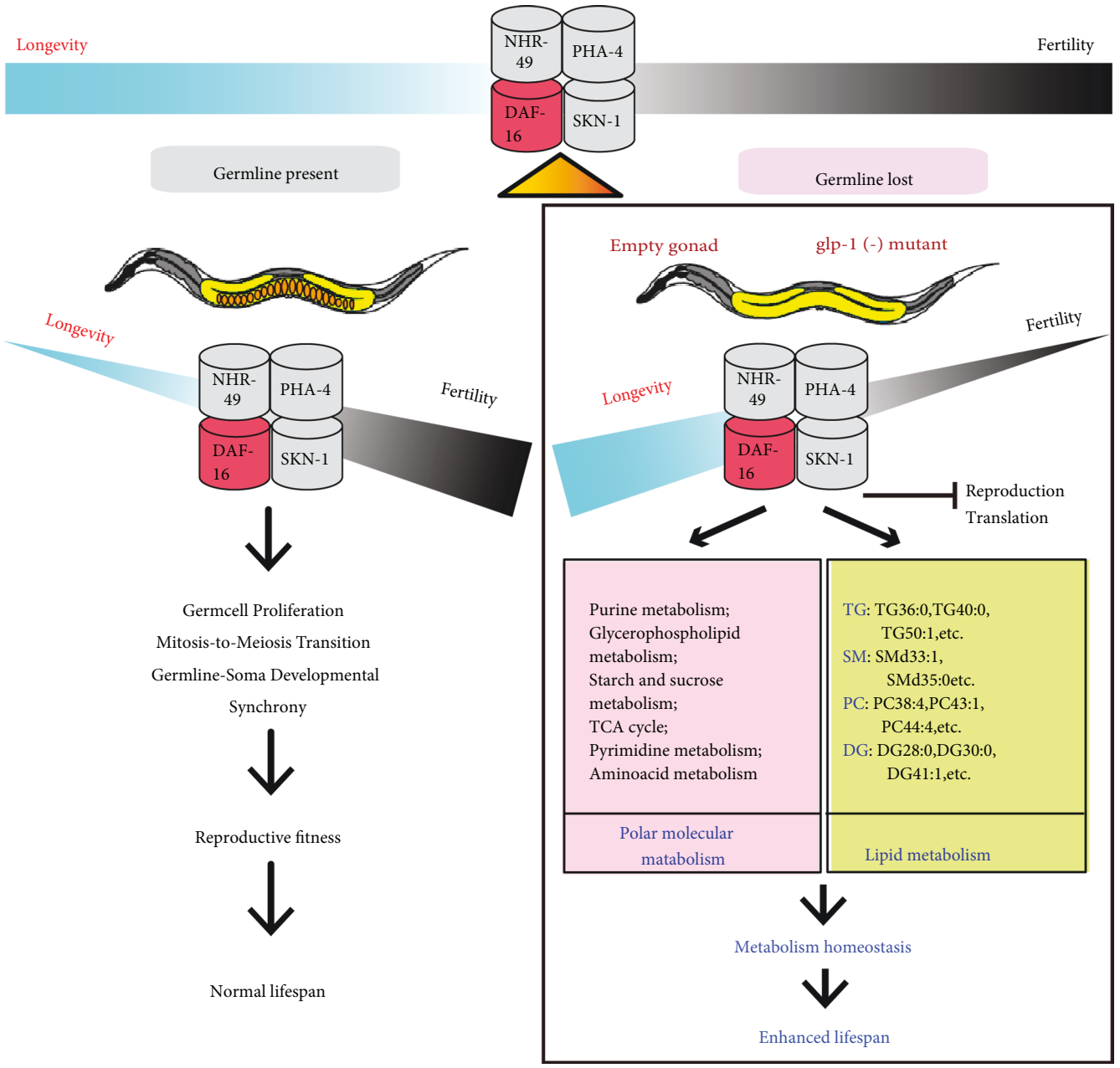


Figure 6: Metabolomic and lipidomic signatures with reproduction-regulated aging in *Caenorhabditis elegans*.

mutant revealed that DAF-16 partially mediated *glp-1*-regulated age-variation lipid metabolism. Indeed, a previous study reported that other downstream target genes also mediated *glp-1* to regulate lipid metabolism to extend lifespan, such as SKN-1 [18], TCER-1 [16], and NHR-49 [17]. Combined with the results of a previous metabolomic studies, there was an inseparable relationship between the extension of the lifespan of *glp-1* and aging-related metabolic changes (Figure 6).

To our knowledge, the present study is the first to use a comprehensive high-resolution lipidome to reveal the relationship between longevity and lipid metabolism. While there are some drawbacks of the lipidomic method, we obtained putative matches for lipids based on databases and references, but these matches often carry considerable uncertainty. In some cases, a single mass-charge ratio may match more than 10 putative known molecules. In addition, some lipids (such as TG (18:1/18:1/18:0) and TGs (18:0/18:2/18:0)) share the same molecular formulas and molecular weights. Thus, the only difference between these molecules is the position of the double bond. These molecules are typically considered to be TGs (54:2). Thus, it is difficult to obtain accurate lipid structure information from lipidomic studies. Moreover, it is difficult to conduct lipid metabolic set enrichment analysis, reflecting the relatively few known lipid metabolic pathways. Therefore,

the present study likely represents only a variation of individual lipid molecules during aging but not the lipid metabolic pathway.

Nevertheless, the results of the present study show the power of using lipidomics to better understand the phenotype of aging and longevity in *C. elegans*. In future studies of aging mechanisms, this knowledge could be linked to functional studies. In any case, the findings of the present study, consistent with the available evidence, clearly suggest that lipid metabolism is closely associated with the aging process and that the long-lived phenotype of *glp-1* is closely related to the regulation of lipid metabolism.

## Data Availability

All the figures and tables used to support the findings of this study are included within the article and supplementary materials.

## Conflicts of Interest

The authors declare that there is no conflict of interest.

## Acknowledgments

We would like to thank the *Caenorhabditis* Genetics Center (CGC) for providing the worm strains, which is funded by NIH Office of Research Infrastructure Programs (P40OD010440). Financial support was received from the Natural Science Foundation of China (81771516, 81801398, and 81671405) and the Science and Technology Cooperation Project of Luzhou and Southwest Medical University (2016LZXNYD-Z05).

## Supplementary Materials

Figure S1: heat map plot listed the lipid variation between YA and 10A N2. Table S1: list of altered lipids of each mutant strain against the wild type in young adults. Table S2: list of altered lipids of each mutant strain against the wild-type days 10 of adult worms. *(Supplementary Materials)*

## References

[1] L. Ferrucci, F. Giallauria, and J. M. Guralnik, "Epidemiology of aging," *Radiologic Clinics of North America*, vol. 46, no. 4, pp. 643–652, 2008.

[2] R. N. Butler, R. A. Miller, D. Perry et al., "New model of health promotion and disease prevention for the 21st century," *BMJ*, vol. 337, article a399, 2008.

[3] C. A. Wijsman, M. P. Rozing, T. C. M. Streefland et al., "Familial longevity is marked by enhanced insulin sensitivity," *Aging Cell*, vol. 10, no. 1, pp. 114–121, 2011.

[4] C. López-Otín, L. Galluzzi, J. M. P. Freije, F. Madeo, and G. Kroemer, "Metabolic control of longevity," *Cell*, vol. 166, no. 4, pp. 802–821, 2016.

[5] R. Pamplona and G. Barja, "An evolutionary comparative scan for longevity-related oxidative stress resistance mechanisms in homeotherms," *Biogerontology*, vol. 12, no. 5, pp. 409–435, 2011.

[6] Q.-L. Wan, X. Shi, J. Liu et al., "Metabolomic signature associated with reproduction-regulated aging in *Caenorhabditis elegans*," *Aging*, vol. 9, no. 2, pp. 447–474, 2017.

[7] H. Hsin and C. Kenyon, "Signals from the reproductive system regulate the lifespan of C. elegans," *Nature*, vol. 399, no. 6734, pp. 362–366, 1999.

[8] N. Arantes-Oliveira, J. Apfeld, A. Dillin, and C. Kenyon, "Regulation of life-span by germ-line stem cells in Caenorhabditis elegans," *Science*, vol. 295, no. 5554, pp. 502–505, 2002.

[9] L. R. Lapierre, S. Gelino, A. Meléndez, and M. Hansen, "Autophagy and lipid metabolism coordinately modulate life span in germline-less C. elegans," *Current Biology*, vol. 21, no. 18, pp. 1507–1514, 2011.

[10] M. C. Wang, E. J. O'rourke, and G. Ruvkun, "Fat metabolism links germline stem cells and longevity in C. elegans," *Science*, vol. 322, no. 5903, pp. 957–960, 2008.

[11] E. T. Judd, F. J. Wessels, M. D. Drewry et al., "Ovariectomy in grasshoppers increases somatic storage, but proportional allocation of ingested nutrients to somatic tissues is unchanged," *Aging Cell*, vol. 10, no. 6, pp. 972–979, 2011.

[12] E. Thomsen and K. Hamburger, "Oxygen consumption of castrated females of the blow-fly, *Calliphora erythrocephala* Meig," *Journal of Experimental Biology*, vol. 32, no. 4, pp. 692–699, 1955.

[13] E. Pallier, R. Aubert, and D. Lemonnier, "Effect of diet and ovariectomy on adipose tissue cellularity in mice," *Reproduction Nutrition Développement*, vol. 20, no. 3A, pp. 631–636, 1980.

[14] M. J. Fettman, C. A. Stanton, L. L. Banks et al., "Effects of neutering on bodyweight, metabolic rate and glucose tolerance of domestic cats," *Research in Veterinary Science*, vol. 62, no. 2, pp. 131–136, 1997.

[15] S. W. Crane, "Occurrence and management of obesity in companion animals," *Journal of Small Animal Practice*, vol. 32, no. 6, pp. 275–282, 1991.

[16] F. R. G. Amrit, E. M. Steenkiste, R. Ratnappan et al., "DAF-16 and TCER-1 facilitate adaptation to germline loss by restoring lipid homeostasis and repressing reproductive physiology in C. elegans," *PLoS Genetics*, vol. 12, no. 2, article e1005788, 2016.

[17] R. Ratnappan, F. R. G. Amrit, S. W. Chen et al., "Germline signals deploy NHR-49 to modulate fatty-acid $\beta$-oxidation and desaturation in somatic tissues of C. elegans," *PLoS Genetics*, vol. 10, no. 12, article e1004829, 2014.

[18] M. J. Steinbaugh, S. D. Narasimhan, S. Robida-Stubbs et al., "Lipid-mediated regulation of SKN-1/Nrf in response to germ cell absence," *eLife*, vol. 4, article e07836, 2015.

[19] M. McCormick, K. Chen, P. Ramaswamy, and C. Kenyon, "New genes that extend Caenorhabditis elegans' lifespan in response to reproductive signals," *Aging Cell*, vol. 11, no. 2, pp. 192–202, 2012.

[20] X. Han, K. Yang, and R. W. Gross, "Multi-dimensional mass spectrometry-based shotgun lipidomics and novel strategies for lipidomic analyses," *Mass Spectrometry Reviews*, vol. 31, no. 1, pp. 134–178, 2012.

[21] C. S. Ejsing, J. L. Sampaio, V. Surendranath et al., "Global analysis of the yeast lipidome by quantitative shotgun mass spectrometry," *Proceedings of the National Academy of Sciences*, vol. 106, no. 7, pp. 2136–2141, 2009.

[22] E. Szymańska, F. A. van Dorsten, J. Troost et al., "A lipidomic analysis approach to evaluate the response to cholesterol-lowering food intake," *Metabolomics*, vol. 8, no. 5, pp. 894–906, 2012.

[23] R. B. Chan, T. G. Oliveira, E. P. Cortes et al., "Comparative lipidomic analysis of mouse and human brain with Alzheimer disease," *Journal of Biological Chemistry*, vol. 287, no. 4, pp. 2678–2688, 2012.

[24] C. Hu, H. Wei, A. M. van den Hoek et al., "Plasma and liver lipidomics response to an intervention of rimonabant in ApoE* 3Leiden. CETP transgenic mice," *PLoS One*, vol. 6, no. 5, p. e19423, 2011.

[25] H. K. Min, S. Lim, B. C. Chung, and M. H. Moon, "Shotgun lipidomics for candidate biomarkers of urinary phospholipids in prostate cancer," *Analytical and Bioanalytical Chemistry*, vol. 399, no. 2, pp. 823–830, 2011.

[26] V. Gonzalez-Covarrubias, M. Beekman, H. W. Uh et al., "Lipidomics of familial longevity," *Aging Cell*, vol. 12, no. 3, pp. 426–434, 2013.

[27] F. Braun, M. M. Rinschen, V. Bartels et al., "Altered lipid metabolism in the aging kidney identified by three layered omic analysis," *Aging (Albany NY)*, vol. 8, no. 3, pp. 441–454, 2016.

[28] I. Montoliu, M. Scherer, F. Beguelin et al., "Serum profiling of healthy aging identifies phospho-and sphingolipid species as markers of human longevity," *Aging (Albany NY)*, vol. 6, no. 1, pp. 9–25, 2014.

[29] J. Graessler, D. Schwudke, P. E. H. Schwarz, R. Herzog, A. Shevchenko, and S. R. Bornstein, "Top-down lipidomics reveals ether lipid deficiency in blood plasma of hypertensive patients," *PLoS One*, vol. 4, no. 7, article e6261, 2009.

[30] K. Suhre, C. Meisinger, A. Döring et al., "Metabolic footprint of diabetes: a multiplatform metabolomics study in an epidemiological setting," *PLoS One*, vol. 5, no. 11, article e13953, 2010.

[31] S. Brenner, "The genetics of *Caenorhabditis elegans*," *Genetics*, vol. 77, no. 1, pp. 71–94, 1974.

[32] S. K. Davies, A. M. Leroi, and J. G. Bundy, "Fluorodeoxyuridine affects the identification of metabolic responses to *daf*-2 status in *Caenorhabditis elegans*," *Mechanisms of Ageing and Development*, vol. 133, no. 1, pp. 46–49, 2012.

[33] M. Witting, T. V. Maier, S. Garvis, and P. Schmitt-Kopplin, "Optimizing a ultrahigh pressure liquid chromatography-time of flight-mass spectrometry approach using a novel sub-2$\mu$m core–shell particle for in depth lipidomic profiling of *Caenorhabditis elegans*," *Journal of Chromatography A*, vol. 1359, pp. 91–99, 2014.

[34] A. Seyer, S. Boudah, S. Broudin, C. Junot, and B. Colsch, "Annotation of the human cerebrospinal fluid lipidome using high resolution mass spectrometry and a dedicated data processing workflow," *Metabolomics*, vol. 12, no. 5, p. 91, 2016.

[35] E. Fahy, M. Sud, D. Cotter, and S. Subramaniam, "LIPID MAPS online tools for lipid research," *Nucleic Acids Research*, vol. 35, Web Server, pp. W606–W612, 2007.

[36] E. Yasugi and K. Watanabe, "LIPIDBANK for Web, the newly developed lipid database," *Tanpakushitsu Kakusan Koso. Protein, Nucleic Acid, Enzyme*, vol. 47, no. 7, pp. 837–841, 2002.

[37] D. S. Wishart, D. Tzur, C. Knox et al., "HMDB: the human metabolome database," *Nucleic Acids Research*, vol. 35, Database, pp. D521–D526, 2007.

[38] J. M. Foster, P. Moreno, A. Fabregat et al., "LipidHome: a database of theoretical lipids optimized for high throughput mass spectrometry lipidomics," *PLoS One*, vol. 8, no. 5, article e61951, 2013.

[39] M. Caffrey and J. Hogan, "LIPIDAT: a database of lipid phase transition temperatures and enthalpy changes. DMPC data subset analysis," *Chemistry and Physics of Lipids*, vol. 61, no. 1, pp. 1–109, 1992.

[40] J. Xia, I. V. Sinelnikov, B. Han, and D. S. Wishart, "MetaboAnalyst 3.0—making metabolomics more meaningful," *Nucleic Acids Research*, vol. 43, no. W1, pp. W251–W257, 2015.

[41] S. Wold, K. Esbensen, and P. Geladi, "Principal component analysis," *Chemometrics and Intelligent Laboratory Systems*, vol. 2, no. 1-3, pp. 37–52, 1987.

[42] J. Trygg and S. Wold, "Orthogonal projections to latent structures (O-PLS)," *Journal of Chemometrics*, vol. 16, no. 3, pp. 119–128, 2002.

[43] P. Caprari, A. Scuteri, A. M. Salvati et al., "Aging and red blood cell membrane: a study of centenarians," *Experimental Gerontology*, vol. 34, no. 1, pp. 47–57, 1999.

[44] R. Pamplona, M. Portero-Otín, D. Riba et al., "Mitochondrial membrane peroxidizability index is inversely related to maximum life span in mammals," *Journal of Lipid Research*, vol. 39, no. 10, pp. 1989–1994, 1998.

[45] J. K. Nicholson, J. C. Lindon, and E. Holmes, "'Metabonomics': understanding the metabolic responses of living systems to pathophysiological stimuli via multivariate statistical analysis of biological NMR spectroscopic data," *Xenobiotica*, vol. 29, no. 11, pp. 1181–1189, 1999.

[46] O. Fiehn, "Metabolomics–the link between genotypes and phenotypes," *Plant Molecular Biology*, vol. 48, no. 1/2, pp. 155–171, 2002.

[47] J. Yeboah, C. McNamara, X. C. Jiang et al., "Association of plasma sphingomyelin levels and incident coronary heart disease events in an adult population," *Arteriosclerosis, Thrombosis, and Vascular Biology*, vol. 30, no. 3, pp. 628–633, 2010.

[48] A. C. I. Boullart, J. de Graaf, and A. F. Stalenhoef, "Serum triglycerides and risk of cardiovascular disease," *Biochimica et Biophysica Acta (BBA) - Molecular and Cell Biology of Lipids*, vol. 1821, no. 5, pp. 867–875, 2012.

[49] M. Miller, N. J. Stone, C. Ballantyne et al., "Triglycerides and cardiovascular disease," *Circulation*, vol. 123, no. 20, pp. 2292–2333, 2011.

[50] M. Piccinini, F. Scandroglio, S. Prioni et al., "Deregulated sphingolipid metabolism and membrane organization in neurodegenerative disorders," *Molecular Neurobiology*, vol. 41, no. 2-3, pp. 314–340, 2010.

[51] J. C. Nelson, X. C. Jiang, I. Tabas, A. Tall, and S. Shea, "Plasma sphingomyelin and subclinical atherosclerosis: findings from the multi-ethnic study of atherosclerosis," *American Journal of Epidemiology*, vol. 163, no. 10, pp. 903–912, 2006.

[52] W. L. Holland and S. A. Summers, "Sphingolipids, insulin resistance, and metabolic disease: new insights from in vivo manipulation of sphingolipid metabolism," *Endocrine Reviews*, vol. 29, no. 4, pp. 381–402, 2008.

[53] E. L. Smith and E. H. Schuchman, "The unexpected role of acid sphingomyelinase in cell death and the pathophysiology of common diseases," *The FASEB Journal*, vol. 22, no. 10, pp. 3419–3431, 2008.

[54] A. R. Smith, F. Visioli, B. Frei, and T. M. Hagen, "Age-related changes in endothelial nitric oxide synthase phosphorylation and nitric oxide dependent vasodilation: evidence for a novel mechanism involving sphingomyelinase and ceramide-activated phosphatase 2A," *Aging Cell*, vol. 5, no. 5, pp. 391–400, 2006.

[55] P. Wiesner, K. Leidl, A. Boettcher, G. Schmitz, and G. Liebisch, "Lipid profiling of FPLC-separated lipoprotein fractions by

electrospray ionization tandem mass spectrometry," *Journal of Lipid Research*, vol. 50, no. 3, pp. 574–585, 2009.

[56] R. Pamplona, M. Portero-Otín, C. Ruiz, R. Gredilla, A. Herrero, and G. Barja, "Double bond content of phospholipids and lipid peroxidation negatively correlate with maximum longevity in the heart of mammals," *Mechanisms of Ageing and Development*, vol. 112, no. , pp. 169–183, 2000.

[57] T. W. Mitchell, R. Buffenstein, and A. J. Hulbert, "Membrane phospholipid composition may contribute to exceptional longevity of the naked mole-rat (*Heterocephalus glaber*): a comparative study using shotgun lipidomics," *Experimental Gerontology*, vol. 42, no. 11, pp. 1053–1062, 2007.

[58] A. A. Puca, P. Andrew, V. Novelli et al., "Fatty acid profile of erythrocyte membranes as possible biomarker of longevity," *Rejuvenation Research*, vol. 11, no. 1, pp. 63–72, 2008.

Hindawi
Oxidative Medicine and Cellular Longevity
Volume 2019, Article ID 1607304, 28 pages
https://doi.org/10.1155/2019/1607304

*Review Article*

# Triclosan: An Update on Biochemical and Molecular Mechanisms

**Mohammad A. Alfhili**[1,2] **and Myon-Hee Lee**[1]

[1]*Department of Medicine (Division of Hematology/Oncology), Brody School of Medicine, East Carolina University, Greenville, NC 27834, USA*
[2]*Department of Clinical Laboratory Sciences, College of Applied Medical Sciences, King Saud University, Riyadh 11433, Saudi Arabia*

Correspondence should be addressed to Myon-Hee Lee; leemy@ecu.edu

Received 30 November 2018; Revised 28 February 2019; Accepted 1 April 2019; Published 2 May 2019

Academic Editor: Demetrios Kouretas



Triclosan (TCS) is a synthetic, chlorinated phenolic antimicrobial agent commonly used in commercial and healthcare products. Items made with TCS include soaps, deodorants, shampoos, cosmetics, textiles, plastics, surgical sutures, and prosthetics. A wealth of information obtained from *in vitro* and *in vivo* studies has demonstrated the therapeutic effects of TCS, particularly against inflammatory skin conditions. Nevertheless, extensive investigations on the molecular aspects of TCS action have identified numerous adversaries associated with the disinfectant including oxidative injury and influence of physiological lifespan and longevity. This review presents a summary of the biochemical alterations pertaining to TCS exposure, with special emphasis on the diverse molecular pathways responsive to TCS that have been elucidated during the present decade.

## 1. Introduction

Triclosan (TCS), or 5-chloro-2-(2,4-dichlorophenoxy)phenol, is a synthetic broad-spectrum antimicrobial developed in the 1960s. As a polychlorinated bisphenolic compound, TCS has a perceptible aromatic odor and is weakly soluble in water. It dissolves well in organic solvents including ethanol, dimethylsulfoxide (DMSO), and methanol [1], and the type of solvent and detergent availability seem to influence TCS activity [2–4]. For example, TCS dissolved in oils (e.g., olive oil) and alkali (e.g., sodium carbonate) exhibits markedly reduced efficacy when compared to other solvents such as glycerol and polyethylene glycol (PEG) [3, 5]. In fact, using propylene glycol (PG) as a solvent renders TCS more effective than using PEG, which is probably due to micellar solubilization of TCS in the larger PEG molecules [3]. Recently, we have shown that the presence of nonionic detergents (e.g., Tween 20) inhibits TCS activity *in vivo*, most likely due to micelle formation [6]. In contrast, sodium dodecyl sulfate (SDS) has been reported to potentiate the antibacterial effect of TCS *in vitro* [7].

TCS has gained enormous popularity in commerce and in healthcare owing to its antibacterial, antiviral, and antifungal properties [8–10]. This efficacy has led to the widespread use of TCS as a preservative in a variety of consumer products, including cosmetics, soaps, mouthwashes, antiperspirants, kitchen utensils, clothing textiles, bedclothes, electronics, plastics, and toys (Triclosan White Paper prepared by the Alliance for the Prudent Use of Antibiotics (APUA)). In clinical practice, TCS is used as a disinfectant and an antiseptic in surgical sutures, scrubs, implants, and medical devices [11, 12]. Annual global production of TCS was estimated at 1500 tons [13], and a total of 132 million liters of TCS-containing products was consumed in a single year in the United States (Safety and Effectiveness of Consumer Antiseptics; Topical Antimicrobial Drug Products for Over-the-Counter Human Use; Proposed Amendment of the Tentative Final Monograph. 2013 https://www.fda.gov/downloads/AboutFDA/ReportsManualsForms/Reports/EconomicAnalyses/UCM379555.pdf).

The high demand for TCS has consequently led to substantial buildup in drinking and wastewater sources and, more alarmingly, accumulation in body fluids [14–20], establishing the antimicrobial as an environmental pollutant. Pharmacokinetic studies in man show that TCS reaches the

systemic circulation by rapid absorption through the skin and mucous membranes of the oral cavity and gastrointestinal tract, and variations in the bioavailability of TCS unsurprisingly affect the rate of urinary excretion [21, 22]. TCS content in commercial products may reach as high as 17 mM and comprise up to 1% of ingredients [12, 19, 23]. Moreover, absorption of up to 25% of applied TCS has been recorded [24], and metabolic studies in rats and mice revealed sulfation, glucuronidation, and hydroxylation products in tissues and excreta [25, 26].

Since the advent of TCS, early studies on the antiseptic have shown evidence of symptomatic relief from acne [27, 28] and contact dermatitis [29, 30] with fewer, or at least comparable, side effects to other therapeutic alternatives [31]. Later, TCS was found to be effective against crural ulcer [32] and chemically induced dermatitis and desquamation [33, 34], which could be attributed to its anti-inflammatory [35], hypoallergenic [36], and analgesic [37] properties. Moreover, a battery of studies collectively indicate that TCS is not a skin or oral mucosal irritant, has a very low sensitization potential (0.1-0.3% of 14,000 subjects), and is unlikely to be phototoxic to human skin (http://ec.europa.eu/health/ph_risk/committees/04_sccp/docs/sccp_o_166.pdf). This is in contrast to the reversible skin and eye irritation caused by up to 10% TCS reported in animals (http://ec.europa.eu/health/ph_risk/committees/04_sccp/docs/sccp_o_166.pdf). Also, in initial studies by Lyman and Furia, it was suggested that TCS is carcinogenic when orally administered to rats [38, 39]. Subsequent investigations in rats and mice disclosed that TCS perturbs microsomal detoxification [40], causes nephrotoxicity and hepatotoxicity [41], reduces prenatal and postnatal survival [42], and leads to central nervous system suppression [43] and hypothermia [44]. In humans, the earliest description of an adverse TCS reaction probably comes from a case report of two patients who developed contact dermatitis following application of deodorants containing 0.12% and 0.2% TCS [45]. Since then, several case reports of the same ailment have thus far been in congruence [46–49]. It is important to mention that, as is the case with healthy subjects, in patients diagnosed with, or suspected to have, contact dermatitis, TCS was similarly found to have a very low sensitization potential (0.6-0.8% of 11,887 patients) (http://ec.europa.eu/health/ph_risk/committees/04_sccp/docs/sccp_o_166.pdf).

In light of the dichotomous debate surrounding TCS, the US Food and Drug Administration (FDA), following extensive examination of available data, has effectively banned antiseptic products containing TCS since September 2016 [19]. In Europe, TCS was approved for use in cosmetics by the European Community Cosmetic Directive in 1986 (http://ec.europa.eu/health/ph_risk/committees/04_sccp/docs/sccp_o_166.pdf). However, the European Commission disapproved the use of TCS for hygienic purposes in 2017, but maintained its legality as a preservative in select cosmetics and mouthwashes in concentrations up to 0.3% and 0.2%, respectively (http://ec.europa.eu/health/scientific_committees/consumer_safety/docs/sccs_o_054.pdf; http://eur-lex.europa.eu/legal-content/EN/TXT/PDF/?uri=OJ:L:2014:107:FULL&from=EN). Furthermore, the Scientific Committee on Consumer Safety (SCCS) expressed its concern over the continued use of TCS in cosmetics, but not in antiseptics, mainly due to the cumulative pattern of exposure (http://ec.europa.eu/health/scientific_committees/consumer_safety/docs/sccs_o_054.pdf). Importantly, the European Chemicals Agency (ECHA) classifies TCS, under the classification, labeling, and packaging (CLP) regulation, as an eye irritant 2 (causes serious eye irritation), skin irritant 2 (causes skin irritation), aquatic acute 1 (very toxic to aquatic life), and aquatic chronic 1 (very toxic to aquatic life with long-lasting effects) (https://echa.europa.eu/documents/10162/21680461/bpc_opinion_triclosan_pt1_en.pdf/efc985e4-8802-4ebb-8245-29708747a358). Because of the previously mentioned ecotoxic properties, TCS is currently a candidate for substitution under the Biocides European Union regulation (Reg 528/2012/EC) (https://echa.europa.eu/potential-candidates-for-substitution-previous-consultations/-/substance-rev/12/term?_viewsubstances_WAR_echarevsubstanceportlet_SEARCH_CRITERIA_EC_NUMBER=222-182-2&_viewsubstances_WAR_echarevsubstanceportlet_DISS=true).

Our aim in this review is to provide an update on current knowledge regarding TCS therapeutic and toxic potential. Emphasis is placed on the biochemical and molecular alterations, either brought about by, or in response to, TCS exposure. Data from both *in vitro* and *in vivo* studies, obtained from humans and other organisms, are incorporated into the analysis, with special attention being given to reports published during the present decade.

## 2. Membrane and Cytoskeletal Damage

Perhaps the earliest report describing the antimicrobial activity of TCS was by Vischer and Regös [50] which was shown through topical application. In a follow-up study, TCS was found to be more effective with the broadest spectrum against bacteria and fungi when compared to other antimicrobials such as gentamicin and clotrimazole [10]. Subsequent efforts, which continue to this day, have focused on dissecting the diverse action mechanisms and cellular targets of TCS. Initially, it was thought that TCS interacts with the prokaryotic cell membrane nonspecifically [9]. This was corroborated by the resistance of Gram-negative bacteria to TCS, which was ascribed to their outer membrane [51, 52]. Investigating the genetic response of *Mycobacterium tuberculosis* to TCS, Betts et al. [53] identified perturbations in a wide assortment of genes involved in cell wall, transport, detoxification, and DNA replication and transcription. Also, *Klebsiella pneumoniae* with inactive efflux pump *KpnGH* exhibit pronounced susceptibility to multiple antibiotics including TCS [54]. Several genes in the membrane stress response pathway were also studied in *Escherichia coli* and *Rhodospirillum rubrum* S1H [55–57]. During the electro-Fenton transformation of TCS, significant changes in expression patterns of genes involved in cell wall and membrane structure, cell envelope, flagella, and multidrug efflux were observed (Table 1). These findings complement an earlier report describing enhanced resistance to TCS due to overexpressed *acrAB* multidrug efflux pump [58]. It was recently

Table 1: Summary of membrane and cytoskeletal targets of TCS.

| Model | Target | | Response |
|---|---|---|---|
| | Gene/protein | Molecular identity | |
| *K. pneumoniae* | *KpnGH* | Efflux pump | Sensitive to TCS |
| *E. coli* | *AcrAB* | Efflux pumps | Upregulated by TCS |
| | *acrE* | | Upregulated by TCS |
| | *mdtE* | | Upregulated by TCS |
| | *acrF* | | Upregulated by TCS |
| | *mdtB* | | Upregulated by TCS |
| | *mdtC* | | Upregulated by TCS |
| | *yddA* | | Upregulated by TCS |
| | *emrA* | | Upregulated by TCS |
| | *emrE* | | Upregulated by TCS |
| | *sanA* | Cell wall/membrane structure | Upregulated by TCS |
| | *dacB* | | Upregulated by TCS |
| | *amiC* | Cell envelope | Upregulated by TCS |
| | *clsA* | | Upregulated by TCS |
| | *ompX* | Membrane porin | Downregulated by TCS |
| | *motA* | Flagellar | Upregulated by TCS |
| | *flgM* | | Upregulated by TCS |
| *R. rubrum* S1H | *sugE* | Small multidrug resistance protein | Upregulated by TCS |
| | *mexF* | RND efflux system, inner membrane transporter | Upregulated by TCS |
| | *mexB* | | Upregulated by TCS |
| | *mexE* | RND efflux system, membrane fusion proteins | Sensitive to TCS |
| | *mexA* | | Upregulated by TCS |
| | *mexM* | | Upregulated by TCS |
| | *oprM* | RND efflux system, outer membrane transporter | Upregulated by TCS |
| | *glmM* | Cell envelope; phosphoglucosamine mutase | Upregulated by TCS |
| | *exoD* | Cell envelope; exopolysaccharide synthesis protein D | Upregulated by TCS |
| | *wbpM* | Cell envelope; polysaccharide biosynthesis protein M | Upregulated by TCS |
| *A. tumefaciens* C58 | *AcrA* | RND efflux system, periplasmic adaptor protein | Upregulated by TCS |
| Human erythrocytes | $Na^+$,$K^+$,$Mg^{2+}$-ATPase | Membrane ion transporter | Sensitive to TCS |
| *C. elegans* | *Pmp-3* | Membrane ABC transporter | Downregulated by TCS |
| *D. rerio* | Actin, cytoplasmic 2 | Cytoskeleton | Downregulated by TCS |
| | Actin $\alpha$1, skeletal muscle | | Downregulated by TCS |
| | Light polypeptide 3 | | Downregulated by TCS |
| | *Desmin* | | Upregulated by TCS |
| | Fast skeletal muscle myosin | | Sensitive to TCS |
| | Keratin, type I cytoskeletal 18 | Cytoskeleton; muscular filament structure | Upregulated by TCS |
| | Tropomyosin $\alpha$-1 chain | | Downregulated by TCS |
| | Type II cytokeratin | | Upregulated by TCS |
| | Lamin B1 | Cytoskeleton; nuclear lamina | Downregulated by TCS |
| *D. polymorpha* | Tubulin $\beta$-2/$\alpha$-4 chain | Cytoskeleton | Upregulated by TCS |
| | Tubulin $\beta$-4 chain | | Upregulated by TCS |
| | Myosin light chain | Cytoskeleton; muscular filament structure | Upregulated by TCS |

Abbreviation: RND: resistance-nodulation-division; ABC: ATP-binding cassette.

suggested that TCS binds to the transcriptional repressor AcrR, causing conformational changes and preventing its binding to the efflux pump *AcrA* promoter in *Agrobacterium tumefaciens* [59].

The interaction of TCS with the cell membrane was also studied in human red blood cells (RBCs; erythrocytes). TCS exposure led to $K^+$ leakage and overt hemolysis, indicating membrane damage, while antagonizing hypotonic lysis,

which may be due to membrane expansion [60]. TCS also inhibited membrane-bound $Na^+$,$K^+$,$Mg^{2+}$-ATPase enzymatic activity [61]. These observations suggest that TCS causes membrane destabilization, perturbs monovalent ion transport, and modulates the overall osmoregulation of erythrocytes. Evidence for membrane damage is further confirmed in numerous studies by means of compromised stability and permeability [62]. To directly observe how TCS interacts with the cell membrane, Guillén and coworkers utilized nuclear magnetic resonance (NMR) spectroscopy to demonstrate that TCS intercalates within hydrophobic pockets in the lipid bilayer, perpendicularly to phospholipid molecules [63]. Furthermore, using neutral red to evaluate membrane integrity, diminished uptake of the dye in hemocytes of the clam *Ruditapes philippinarum* and mussel *Mytilus galloprovincialis* was related to TCS-induced suppression of pinocytosis and disturbed phagocytosis [64, 65].

Along those lines, our recent findings indicate that TCS blunts the expression of the *pmp3* membrane transporter in *Caenorhabditis elegans* nematodes and that *pmp3(ok1087)* mutants exhibit increased sensitivity to the disinfectant [66]. Finally, a proteomic analysis of zebrafish (*Danio rerio*) larvae and gills of freshwater mussel *Dreissena polymorpha* revealed alterations in cytoskeletal protein levels following TCS exposure (summarized in Table 1) [67, 68].

There is a consensus in the literature regarding the membranotropic nature of TCS in different membrane models across various species. The cell membrane is a primary target for TCS and among the first cellular obstacles that must be overcome by the antiseptic to exert its effects. Although evidence implicating membrane-associated efflux pumps as part of the cellular response to TCS is strong, there is paucity in reports describing TCS modulation of structural or functional membrane components in human-based systems. Similarly lacking is an understanding of the role of membrane receptors not only in pumping out TCS molecules but also in transducing both inter- and intracellular signals as a consequence to TCS presence.

## 3. Cellular Longevity

The interest in TCS and ultimate cell fate has originally stemmed from its use in oral hygiene products, which is reflected in two seminal studies on human gingival cells [69, 70]. TCS was shown to be cytotoxic to gingival fibroblasts and epithelial cells, identifying it as a novel stimulator of apoptosis in the latter.

Investigations have thus far followed a more comprehensive approach, relating cell death induced by TCS to other cellular adversaries, utilizing both human and non-human model systems. When TCS was treated to human choriocarcinoma placental cells (JEG-3), multiple dose- and time-dependent responses were observed [71]. While there was a proportional increase in estradiol and progesterone secretion, $\beta$-human chorionic gonadotropin ($\beta$-hCG) release was nevertheless inhibited with increasing TCS concentrations [71]. In addition to blunted proliferation, significant cell death was recognized as apoptotic in nature evidenced by activated caspase-3 and Hoechst 33342-stained fragmented DNA [71]. Similarly, using anoikis-resistant H460 human lung cancer cells, Winitthana et al. demonstrated that 24-hour exposure to 10 $\mu$M TCS causes cell death and apoptosis. Nontoxic levels ($\leq$7.5 $\mu$M), however, enhanced cell growth (increased colony number and reduced size) without altering proliferation. TCS also promoted epithelial-to-mesenchymal transition (EMT), along with the migratory and invasive abilities of the cells [72].

A research group performed a series of *in vivo* and *in vitro* studies on the effect of TCS on growth and proliferation of human BG-1 ovarian cancer cells. Results from these studies indicate that TCS increases cellular proliferation and both gene expression and protein levels of cyclin D1 and decreases p21 and Bax gene expression and protein levels [73]. These effects were significantly antagonized by the estrogen receptor (ER) antagonist ICI 182,780, implicating ER in TCS-induced cell cycle progression and in its antiapoptotic role. Investigators from the same group also reported a similar response to TCS by MCF-7 breast cancer cells and LNCaP prostate cancer cells. In MCF-7 cells, 1 $\mu$M TCS enhanced growth and proliferation during a six-day period, which was associated with increased cyclin D1 and reduced p21 expression levels. When mice were treated with TCS for 8 weeks, brdU-positive breast tumor cells were significantly increased compared to the control group treated with corn oil [74]. Similar to BG-1 cells, TCS-promoted proliferation of MCF-7 cells was mediated through ER$\alpha$ signaling, demonstrated as antagonism by kaempferol and 3,3′-diindolylmethane (DIM), two phytoestrogens [75]. In addition to cyclin D1 and p21, TCS caused an increase in cyclin E and a decrease in Bax and induced metastasis through elevated cathepsin D protein expression. These observations were paralleled *in vivo* using xenografted mouse models. Researchers from this report expanded their findings to VM7Luc4E2 cells, a variant of the MCF-7 model, to show that TCS (0.1-10 $\mu$M) is pro-proliferative and antiapoptotic by inhibiting oxidative stress, with both effects being antagonized by kaempferol [76]. In LNCaP cells exposed to concentrations of TCS ranging from 0.01 to 10 $\mu$M for up to 5 days showed enhanced proliferation and migration and reduced p21 protein expression [77]. In primary human syncytiotrophoblasts, TCS at 0.001 to 10 $\mu$M induced apoptosis as seen by condensed nuclei and fragmented DNA [78]. TCS also reduced 11$\beta$-hydroxysteroid dehydrogenase type 2 (11$\beta$-HSD2) via a caspase-dependent mechanism. Other targets included both Bax and Bcl-2 proteins.

Similar to human cells, both pro- and antiapoptotic properties were observed in rodent cells treated with TCS. Beside its cytotoxicity, TCS caused caspase-dependent apoptosis in rat neural stem cells along with elevated Bax and reduced Bcl-2 [79]. In a series of studies, [80–82] mouse neurons were used to show that TCS is apoptotic through the Fas receptor (FasR), aryl hydrocarbon receptor (AhR), and caspase activation involving N-methyl-D-aspartate receptors (NMDARs). In agreement with the cytotoxicity data, TCS-treated mouse lung epithelial cells were deformed with reduced viability [83]. Conversely, TCS stimulated the proliferation of mouse epidermis-derived JB6 Cl 41-5a cells, by increasing cyclins

D1 and A and reducing p27(Kip1) protein levels [84]. Examining these effects *in vivo*, B6C3F1 mice exhibited epidermal hyperplasia and focal necrosis following topical administration of TCS. Moreover, the pluripotency markers of mouse embryonic stem cells were analyzed following TCS exposure [85]. Alkaline phosphatase (*Alp*), *Sox2*, *Oct4*, and *Nanog* were all reduced, while miRNA-134 was elevated.

Unlike human and rodent cells, *in vivo* and *in vitro* studies on aquatic organisms uniformly agree that TCS is solely proapoptotic in these animals. Pyknotic apoptosis in the central nervous system of zebrafish *D. rerio* was observed following treatment with either TCS alone or TCS combined with derivatives 2,4,6-trichlorophenol (2,4,6-TCP) and 2,4-dichlorophenol (2,4-DCP) [86, 87]. The TCS-derivative mixture caused pronounced deformities and behavioral abnormalities and perturbed the expression of a panel of neurodevelopmental and apoptotic genes (Table 2). Also, TCS, following both *in vivo* and *in vitro* exposure, induced a dose- and time-dependent increase in apoptotic hemocytes of *D. polymorpha* [88, 89]. Likewise, when the saltwater clam *Ruditapes philippinarum* was treated with TCS, hemocytes exhibited significant cell death, blunted proliferation, reduced size, and promiment apoptotic DNA fragmentation [65]. TCS-induced apoptosis, or apoptosis-like cell death, was also detected in unicellular organisms, such as the green alga *Chlamydomonas reinhardtii* and the pathogenic fungus *Cryptococcus neoformans* [90, 91].

Collectively, studies on TCS influence on cell fate indicate estrogenic, proliferative, and apoptotic activities. Genes and proteins governing the regulation of cell cycle and apoptosis are particularly sensitive to TCS modulation. The disparity in ultimate cell fate seems to point at an interspecies variation and a dose-specific response, among other experimental details such as cell type and duration of exposure. Elucidating the existence and the identity of a specific molecular "switch" that may tip the scales in favor of either cell death or survival could be an important inquiry for future investigations.

## 4. Oxidative Stress

Overwhelming evidence has recently accumulated in support of the prooxidative action of TCS. It is prudent to provide an overview of human-based studies first before summarizing notable findings obtained from other model organisms.

In Puerto Rican pregnant women, a correlation between exposure to TCS during pregnancy and oxidative damage, as measured by urinary 8-hydroxyguanosine (8-OHdG), and inflammation was suggested [92]. Similar observations were also mirrored in Chinese and Brazilian children [93, 94]. Conversely, in a global effort comprising nine countries from Asia, Europe, and North America, no relation between urinary TCS and 8-OHdG was established [95].

*In vitro* studies on human cells have also shed some light on the oxidative potential of TCS. In peripheral blood mononuclear cells (PBMC), 2,4-dichlorophenol (2,4-DCP)—a product of TCS transformation—promoted reactive oxygen species (ROS) generation, with subsequent lipid peroxidation and protein carbonylation [96]. Similarly, TCS caused elevated ROS in Nthy-ori 3-1 human follicular thyroid cells [97] and lipid peroxidation in retinoblastoma (Y79 RB) cells [98]. Our recent investigations on mesenchymal stem cells also showed TCS interference with the activation of nuclear factor (erythroid-derived 2)-like 2 (Nrf2), the "master regulator" of detoxification, and its downstream targets, heme oxygenase 1 (HO-1) and NAD(P)H dehydrogenase [quinone 1] (NQO-1) [66]. Consistently, TCS incorporated in mouthrinse did not exhibit antioxidant activity on fibroblasts [99]. In contrast, TCS reduced ROS levels in VM7Luc4E2 cells, which contributed to its antiapoptotic activity in these malignant breast cells [76].

Mitochondrial damage was also evident in multiple mammalian cells including human PBMC and keratinocytes, exposed to 3.5-350 $\mu$M TCS [100]. At concentrations up to 100 $\mu$M, TCS caused depolarization of mitochondrial membrane, reduced oxidative phosphorylation, and suppressed ATP synthesis. Weatherly et al. [101] utilized human HMC-1.2 mast cells and primary keratinocytes to show that TCS is a proton ionophore uncoupler and interferes with ATP production.

Animal studies conducted on mice and rats have revealed a profound response in the cellular antioxidant machinery upon TCS treatment. In rat thymocytes, superoxide anions were found to be elevated following TCS treatment [102] which, as Yueh et al. [103] showed, was met with increased expression of key antioxidant enzymes including HO-1, NQO-1, and glutathione S-transferase (GST) in mouse liver. Evidence for testicular DNA damage, elevated malondialdehyde (MDA), and superoxide dismutase (SOD), in addition to diminished catalase (CAT), was related to TCS treatment in weanling rats [104]. Similarly, in lung homogenates of female albino rats, TCS was found to induce lipid peroxidation and severely deplete the levels of other crucial antioxidants: SOD, CAT, and glutathione (GSH) [105]. Increased expression of glutathione peroxidase 1 (*Gpx1*) and aldehyde oxidase 1 (*Aox1*) was also observed as a consequence to TCS exposure in C57BL/6 mice [106]. Most recently, Zhang et al. [97] showed downregulation of antioxidant enzymes, *Gpx3*, *Cat*, and *Sod2*, along with elevated MDA, in the hypothalamus of Sprague-Dawley rats. Moreover, it was found that TCS treatment leads to increased ROS and reduced GSH activity in rat neural stem cells [79]. TCS also increased ROS levels in mouse neocortical neurons, along with perturbed regulation of cytochrome P450 family 1, subfamily a, member 1 (CYP1a1) and CYP1b1 [81, 82]. Effects of TCS on cytochromes and hepatic detoxification were also demonstrated in Sprague-Dawley rats, showing increased levels of UDP-glucuronosyltransferase 1-1 (Ugt1a), Ugt2b1, CYP1a1, CYP1a2, CYP2b1, CYP3a1, and sulfotransferase family 1E member 1 (Sult1e1) [97].

Several terrestrial organisms have been employed in the study of TCS toxicology. *Caenorhabditis elegans* is among the best-studied animal models due to its ease of maintenance and high genetic homology to humans. We have recently shown that TCS leads to overproduction of ROS, inhibition of nuclear translocation of protein skinhead-1 (SKN-1) antioxidant transcription factor, and

Table 2: Summary of cell survival molecules modulated by TCS.

| Model | Target | | Response |
|---|---|---|---|
| | Gene/protein | Molecular identity | |
| JEG-3 cells | Estradiol | Major female sex hormones | Upregulated by TCS |
| | Progesterone | | Upregulated by TCS |
| | $\beta$-hCG | Maintenance of pregnancy | Downregulated by TCS |
| | Caspase-3 | Apoptosis regulator; proapoptotic | Upregulated by TCS |
| BG-1 cells | Cyclin D1 | Cell cycle regulators | Upregulated by TCS |
| | p21 | | Downregulated by TCS |
| | Bax | Apoptosis regulator; proapoptotic | Downregulated by TCS |
| MCF-7 cells | Cyclin D1 | Cell cycle regulators | Upregulated by TCS |
| | Cyclin E | | Upregulated by TCS |
| | p21 | | Downregulated by TCS |
| | Bax | Apoptosis regulator; proapoptotic | Downregulated by TCS |
| | Cathepsin B | Metastasis markers | Upregulated by TCS |
| | Cathepsin D | | Upregulated by TCS |
| | MMP-9 | | Upregulated by TCS |
| | MMP-2 | | Upregulated by TCS |
| | CXCR4 | | Upregulated by TCS |
| | Snail | Mesenchymal markers | Upregulated by TCS |
| | Slug | | Upregulated by TCS |
| LNCaP | p21 | Cell cycle regulator | Downregulated by TCS |
| Primary human syncytiotrophoblasts | 11$\beta$-HSD2 | Fetal development; anticortisol | Downregulated by TCS |
| | Caspase-3 | Apoptosis regulators; proapoptotic | Upregulated by TCS |
| | Bax | | Upregulated by TCS |
| | Bcl-2 | Apoptosis regulator; antiapoptotic | Downregulated by TCS |
| Rat neural stem cells | Caspase-3 | Apoptosis regulators; proapoptotic | Upregulated by TCS |
| | Bax | | Upregulated by TCS |
| | Bcl-2 | Apoptosis regulator; antiapoptotic | Downregulated by TCS |
| Mouse neocortical neurons | *GluN1* | Ionotropic glutamate receptors; neurotransmission | Downregulated by TCS |
| | GluN1 | | Downregulated by TCS |
| | *GluN2A* | | Downregulated by TCS |
| | GluN2A | | Downregulated by TCS |
| | *GluN2B* | | Upregulated by TCS |
| | GluN2B | | Downregulated by TCS |
| | FasR | Apoptosis regulators; proapoptotic | Upregulated by TCS |
| | Caspase-8 | | Upregulated by TCS |
| | Caspase-9 | | Upregulated by TCS |
| | Caspase-3 | | Upregulated by TCS |
| | AhR | Ligand-activated receptor; detoxification | Upregulated by TCS |
| JB6 Cl 41-5a cells | Cyclin D1 | Cell cycle regulators | Upregulated by TCS |
| | Cyclin A | | Upregulated by TCS |
| | p27 | | Downregulated by TCS |
| B6C3F1 mice | *Alp* | Pluripotency markers; stem cell self-renewal and differentiation regulators | Downregulated by TCS |
| | *Oct4* | | Downregulated by TCS |
| | *Nanog* | | Downregulated by TCS |
| | ALP | | Downregulated by TCS |
| | Oct 4 | | Downregulated by TCS |

Table 2: Continued.

| Model | Target | | Response |
|---|---|---|---|
| | Gene/protein | Molecular identity | |
| | Nanog | | Downregulated by TCS |
| | Sox 2 | | Downregulated by TCS |
| | miRNA-134 | Transcriptional regulator of pluripotency markers | Upregulated by TCS |
| *D. rerio* | *Oct4* | Pluripotency markers | Downregulated by TCS |
| | *Nanog* | | Downregulated by TCS |
| | *Sox2* | | Upregulated by TCS |
| | *p53* | Cell cycle regulator; tumor suppressor | Upregulated by TCS |
| | *Casp3* | Apoptosis regulators; proapoptotic | Upregulated by TCS |
| | *Casp8* | | Upregulated by TCS |
| | *Shha* | Early neurogenesis | Sensitive to TCS sensitive to TCS |
| | *Ngn1* | | Upregulated by TCS |
| | *Nrd* | | Upregulated by TCS |
| | *Elavl3* | | Upregulated by TCS |
| | *α1-tubulin* | | Upregulated by TCS |
| | *Gap43* | Neural maturation | Upregulated by TCS |
| | *Gfap* | | Downregulated by TCS |
| | *Mbp* | | Downregulated by TCS |

Abbreviation: *Shha*: sonic hedgehog a; *Ngn1*: neurogenin 1; *Nrd*: NeuroD; *Elavl3*: ELAV-like, neuron-specific RNA-binding protein 3; *Gap43*: growth-associated protein 43; *Gfap*: glial fibrillary acidic protein; *Mbp*: myelin basic protein.

downregulation of gamma-glutamyl cysteine synthetase (*Gcs1*) [66]. In a subsequent report, *Skn1* expression was found to be upregulated by TCS along with *Sod1*, *Sod4*, heat shock proteins (*Hsp*)-*3*, *-4*, *-16.2*, and *-70*; and cytochromes *Cyp29A2* and *Cyp34A9* (https://app.dimensions.ai/details/publication/pub.1103154992#readcube-epdf). TCS also enhanced nuclear translocation of stress-related factor DAF-16, suggesting the occurrence of oxidative stress [107]. In the Earthworm *Eisenia fetida*, oxidative damage by TCS was manifested as a transient elevation in CAT and GST enzymes, increased MDA, and DNA damage [108]. In a follow-up study by the same group, SOD was also increased and decreased by TCS depending on the concentration used [109], a response mirrored by CAT in the snail *Achatina fulica* [110]. In that study, TCS caused diminished levels of SOD and peroxidase (POD), along with elevated MDA, among other morphological anomalies.

The ubiquity of TCS in aquatic environments has made animal models from that habitat the subject of extensive investigations on TCS toxicity. Perhaps the most relevant aquatic organism is the zebrafish *D. rerio*, owing to a strong structural and molecular resemblance to humans. Elucidating the interaction between TCS and the antioxidant system in ZFL liver cells, Zhou et al. [111] showed evidence of induced CYP1A activity along with a general trend of suppression in phase I and II detoxification enzymes. Elevated MDA, along with perturbed homeostasis of GSH, peroxiredoxin-2 (PRD-2), and HSPs, were observed in zebrafish larvae grown in the presence of TCS ([67, 87]).

TCS has been shown to induce MDA and cause oscillations in CAT, ethoxyresorufin-O-deethylase (EROD), erythromycin N-demethylase (ERND), and aminopyrine N-demethylase (APND) in *Daphnia magna* [112]. Moreover, elevated amino acids, including glutamine, glutamate, and proline, have been attributed to a general oxidative stress state in daphnids [113]. Also, stress-related proteins, including glyceraldehyde 3-phosphate dehydrogenase (GAPDH) and hsp-70, were modulated by TCS in *D. polymorpha*, in addition to lipid peroxidation [68]. TCS exposure demonstrated reduced oxyradicals and lipofuscin and elevated oxidized glutathione (GSSG) in the digestive gland of swollen river mussels *Unio tumidus* [114]. In *Tigriopus japonicus* copepods treated with TCS, increased ROS, SOD, GST, GPx, and GSH content was noted [115]. TCS also caused perturbations in expressional profiles of *Cyps*, *Sod*, *Gst*, and *Cat* proteins (Table 3) [115].

TCS treatment in the yellow catfish *Pelteobagrus fulvidraco* revealed induced CAT, EROD, ERND, and APND [116]. Expressional profiling of *Cyp1a*, *Cyp3a*, and *Gst* showed both up- and downregulation depending on TCS concentration and length of exposure, a pattern that was also seen with MDA formation. When another catfish, *Heteropneustes fossilis*, was treated with a cosmetic effluent rich in TCS, increased SOD and CAT activities and reduced GSH, GST, and GPx were noted [117].

Oxidative damage by TCS was also evident in the goldfish *Carassius auratus*, as MDA, CAT, and GSH were elevated in addition to a reduced total antioxidant capacity [118]. Variable responses by antioxidant enzymes and in MDA

Table 3: Oxidative stress patterns elicited by TCS.

| Model | Target | | Response |
|---|---|---|---|
| | Biomarker | Molecular identity | |
| Humans (pregnant women; children) | Urinary 8-OHdG | Oxidized deoxyguanosine; DNA damage | Upregulated by TCS |
| Nthy-ori 3-1 cells | ROS | Metabolic oxygen by-products | Upregulated by TCS |
| PBMC* | ROS | | Upregulated by TCS |
| | Lipid peroxidation | Oxidized lipids | Upregulated by TCS |
| | Protein carbonylation | Oxidized proteins | Upregulated by TCS |
| Y79 RB cells | Lipid peroxidation | Oxidized lipids | Upregulated by TCS |
| Human bone marrow-derived mesenchymal stem cells | Nrf2 | Antioxidant regulator | Downregulated by TCS |
| | *Ho-1* | Antioxidant enzymes | Downregulated by TCS |
| | *Nqo-1* | | Downregulated by TCS |
| VM7Luc4E2 cells | ROS | Metabolic oxygen by-products | Upregulated by TCS |
| Mouse liver | $O_2^-$ | Antioxidant enzymes | Upregulated by TCS |
| | HO-1 | | Upregulated by TCS |
| | NQO-1 | | Upregulated by TCS |
| | GST | | Upregulated by TCS |
| Weanling rats | MDA | Oxidized lipid marker | Upregulated by TCS |
| | SOD | Antioxidant enzymes | Upregulated by TCS |
| | CAT | | Downregulated by TCS |
| Female albino rat lung homogenates | Lipid peroxidation | Oxidized lipids | Upregulated by TCS |
| | SOD | Antioxidants | Downregulated by TCS |
| | CAT | | Downregulated by TCS |
| | GSH | | Downregulated by TCS |
| C57BL/6 mice liver | *Gpx1* | Antioxidant enzyme; glutathione homeostasis | Upregulated by TCS |
| | *Aox1* | Superoxide and hydrogen peroxide formation | Upregulated by TCS |
| Sprague-Dawley rat hypothalamus | MDA | Oxidized lipid marker | Upregulated by TCS |
| | *Gpx3* | Antioxidant enzyme; glutathione homeostasis | Downregulated by TCS |
| | *Cat* | Antioxidant enzymes | Downregulated by TCS |
| | *Sod2* | | Downregulated by TCS |
| Rat neural stem cells | ROS | Metabolic oxygen by-products | Upregulated by TCS |
| | GSH | Antioxidant | Downregulated by TCS |
| Mouse neocortical neurons | ROS | Metabolic oxygen by-products | Upregulated by TCS |
| | *Cyp1a1* | Cytochrome family enzymes; detoxification | Downregulated by TCS |
| | CYP1a1 | | Downregulated by TCS |
| | *Cyp1b1* | | Downregulated by TCS |
| Sprague-Dawley rat liver | Cyp1b1 | | Upregulated by TCS |
| | *Cyp1a1* | | Upregulated by TCS |
| | *Cyp1a2* | | Upregulated by TCS |
| | *Cyp2b1* | | Upregulated by TCS |
| | CYP2b1 | | Upregulated by TCS |
| | *Cyp3a1* | | Upregulated by TCS |
| | *Ugt2b1* | Glucuronidation enzymes; detoxification | Upregulated by TCS |
| | Ugt2b1 | | Upregulated by TCS |
| | *Sult1e1* | Sulfation enzyme; detoxification | Upregulated by TCS |
| | Sult1e1 | | Upregulated by TCS |
| *C. elegans* | ROS | Metabolic oxygen by-products | Upregulated by TCS |
| | *Skn1* | Stress response regulator | Upregulated by TCS |
| | SKN-1 | | Downregulated by TCS |

Table 3: Continued.

| Model | Target | | Response |
|---|---|---|---|
| | Biomarker | Molecular identity | |
| | *Gcs1* | Antioxidant enzymes | Downregulated by TCS |
| | *Sod1* | | Upregulated by TCS |
| | *Sod4* | | Upregulated by TCS |
| | *Hsp-3* | Stress response; protein stabilization | Upregulated by TCS |
| | *Hsp-4* | | Upregulated by TCS |
| | *Hsp-16.2* | | Upregulated by TCS |
| | *Hsp-70* | | Upregulated by TCS |
| | *Cyp29A2* | Cytochrome family enzymes; detoxification | Upregulated by TCS |
| | *Cyp34A9* | | Upregulated by TCS |
| | DAF-16 | Stress response | Upregulated by TCS |
| *E. fetida* | MDA | Oxidized lipid marker | Upregulated by TCS |
| | CAT | Antioxidant enzymes | Upregulated by TCS |
| | GST | | Upregulated by TCS |
| | SOD | | Sensitive to TCS to TCS |
| *A. fulica* | MDA | Oxidized lipid marker | Upregulated by TCS |
| | CAT | Antioxidant enzymes | Sensitive to TCS to TCS |
| | SOD | | Downregulated by TCS |
| | POD | | Downregulated by TCS |
| ZFL liver cells | CYP1A | Cytochrome family enzyme; detoxification | Upregulated by TCS |
| *D. rerio* larvae | GPx | Antioxidant enzymes; glutathione homeostasis | Upregulated by TCS |
| | GR | | Downregulated by TCS |
| | PRD-2 | Antioxidant enzyme | Downregulated by TCS |
| | Hsp-5 | Stress response; protein stabilization | Upregulated by TCS |
| | Hsp-90 $\beta$ | | Upregulated by TCS |
| *D. magna* | MDA | Oxidized lipid marker | Upregulated by TCS |
| | CAT | Antioxidant enzymes | Sensitive to TCS to TCS |
| | EROD | Detoxification enzymes | Sensitive to TCS to TCS |
| | ERND | | Sensitive to TCS to TCS |
| | APND | | Sensitive to TCS to TCS |
| | Glutamine | Amino acids; markers of protein oxidation/breakdown | Upregulated by TCS |
| | Glutamate | | Upregulated by TCS |
| | Proline | | Upregulated by TCS |
| *D. polymorpha* gills | Hsp-70 | Stress response; protein stabilization | Sensitive to TCS to TCS |
| *U. tumidus* digestive gland | GAPDH | Oxidoreductase; glucose metabolism | Sensitive to TCS to TCS |
| | GSSG | Oxidized glutathione; antioxidant | Upregulated by TCS |
| | Oxyradicals | Oxygen-containing radicals; prooxidants | Downregulated by TCS |
| | Lipofuscin | Lysosomal pigment granules; toxicity marker | Downregulated by TCS |
| *T. japonicus* | ROS | Metabolic oxygen by-products | Upregulated by TCS |
| | *Sod* | Antioxidant enzymes | Sensitive to TCS to TCS |
| | SOD | | Upregulated by TCS |
| | *Cat* | | Sensitive to TCS to TCS |
| | *Gst* variants | Antioxidants; glutathione homeostasis | Sensitive to TCS to TCS |
| | GST | | Upregulated by TCS |
| | GPx | | Upregulated by TCS |
| | GSH | | Upregulated by TCS |
| | *Cyp3026a3* | Cytochrome family enzymes; detoxification | Upregulated by TCS |
| | *Cyp3037a1* | | Upregulated by TCS |

Table 3: Continued.

| Model | Target | | Response |
|---|---|---|---|
| | Biomarker | Molecular identity | |
| *P. fulvidraco* | MDA | Oxidized lipid marker | Sensitive to TCS to TCS |
| | CAT | Antioxidant enzyme | Upregulated by TCS |
| | *Gst* | Antioxidant enzyme; glutathione homeostasis | Sensitive to TCS to TCS |
| | EROD | Detoxification enzymes | Upregulated by TCS |
| | ERND | | Upregulated by TCS |
| | APND | | Upregulated by TCS |
| | *Cyp1a* | Cytochrome family enzymes; detoxification | Sensitive to TCS to TCS |
| | *Cyp3a* | | Sensitive to TCS to TCS |
| *H. fossilis* | CAT | Antioxidant enzymes | Upregulated by TCS |
| | SOD | | Upregulated by TCS |
| | GSH | Antioxidants; glutathione homeostasis | Downregulated by TCS |
| | GST | | Downregulated by TCS |
| | GPx | | Downregulated by TCS |
| *C. auratus* | MDA | Oxidized lipid marker | Upregulated by TCS |
| | CAT | Antioxidant enzymes | Upregulated by TCS |
| | SOD | | Downregulated by TCS |
| | GSH | Antioxidant; glutathione homeostasis | Upregulated by TCS |
| *Brachionus koreanus* | ROS | Metabolic oxygen by-products | Upregulated by TCS |
| | *Gst* variants | Stress response; protein stabilization | Sensitive to TCS to TCS |
| | *Gpx* | Antioxidant enzyme; glutathione homeostasis | Sensitive to TCS to TCS |
| | GST | Stress response; protein stabilization | Upregulated by TCS |
| | *Sod* | Antioxidant enzymes | Sensitive to TCS to TCS |
| | *Cat* | | Sensitive to TCS to TCS |
| | *Cyp3042a1* | Cytochrome family enzymes; detoxification | Sensitive to TCS to TCS |
| | *Cyp43a1* | | Sensitive to TCS to TCS |
| | *Hsp10* | Stress response; protein stabilization | Sensitive to TCS to TCS |
| | *Hsp21* | | Upregulated by TCS |
| | *Hsp27* | | Upregulated by TCS |
| | *Hsp30* | | Sensitive to TCS to TCS |
| | *Hsp40* | | Sensitive to TCS to TCS |
| | *Hsp40h* | | Sensitive to TCS to TCS |
| | *Hsp60* | | Sensitive to TCS to TCS |
| | *Hsp70* | | Upregulated by TCS |
| | *Hsc70* | | Upregulated by TCS |
| | *Hsp90α1* | | Sensitive to TCS to TCS |
| | *Hsp90α2* | | Sensitive to TCS to TCS |
| | *Hsp90β* | | Sensitive to TCS to TCS |
| *B. gargarizans* liver | *Sod* | Antioxidant enzyme | Downregulated by TCS |
| | *Phgpx* | Antioxidant enzyme; glutathione homeostasis | Downregulated by TCS |
| *P. perezi* larvae | GST | | Upregulated by TCS |
| *R. philippinarum* digestive gland | MDA | Oxidized lipid marker | Upregulated by TCS |
| | CAT | Antioxidant enzymes | Sensitive to TCS to TCS |
| | SOD | | Sensitive to TCS to TCS |
| | GPx variants | | Sensitive to TCS to TCS |
| | GST | Antioxidant enzymes; glutathione homeostasis | Sensitive to TCS to TCS |
| | GR | | Sensitive to TCS to TCS |
| | EROD | Detoxification enzyme | Sensitive to TCS to TCS |

Table 3: Continued.

| Model | Target | | Response |
|---|---|---|---|
| | Biomarker | Molecular identity | |
| *O. mykiss* liver and kidney | *Cat* | Antioxidant enzymes | Downregulated by TCS |
| | *Sod* | | Upregulated by TCS |
| | *Gpx* variants | Antioxidant enzymes; glutathione homeostasis | Upregulated by TCS |
| | *Gsta* | | Upregulated by TCS |
| | *Hsp90bb* | Stress response; protein stabilization | Upregulated by TCS |
| | *Hsp90ba* | | Upregulated by TCS |
| | *Hsc70a* | | Upregulated by TCS |
| *C. reinhardtii* | ROS | Metabolic oxygen by-products | Upregulated by TCS |
| | MDA | Oxidized lipid marker | Upregulated by TCS |
| | *Sod* | Antioxidant enzyme | Upregulated by TCS |
| | *Gpx* | Antioxidant enzyme; glutathione homeostasis | Upregulated by TCS |
| | *Gpx* | | Upregulated by TCS |
| | *GrxC* | Antioxidant enzymes; glutathione homeostasis | Upregulated by TCS |
| | *TrxB* | | Upregulated by TCS |
| | *OsmC* | Antioxidant enzyme | Upregulated by TCS |
| | *DnaJ* | Heat shock protein; general stress marker | Upregulated by TCS |
| *R. rubrum* S1H | *RpoN* | RNA polymerase factor sigma-54; general stress marker | Downregulated by TCS |
| | *TerA* | Tellurite resistance protein A; general stress marker | Upregulated by TCS |
| | *Psp* variants | Phage shock proteins; general stress markers | Sensitive to TCS to TCS |
| | *ClpP* | ATP-dependent protease, proteolytic subunit; general stress marker | Upregulated by TCS |
| | *HrcA* | Heat-inducible transcription suppressor; general stress marker | Upregulated by TCS |
| *E. coli* K12, MG1655 | *OxyR* | ROS sensor proteins | Upregulated by TCS |
| | *Grx* | Antioxidant enzymes; glutathione homeostasis | Upregulated by TCS |
| | *Sod* variants | Antioxidant enzymes | Upregulated by TCS |
| | *Cat* variants | | Upregulated by TCS |
| | *Ahp* variants | Antioxidant enzymes | Upregulated by TCS |
| *E. coli* | ROS | Metabolic oxygen by-products | Upregulated by TCS |
| | *YgiW* | Antioxidant proteins | Downregulated by TCS |
| | *SoxS* | | Downregulated by TCS |
| | *YhcN* | | Downregulated by TCS |

Abbreviation: *TrxB*: thioredoxin; *OsmC*: peroxiredoxin osmotically inducible protein C-like. *Effects of 2,4-DCP, a by-product of TCS degradation.

levels were recorded in the goldfish's liver after TCS treatment under a pH range of 6 to 9 [119]. The oxidative potential of TCS was also evident in the rotifer *Brachionus koreanus*, detected as ROS overproduction and enhanced GST activity, in addition to transcriptional modulation of cytochromes, antioxidant genes *Gst*, *Gpx*, *Sod*, and *Cat* and chaperons (Table 3) [120]. Moreover, TCS inhibited *Sod* and phospholipid hydroperoxide glutathione peroxidase (*Phgpx*) expression in the liver of *Bufo gargarizans* tadpoles [121] and induced GST in *Pelophylax perezi* frog larvae [122].

Sendra et al. [123] studied the combined effect of titanium dioxide ($TiO_2$) and a heterogeneous mixture of organic compounds including TCS using the clam *Ruditapes philippinarum*. Modulations in EROD, SOD, CAT, GPx, GST, and GR enzyme activities were noted in the clam's digestive gland, in parallel with increased lipid peroxidation. TCS exposure caused alterations in *Cat*, *Sod*, *Gpx1*, *Gpx2*, *Gsta*, *Hsp90bb*, *Hsp90ba*, and *Hsc70a* genes in rainbow trout *Oncorhynchus mykiss* [124]. Although in one report TCS failed to elicit oxidative stress in the green algae *Chlamydomonas reinhardtii* [125], another report detected ROS formation following TCS exposure [90], which was also most recently confirmed by significantly increased MDA, downregulated *Gpx*, and upregulated *Sod* expression [126].

The antimicrobial nature of TCS makes bacteria an appropriate target for mechanistic studies. Using *Rhodospirillum rubrum* S1H, Pycke et al. [57] detected upregulation in a host of TCS-induced oxidative response genes, most

notably *Gpx*. In *E. coli* K12, MG1655, the electro-Fenton transformation of TCS caused activation of genes related to ROS sensing, along with reduced glutaredoxin (*Grx*), *Sod*, *Cat*, and alkyl hydroperoxide reductase (*Ahpr*) [55]. Very recently, ROS formation by TCS was associated with diminished expression of antioxidants in *E. coli* (Table 3), an event that preceded mutagenesis and enhanced drug resistance in that species [56]. TCS was also recently used to validate novel self-luminescent bioreporter strains of *Nostoc* sp. PCC 7120 using *Sod* promoters [127].

Collectively, monumental evidence demonstrates the prooxidant properties of TCS evident as both overproduction of ROS and interference with the cellular antioxidant defensome. TCS is toxic in part by inducing oxidative damage in a wide range of organisms and by targeting a defined cluster of proteins in a fashion that is conserved among diverse species. Nonetheless, the vast majority of data are collected from non-human models, and, as is the case with other toxicological reports of TCS, studies conducted on man or human-derived tissues are severely lacking.

## 5. Immunity and Inflammation

TCS has, for a long time, been recognized as an effective therapy for infectious dermatitis [29–31], and the observed curative capacity of the compound was solely attributed to its antimicrobial activity. It was not until the end of last century that associations between TCS exposure and remission of noninfectious inflammation were made [33, 35, 36], and the use of antibacterials as anti-inflammatory agents has gained deserved attention during the past two decades. For example, an appreciable number of antibiotics, including macrolides and quinolones, have been shown to possess anti-inflammatory activity [128–132]. Follow-up efforts have successfully provided solid evidence for the direct interaction of TCS with inflammatory pathways.

Gaffar et al. [133] reported that TCS inhibits cyclooxygenase-1 (COX-1) and COX-2, 5-lipoxygenase and (LPO), 15-LPO, and interleukin- (IL-) 1$\beta$-induced prostaglandin E2 (PGE2) in gingival cells. TCS was also shown to suppress a wider range of inflammatory mediators including IL-1$\beta$-induced prostaglandin I2 (PGI2) and arachidonic acid, tumor necrosis factor (TNF)$\alpha$-induced PGE2, phospholipase A2 (PLA2), and COX [134]. Moreover, in a double-blind crossover study, participants who used a mouthrinse with added 0.15% TCS developed significantly less oral erythematous lesions than those who used a TCS-free mouthrinse [135]. By then, the anti-inflammatory properties of TCS were established and were widely accepted within the scientific and medical communities.

TCS in prosthetic devices was found to have no influence on the acute phase response [136], and only modest differences were seen between TCS and stannous fluoride dentrifice [137]. Nevertheless, TCS, when applied intracrevicularly, improved clinical parameters of gingivitis [138]. In a recent double-blind, randomized, crossover study, it was concluded that TCS-containing toothpaste inhibits inflammation in peri-implant tissue [139].

To date, elaborations on the anti-inflammatory nature of TCS have been the focus of subsequent studies. Mustafa et al. [140–142] identified IL-1$\beta$, interferon (IFN)$\gamma$, major histocompatibility complex (MHC) class II, and PGE synthase-1, as targets of TCS in human gingival fibroblasts. Of note, studies to discern the subcellular localization of TCS show preference for nuclear, as opposed to cytosolic, accumulation. Although initial uptake was considerably higher in the cytoplasm, a great proportion of cytosolic TCS was eliminated after repeated washing, while nuclear retention was observed [143]. This may explain the perturbed inflammatory signaling associated with TCS. Moreover, in primary human oral epithelial cells, TCS attenuated LPS-induced cytokine response including IL-8, IL-1$\alpha$, and TNF$\alpha$ and aggravated the antimicrobial response, which was mediated through microRNA (miRNA) regulation of the toll-like receptor (TLR) pathway [144]. The findings were also reciprocated in cells derived from diabetic patients, with an exaggerated TLR response [145]. It was revealed that TCS, nevertheless, abrogated LPS-induced TLR response, again, through regulating miRNAs (stimulating miR146a and inhibiting miR155s).

In skin and leukocytes of mice topically treated with TCS, alterations in inflammatory responses were mediated through TLR4 [146]. Likewise, TCS downregulated parathyroid hormone- (PTH-) or PGE2-stimulated matrix metalloproteinase-13 (MMP-13) expression in rat osteoblastic osteosarcoma cells [147]. Since hyperactive MMP-13 is implicated in periodontal disease, it was suggested that TCS might have a protective role against oral inflammatory conditions through its action on that enzyme, among others [148].

Interestingly, favorable results have been observed for TCS against other inflammatory conditions including cardiovascular disease and hidradenitis suppurativa [149, 150]. Moreover, the use of TCS-impregnated ureteral stents seems to be a promising approach to combat urinary tract infections (UTI) and associated inflammation [151, 152]. Along those lines, an increased urinary TCS was related to increased serum IL-6 in pregnant women [92], pointing at a possible pro- or anti-inflammatory role.

In a unique effort by Barros et al. [153], TCS modulation of the inflammatory response in an ex vivo whole blood stimulation assay was investigated. In that study, TCS inhibited multiple inflammatory mediators induced by LPS, including interleukins, most notably IL-1 & IL-6, IFNs, and colony-stimulating factor (CSF) 2. Activation of type 1 T helper lymphocytes was interrupted through the action of TCS on CD70. In a related report, TCS also reduced the capacity of natural killer (NK) lymphocytes to lyse chronic myelogenous leukemia K562 cells [154]. Recently, chitosan-TCS particles reduced the expression of IL-1$\beta$-induced *Cox2* and *Il6*, among other immune molecules in gingival fibroblasts (Table 4) [155], showcasing the vast amenability of this antimicrobial to nanoparticle manipulation.

Other *in vivo* studies on rodents and marine organisms clarified further the immunomodulatory properties of TCS. For instance, in mice subjected to an acute, systemic *E. coli* infection, Sharma et al. [156] demonstrated that cotreatment with TCS significantly reversed the damage caused by the

Table 4: Inflammatory and immune mediators responsive to TCS.

| Model | Target | | Response |
|---|---|---|---|
| | Biomarker | Molecular identity | |
| Human gingival fibroblasts | COX-1/2 | Inflammatory mediators | Downregulated by TCS |
| | 5/15-LPO | | Downregulated by TCS |
| | PGE2 | | Downregulated by TCS |
| | PGI2 | | Downregulated by TCS |
| | Arachidonic acid | | Downregulated by TCS |
| | PLA2 | | Downregulated by TCS |
| | PGE synthase-1 | | Downregulated by TCS |
| | IFN$\gamma$ | Immune/inflammatory cytokines | Downregulated by TCS |
| | IL-1$\beta$ | | Downregulated by TCS |
| | MHC II | Cell surface proteins; adaptive immunity regulators | Downregulated by TCS |
| | *Cox2* | Inflammatory mediator | Downregulated by TCS |
| | *Il6* | Immune/inflammatory cytokines | Downregulated by TCS |
| | *Il1b* | | Downregulated by TCS |
| | *Tlr6* | Innate immunity receptor | Upregulated by TCS |
| Human primary oral epithelial cells | IL-8 | Immune/inflammatory cytokines | Downregulated by TCS |
| | IL-1$\alpha$ | | Downregulated by TCS |
| | TNF$\alpha$ | | Downregulated by TCS |
| | miR146a | Transcriptional regulators of TLR response | Upregulated by TCS |
| | miR155s | | Downregulated by TCS |
| Mouse skin and leukocytes | S100A8/A9 | Inflammatory modulator; $Ca^{2+}$-binding protein | Upregulated by TCS |
| | *Tlr4* | Innate immunity receptors | Upregulated by TCS |
| | TLR4 | | Upregulated by TCS |
| | *Tlr1* | | Upregulated by TCS |
| | *Tlr2* | | Upregulated by TCS |
| | *Tlr6* | | Upregulated by TCS |
| Rat osteoblastic osteosarcoma cells | MMP-13 | Endopeptidase; collagen degradation | Downregulated by TCS |
| Human oral fluids | IL-1$\alpha$ | Immune/inflammatory cytokines | Downregulated by TCS |
| | IL-1$\beta$ | | Sensitive to TCS |
| | IL-8 | | Sensitive to TCS |
| | MCP-1 | | Sensitive to TCS |
| | TIMP-2 | MMP regulator proteins | Sensitive to TCS |
| | TIMP-1 | | Downregulated by TCS |
| | MMP-8/9 | Endopeptidases; extracellular matrix degradation | Downregulated by TCS |
| Human urine | IL-6 | Immune/inflammatory cytokines | Upregulated by TCS |
| Sprague-Dawley rats | TNF$\alpha$ | | Upregulated by TCS |
| | IL-6 | | Upregulated by TCS |
| Human whole blood leukocytes | *Csf2* | Hematopoietic stem cell growth and maintenance | Downregulated by TCS |
| | *Ifna1* | Immune/inflammatory cytokines | Downregulated by TCS |
| | *Ifna2* | | Downregulated by TCS |
| | *Ifna4* | | Downregulated by TCS |
| | *Ifna8* | | Downregulated by TCS |
| | *Il-1f10* | | Downregulated by TCS |
| | *Il-1f5* | | Downregulated by TCS |
| | *Il-1f7* | | Downregulated by TCS |
| | *Il-1f8* | | Downregulated by TCS |
| | *Il-1f9* | | Downregulated by TCS |
| | *Il-6* | | Downregulated by TCS |

Table 4: Continued.

| Model | Target | | Response |
|---|---|---|---|
| | Biomarker | Molecular identity | |
| | *Il-11* | | Downregulated by TCS |
| | *Il-13* | | Downregulated by TCS |
| | *Il-25* | | Downregulated by TCS |
| | *Il-19* | | Downregulated by TCS |
| | *Il-21* | | Downregulated by TCS |
| | *Il-9* | | Downregulated by TCS |
| | *Cd70* | Cell surface receptor/ligand; activated lymphocytes | Downregulated by TCS |
| | *Bmp2* | Growth factors; bone and cartilage development | Upregulated by TCS |
| | *Bmp6* | | Upregulated by TCS |
| | *Tnfrsf11b* | TNFSF11 receptor | Downregulated by TCS |
| | *Gdf3* | | Downregulated by TCS |
| | *Gdf2* | Growth/differentiation factors | Downregulated by TCS |
| | *Gdf5* | | Downregulated by TCS |
| | *Gdf9* | | Downregulated by TCS |
| | *Inhba* | Hypothalamus-pituitary axis regulator | Downregulated by TCS |
| | *Lefty2* | Left-right determination factor 2; left-right asymmetry of organs | Downregulated by TCS |
| Sprague-Dawley rats | TNF$\alpha$ | Immune/inflammatory cytokine | Upregulated by TCS |
| | IL-6 | | Upregulated by TCS |

Abbreviation: MCP: monocyte chemoattractant protein; TIMP: tissue inhibitor of metalloproteinase; *Bmp*: bone morphogenetic protein; *Gdf*: growth differentiation factor; *Inhba*: inhibin beta A chain.

bacteria. Specifically, TCS prolonged survival; lessened hepatic congestion, hemorrhage, and fatty changes; and reduced blood liver enzymes, serum TNF$\alpha$, and the severity of bacteremia. In accordance with published data, TCS was similarly immunosuppressive in aquatic mussels (*M. galloprovincialis*) and clams (*R. philippinarum*) [64, 65].

Contrary to the overwhelming evidence of the anti-inflammatory function of TCS, a number of studies have nonetheless identified a proinflammatory role by the antiseptic. For example, upon intratracheal instillation of TCS in Sprague-Dawley rats, elevated total cell (TC) count, polymorphonuclear leukocytes (PMNs), total protein (TP), LDH, TNF$\alpha$, and IL-6 were observed in bronchoalveolar lavage (BAL) fluid [83], which, except for TP, returned to baseline levels 14 days after exposure. Consonantly, it has also been demonstrated that TCS exacerbates diethylnitrosamine-induced hepatocellular carcinoma in C57BL/6 mice [103]. Likewise, TCS was very recently found to increase *Tlr4* expression to promote colitis and aggravate colitis-related cancer in C57BL/6 mice [157].

It is evident from the wealth of information present that TCS is a modulator of immune and inflammatory reactions. The sum of data from *in vitro* and *in vivo* studies indicates that TCS, on its own, is immunosuppressive. Nevertheless, increasing evidence seems to suggest that in the presence of an existing adverse condition, such as inflammation or tumor, TCS further potentiates and worsens the eventual outcome. Investigations into the molecular basis behind this unique behavior are particularly warranted.

## 6. Genotoxicity and Carcinogenicity

Among the most important aspects of toxicological profiling of compounds is their interaction with the molecule of life—the DNA. Early efforts [42, 158] point at a possible role for TCS in somatic mutations observed in mice. TCS also caused a significant reduction in global DNA methylation in human hepatocellular carcinoma HepG2 cells, a finding associated with liver tumor [159]. Similarly, TCS caused a dose-responsive increase in chromosomal aberrations in lung fibroblast V79 cells, but not in ovary CHO cells, of the Chinese hamster *Cricetulus griseus* [12]. In a comparative study on *Drosophila melanogaster* using three mouthwashes, namely, Cepacol® (0.05% cetylpyridinium chloride), Periogard® (0.12% chlorhexidine digluconate), and Plax® (0.03% TCS), it was concluded that only the ethanol content in Cepacol®, but not other active ingredients, caused mitotic recombination between homologous chromosomes [160]. On the other hand, TCS induced dose-responsive DNA damage in hemocytes of the zebra mussel *D. polymorpha* [88], and strand breaks in the digestive gland of *U. tumidus* mussels [114]. A similar dose-dependent DNA damage was also observed in the earthworm *E. fetida* [108, 109], but not in *E. andrei* [161].

Comparing TCS to other toxicants in the larvae of freshwater insect *Chironomus riparius*, Martinez-Paz et al. [162] found TCS, along with nonylphenol, to be the most potent in causing DNA breakage. It was also noted that TCS, either alone or in combination with carbendazim, induced DNA

Table 5: TCS genotoxicity and carcinogenicity.

| Model | Effect | Classification |
|---|---|---|
| HepG2 cells | Global DNA hypomethylation | Limited evidence of carcinogenicity |
| V79 cells | Chromosomal aberrations | |
| Mouse | Somatic mutation (positive spot test)<br>Increased incidence of liver tumors<br>Aggravated hepatocellular carcinoma<br>Exacerbated colon tumorigenesis | |
| *D. polymorpha* | DNA damage (positive comet assay) | N/A |
| *U. tumidus* | DNA strand breaks (Hoescht 33342 fluorescence) | |
| *E. Fetida* | DNA damage (positive Comet assay) | |
| *D. magna* | DNA damage (positive Comet assay) | |
| *A. salina* | DNA damage (positive Comet assay) | |
| *H. fossilis* | DNA damage (positive Comet assay) | |
| *C. auratus* | DNA damage (positive Comet assay) | |
| *O. mykiss* | DNA damage (positive Comet assay) | |
| *T. thermophila* | DNA damage (positive Comet assay) | |
| *A. cepa* | Chromosomal stickiness, reduced mitotic activity, and ana-telophase bridges (positive Feulgen reaction) | |

N/A = data from non-mammalian animals are not considered for ECHA mutagenicity/carcinogenicity classification.

damage in *D. magna* [163]. Using the brine shrimp *Artemia salina*, a time-dependent pattern of TCS-induced genotoxicity was identified [164]. Moreover, TCS was genotoxic in the catfish *Heteropneustes fossilis*, goldfish *C. auratus*, and rainbow trout *O. mykiss* [117, 118, 124]. Importantly, when TCS at an environmentally relevant concentration (3 nM) was treated to the freshwater protozoan *Tetrahymena thermophila*, notable DNA damage, without significant perturbation in growth or cell viability, was evident [165]. In a more detailed study on *E. coli*, Gou et al. [55] revealed that the electro-Fenton transformation of TCS caused upregulation of a host of genes involved in the DNA repair machinery, indicative of DNA stress. These genes belong to base excision repair (*mutT* and *nfo*), nucleotide excision repair (*uvrA* and *uvrD*), mismatch repair (*uvrD* and *ssb*), and double-strand break repair (*ssb* and *recN*). Chromosomal stickiness, reduced mitotic activity, and ana-telophase bridges were also noticeable in the bulb onion *Allium cepa* following TCS treatment [166].

In a recent proof-of-concept study, the promising potential of a toxicogenomic approach as a follow-up to positive *in vitro* genotoxicity data was evaluated. Using TCS as a testing compound, it was shown that the antimicrobial is non-DNA reactive and that it is genotoxic solely *in vitro* as opposed to *in vivo* [167].

Ambiguity surrounding the carcinogenicity of TCS still remains today. Investigators have generally been able to provide evidence for carcinogenic effects in animal models but not in humans. Of the earliest studies in this regard was a report by Lyman and Furia [38] identifying TCS as a carcinogen in mice. Other studies on mice have been in agreement with that conclusion. For example, it was noted that chronic TCS exposure increased the incidence of liver neoplasms [12] and aggravated hepatocellular carcinoma [103]. Furthermore, TCS caused colonic inflammation and worsened colitis or tumorigenesis induced by dextran sodium sulfate [168]. These findings, were, however, not paralleled in rats, hamsters, or baboons [12, 169]. More importantly, *in vivo* human studies of TCS are scarce, and aspects related to TCS-induced oncogenesis are lacking. Consequently, whether TCS poses a carcinogenic hazard to humans is unknown and requires further investigation. Nonetheless, the interaction of TCS with human-derived cancer cells *in vitro* has recently gained considerable attention (reviewed under Therapeutic Proposals).

In light of available data (Table 5), TCS demonstrates carcinogenicity solely in mice and within a narrow range of tissues (the liver and colon), which constitutes limited evidence of carcinogenicity according to ECHA (https://echa.europa.eu/documents/10162/23036412/clp_en.pdf/58b5dc6d-ac2a-4910-9702-e9e1f5051cc5). Hence, TCS is not classifiable as a carcinogen (http://ec.europa.eu/health/scientific_committees/consumer_safety/docs/sccs_o_054.pdf). It must be noted that in case future assessment conclusively rules out TCS as a human carcinogen, caution with its use must still be exercised given the established carcinogenicity of its transformation products—dioxins, chloroform, and anilines [170].

## 7. Cellular Signaling

Adaptations to the ever-changing intracellular and surrounding environments are achieved, in large part, by effective communication. Transmission of information that carries specific instructions is executed by messengers that function in tandem within a defined pathway. Tasks, however, are usually accomplished through the sequential transduction of multiple messages along a complex, intertwining network that involves a wide assortment of mediators [171]. Hence, the participation of cell signaling cascades in the response to xenobiotics cannot be overlooked.

The use of human cell lines has provided a wealth of information particularly regarding the study of signaling molecules responsive to stressors and xenobiotics, including TCS. In H460 lung cancer cells, TCS promoted migration and invasion through focal adhesion kinase/ATP-dependent tyrosine kinase (FAK/Akt) and Ras-related C3 botulinum toxin substrate 1 (Rac1) [72]. Evidence similarly exists for the classical mitogen-activated protein kinases (MAPK) as targets of TCS. For example, proliferation of JB6 Cl 41-5a cells as induced by TCS was accompanied by activation of extracellular signal-regulated kinases 1/2 (ERK1/2), c-Jun N-terminal kinases (JNK), and p38 MAPKs, in addition to Akt [84]. Importantly, blocking either MEK1/2 or phosphoinositide 3-kinase (PI3K) significantly attenuated TCS-induced proliferation. In another study on rat neural stem cells, TCS-induced cytotoxicity and apoptosis were accompanied by activation of p38 and JNK and suppression of ERK, Akt, and PI3K [79]. This points at the involvement of these proteins in both cellular survival and death as brought about by TCS. Recently, TCS was shown to activate p38 and JNK *in vivo* as detected in the hypothalamus of Sprague-Dawley rats and *in vitro* utilizing human Nthy-ori 3-1 thyroid follicular cells [97]. In that study, TCS stimulated the thyrotropin-releasing hormone receptor through p38 MAPK, which, in turn, influenced the thyroid peroxidase (TPO) level.

In suppressing TLR signaling in whole blood leukocytes, TCS downregulated the expression of several signaling mediators, most notably, NF-$\kappa$B-inducing kinase (*Nik*) and *C-jun*, which accounted for the overall blunted inflammatory response to LPS in these cells [153]. Furthermore, suppression of *Mmp-13* expression in mouse osteoblastic osteocarcinoma cells by TCS was possibly related to its inhibition of Fos/Jun and AP-1 sequence binding in both the *Mmp-13* and *C-fos* promoters [147].

The endocrine-disrupting activity of TCS, specifically its estrogenicity, has been of great interest to researchers. Kim et al. [73] utilized BG-1 ovarian cancer cells to show that the proliferative effects of TCS were mediated through ER$\alpha$. Confirming the ER's role, the use of ICI 182,780 reversed the proliferative properties of TCS along with associated perturbations in cyclin D1, p21, and Bax expression and protein levels. Likewise, the ER is implicated in TCS-induced proliferation of MCF-7 cells and increased breast tumor mass in mice [74, 75, 172]. This was similarly indicated by TCS inhibition with ICI 182,780 or kaempferol and the stimulation of insulin-like growth factor (IGF) signaling, namely, phosphorylated insulin receptor substrate (pIRS-1), pAkt, pMEK1/2, and pERK1/2 [75]. Notably, kaempferol also inhibited TCS-induced VM7Luc4E2 cell growth [76]. These observations are in congruence with an earlier report by Huang et al. [173] describing the estrogenic activities of nanomolar concentrations of TCS in the same cells. Investigating ER-responsive genes on the transcriptional and translational levels, it was shown that TCS induced pS2 but blunted ER$\alpha$ mRNA and protein levels, the latter of which was related to elevated miR-22, miR-206, and miR-193b miRNAs.

Recent studies have also argued for the dual effect of TCS on ER signaling. For example, Henry and Fair [174] demonstrated that, when administered alone to MCF7 cells, TCS at 7 nM to 700 $\mu$M exhibits estrogenic activity but becomes antiestrogenic in the presence of E2. Along those lines, it was shown that TCS, on its own, lacked any effect on rat uterine growth, but could still potentiate the effect of ethinylestradiol (EE) [175]. In a follow-up investigation, it was reported that TCS promotes EE-induced inhibition of ER$\alpha$ and ER$\beta$ expression and when given alone does not activate ER at concentrations from 30 nM to 100 $\mu$M [176]. Furthermore, TCS diminished E2 and estrogen sulfotransferase in sheep placenta [177]. This is in contrast to the increased activity of ER$\beta$ but not ER$\alpha$ caused by a TCS-derivative mixture, which led to neurological and behavioral abnormalities in zebrafish [87]. Also, Sprague-Dawley rats given TCS showed increased uterine weight and *Calbindin-d(9*k) (CaBP-9k) expression, which was also reciprocated in pituitary GH3 cells [178]. Reversal of both anomalies by ICI 182,780 and RU 486 points at a possible estrogenic role of the antimicrobial.

Very recently, Serra et al. [179] challenged accumulating evidence of TCS estrogenicity by showing the lack of agonistic or antagonistic effect *in vivo* and *in vitro*. While up to 0.3 $\mu$M TCS did not modulate ER-dependent brain aromatase in zebrafish embryos, interference with the enzyme's activity, and with E2 activation of the enzyme observed at 1 $\mu$M, was not attributed to TCS-ER interaction. Moreover, up to 10 $\mu$M TCS lacked estrogenic effects in ER-expressing zebrafish liver cells as well as in MCF-7 cells [179]. Additionally, in a screening study of the estrogenicity of a group of endocrine-disrupting chemicals on fish species, TCS failed to significantly elicit a response in an *in vitro* ER$\alpha$ reporter gene assay [180].

In light of available evidence, the general consensus seems to indicate that the estrogenicity of TCS is contingent upon multiple factors, including concentration, species, duration of exposure, and whether TCS is administered alone or in combination with other molecules.

With regard to the androgenic properties of TCS, it was revealed that TCS interferes with testosterone- (TSN-) related transcription but promotes that dependent on androgen [181, 182]. In a recent *in vivo* study on weanling male rats, Riad et al. [104] reported that TCS, either alone or combined with butylparaben, reduced TSN, leutinizing hormone (LH), and follicle-stimulating hormone (FSH), while increased E2 was observed upon single TCS administration Also, TCS-induced proliferation and migration of LNCaP cells were significantly reduced in presence of bicalutamide, an androgen receptor (AR) antagonist [77]. These findings support a previous report by Ahn et al. [183] in which 1 $\mu$M TCS reduced E2-induced ER activation by 50% and AR in human BG1Luc4E2 ovarian adenocarcinoma cells and T47D-ARE breast cancer cells, respectively. Evidence for TCS estrogenicity was detected in MCF7 cells when [(3)H]estradiol was successfully displaced from the ER by the antimicrobial [184]. Furthermore, 10 $\mu$M TCS attenuated E2-dependent ERE-CAT reporter gene induction, while 0.1 and 1 $\mu$M TCS inhibited TSN-stimulated LTR-CAT reporter gene in both T47D cells and S115 mouse mammary tumor cells [184]. TCS was also determined to have a weak

effect on AhR in recombinant rat hepatoma (H4L1.1c4) cells. Finally, Forgacs et al. [185] showed that TCS interferes with recombinant hCG stimulation of TSN in a novel BLTK1 murine Leydig cell model. Most recently, however, no significant influence on androgen synthesis or activity by TCS was observed in Wistar rats [186].

Controversy surrounding the interaction between TCS and members of the peroxisome proliferator-activated receptors (PPARs) has gained considerable attention as of late. This has essentially stemmed from the apparent discrepancy between data obtained from humans and those from rodents. In comparing the differential modulation of TCS on PPAR$\alpha$ in HepG2 cells and mouse hepatoma Hepa1c1c7 cells, distinct responses were observed by Wu et al. [187]. Protein levels of PPAR$\alpha$ downstream target, acyl-coenzyme A oxidase, were decreased in HepG2 cells but were increased in Hepa1c1c7, which also showed higher DNA synthesis and blunted apoptosis through transforming growth factor (TGF-$\beta$). PPAR signaling was similarly identified as a target of TCS through genome-wide CRISPR-Cas9 screening in HepG2 cells [188], zebrafish [189], and *Gallus gallus* chicken embryos [190]. In the latter model, PPAR signaling members *Cyp7a1*, fatty acid-binding protein 1 (*Fabp1*), acyl-CoA synthetase long-chain family member 5 (*Acsl5*), acyl-CoA oxidase 2 (*Acox2*), and perilipin 1 (*Plin1*) were upregulated, whereas angiopoietin-like 4 (*Angptl*) was downregulated.

TCS administered to pregnant mice caused insulin resistance, hypothyroidism, diminished glucose transporter 4 (GLUT4) expression, and inhibition of Akt and mTOR phosphorylation [191, 192]. While thyroxine corrected these adversaries, PPAR$\gamma$ activator, rosiglitazone, solely reversed the decrease in Akt phosphorylation in adipose tissue and in muscle [192]. PPAR$\gamma$ is known to ameliorate mTOR suppression-induced glucose intolerance in rats [193], further underlining the far-reaching effects of TCS action.

Although TCS has been reported to promote hepatocyte proliferation in mice through PPAR [12], Yueh et al. [103] found no appreciable induction of PPAR$\alpha$ following TCS treatment. Importantly, the authors also identified constitutive androstane receptor (CAR) as a possible aggravator of TCS-induced tumorigenesis, given the halved tumor number in $Car^{-/-}$ mice compared to their $Car^{+/-}$ counterparts. TCS, as is the case with PPARs, is reported to exhibit varying affinities for CAR and pregnane X receptor (PXR) in humans and rodents. A weak agonist for human CAR, TCS was found to be a reverse agonist for rodent CAR, an agonist for human PXR, and had no effect on rodent PXR [194].

Calcium concentration within cells influences protein conformation and dynamics. Protein binding of $Ca^{2+}$, on the other hand, maintains the ion's content within a physiological range and sets forth diverse cellular activities related to gene expression, motility, secretion, and survival [195]. Beside proteins, intracellular $Ca^{2+}$ levels are modulated by a variety of stimuli, including xenobiotic exposure. Through the $Ca^{2+}$ channel ryanodine (Ry) receptor type 1 (RyR1), TCS increased cytosolic $Ca^{2+}$ dose-dependently in primary skeletal myotubes irrespective of extracellular $Ca^{2+}$ [183]. Accordingly, muscle contractility was compromised upon TCS exposure *in vitro* and *in vivo* [196]. Results from this study indicate that TCS impaired excitation-contraction coupling (ECC) in cardiac and skeletal muscles and enhanced electrically induced $Ca^{2+}$ transients in myotubes without depleting intracellular $Ca^{2+}$ and notwithstanding RyR1 blockage. TCS also efficiently blocked excitation-coupled $Ca^{2+}$ entry and interfered with the bidirectional signaling between RyR1 channels and $Ca^{2+}$ ions. Likewise, TCS compromised ECC in larval fathead minnows *Pimephales promelas*, as evidenced by altered RyR and dihydropyridine receptor (DHPR) mRNA and protein levels and weakened ligand binding to both receptors in adult muscle homogenates [197].

In rat thymocytes, TCS elevated intracellular $Ca^{2+}$ levels and opened $Ca^{2+}$-responsive $K^+$ channels, eventually leading to membrane hyperpolarization [198]. Also, TCS prevented $Ca^{2+}$-induced mitochondrial swelling in rat liver [199]. A more in-depth analysis of TCS modulation of $Ca^{2+}$ homeostasis was conducted on rat basophilic leukemia (RBL) mast cells [24]. In this cell type, TCS caused mitochondrial fission and diminished membrane potential and translocation, with compromised ATP production and elevated ROS. These changes were associated with perturbed mitochondrial and endoplasmic reticulum $Ca^{2+}$ and depleted cytosolic $Ca^{2+}$ levels following antigen stimulation. Accordingly, TCS-induced degranulation of mast cell may at least in part be attributed to $Ca^{2+}$ mobilization.

Calcium modulation by TCS has also been investigated in other organisms. In *C. reinhardtii* exposed to 14 $\mu$M TCS, increased $Ca^{2+}$ levels with oxidative stress, cell and mitochondrial membrane depolarization, compromised photosynthesis, and caspase activation were noted [90]. Importantly, chelation of intracellular $Ca^{2+}$ ions by BAPTA-AM protected the algae from TCS-induced $Ca^{2+}$ dysregulation. These observations strongly implicate $Ca^{2+}$ as a mediator of a wide array of toxic anomalies attributed to TCS.

Literature concerning the xenobiotic response to TCS has revealed important signaling pathways activated or suppressed by TCS (Table 6). Distinct outcomes exist among species and even within the same species based on experimental conditions and model under investigation. Although important milestones in TCS signaling have been achieved so far, there remains a lot to be discovered, especially in human-based systems, about the modulatory effects of TCS on cellular physiology. In particular, the response of many human cell types and tissues to TCS treatment is unknown, and identification of signaling pathways and their roles in cellular growth, metabolism, and overall function is therefore advised.

## 8. Therapeutic Proposals

The first specific action mechanism of TCS in prokaryotes was only demonstrated 20 years ago, when inhibition of fatty acid synthesis in *Escherichia coli* was noted following exposure to TCS [200, 201]. TCS irreversibly inhibited the fatty acid biosynthesis enzyme, enoyl–acyl carrier protein reductase (ACP), by mimicking its natural substrate *in vivo*.

Table 6: TCS modulation of signaling pathways.

| Model | Target | | Response |
|---|---|---|---|
| | Pathways | TCS role | |
| H460 cells | FAK/Akt | Cellular migration and invasion | Upregulated by TCS |
| | Rac1 | | Upregulated by TCS |
| JB6 Cl 41-5a cells | ERK1/2 | Cell proliferation | Upregulated by TCS |
| | JNK | | Upregulated by TCS |
| | p38 | | Upregulated by TCS |
| | Akt | | Upregulated by TCS |
| | PI3K | | Upregulated by TCS |
| Rat neural stem cells | JNK | Cytotoxicity and apoptosis | Upregulated by TCS |
| | p38 | | Upregulated by TCS |
| | ERK | | |
| | Akt | | Downregulated by TCS |
| | PI3K | | Downregulated by TCS |
| | | | Downregulated by TCS |
| Sprague-Dawley rats hypothalamus and Nthy-ori 3-1 cells | JNK | Reduced TPO; hypothyroidism | Upregulated by TCS |
| | p38 | | Upregulated by TCS |
| Whole blood leukocytes | *Nik* | Anti-inflammatory response | Downregulated by TCS |
| | *Cjun* | | Downregulated by TCS |
| Mouse osteoblastic osteocarcinoma | *Fos* | | Downregulated by TCS |
| | *Jun* | | Downregulated by TCS |
| | *Ap1* | | Downregulated by TCS |
| BG-1 | ER$\alpha$ | Cell proliferation | Upregulated by TCS |
| | ER$\alpha$* | | Sensitive to TCS |
| MCF-7 cells | pIRS-1 | | Upregulated by TCS |
| | pAKT | | Upregulated by TCS |
| | pMEK1/2 | | Upregulated by TCS |
| | pERK1/2 | | Upregulated by TCS |
| | *Er$\alpha$* | | Downregulated by TCS |
| | *Ps2* | | Upregulated by TCS |
| VM7Luc4E2 cells | ER$\alpha$ | | Downregulated by TCS |
| | pS2 | | Upregulated by TCS |
| | miR-22 | | Upregulated by TCS |
| | miR-206 | | Upregulated by TCS |
| | miR-193b | | Upregulated by TCS |
| Sheep placenta | E2 | Anti-estrogenicity | Downregulated by TCS |
| | Estrogen sulfotransferase | | Downregulated by TCS |
| BG1Luc4E2 cells | ER* | | Downregulated by TCS |
| Sprague-Dawley rats and GH3 cells | *CaBP-9* k | Estrogenicity | Upregulated by TCS |
| LNCaP | AR | Androgenicity; cell proliferation, and migration | Upregulated by TCS |
| T47D-ARE cells | AR | Anti-androgenicity | Downregulated by TCS |
| H4L1.1c4 cells | AR | Pro(anti)-androgenicity | Sensitive to TCS |
| HepG2 cells | Acyl-coenzyme A oxidase | Blunted lipid metabolism | Downregulated by TCS |
| Hepa1c1c7 cells | Acyl-coenzyme A oxidase | Enhanced lipid metabolism and DNA synthesis | Upregulated by TCS |
| | TGF-$\beta$ | Antiapoptosis | Downregulated by TCS |
| *D. rerio* | PPAR$\alpha$ | Enhanced lipid metabolism | Upregulated by TCS |
| | PPAR$\gamma$ | | Upregulated by TCS |
| *G. gallus* embryo livers | PPAR$\alpha$ | | Upregulated by TCS |

Table 6: Continued.

| Model | Target | | Response |
|---|---|---|---|
| | Pathways | TCS role | |
| ICR mice | Akt | Impaired glucose metabolism | Downregulated by TCS |
| | mTOR | | Downregulated by TCS |
| C57BL/6 mice | CAR | Tumorigenesis | Upregulated by TCS |
| HepG2 cells | CAR | Enhanced hepatic catabolism | Upregulated by TCS |
| | PXR | | Upregulated by TCS |
| Rodent FAO hepatoma cells | CAR | Reduced hepatic catabolism | Downregulated by TCS |
| Primary skeletal myotubes | $Ca^{2+}$ | Diminished muscle contractility | Upregulated by TCS |
| | RyR1 | | Upregulated by TCS |
| *P. promelas* muscle homogenates | *Ryr2* | | Sensitive to TCS |
| | *Ryr3* | | Downregulated by TCS |
| | RyR | | Downregulated by TCS |
| Rat thymocytes | $Ca^{2+}$ | Cell membrane hyperpolarization | Upregulated by TCS |
| RBL cells | $Ca^{2+}$ | Mast cell degranulation | Downregulated by TCS |
| *C. reinhardtii* | $Ca^{2+}$ | Dampened photosynthesis | Upregulated by TCS |

*TCS is anti-estrogenic in the presence of E2.

Further, a mutated or overexpressed ACP, encoded by *fabI*, was shown to confer TCS resistance in the bacterium. These findings established ACP as a specific, subcellular TCS target. Efforts have thus far revealed the susceptibility of a host of other pathogens to inhibition of fatty acid synthesis by TCS. These include *Staphylococcus aureus*, *M. tuberculosis*, *Helicobacter pylori*, *Haemophilus influenzae*, *Plasmodium falciparum*, *Toxoplasma gondii*, *Leishmania* spp., and *Trypanosoma* spp. [52, 202–208]. In humans, fatty acid synthase (FAS) is the only multienzyme complex that is responsible for the endogenous synthesis of saturated fatty acids from acetyl-CoA and malonyl-CoA [209, 210]. Although a BLAST analysis of *E. coli* FabI protein and FAS showed no homology, appreciable sequence similarities were nevertheless found with polyketide synthase and type I FAS of *M. tuberculosis* [211].

The success of cerulenin, a mycotoxin with fatty acid inhibitory action, in suppressing tumor progression *in vivo* has spawned several reports in support of fatty acid synthesis inhibition as an emerging target for chemotherapy [212]. The earliest study in this regard investigated the cytotoxicity of TCS in MCF-7 and SKBr-3 breast cancer cells [211]. It was revealed that TCS at 10-50 $\mu$M is cytotoxic and antiproliferative, induces morphological alterations, and inhibits FAS. These findings corroborate an earlier observation linking FAS inhibition with apoptotic death of breast cancer cells [211, 213, 214]. TCS was similarly found to inhibit the development of methylnitrosourea-induced breast cancer in Sprague-Dawley rats [209]. In human A-375 melanoma cells, TCS inhibited growth at 40 $\mu$M [215]. TCS was similarly found to be dose-dependently proapoptotic in prostate cancer cells, with $IC_{50}$ values as low as 4.5-7.8 $\mu$M [216]. Whereas no cytotoxicity was observed in NIH3T3 fibroblasts at concentrations up to 60 $\mu$M, values of $IC_{50}$ ranging from 0.74 to 62 $\mu$M were nonetheless observed in nonmalignant prostate cells. This suggests two things; first, that prostate cells are relatively more sensitive to TCS toxicity than fibroblasts and presumably other nonmalignant cell types, and second, that malignant prostate cells exhibit higher chemosensitivity compared to their nonmalignant counterparts. This differential susceptibility could be due to overexpressed FAS in malignant cells. However, in contrast to these reports, at concentrations up to 345 $\mu$M, TCS was found to be preferentially cytotoxic to Y79 RB cells over mouse 3T3 fibroblasts and human MIO-M1 Müller glial cells as indicated by $IC_{50}$ values, creating a large therapeutic index of 7.1 and 5.3, respectively [217]. FAS suppression, depleted fatty acid content, lipid peroxidation, and apoptotic death were noted in Y79 RB cells at the same TCS concentration range [98]. Recently, TCS at 40 $\mu$M was also shown to be effective against MiaPaCa-2 and AsPC-1 pancreatic cancer cells suppressing proliferation and eliciting apoptotic death [218]. Of note, in a related study, TCS impeded mouse preadipocyte differentiation [219]. Given the regulation of food intake by FAS, and the susceptibility of adipocyte development to TCS inhibition, it was suggested that TCS may possess anti-obesogenic properties.

The differential expression and activity of FAS in healthy and malignant tissues, where it is upregulated in the latter [220, 221], indicate a possibly high therapeutic index. The long history of human use, and the ubiquity of TCS in consumer products, coupled with encouraging *in vivo* results, cements the antimicrobial as a promising candidate for chemotherapy. As noted earlier, it must be stressed that variations in the final outcome of TCS treatment largely depend on experimental setup. Moreover, limited data from animal studies suggest that in the presence of a preexisting tumor, TCS administration seems to exacerbate the condition. This observation is concerning and indeed warrants further investigation before TCS can be invested in for clinical trials.

## 9. Conclusion

TCS is a synthetic antimicrobial with a long history of human use. At concentrations well below those present in commercial products, data from *in vitro* and *in vivo* studies have provided evidence of adverse effects on diverse molecular pathways. Most alarmingly is TCS enhancement of malignant cell proliferation *in vitro* and tumor growth *in vivo*. On the other hand, TCS has also been shown to be protective against malignant cell growth and proliferation, possibly opening the door for its use in chemotherapy. Clearly, dose and time dependence is an important factor in determining the eventual denouement of the chemical. In spite of the numerous publications dissecting the signaling pathways responsive to TCS, it is evident that a severe paucity surrounding human-based *in vivo* and *in vitro* studies still remains today. Future studies, thus, should focus on identifying signaling molecules differentially regulated by TCS and characterize their roles in toxic or protective effects in different cell types. Insights gained from such revelations will be invaluable to possibly validate targets for drug development or devise possible TCS adjuvants or inhibitors.

## Conflicts of Interest

The authors declare that there are no conflicts of interest regarding the publication of this paper.

## Acknowledgments

We thank the members of the Lee Laboratory for helpful advice and discussion during this work. This work was supported in part by the Brody Brothers Grant (BBE216102), NIH (1R15AG060373-01) to M-H.L., and the Saudi Government Graduate Scholarship (through King Saud University) to M.A.A.

## References

[1] R. Montville and D. W. Schaffner, "A meta-analysis of the published literature on the effectiveness of antimicrobial soaps," *Journal of Food Protection*, vol. 74, no. 11, pp. 1875–1882, 2011.

[2] V. Kjaerheim, A. Skaare, P. Barkvoll, and G. Rolla, "Antiplaque, antibacterial, and anti-inflammatory properties of triclosan mouthrinses in combination with zinc citrate or polyvinylmethylether maleic acid (PVM-MA) copolymer," *European Journal of Oral Sciences*, vol. 104, no. 5-6, pp. 529–534, 1996.

[3] V. Kjaerheim, S. M. Waaler, and G. Rolla, "Organic solvents and oils as vehicles for triclosan in mouthrinses: a clinical study," *Scandinavian Journal of Dental Research*, vol. 102, no. 5, pp. 306–308, 1994.

[4] A. B. Skaare, V. Kjaerheim, P. Barkvoll, and G. Rolla, "Does the nature of the solvent affect the anti-inflammatory capacity of triclosan? An experimental study," *Journal of Clinical Periodontology*, vol. 24, no. 2, pp. 124–128, 1997.

[5] V. Kjaerheim, S. M. Waaler, and G. Rolla, "Significance of choice of solvents for the clinical effect of triclosan-containing mouthrinses," *Scandinavian Journal of Dental Research*, vol. 102, no. 4, pp. 202–205, 1994.

[6] M. A. Alfhili, D. S. Yoon, T. A. Faten et al., "Non-ionic surfactants antagonize toxicity of potential phenolic endocrine-disrupting chemicals, including Triclosan in *Caenorhabditis elegans*," *Molecules and Cells*, vol. 41, no. 12, pp. 1052–1060, 2018.

[7] S. M. Waaler, G. Rölla, K. K. Skjörland, and B. Ögaard, "Effects of oral rinsing with triclosan and sodium lauryl sulfate on dental plaque formation: a pilot study," *Eropean Journal of Oral Sciences*, vol. 101, no. 4, pp. 192–195, 1993.

[8] K. Bellamy, R. Alcock, J. R. Babb, J. G. Davies, and G. A. J. Ayliffe, "A test for the assessment of 'hygienic' hand disinfection using rotavirus," *The Journal of Hospital Infection*, vol. 24, no. 3, pp. 201–210, 1993.

[9] J. Regos and H. R. Hitz, "Investigations on the mode of action of Triclosan, a broad spectrum antimicrobial agent," *Zentralblatt fur Bakteriologie, Parasitenkunde, Infektionskramkheiten und hygiene, Erste Abteilung Originale, Reihe A: Medizinische Mikrobiologie und Parasitologie*, vol. 226, no. 3, pp. 390–401, 1974.

[10] J. Regös, O. Zak, R. Solf, W. A. Vischer, and E. G. Weirich, "Antimicrobial spectrum of triclosan, a broad-spectrum antimicrobial agent for topical application. II. Comparison with some other antimicrobial agents," *Dermatologica*, vol. 158, no. 1, pp. 72–79, 1979.

[11] R. C. Petersen, "Triclosan antimicrobial polymers," *AIMS Molecular Science*, vol. 3, no. 1, pp. 88–103, 2016.

[12] J. V. Rodricks, J. A. Swenberg, J. F. Borzelleca, R. R. Maronpot, and A. M. Shipp, "Triclosan: a critical review of the experimental data and development of margins of safety for consumer products," *Critical Reviews in Toxicology*, vol. 40, no. 5, pp. 422–484, 2010.

[13] X. Chen, J. L. Nielsen, K. Furgal, Y. Liu, I. B. Lolas, and K. Bester, "Biodegradation of triclosan and formation of methyl-triclosan in activated sludge under aerobic conditions," *Chemosphere*, vol. 84, no. 4, pp. 452–456, 2011.

[14] M. Adolfsson-Erici, M. Pettersson, J. Parkkonen, and J. Sturve, "Triclosan, a commonly used bactericide found in human milk and in the aquatic environment in Sweden," *Chemosphere*, vol. 46, no. 9-10, pp. 1485–1489, 2002.

[15] T. Geens, H. Neels, and A. Covaci, "Distribution of bisphenol-A, triclosan and n-nonylphenol in human adipose tissue, liver and brain," *Chemosphere*, vol. 87, no. 7, pp. 796–802, 2012.

[16] L. Hovander, T. Malmberg, M. Athanasiadou et al., "Identification of hydroxylated PCB metabolites and other phenolic halogenated pollutants in human blood plasma," *Archives of Environmental Contamination and Toxicology*, vol. 42, no. 1, pp. 105–117, 2002.

[17] L. W. B. Olaniyan, N. Mkwetshana, and A. I. Okoh, "Triclosan in water, implications for human and environmental health," *Springerplus*, vol. 5, no. 1, p. 1639, 2016.

[18] J. Schulze, F. H. Marquardt, F. Lyman, and C. Spitzer, "Determination of free and conjugated triclosan-1 in blood by electron capture gas liquid chromatography-2," *Journal of the American Oil Chemists' Society*, vol. 52, no. 7, pp. 215–218, 1975.

[19] L. M. Weatherly and J. A. Gosse, "Triclosan exposure, transformation, and human health effects," *Journal of Toxicology and Environmental Health Part B, Critical Reviews*, vol. 20, no. 8, pp. 447–469, 2017.

[20] Q. Wu, H. Shi, C. D. Adams, T. Timmons, and Y. Ma, "Oxidative removal of selected endocrine-disruptors and pharmaceuticals in drinking water treatment systems, and identification of degradation products of triclosan," *Science of The Total Environment*, vol. 439, pp. 18–25, 2012.

[21] C. Queckenberg, J. Meins, B. Wachall et al., "Absorption, pharmacokinetics, and safety of triclosan after dermal administration," *Antimicrobial Agents and Chemotherapy*, vol. 54, no. 1, pp. 570–572, 2010.

[22] G. Sandborgh-Englund, M. Adolfsson-Erici, G. Odham, and J. Ekstrand, "Pharmacokinetics of triclosan following oral ingestion in humans," *Journal of Toxicology and Environmental Health Part A*, vol. 69, no. 20, pp. 1861–1873, 2006.

[23] S. B. Levy, "Antibacterial household products: cause for concern," *Emerging Infectious Diseases*, vol. 7, Supplement 3, pp. 512–515, 2001.

[24] L. M. Weatherly, A. J. Nelson, J. Shim et al., "Antimicrobial agent triclosan disrupts mitochondrial structure, revealed by super-resolution microscopy, and inhibits mast cell signaling via calcium modulation," *Toxicology and Applied Pharmacology*, vol. 349, pp. 39–54, 2018.

[25] J. L. Fang, M. Vanlandingham, G. G. da Costa, and F. A. Beland, "Absorption and metabolism of triclosan after application to the skin of B6C3F1 mice," *Environmental Toxicology*, vol. 31, no. 5, pp. 609–623, 2016.

[26] T. Moss, D. Howes, and F. M. Williams, "Percutaneous penetration and dermal metabolism of triclosan (2,4, 4′-trichloro-2′-hydroxydiphenyl ether)," *Food and Chemical Toxicology*, vol. 38, no. 4, pp. 361–370, 2000.

[27] E. Franz and S. Weidner-Strahl, "The effectiveness of topical antibacterials in acne: a double-blind clinical study," *The Journal of International Medical Research*, vol. 6, no. 1, pp. 72–77, 1978.

[28] T. W. Lee, J. C. Kim, and S. J. Hwang, "Hydrogel patches containing triclosan for acne treatment," *European Journal of Pharmaceutics and Biopharmaceutics*, vol. 56, no. 3, pp. 407–412, 2003.

[29] P. Kalliomaki and K. Kuokkanen, "Comparative study on the efficacy and tolerance of the ointments CGP433 and GP41′ 353 in the treatment of infectious dermatitis," *Zeitschrift für Hautkrankheiten*, vol. 54, no. 14, pp. 668–670, 1979.

[30] H. Weitgasser, C. Schindléry, and V. Macarol, "A comparative multicentre trial of halometasone/triclosan cream and betamethasone dipropionate/gentamicin sulphate cream in the treatment of infected acute eczematous dermatitis," *The Journal of International Medical Research*, vol. 11, Supplment 1, pp. 43–47, 1983.

[31] A. Aliaga, A. Castells, D. Kriznik et al., "An overview of two comparative multicentre trials with halometasone/triclosan cream in acute superficial bacterial skin infections," *The Journal of International Medical Research*, vol. 11, Supplement 1, pp. 53–57, 1983.

[32] L. Huber, "Role of Klion ointment in the treatment of crural ulcer," *Therapia Hungarica*, vol. 39, no. 3, pp. 148–150, 1991.

[33] P. Barkvoll and G. Rolla, "Triclosan protects the skin against dermatitis caused by sodium lauryl sulphate exposure," *Journal of Clinical Periodontology*, vol. 21, no. 10, pp. 717–719, 1994.

[34] A. Skaare, G. Eide, B. Herlofson, and P. Barkvoll, "The effect of toothpaste containing triclosan on oral mucosal desquamation. A model study," *Journal of Clinical Periodontology*, vol. 23, no. 12, pp. 1100–1103, 1996.

[35] V. Kjaerheim, P. Barkvoll, S. M. Waaler, and G. Rolla, "Triclosan inhibits histamine-induced inflammation in human skin," *Journal of Clinical Periodontology*, vol. 22, no. 6, pp. 423–426, 1995.

[36] P. Barkvoll and G. Rolla, "Triclosan reduces the clinical symptoms of the allergic patch test reaction (APR) elicited with 1% nickel sulphate in sensitised patients," *Journal of Clinical Periodontology*, vol. 22, no. 6, pp. 485–487, 1995.

[37] V. Kjaerheim, A. Roed, P. Brodin, and G. Rolla, "Effects of triclosan on the rat phrenic nerve-diaphragm preparation," *Journal of Clinical Periodontology*, vol. 22, no. 6, pp. 488–493, 1995.

[38] F. L. Lyman and T. Furia, "Toxicology of 2, 4, 4′-trichloro-2′-hydroxy-diphenyl ether," *IMS, Industrial Medicine and Surgery*, vol. 38, no. 2, pp. 64–71, 1969.

[39] F. L. Lyman and T. E. Furia, "Toxicology of 2,4,4′-trichloro-2′-hydroxyphenyl ether," *IMS, Industrial Medicine and Surgery*, vol. 37, no. 7, p. 546, 1968.

[40] E. Arrhenius, L. Renberg, L. Johansson, and M. A. Zetterqvist, "Disturbance of microsomal detoxication mechanisms in liver by chlorophenol pesticides," *Chemico-Biological Interactions*, vol. 18, no. 1, pp. 35–46, 1977.

[41] A. Y. K. Chow, G. H. Hirsch, and H. S. Buttar, "Nephrotoxic and hepatotoxic effects of triclosan and chlorhexidine in rats," *Toxicology and Applied Pharmacology*, vol. 42, no. 1, pp. 1–10, 1977.

[42] L. B. Russell and C. S. Montgomery, "Use of the mouse spot test to investigate the mutagenic potential of triclosan (Irgasan DP300)," *Mutation Research*, vol. 79, no. 1, pp. 7–12, 1980.

[43] T. L. Miller, D. J. Lorusso, and M. L. Deinzer, "The acute toxicity of nonachloropredioxin and 3- and 4-hydroxynonachlorodiphenyl ether in mice," *Journal of Toxicology and Environmental Health*, vol. 10, no. 4-5, pp. 699–707, 1982.

[44] T. L. Miller, D. J. Lorusso, M. L. Walsh, and M. L. Deinzer, "The acute toxicity of penta-, hexa-, and heptachlorohydroxydiphenyl ethers in mice," *Journal of Toxicology and Environmental Health*, vol. 12, no. 2-3, pp. 245–253, 1983.

[45] J. Roed-Petersen, G. Auken, and N. Hjorth, "Contact sensitivity to Irgasan DP 300," *Contact Dermatitis*, vol. 1, no. 5, pp. 293-294, 1975.

[46] B. Steinkjer and L. R. Braathen, "Contact dermatitis from triclosan (Irgasan DP 300)," *Contact Dermatitis*, vol. 18, no. 4, pp. 243-244, 1988.

[47] E. Storer, K. J. Koh, and L. Warren, "Severe contact dermatitis as a result of an antiseptic bath oil," *The Australasian Journal of Dermatology*, vol. 45, no. 1, pp. 73–75, 2004.

[48] S. Veronesi, S. M. P. de Padova, D. Vanni, and M. Melino, "Contact dermatitis to triclosan," *Contact Dermatitis*, vol. 15, no. 4, pp. 257-258, 1986.

[49] C. S. M. Wong and M. H. Beck, "Allergic contact dermatitis from triclosan in antibacterial handwashes," *Contact Dermatitis*, vol. 45, no. 5, p. 307, 2001.

[50] W. A. Vischer and J. Regös, "Antimicrobial spectrum of Triclosan, a broad-spectrum antimicrobial agent for topical application," *Zentralblatt fur Bakteriologie, Parasitenkunde, Infektionskramkheiten und hygiene, Erste Abteilung Originale, Reihe A: Medizinische Mikrobiologie und Parasitologie*, vol. 226, no. 3, pp. 376–389, 1974.

[51] P. Gilbert and A. J. McBain, "Literature-based evaluation of the potential risks associated with impregnation of medical devices and implants with triclosan," *Surgical Infections*, vol. 3, Supplement 1, pp. S55–S63, 2002.

[52] R. J. Heath, J. Li, G. E. Roland, and C. O. Rock, "Inhibition of the Staphylococcus aureus NADPH-dependent enoyl-acyl carrier protein reductase by triclosan and hexachlorophene," *The Journal of Biological Chemistry*, vol. 275, no. 7, pp. 4654–4659, 2000.

[53] J. C. Betts, A. McLaren, M. G. Lennon et al., "Signature gene expression profiles discriminate between isoniazid-, thiolactomycin-, and triclosan-treated Mycobacterium tuberculosis," *Antimicrobial Agents and Chemotherapy*, vol. 47, no. 9, pp. 2903–2913, 2003.

[54] V. B. Srinivasan, B. B. Singh, N. Priyadarshi, N. K. Chauhan, and G. Rajamohan, "Role of novel multidrug efflux pump involved in drug resistance in Klebsiella pneumoniae," *PLoS One*, vol. 9, no. 5, article e96288, 2014.

[55] N. Gou, S. Yuan, J. Lan, C. Gao, A. N. Alshawabkeh, and A. Z. Gu, "A quantitative toxicogenomics assay reveals the evolution and nature of toxicity during the transformation of environmental pollutants," *Environmental Science & Technology*, vol. 48, no. 15, pp. 8855–8863, 2014.

[56] J. Lu, M. Jin, S. H. Nguyen et al., "Non-antibiotic antimicrobial triclosan induces multiple antibiotic resistance through genetic mutation," *Environment International*, vol. 118, pp. 257–265, 2018.

[57] B. F. G. Pycke, G. Vanermen, P. Monsieurs et al., "Toxicogenomic response of *Rhodospirillum rubrum* S1H to the micropollutant triclosan," *Applied and Environmental Microbiology*, vol. 76, no. 11, pp. 3503–3513, 2010.

[58] L. M. McMurry, M. Oethinger, and S. B. Levy, "Overexpression of marA, soxS, or acrAB produces resistance to triclosan in laboratory and clinical strains of Escherichia coli," *FEMS Microbiology Letters*, vol. 166, no. 2, pp. 305–309, 1998.

[59] P. Nuonming, S. Khemthong, T. Dokpikul, R. Sukchawalit, and S. Mongkolsuk, "Characterization and regulation of AcrABR, a RND-type multidrug efflux system, in *Agrobacterium tumefaciens* C58," *Microbiological Research*, vol. 214, pp. 146–155, 2018.

[60] T. L. Miller and M. L. Deinzer, "Effects of nonachloropredioxin and other hydroxychlorodiphenyl ethers on biological membranes," *Journal of Toxicology and Environmental Health*, vol. 6, no. 1, pp. 11–25, 1980.

[61] D. J. Lorusso, T. L. Miller, and M. L. Deinzer, "Effect of hydroxychlorodiphenyl ethers (chlorinated pre-and isopredioxins) on erythrocyte membrane adenosinetriphosphatase activity," *Journal of Toxicology and Environmental Health*, vol. 8, no. 1-2, pp. 215–223, 1981.

[62] J. Villalain, C. R. Mateo, F. J. Aranda, S. Shapiro, and V. Micol, "Membranotropic effects of the antibacterial agent Triclosan," *Archives of Biochemistry and Biophysics*, vol. 390, no. 1, pp. 128–136, 2001.

[63] J. Guillén, A. Bernabeu, S. Shapiro, and J. Villalaín, "Location and orientation of Triclosan in phospholipid model membranes," *European Biophysics Journal*, vol. 33, no. 5, pp. 448–453, 2004.

[64] L. Canesi, C. Ciacci, L. C. Lorusso et al., "Effects of Triclosan on Mytilus galloprovincialis hemocyte function and digestive gland enzyme activities: possible modes of action on non target organisms," *Comparative Biochemistry and Physiology Part C: Toxicology & Pharmacology*, vol. 145, no. 3, pp. 464–472, 2007.

[65] V. Matozzo, A. Costa Devoti, and M. G. Marin, "Immunotoxic effects of triclosan in the clam Ruditapes philippinarum," *Ecotoxicology*, vol. 21, no. 1, pp. 66–74, 2012.

[66] D. S. Yoon, Y. Choi, D. S. Cha et al., "Triclosan disrupts SKN-1/Nrf2-mediated oxidative stress response in *C. elegans* and human mesenchymal stem cells," *Scientific Reports*, vol. 7, no. 1, article 12592, 2017.

[67] E. Falisse, A. S. Voisin, and F. Silvestre, "Impacts of triclosan exposure on zebrafish early-life stage: toxicity and acclimation mechanisms," *Aquatic Toxicology*, vol. 189, pp. 97–107, 2017.

[68] C. Riva, S. Cristoni, and A. Binelli, "Effects of triclosan in the freshwater mussel Dreissena polymorpha: a proteomic investigation," *Aquatic Toxicology*, vol. 118-119, pp. 62–71, 2012.

[69] H. Babich and J. P. Babich, "Sodium lauryl sulfate and triclosan: in vitro cytotoxicity studies with gingival cells," *Toxicology Letters*, vol. 91, no. 3, pp. 189–196, 1997.

[70] H. L. Zuckerbraun, H. Babich, R. May, and M. C. Sinensky, "Triclosan: cytotoxicity, mode of action, and induction of apoptosis in human gingival cells in vitro," *European Journal of Oral Sciences*, vol. 106, no. 2, Part 1, pp. 628–636, 1998.

[71] E. Honkisz, D. Zieba-Przybylska, and A. K. Wojtowicz, "The effect of triclosan on hormone secretion and viability of human choriocarcinoma JEG-3 cells," *Reproductive Toxicology*, vol. 34, no. 3, pp. 385–392, 2012.

[72] T. Winitthana, S. Lawanprasert, and P. Chanvorachote, "Triclosan potentiates epithelial-to-mesenchymal transition in anoikis-resistant human lung cancer cells," *PLoS One*, vol. 9, no. 10, article e110851, 2014.

[73] Y. S. Kim, H. W. Seo, M. H. Lee, D. K. Kim, H. Jeon, and D. S. Cha, "Protocatechuic acid extends lifespan and increases stress resistance in Caenorhabditis elegans," *Archives of Pharmacal Research*, vol. 37, no. 2, pp. 245–252, 2014.

[74] H. R. Lee, K. A. Hwang, K. H. Nam, H. C. Kim, and K. C. Choi, "Progression of breast cancer cells was enhanced by endocrine-disrupting chemicals, triclosan and octylphenol, via an estrogen receptor-dependent signaling pathway in cellular and mouse xenograft models," *Chemical Research in Toxicology*, vol. 27, no. 5, pp. 834–842, 2014.

[75] S. H. Kim, K. A. Hwang, and K. C. Choi, "Treatment with kaempferol suppresses breast cancer cell growth caused by estrogen and triclosan in cellular and xenograft breast cancer models," *The Journal of Nutritional Biochemistry*, vol. 28, pp. 70–82, 2016.

[76] G. A. Lee, K. C. Choi, and K. A. Hwang, "Treatment with phytoestrogens reversed triclosan and bisphenol A-induced anti-apoptosis in breast cancer cells," *Biomolecules & Therapeutics*, vol. 26, no. 5, pp. 503–511, 2018.

[77] S. H. Kim, K. A. Hwang, S. M. Shim, and K. C. Choi, "Growth and migration of LNCaP prostate cancer cells are promoted by triclosan and benzophenone-1 via an androgen receptor signaling pathway," *Environmental Toxicology and Pharmacology*, vol. 39, no. 2, pp. 568–576, 2015.

[78] N. Zhang, W. Wang, W. Li et al., "Inhibition of 11$\beta$-HSD2 expression by triclosan via induction of apoptosis in human placental syncytiotrophoblasts," *The Journal of Clinical Endocrinology and Metabolism*, vol. 100, no. 4, pp. E542–E549, 2015.

[79] B. K. Park, E. L. T. Gonzales, S. M. Yang, M. Bang, C. S. Choi, and C. Y. Shin, "Effects of triclosan on neural stem cell viability and survival," *Biomolecules & Therapeutics*, vol. 24, no. 1, pp. 99–107, 2016.

[80] K. A. Szychowski, A. M. Sitarz, and A. K. Wojtowicz, "Triclosan induces Fas receptor-dependent apoptosis in mouse neocortical neurons in vitro," *Neuroscience*, vol. 284, pp. 192–201, 2015.

[81] K. A. Szychowski, A. Wnuk, M. Kajta, and A. K. Wojtowicz, "Triclosan activates aryl hydrocarbon receptor (AhR)-dependent apoptosis and affects Cyp1a1 and Cyp1b1 expression in mouse neocortical neurons," *Environmental Research*, vol. 151, pp. 106–114, 2016.

[82] K. A. Szychowski, A. Wnuk, J. Rzemieniec, M. Kajta, T. Leszczyńska, and A. K. Wójtowicz, "Triclosan-evoked neurotoxicity involves NMDAR subunits with the specific role of GluN2A in caspase-3-dependent apoptosis," *Molecular Neurobiology*, vol. 56, no. 1, pp. 1–12, 2019.

[83] J. T. Kwon, Y. S. Yang, M. S. Kang et al., "Pulmonary toxicity screening of triclosan in rats after intratracheal instillation," *The Journal of Toxicological Sciences*, vol. 38, no. 3, pp. 471–475, 2013.

[84] Y. Wu, F. A. Beland, S. Chen, and J. L. Fang, "Extracellular signal-regulated kinases 1/2 and Akt contribute to triclosan-stimulated proliferation of JB6 Cl 41-5a cells," *Archives of Toxicology*, vol. 89, no. 8, pp. 1297–1311, 2015.

[85] X. Chen, B. Xu, X. Han et al., "The effects of triclosan on pluripotency factors and development of mouse embryonic stem cells and zebrafish," *Archives of Toxicology*, vol. 89, no. 4, pp. 635–646, 2015.

[86] J. Kim, H. Oh, B. Ryu et al., "Triclosan affects axon formation in the neural development stages of zebrafish embryos (Danio rerio)," *Environmental Pollution*, vol. 236, pp. 304–312, 2018.

[87] J. Liu, L. Sun, H. Zhang et al., "Response mechanisms to joint exposure of triclosan and its chlorinated derivatives on zebrafish (*Danio rerio*) behavior," *Chemosphere*, vol. 193, pp. 820–832, 2018.

[88] A. Binelli, D. Cogni, M. Parolini, C. Riva, and A. Provini, "Cytotoxic and genotoxic effects of *in vitro* exposure to triclosan and trimethoprim on zebra mussel (*Dreissena polymorpha*) hemocytes," *Comparative Biochemistry and Physiology Part C: Toxicology & Pharmacology*, vol. 150, no. 1, pp. 50–56, 2009.

[89] A. Binelli, D. Cogni, M. Parolini, C. Riva, and A. Provini, "*In vivo* experiments for the evaluation of genotoxic and cytotoxic effects of Triclosan in Zebra mussel hemocytes," *Aquatic Toxicology*, vol. 91, no. 3, pp. 238–244, 2009.

[90] M. Gonzalez-Pleiter, C. Rioboo, M. Reguera et al., "Calcium mediates the cellular response of *Chlamydomonas reinhardtii* to the emerging aquatic pollutant Triclosan," *Aquatic Toxicology*, vol. 186, pp. 50–66, 2017.

[91] E. Movahed, G. M. Y. Tan, K. Munusamy et al., "Triclosan demonstrates synergic effect with amphotericin B and fluconazole and induces apoptosis-like cell death in Cryptococcus neoformans," *Frontiers in Microbiology*, vol. 7, p. 360, 2016.

[92] D. J. Watkins, K. K. Ferguson, L. V. Anzalota Del Toro, A. N. Alshawabkeh, J. F. Cordero, and J. D. Meeker, "Associations between urinary phenol and paraben concentrations and markers of oxidative stress and inflammation among pregnant women in Puerto Rico," *International Journal of Hygiene and Environmental Health*, vol. 218, no. 2, pp. 212–219, 2015.

[93] Y. Lv, C. Rui, Y. Dai et al., "Exposure of children to BPA through dust and the association of urinary BPA and triclosan with oxidative stress in Guangzhou, China," *Environmental Science: Processes & Impacts*, vol. 18, no. 12, pp. 1492–1499, 2016.

[94] B. A. Rocha, A. G. Asimakopoulos, M. Honda et al., "Advanced data mining approaches in the assessment of urinary concentrations of bisphenols, chlorophenols, parabens and benzophenones in Brazilian children and their association to DNA damage," *Environment International*, vol. 116, pp. 269–277, 2018.

[95] A. P. Iyer, J. Xue, M. Honda et al., "Urinary levels of triclosan and triclocarban in several Asian countries, Greece and the USA: association with oxidative stress," *Environmental Research*, vol. 160, pp. 91–96, 2018.

[96] B. Bukowska, P. Wieteska, M. Kwiatkowska, P. Sicinska, and J. Michalowicz, "Evaluation of the effect of 2,4-dichlorophenol on oxidative parameters and viability of human blood mononuclear cells (in vitro)," *Human & Experimental Toxicology*, vol. 35, no. 7, pp. 775–784, 2016.

[97] P. Zhang, M. Yang, L. Zeng, and C. Liu, "P38/TRHr-dependent regulation of TPO in thyroid cells contributes to the hypothyroidism of triclosan-treated rats," *Cellular Physiology and Biochemistry*, vol. 45, no. 4, pp. 1303–1315, 2018.

[98] S. Vandhana, K. Coral, U. Jayanthi, P. R. Deepa, and S. Krishnakumar, "Biochemical changes accompanying apoptotic cell death in retinoblastoma cancer cells treated with lipogenic enzyme inhibitors," *Biochimica et Biophysica Acta (BBA) - Molecular and Cell Biology of Lipids*, vol. 1831, no. 9, pp. 1458–1466, 2013.

[99] M. Battino, M. S. Ferreiro, D. Fattorini, and P. Bullon, "In vitro antioxidant activities of mouthrinses and their components," *Journal of Clinical Periodontology*, vol. 29, no. 5, pp. 462–467, 2002.

[100] C. Ajao, M. A. Andersson, V. V. Teplova et al., "Mitochondrial toxicity of triclosan on mammalian cells," *Toxicology Reports*, vol. 2, pp. 624–637, 2015.

[101] L. M. Weatherly, J. Shim, H. N. Hashmi, R. H. Kennedy, S. T. Hess, and J. A. Gosse, "Antimicrobial agent triclosan is a proton ionophore uncoupler of mitochondria in living rat and human mast cells and in primary human keratinocytes," *Journal of Applied Toxicology*, vol. 36, no. 6, pp. 777–789, 2016.

[102] I. Tamura, Y. Kanbara, M. Saito et al., "Triclosan, an antibacterial agent, increases intracellular $Zn^{2+}$ concentration in rat thymocytes: its relation to oxidative stress," *Chemosphere*, vol. 86, no. 1, pp. 70–75, 2012.

[103] M. F. Yueh, K. Taniguchi, S. Chen et al., "The commonly used antimicrobial additive triclosan is a liver tumor promoter," *Proceedings of the National Academy of Sciences of the United States of America*, vol. 111, no. 48, pp. 17200–17205, 2014.

[104] M. A. Riad, M. M. Abd-Rabo, S. A. Abd El Aziz, A. M. El Behairy, and M. M. Badawy, "Reproductive toxic impact of subchronic treatment with combined butylparaben and triclosan in weanling male rats," *Journal of Biochemical and Molecular Toxicology*, vol. 32, no. 3, article e22037, 2018.

[105] A. T. Mohammed, A. A.-R. Mohamed, and H. Ali, "Pulmonary apoptotic and oxidative damaging effects of Triclosan alone or in combination with fluoride in Sprague Dawley rats," *Acta Histochemica*, vol. 119, no. 4, pp. 357–363, 2017.

[106] Z. Wang, X. Li, and J. E. Klaunig, "Investigation of the mechanism of triclosan induced mouse liver tumors," *Regulatory Toxicology and Pharmacology*, vol. 86, pp. 137–147, 2017.

[107] K. A. Lenz, C. Pattison, and H. Ma, "Triclosan (TCS) and triclocarban (TCC) induce systemic toxic effects in a model organism the nematode Caenorhabditis elegans," *Environmental Pollution*, vol. 231, Part 1, pp. 462–470, 2017.

[108] D. Lin, Q. Zhou, X. Xie, and Y. Liu, "Potential biochemical and genetic toxicity of triclosan as an emerging pollutant on earthworms (*Eisenia fetida*)," *Chemosphere*, vol. 81, no. 10, pp. 1328–1333, 2010.

[109] D. Lin, X. Xie, Q. Zhou, and Y. Liu, "Biochemical and genotoxic effect of triclosan on earthworms (*Eisenia fetida*) using contact and soil tests," *Environmental Toxicology*, vol. 27, no. 7, pp. 385–392, 2012.

[110] X. Wang, Z. Liu, W. Wang et al., "Assessment of toxic effects of triclosan on the terrestrial snail (*Achatina fulica*)," *Chemosphere*, vol. 108, pp. 225–230, 2014.

[111] Z. Zhou, J. Yang, and K. M. Chan, "Toxic effects of triclosan on a zebrafish (*Danio rerio*) liver cell line, ZFL," *Aquatic Toxicology*, vol. 191, pp. 175–188, 2017.

[112] Y. Peng, Y. Luo, X. P. Nie, W. Liao, Y. F. Yang, and G. G. Ying, "Toxic effects of triclosan on the detoxification system and breeding of *Daphnia magna*," *Ecotoxicology*, vol. 22, no. 9, pp. 1384–1394, 2013.

[113] V. Kovacevic, A. J. Simpson, and M. J. Simpson, "(1)H NMR-based metabolomics of Daphnia magna responses after sublethal exposure to triclosan, carbamazepine and ibuprofen," *Comparative Biochemistry and Physiology Part D, Genomics & Proteomics*, vol. 19, pp. 199–210, 2016.

[114] H. I. Falfushynska, L. L. Gnatyshyna, O. Y. Osadchuk et al., "Diversity of the molecular responses to separate wastewater effluents in freshwater mussels," *Comparative Biochemistry and Physiology Part C: Toxicology & Pharmacology*, vol. 164, pp. 51–58, 2014.

[115] J. C. Park, J. Han, M. C. Lee, J. S. Seo, and J. S. Lee, "Effects of triclosan (TCS) on fecundity, the antioxidant system, and oxidative stress-mediated gene expression in the copepod *Tigriopus japonicus*," *Aquatic Toxicology*, vol. 189, pp. 16–24, 2017.

[116] P. Ku, X. Wu, X. Nie et al., "Effects of triclosan on the detoxification system in the yellow catfish (Pelteobagrus fulvidraco): expressions of CYP and GST genes and corresponding enzyme activity in phase I, II and antioxidant system," *Comparative Biochemistry and Physiology Part C: Toxicology & Pharmacology*, vol. 166, pp. 105–114, 2014.

[117] P. Banerjee, T. K. Dey, S. Sarkar, S. Swarnakar, A. Mukhopadhyay, and S. Ghosh, "Treatment of cosmetic effluent in different configurations of ceramic UF membrane based bioreactor: toxicity evaluation of the untreated and treated wastewater using catfish (Heteropneustes fossilis)," *Chemosphere*, vol. 146, pp. 133–144, 2016.

[118] F. Wang, R. Xu, F. Zheng, and H. Liu, "Effects of triclosan on acute toxicity, genetic toxicity and oxidative stress in goldfish (*Carassius auratus*)," *Experimental Animals*, vol. 67, no. 2, pp. 219–227, 2018.

[119] C. Li, R. Qu, J. Chen et al., "The pH-dependent toxicity of triclosan to five aquatic organisms (*Daphnia magna, Photobacterium phosphoreum, Danio rerio, Limnodrilus hoffmeisteri, and Carassius auratus*)," *Environmental Science and Pollution Research International*, vol. 25, no. 10, pp. 9636–9646, 2018.

[120] J. Han, E. J. Won, U. K. Hwang, I. C. Kim, J. H. Yim, and J. S. Lee, "Triclosan (TCS) and Triclocarban (TCC) cause lifespan reduction and reproductive impairment through oxidative stress-mediated expression of the defensome in the monogonont rotifer (*Brachionus koreanus*)," *Comparative Biochemistry and Physiology Part C: Toxicology & Pharmacology*, vol. 185-186, pp. 131–137, 2016.

[121] L. Chai, A. Chen, P. Luo, H. Zhao, and H. Wang, "Histopathological changes and lipid metabolism in the liver of Bufo gargarizans tadpoles exposed to Triclosan," *Chemosphere*, vol. 182, pp. 255–266, 2017.

[122] D. Martins, M. S. Monteiro, A. M. V. M. Soares, and C. Quintaneiro, "Effects of 4-MBC and triclosan in embryos of the frog Pelophylax perezi," *Chemosphere*, vol. 178, pp. 325–332, 2017.

[123] M. Sendra, M. G. Pintado-Herrera, G. V. Aguirre-Martinez et al., "Are the TiO2 NPs a "Trojan horse" for personal care products (PCPs) in the clam Ruditapes philippinarum?," *Chemosphere*, vol. 185, pp. 192–204, 2017.

[124] E. Capkin, T. Ozcelep, S. Kayis, and I. Altinok, "Antimicrobial agents, triclosan, chloroxylenol, methylisothiazolinone and borax, used in cleaning had genotoxic and histopathologic effects on rainbow trout," *Chemosphere*, vol. 182, pp. 720–729, 2017.

[125] A. C. Almeida, T. Gomes, K. Langford, K. V. Thomas, and K. E. Tollefsen, "Oxidative stress in the algae *Chlamydomonas reinhardtii* exposed to biocides," *Aquatic Toxicology*, vol. 189, pp. 50–59, 2017.

[126] C. G. Pan, F. J. Peng, W. J. Shi, L. X. Hu, X. D. Wei, and G. G. Ying, "Triclosan-induced transcriptional and biochemical alterations in the freshwater green algae Chlamydomonas reinhardtii," *Ecotoxicology and Environmental Safety*, vol. 148, pp. 393–401, 2018.

[127] J. Hurtado-Gallego, K. Martin-Betancor, I. Rodea-Palomares, F. Leganes, R. Rosal, and F. Fernandez-Pinas, "Two novel cyanobacterial bioluminescent whole-cell bioreporters based on superoxide dismutases MnSod and FeSod to detect superoxide anion," *Chemosphere*, vol. 201, pp. 772–779, 2018.

[128] O. Culic, V. Erakovic, and M. J. Parnham, "Anti-inflammatory effects of macrolide antibiotics," *European Journal of Pharmacology*, vol. 429, no. 1-3, pp. 209–229, 2001.

[129] Y. Iino, M. Toriyama, Y. Natori, K. Kudo, and A. Yuo, "Erythromycin inhibition of lipopolysaccharide-stimulated tumor necrosis factor alpha production by human monocytes in vitro," *The Annals of Otology, Rhinology & Laryngology. Supplement*, vol. 101, 10 Supplement, pp. 16–20, 1992.

[130] O. M. Korzeniowski, "Effects of antibiotics on the mammalian immune system," *Infectious Disease Clinics of North America*, vol. 3, no. 3, pp. 469–478, 1989.

[131] S. M. Uriarte, R. E. Molestina, R. D. Miller et al., "Effects of fluoroquinolones on the migration of human phagocytes through Chlamydia pneumoniae-infected and tumor necrosis factor alpha-stimulated endothelial cells," *Antimicrobial Agents and Chemotherapy*, vol. 48, no. 7, pp. 2538–2543, 2004.

[132] B. Van Vlem, R. Vanholder, P. De Paepe, S. Ringoir, and D. Vogelaers, "Immunomodulating effects of antibiotics: literature review," *Infection*, vol. 24, no. 4, pp. 275–291, 1996.

[133] A. Gaffar, D. Scherl, J. Afflitto, and E. J. Coleman, "The effect of triclosan on mediators of gingival inflammation," *Journal of Clinical Periodontology*, vol. 22, no. 6, pp. 480–484, 1995.

[134] T. Modéer, A. Bengisson, and G. Rölla, "Triclosan reduces prostaglandin biosynthesis in human gingival fibroblasts challenged with interleukin-1 in vitro," *Journal of Clinical Periodontology*, vol. 23, no. 10, pp. 927–933, 1996.

[135] A. B. Skaare, G. Rolla, and P. Barkvoll, "The influence of triclosan, zinc or propylene glycol on oral mucosa exposed to sodium lauryl sulphate," *European Journal of Oral Sciences*, vol. 105, no. 5, Part 2, pp. 527–533, 1997.

[136] T. M. Hernandez-Richter, M. W. Wichmann, W. Schrodl, M. K. Angele, K. Heinritzi, and F. W. Schildberg, "The acute phase response following implantation of triclosan-bonded vascular prostheses," *Clinical and Experimental Medicine*, vol. 1, no. 1, pp. 35–41, 2001.

[137] S. Kumar, "Little difference between triclosan and stannous fluoride dentifrices on gingival inflammation," *Evidence-Based Dentistry*, vol. 16, no. 1, pp. 13-14, 2015.

[138] D. K. Suresh, K. L. Vandana, and D. S. Mehta, "Intracrevicular application of 0.3% Flurbiprofen gel and 0.3% Triclosan gel as anti inflammatory agent. A comparative clinical study," *Indian Journal of Dental Research*, vol. 12, no. 2, pp. 105–112, 2001.

[139] F. V. Ribeiro, M. Z. Casati, R. C. Casarin et al., "Impact of a triclosan-containing toothpaste during the progression of experimental peri-implant mucositis: clinical parameters and local pattern of osteo-immunoinflammatory mediators in peri-implant fluid," *Journal of Periodontology*, vol. 89, no. 2, pp. 203–212, 2018.

[140] M. Mustafa, M. Bakhiet, B. Wondimu, and T. Modeer, "Effect of triclosan on interferon-gamma production and major histocompatibility complex class II expression in human gingival fibroblasts," *Journal of Clinical Periodontology*, vol. 27, no. 10, pp. 733–737, 2000.

[141] M. Mustafa, B. Wondimu, M. Ibrahim, and T. Modeer, "Effect of triclosan on interleukin-1beta production in human gingival fibroblasts challenged with tumor necrosis factor alpha," *European Journal of Oral Sciences*, vol. 106, no. 2, Part 1, pp. 637–643, 1998.

[142] M. Mustafa, B. Wondimu, T. Yucel-Lindberg, A. T. Kats-Hallstrom, A. S. Jonsson, and T. Modeer, "Triclosan reduces microsomal prostaglandin E synthase-1 expression in human gingival fibroblasts," *Journal of Clinical Periodontology*, vol. 32, no. 1, pp. 6–11, 2005.

[143] M. Mustafa, B. Wondimu, K. Hultenby, T. Yucel-Lindberg, and T. Modeer, "Uptake, distribution and release of 14C-triclosan in human gingival fibroblasts," *Journal of Pharmaceutical Sciences*, vol. 92, no. 8, pp. 1648–1653, 2003.

[144] M. A. Wallet, N. L. Calderon, T. R. Alonso et al., "Triclosan alters antimicrobial and inflammatory responses of epithelial cells," *Oral Diseases*, vol. 19, no. 3, pp. 296–302, 2013.

[145] K. G. Neiva, N. L. Calderon, T. R. Alonso, F. Panagakos, and S. M. Wallet, "Type 1 diabetes-associated TLR responsiveness of oral epithelial cells," *Journal of Dental Research*, vol. 93, no. 2, pp. 169–174, 2014.

[146] N. B. Marshall, E. Lukomska, A. P. Nayak, C. M. Long, J. M. Hettick, and S. E. Anderson, "Topical application of the antimicrobial chemical triclosan induces immunomodulatory responses through the S100A8/A9-TLR4 pathway," *Journal of Immunotoxicology*, vol. 14, no. 1, pp. 50–59, 2017.

[147] V. M. Barnes, T. Xu, E. Shimizu et al., "Triclosan blocks MMP-13 expression in hormone-stimulated osteoblasts," *Journal of Periodontology*, vol. 84, no. 11, pp. 1–9, 2013.

[148] B. A. Pancer, D. Kott, J. V. Sugai et al., "Effects of triclosan on host response and microbial biomarkers during experimental gingivitis," *Journal of Clinical Periodontology*, vol. 43, no. 5, pp. 435–444, 2016.

[149] M. P. Cullinan, J. E. Palmer, M. J. Faddy et al., "The influence of triclosan on biomarkers of cardiovascular risk in patients in the Cardiovascular and Periodontal Study (CAPS): a randomized controlled trial," *Journal of Periodontology*, vol. 86, no. 7, pp. 847–855, 2015.

[150] S. Hessam, M. Sand, N. M. Meier, T. Gambichler, L. Scholl, and F. G. Bechara, "Combination of oral zinc gluconate and topical triclosan: an anti-inflammatory treatment modality for initial hidradenitis suppurativa," *Journal of Dermatological Science*, vol. 84, no. 2, pp. 197–202, 2016.

[151] P. A. Cadieux, B. H. Chew, B. E. Knudsen et al., "Triclosan loaded ureteral stents decrease proteus mirabilis 296 infection in a rabbit urinary tract infection model," *The Journal of Urology*, vol. 175, no. 6, pp. 2331–2335, 2006.

[152] C. N. Elwood, B. H. Chew, S. Seney, J. Jass, J. D. Denstedt, and P. A. Cadieux, "Triclosan inhibits uropathogenic Escherichia coli-stimulated tumor necrosis factor-alpha secretion in T24 bladder cells in vitro," *Journal of Endourology*, vol. 21, no. 10, pp. 1217–1222, 2007.

[153] S. P. Barros, S. Wirojchanasak, D. A. Barrow, F. S. Panagakos, W. Devizio, and S. Offenbacher, "Triclosan inhibition of acute and chronic inflammatory gene pathways," *Journal of Clinical Periodontology*, vol. 37, no. 5, pp. 412–418, 2010.

[154] F. Udoji, T. Martin, R. Etherton, and M. M. Whalen, "Immunosuppressive effects of triclosan, nonylphenol, and DDT on human natural killer cells *in vitro*," *Journal of Immunotoxicology*, vol. 7, no. 3, pp. 205–212, 2010.

[155] L. Pavez, N. Tobar, C. Chacon et al., "Chitosan-triclosan particles modulate inflammatory signaling in gingival fibroblasts," *Journal of Periodontal Research*, vol. 53, no. 2, pp. 232–239, 2018.

[156] S. Sharma, T. N. C. Ramya, A. Surolia, and N. Surolia, "Triclosan as a systemic antibacterial agent in a mouse model of acute bacterial challenge," *Antimicrobial Agents and Chemotherapy*, vol. 47, no. 12, pp. 3859–3866, 2003.

[157] H. Yang, W. Wang, K. A. Romano et al., "A common antimicrobial additive increases colonic inflammation and colitis-associated colon tumorigenesis in mice," *Science Translational Medicine*, vol. 10, no. 443, article eaan4116, 2018.

[158] A. Kanetoshi, E. Katsura, H. Ogawa, T. Ohyama, H. Kaneshima, and T. Miura, "Acute toxicity, percutaneous absorption and effects on hepatic mixed function oxidase activities of 2,4,4′-trichloro-2′-hydroxydiphenyl ether (Irgasan DP300) and its chlorinated derivatives," *Archives of Environmental Contamination and Toxicology*, vol. 23, no. 1, pp. 91–98, 1992.

[159] H. Ma, L. Zheng, Y. Li et al., "Triclosan reduces the levels of global DNA methylation in HepG2 cells," *Chemosphere*, vol. 90, no. 3, pp. 1023–1029, 2013.

[160] F. Rodrigues, M. Lehmann, V. S. do Amaral, M. L. Reguly, and H. H. R. de Andrade, "Genotoxicity of three mouthwash products, Cepacol®, Periogard®, and Plax®, in the Drosophila wing-spot test," *Environmental and Molecular Mutagenesis*, vol. 48, no. 8, pp. 644–649, 2007.

[161] F. Chevillot, M. Guyot, M. Desrosiers et al., "Accumulation and sublethal effects of triclosan and its transformation product methyl-triclosan in the earthworm Eisenia andrei exposed to environmental concentrations in an artificial soil,"

*Environmental Toxicology and Chemistry*, vol. 37, no. 7, pp. 1940–1948, 2018.

[162] P. Martinez-Paz, M. Morales, J. L. Martinez-Guitarte, and G. Morcillo, "Genotoxic effects of environmental endocrine disruptors on the aquatic insect Chironomus riparius evaluated using the comet assay," *Mutation Research*, vol. 758, no. 1-2, pp. 41–47, 2013.

[163] A. R. R. Silva, D. N. Cardoso, A. Cruz et al., "Ecotoxicity and genotoxicity of a binary combination of triclosan and carbendazim to *Daphnia magna*," *Ecotoxicology and Environmental Safety*, vol. 115, pp. 279–290, 2015.

[164] X. Xu, Y. Lu, D. Zhang et al., "Toxic assessment of triclosan and triclocarban on Artemia salina," *Bulletin of Environmental Contamination and Toxicology*, vol. 95, no. 6, pp. 728–733, 2015.

[165] L. Gao, T. Yuan, P. Cheng et al., "Effects of triclosan and triclocarban on the growth inhibition, cell viability, genotoxicity and multixenobiotic resistance responses of Tetrahymena thermophila," *Chemosphere*, vol. 139, pp. 434–440, 2015.

[166] O. Herrero, J. M. Perez Martin, P. Fernandez Freire, L. Carvajal Lopez, A. Peropadre, and M. J. Hazen, "Toxicological evaluation of three contaminants of emerging concern by use of the Allium cepa test," *Mutation Research*, vol. 743, no. 1-2, pp. 20–24, 2012.

[167] T. Y. Doktorova, G. Ates, M. Vinken, T. Vanhaecke, and V. Rogiers, "Way forward in case of a false positive in vitro genotoxicity result for a cosmetic substance?," *Toxicology In Vitro*, vol. 28, no. 1, pp. 54–59, 2014.

[168] K. Z. Sanidad, H. Xiao, and G. Zhang, "Triclosan, a common antimicrobial ingredient, on gut microbiota and gut health," *Gut Microbes*, pp. 1–4, 2018.

[169] H. N. Bhargava and P. A. Leonard, "Triclosan: applications and safety," *American Journal of Infection Control*, vol. 24, no. 3, pp. 209–218, 1996.

[170] R. U. Halden, A. E. Lindeman, A. E. Aiello et al., "The Florence statement on triclosan and triclocarban," *Environmental Health Perspectives*, vol. 125, no. 6, article 064501, 2017.

[171] I. J. Uings and S. N. Farrow, "Cell receptors and cell signalling," *Molecular Pathology*, vol. 53, no. 6, pp. 295–299, 2000.

[172] G. A. Lee, K. A. Hwang, and K. C. Choi, "Inhibitory effects of 3,3′-diindolylmethane on epithelial-mesenchymal transition induced by endocrine disrupting chemicals in cellular and xenograft mouse models of breast cancer," *Food and Chemical Toxicology*, vol. 109, Part 1, pp. 284–295, 2017.

[173] H. Huang, G. Du, W. Zhang et al., "The in vitro estrogenic activities of triclosan and triclocarban," *Journal of Applied Toxicology*, vol. 34, no. 9, pp. 1060–1067, 2014.

[174] N. D. Henry and P. A. Fair, "Comparison of in vitro cytotoxicity, estrogenicity and anti-estrogenicity of triclosan, perfluorooctane sulfonate and perfluorooctanoic acid," *Journal of Applied Toxicology*, vol. 33, no. 4, pp. 265–272, 2013.

[175] T. E. Stoker, E. K. Gibson, and L. M. Zorrilla, "Triclosan exposure modulates estrogen-dependent responses in the female Wistar rat," *Toxicological Sciences*, vol. 117, no. 1, pp. 45–53, 2010.

[176] G. W. Louis, D. R. Hallinger, and T. E. Stoker, "The effect of triclosan on the uterotrophic response to extended doses of ethinyl estradiol in the weanling rat," *Reproductive Toxicology*, vol. 36, pp. 71–77, 2013.

[177] M. O. James, W. Li, D. P. Summerlot, L. Rowland-Faux, and C. E. Wood, "Triclosan is a potent inhibitor of estradiol and estrone sulfonation in sheep placenta," *Environment International*, vol. 36, no. 8, pp. 942–949, 2010.

[178] E. M. Jung, B. S. An, K. C. Choi, and E. B. Jeung, "Potential estrogenic activity of triclosan in the uterus of immature rats and rat pituitary GH3 cells," *Toxicology Letters*, vol. 208, no. 2, pp. 142–148, 2012.

[179] H. Serra, F. Brion, J. M. Porcher, H. Budzinski, and S. Ait-Aissa, "Triclosan lacks anti-estrogenic effects in zebrafish cells but modulates estrogen response in zebrafish embryos," *International Journal of Molecular Sciences*, vol. 19, no. 4, p. 1175, 2018.

[180] S. Miyagawa, A. Lange, I. Hirakawa et al., "Differing species responsiveness of estrogenic contaminants in fish is conferred by the ligand binding domain of the estrogen receptor," *Environmental Science & Technology*, vol. 48, no. 9, pp. 5254–5263, 2014.

[181] J. Chen, K. C. Ahn, N. A. Gee, S. J. Gee, B. D. Hammock, and B. L. Lasley, "Antiandrogenic properties of parabens and other phenolic containing small molecules in personal care products," *Toxicology and Applied Pharmacology*, vol. 221, no. 3, pp. 278–284, 2007.

[182] V. Christen, P. Crettaz, A. Oberli-Schrammli, and K. Fent, "Some flame retardants and the antimicrobials triclosan and triclocarban enhance the androgenic activity in vitro," *Chemosphere*, vol. 81, no. 10, pp. 1245–1252, 2010.

[183] K. C. Ahn, B. Zhao, J. Chen et al., "*In vitro* biologic activities of the antimicrobials triclocarban, its analogs, and triclosan in bioassay screens: receptor-based bioassay screens," *Environmental Health Perspectives*, vol. 116, no. 9, pp. 1203–1210, 2008.

[184] R. H. Gee, A. Charles, N. Taylor, and P. D. Darbre, "Oestrogenic and androgenic activity of triclosan in breast cancer cells," *Journal of Applied Toxicology*, vol. 28, no. 1, pp. 78–91, 2008.

[185] A. L. Forgacs, Q. Ding, R. G. Jaremba, I. T. Huhtaniemi, N. A. Rahman, and T. R. Zacharewski, "BLTK1 murine Leydig cells: a novel steroidogenic model for evaluating the effects of reproductive and developmental toxicants," *Toxicological Sciences*, vol. 127, no. 2, pp. 391–402, 2012.

[186] W. T. Farmer, G. W. Louis, A. R. Buckalew, D. R. Hallinger, and T. E. Stoker, "Evaluation of triclosan in the Hershberger and H295R steroidogenesis assays," *Toxicology Letters*, vol. 291, pp. 194–199, 2018.

[187] Y. Wu, Q. Wu, F. A. Beland, P. Ge, M. G. Manjanatha, and J. L. Fang, "Differential effects of triclosan on the activation of mouse and human peroxisome proliferator-activated receptor alpha," *Toxicology Letters*, vol. 231, no. 1, pp. 17–28, 2014.

[188] P. Xia, X. Zhang, Y. Xie, M. Guan, D. L. Villeneuve, and H. Yu, "Functional toxicogenomic assessment of triclosan in human HepG2 cells using genome-wide CRISPR-Cas9 screening," *Environmental Science & Technology*, vol. 50, no. 19, pp. 10682–10692, 2016.

[189] D. E. Haggard, P. D. Noyes, K. M. Waters, and R. L. Tanguay, "Phenotypically anchored transcriptome profiling of developmental exposure to the antimicrobial agent, triclosan, reveals hepatotoxicity in embryonic zebrafish," *Toxicology and Applied Pharmacology*, vol. 308, pp. 32–45, 2016.

[190] J. Guo, S. Ito, H. T. Nguyen et al., "Effects of prenatal exposure to triclosan on the liver transcriptome in chicken embryos," *Toxicology and Applied Pharmacology*, vol. 347, pp. 23–32, 2018.

[191] X. Cao, X. Hua, X. Wang, and L. Chen, "Exposure of pregnant mice to triclosan impairs placental development and nutrient transport," *Scientific Reports*, vol. 7, no. 1, article 44803, 2017.

[192] X. Hua, X. Y. Cao, X. L. Wang, P. Sun, and L. Chen, "Exposure of pregnant mice to triclosan causes insulin resistance via thyroxine reduction," *Toxicological Sciences*, vol. 160, no. 1, pp. 150–160, 2017.

[193] W. T. Festuccia, P. G. Blanchard, T. Belchior et al., "PPARγ activation attenuates glucose intolerance induced by mTOR inhibition with rapamycin in rats," *American Journal of Physiology Endocrinology and Metabolism*, vol. 306, no. 9, pp. E1046–E1054, 2014.

[194] K. B. Paul, J. T. Thompson, S. O. Simmons, J. P. Vanden Heuvel, and K. M. Crofton, "Evidence for triclosan-induced activation of human and rodent xenobiotic nuclear receptors," *Toxicology In Vitro*, vol. 27, no. 7, pp. 2049–2060, 2013.

[195] D. E. Clapham, "Calcium signaling," *Cell*, vol. 131, no. 6, pp. 1047–1058, 2007.

[196] G. Cherednichenko, R. Zhang, R. A. Bannister et al., "Triclosan impairs excitation-contraction coupling and Ca2+ dynamics in striated muscle," *Proceedings of the National Academy of Sciences of the United States of America*, vol. 109, no. 35, pp. 14158–14163, 2012.

[197] E. B. Fritsch, R. E. Connon, I. Werner et al., "Triclosan impairs swimming behavior and alters expression of excitation-contraction coupling proteins in fathead minnow (*Pimephales promelas*)," *Environmental Science & Technology*, vol. 47, no. 4, pp. 2008–2017, 2013.

[198] T. Kawanai, "Triclosan, an environmental pollutant from health care products, evokes charybdotoxin-sensitive hyperpolarization in rat thymocytes," *Environmental Toxicology and Pharmacology*, vol. 32, no. 3, pp. 417–422, 2011.

[199] V. V. Teplova, K. N. Belosludtsev, and A. G. Kruglov, "Mechanism of triclosan toxicity: mitochondrial dysfunction including complex II inhibition, superoxide release and uncoupling of oxidative phosphorylation," *Toxicology Letters*, vol. 275, pp. 108–117, 2017.

[200] G. McDonnell and A. D. Russell, "Antiseptics and disinfectants: activity, action, and resistance," *Clinical Microbiology Reviews*, vol. 12, no. 1, pp. 147–179, 1999.

[201] L. M. McMurry, M. Oethinger, and S. B. Levy, "Triclosan targets lipid synthesis," *Nature*, vol. 394, no. 6693, pp. 531-532, 1998.

[202] J. G. Beeson, P. A. Winstanley, G. I. McFadden, and G. V. Brown, "New agents to combat malaria," *Nature Medicine*, vol. 7, no. 2, pp. 149-150, 2001.

[203] H. H. Lee, J. Yun, J. Moon et al., "Crystallization and preliminary X-ray crystallographic analysis of enoyl-acyl carrier protein reductase from *Helicobacter pylori*," *Acta Crystallographica Section D, Biological Crystallography*, vol. 58, no. 6, pp. 1071–1073, 2002.

[204] J. Marcinkeviciene, W. Jiang, L. M. Kopcho, G. Locke, Y. Luo, and R. A. Copeland, "Enoyl-ACP reductase (FabI) of Haemophilus influenzae: steady-state kinetic mechanism and inhibition by triclosan and hexachlorophene," *Archives of Biochemistry and Biophysics*, vol. 390, no. 1, pp. 101–108, 2001.

[205] R. McLeod, S. P. Muench, J. B. Rafferty et al., "Triclosan inhibits the growth of Plasmodium falciparum and Toxoplasma gondii by inhibition of apicomplexan Fab I," *International Journal for Parasitology*, vol. 31, no. 2, pp. 109–113, 2001.

[206] S. L. Parikh, G. Xiao, and P. J. Tonge, "Inhibition of InhA, the enoyl reductase from Mycobacterium tuberculosis, by triclosan and isoniazid," *Biochemistry*, vol. 39, no. 26, pp. 7645–7650, 2000.

[207] C. W. Roberts, R. McLeod, D. W. Rice, M. Ginger, M. L. Chance, and L. J. Goad, "Fatty acid and sterol metabolism: potential antimicrobial targets in apicomplexan and trypanosomatid parasitic protozoa," *Molecular and Biochemical Parasitology*, vol. 126, no. 2, pp. 129–142, 2003.

[208] N. Surolia and A. Surolia, "Triclosan offers protection against blood stages of malaria by inhibiting enoyl-ACP reductase of Plasmodium falciparum," *Nature Medicine*, vol. 7, no. 2, pp. 167–173, 2001.

[209] S. Lu and M. C. Archer, "Fatty acid synthase is a potential molecular target for the chemoprevention of breast cancer," *Carcinogenesis*, vol. 26, no. 1, pp. 153–157, 2005.

[210] R. Lupu and J. Menendez, "Pharmacological inhibitors of fatty acid synthase (FASN)–catalyzed endogenous fatty acid biogenesis: a new family of anti-cancer agents?," *Current Pharmaceutical Biotechnology*, vol. 7, no. 6, pp. 483–494, 2006.

[211] B. Liu, Y. Wang, K. Fillgrove, and V. Anderson, "Triclosan inhibits enoyl-reductase of type I fatty acid synthase in vitro and is cytotoxic to MCF-7 and SKBr-3 breast cancer cells," *Cancer Chemotherapy and Pharmacology*, vol. 49, no. 3, pp. 187–193, 2002.

[212] E. S. Pizer, C. Jackisch, F. D. Wood, G. R. Pasternack, N. E. Davidson, and F. P. Kuhajda, "Inhibition of fatty acid synthesis induces programmed cell death in human breast cancer cells," *Cancer Research*, vol. 56, no. 12, pp. 2745–2747, 1996.

[213] F. P. Kuhajda, K. Jenner, F. D. Wood et al., "Fatty acid synthesis: a potential selective target for antineoplastic therapy," *Proceedings of the National Academy of Sciences of the United States of America*, vol. 91, no. 14, pp. 6379–6383, 1994.

[214] F. P. Kuhajda, E. S. Pizer, J. N. Li, N. S. Mani, G. L. Frehywot, and C. A. Townsend, "Synthesis and antitumor activity of an inhibitor of fatty acid synthase," *Proceedings of the National Academy of Sciences of the United States of America*, vol. 97, no. 7, pp. 3450–3454, 2000.

[215] T. S. Ho, Y. P. Ho, W. Y. Wong, L. Chi-Ming Chiu, Y. S. Wong, and V. Eng-Choon Ooi, "Fatty acid synthase inhibitors cerulenin and C75 retard growth and induce caspase-dependent apoptosis in human melanoma A-375 cells," *Biomedicine & Pharmacotherapy*, vol. 61, no. 9, pp. 578–587, 2007.

[216] M. C. Sadowski, R. H. Pouwer, J. H. Gunter, A. A. Lubik, R. J. Quinn, and C. C. Nelson, "The fatty acid synthase inhibitor triclosan: repurposing an anti-microbial agent for targeting prostate cancer," *Oncotarget*, vol. 5, no. 19, pp. 9362–9381, 2014.

[217] P. R. Deepa, S. Vandhana, U. Jayanthi, and S. Krishnakumar, "Therapeutic and toxicologic evaluation of anti-lipogenic agents in cancer cells compared with non-neoplastic cells," *Basic & Clinical Pharmacology & Toxicology*, vol. 110, no. 6, pp. 494–503, 2012.

[218] K. Nishi, K. Suzuki, J. Sawamoto et al., "Inhibition of fatty acid synthesis induces apoptosis of human pancreatic cancer cells," *Anticancer Research*, vol. 36, no. 9, pp. 4655–4660, 2016.

[219] B. Schmid, J. F. Rippmann, M. Tadayyon, and B. S. Hamilton, "Inhibition of fatty acid synthase prevents preadipocyte differentiation," *Biochemical and Biophysical Research Communications*, vol. 328, no. 4, pp. 1073–1082, 2005.

[220] E. S. Pizer, R. J. Kurman, G. R. Pasternack, and F. P. Kuhajda, "Expression of fatty acid synthase is closely linked to proliferation and stromal decidualization in cycling endometrium," *International Journal of Gynecological Pathology*, vol. 16, no. 1, pp. 45–51, 1997.

[221] R. E. Wilentz, L. A. Witters, and E. S. Pizer, "Lipogenic enzymes fatty acid synthase and acetyl-coenzyme A carboxylase are coexpressed with sterol regulatory element binding protein and Ki-67 in fetal tissues," *Pediatric and Developmental Pathology*, vol. 3, no. 6, pp. 525–531, 2000.